IN-VITRO CELLULAR INTERACTION OF QUANTUM DOTS AND SILICONE SURFACES

A thesis submitted to the National University of Ireland, Galway
in fulfilment of the requirement for degree of

Doctor of Philosophy

By

Babu Rajendra Prasad Bodi

Bachelor of Medicine and Bachelor of Surgery (M.B;B.S)

National Centre for Biomedical Engineering Science
National University of Ireland, Galway

Thesis Supervisors: **Dr. Yury Rochev and Prof. Terry J. Smith**

September 2011

TABLE OF CONTENTS

I wish to dedicate this work

to

The Supreme divine couple

Sree Sree Radha Govinda

and

Jagad Guru

A. C. Bhaktivedanta Swami Srila Prabhupada

and

Sree Guru

and

Sree Gauranga

ACKNOWLEDGEMENTS

I would like to firstly thank my supervisors Prof. Terry J. Smith and Dr. Yury Rochev for providing me the opportunity to do this PhD and for all the support, encouragement and guidance throughout this research project and in difficult times.

I would like to thank Prof. Yurii K. Gun'ko for giving me the opportunity to spend time in the SNIAM lab in Trinity to observe the synthesis process of our QDs.

I would also like to thank Dr. Natalia, Dr. Enda O'Connell, David Connolly and Eoidan O'Timmins for the patience and support with all the cell culture work, Microarray analysis, Confocal microscopy and Atomic force Microscopy work respectively and for all thier efforts to ensure I got good results.

I would like to thank Dr. Stephen J. Byrne, Valerie A. Gerard and Gemma Louis Davis for all the patience and help with my constant questions on QDs.

I would like to thank Dr. Una Fitzgerald for all the feedbacks as Graduate Research comitee member for her time and effort.

I would like to thank the NCBES and REMEDI for the use of the facilities.

I would like to thank Dr. Alan Ryder and his Biophotonics group for helping and using their facility in measuring QDs with the Spectrophotometer.

I would like to thank Maria Nash, Jennifer Alexander and Rong Bing Yang from our biomaterials group who always had time to answer any of my questions.

I would like to thank my parents, brother and all the family relatives at home for their constant support and help.

I would also like to thank my spiritual house-mates and also my best friends Vrajendra Prabhu and Maharani mataji, Dr. Mangesh Kulkarni and Aleksandra Leszczynska, Sri Vamsi Chekinarapu, Dr. Dmitry Tkachenko, Dr. Sudhir Sunkara and Dr. Kalyani, Iniya Kumar Muniraj and his wife, Aditya Vaishya and his wife, Oisin and Niall, Rajiv Krishna, Ajay Babu, Sreenath Chandran, Ayswaria Deepti, Biraja Dash, Siva Rama Krishna Ramadurai, Venkatesh Kodgi, Naveen, Yashwant, Gopi Krishna Chakka and Parimala, Srinivas and Nalini, Krishnan Sathyakumar and Swatika, Prasad. V. V and his wife, Rao Rapolu and Kalyani, Rama Krishna and his wife, Abhijyan and his wife, Pramodh and his wife, Ramesh Kumar and his wife, Senthil Kumar, Rama Krishna and his family, Narayana, Raja Mohan for all their support and help for making this PhD project and the life in Galway such an enjoyable one.

ABBREVIATIONS

µg	Micro grams
µl	Micro-litres
µm	Micrometers
µM	Micro Molar
BSA/PBS	Bovine serum albumin / phosphate-buffered saline
Cd^{2+}	Cadmium ions
$CdCl_2$	Cadmium Chloride
CdS	Cadmium Sulphide
CdSe	Cadmium Selenide
CdTe	Cadmium Telluride
CTAB	Cetyltrimethylammonium Bromide
Cys	Cysteamine
DAPI	4, 6-diamidino-2-phenylindole
DHLA	Dihydrolipoic acid
DIC	Differential Interference Contrast
DMEM	Dulbecco's Modification of Eagle Medium EDTA
DNA	Deoxy-ribonucleic acid
EDTA	Ethylene-diamine tetra-acetic acid
Gel-QDs	Gelatinated QDs
gm	Grams
HBSS	Hank's Balanced Salt Solution
HPMEC	Human Pulmonary Microvascular Endothelial cells
M-199	Medium 199
mg	Milligrams
ml	Millilitres
MPA	Mercaptopropionic acid
MUA	Mercapto-undecanoic acid,
NAC	N-acetyl Cysteine
NGF	Nerve growth factor
nm	Nanometers

Non-gel QDs	Non-gelatinated QDs
PAH	Poly(allylaminehydrochloride)
PC12	Pheochromocytoma 12
PDMS	Poly(dimethylsiloxane)
PEG	Polyethylene Glycol
PEI	Polyethylene Imine
PL	Photoluminescence
PLA	Polylactic acid
PLL	Poly-L-Lysine
PSS	Poly(styrenesulfonate)
QDMC	Quantum dot loaded microcapsules
QDs	QuantumDots
RNA	Ribo-nucleic acid
RT	Room temperature
SDS	Sodium dodecyl sulfate
SSA	Sodium Sulphate Anhydrous
TGA	Thioglycolic Acid
TOPO	Trioctylphosphine oxide
UV	Ultraviolet
Vs	Versus
λ_{ex}	Excitation wave length
ZnS	Zinc Sulphide

ABSTRACT

The main hypothesis on which this study has been based is that the surface modification of nano-particles of different size (Quantum Dots) and varying nano-surfaces roughness (Silicones of nanosurface roughness) can make them highly biocompatible in various applications of biology and medicine. In this work, attempts were made to investigate if the surface modification of nano-particles by gelatination of different size (Quantum Dots) makes them more biocompatible by reducing the toxicity on the cells and increasing the nano-surface roughness (Silicones of nanosurface roughness ranging from ~88 nm to ~650 nm) makes them more biocompatible by reducing the fibroblast growth of the cells *in vitro.*

To address these questions, the nano-particles [CdTe Quantum dots of thioglycolic acid (TGA) capped gelatinated and non-gelatinated] and nano-surfaces (Silicones of nanosurface roughness) were characterised and then three different types of cells were used to check the biocompatibility in *in vitro* cell lines. At first, the Quantum Dots (QDs) were co-incubated with undifferentiated Pheochromocytoma12 (PC12) cells and investigated the cellular interaction, uptake and resultant toxic influence of the QD – cell interplay was explored as the QD concentrations were varied over extended (up to 72 hours) co-incubation periods. Following this, QDs have been co-incubated with differentiated pheochromocytoma 12 (PC12) cells and the apoptotic process involved in the cell death machinery and also the intrinsic behaviour of QDs upon uptake by the cells have been analysed to extended (up to 17 days) co-incubation periods. In the same experiment, differentiated PC12 cells were also exposed to QDs after the neurites were grown for 10 days. Subsequently QDs were co-incubated with Human Pulmonary Microvascular Endothelial (HPMEC-ST1.6R) cells and analysed their cytotoxicity, differentially expressed genes and also their pathways involved to extended (up to 72 hours) co-incubation periods. Finally, the nano-surface roughnesses of silicone elastomer samples with rms surface roughnesses varying from ~88 nm to ~650 nm were co-incubated with NIH-3T3 fibroblast cells and analysed the total amount of DNA to extended (up to 24 hours) co-incubation periods.

In conclusion, it was shown here that the surface modification of nano-particles (Quantum Dots) and nano-surfaces (Silicones of nanosurface roughness) were more biocompatible *in vitro.*

CHAPTER 1:INTRODUCTION

1.1 Background

The term “Quantum Dot” was first coined by Mark A. Reed in 1988 (Drummen 2010). Quantum dots (QDs) are nanometer-scale semiconductor crystals, are promising zero-dimensional advanced materials because of their nanoscale size (Mansur 2010), and are defined as particles with dimensions physically smaller than the exciton Bohr radius (Chan W. C. et al. 2002a). When a photon of visible wavelength is absorbed by such a semiconductor, it emits electrons of higher energy states and upon returning to their ground state, they will emit a photon of certain frequency characteristic of that material (Chan W. C. et al. 2002a). QDs are nano-crystalline semiconducting inorganic fluorophores, whose excitons are confined in all three dimensions spatially called quantum confinement having typically diameters of 2–20 nm (Drummen 2010). This quantum confinement has charge carriers with electrons and holes confined in all the three dimensions occupying a volume which is determined by the physical properties of the material the QDs were made. This quantum confinement occurs due to shrinkage in dimension of QD material which is smaller than characteristic volume with new physical properties not observed in the original bulk material as shown in figure 1.1. This quantum confinement can be observed based on their relationship between emission color of QDs and their size (Bentolila et al. 2009, Bhirde et al. 2011). QDs in the size range of 2–6nm are extremely very important, because of their similarities in physical dimensions with biological macromolecules such as nucleic acids (RNA and DNA) and proteins (Chan W. C. et al. 2002a).

Because of their unique physical properties, QDs are predominantly used as bioimaging agents (Drummen 2010). Optical properties like strong light absorbance, size-tunable emission means minute changes in the radius of QDs manifests as visible colour changes of the QDs in solution. This property may lead to their potential use as simultaneous multiple colour labels (Pathak et al. 2006a, Vanmaekelbergh and Liljeroth 2005, Yu et al. 2003). Bright fluorescence/high quantum yield, narrow symmetric emission bands (Alivisatos 2004, Chan Warren C. W. et al. 2002b, Han et al. 2001, Larson et al. 2003), high photo-stability and highly resistant to photo-bleaching (Bruchez Marcel, Jr. et al. 1998b, Chan Warren C. and Nie 1998a, Chen and Gerion 2004, Gao Xiaohu et al. 2004a), and their broad absorption ranges allow for their excitation and multiplexed detection across a wide spectrum of wavelengths (Alivisatos

2004, Chan Warren C. W. et al. 2002b, Drummen 2010, Han et al. 2001, Larson et al. 2003).

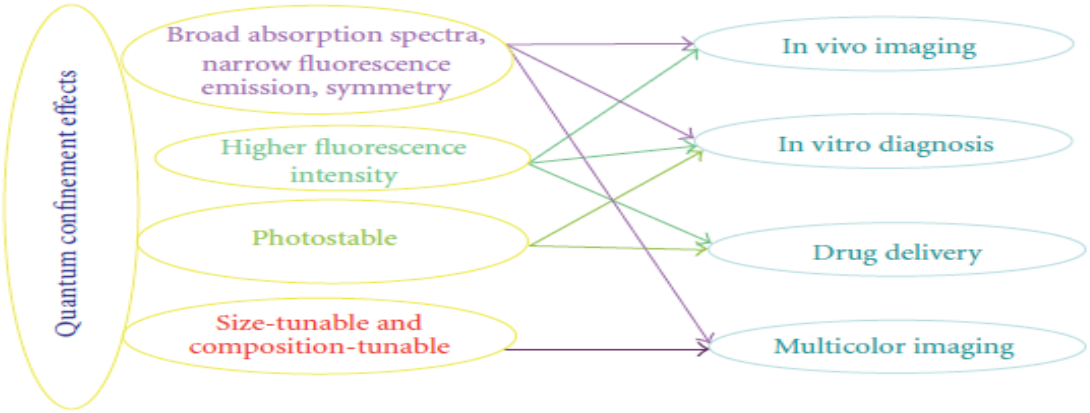

Figure 1.1: Showing quantum confinement effects of QDs are the characteristics of broad absorption spectra, narrow fluorescence emission, high levels of fluorescence and photostability, size and composition-tunable QDs and its applications in in vitro and in vivo multicolor imaging and diagnosis along with targeted drug delivery [Adapted from (Peng C. W. and Li 2010)]. Permission to reproduce this figure has been granted by Yan Li.

1.2 Properties of QDs

The difference in properties of QDs is due to different combinations of chemicals used in synthesizing them. Various combinations like CdTe, CdSe and CdS is used during synthesis of QDs. These combinations will show different properties and their effects on cellular activity differ upon interfering with cells (Peng X. G. and Peng 2001). Previously the QDs were hydrophobic and are not of any use in biological research as they cannot interact with cells and tissues due to diminution of fluorescence in aqueous media (Lovric et al. 2005b). To render them hydrophilic (Nie and Chan 1998) and make them useful in biological research, QDs were capped with bifunctional molecules i.e, hydrophilic on one side and hydrophobic on other side, such as Mercaptopropionic acid (MPA) (Zhang W. et al. 2009b), Thioglycolic acid (TGA) (Ji et al. 2008, Komarala et al. 2006), 2-mercaptoethylamine (MEM) and 3-mercapto-1,2-propanediol (MPD) (Komarala et al. 2006) etc .

The inherent nature of QDs is that the size depends directly on their physical properties. The size of QDs is inversely proportional to the surface area of the QDs as shown in figure 1.2. The decrease in size of QDs leads to percentage increase in the atoms or molecules displayed over the surface of QDs instead of seating in the interior of the material. This increase in surface area of QDs will ultimately determine the numerous potential of various reactive elements or groups over their surface. By the decrease in size of QDs and thereby changing the structural and physicochemical properties of QDs lead to interaction with different materials finally causing toxicological effects. So the size and surface area of QDs plays a pivotal role in respect to their toxicological studies (Nel A. et al. 2006b). QDs are less susceptible to photo-bleaching than organic dyes because of their stable emitting light owing to their inorganic composition (Alivisatos 1999, Michalet et al. 2001). High fluorescence intensity or photo-brightening of QDs is also a very important characteristic of QDs (Gerion et al. 2001, Kloepfer et al. 2003). QDs have larger diffusion coefficient than organic dyes, this property helps in tracking the QDs and analyses their trajectories. Because of the small size, QDs effect on molecules motion is very significant. This small size and high photo-stability makes QDs very useful in single-molecule experiments as a suitable and reliable probe than organic dyes (Alivisatos et al. 2005, Dahan et al. 2003).

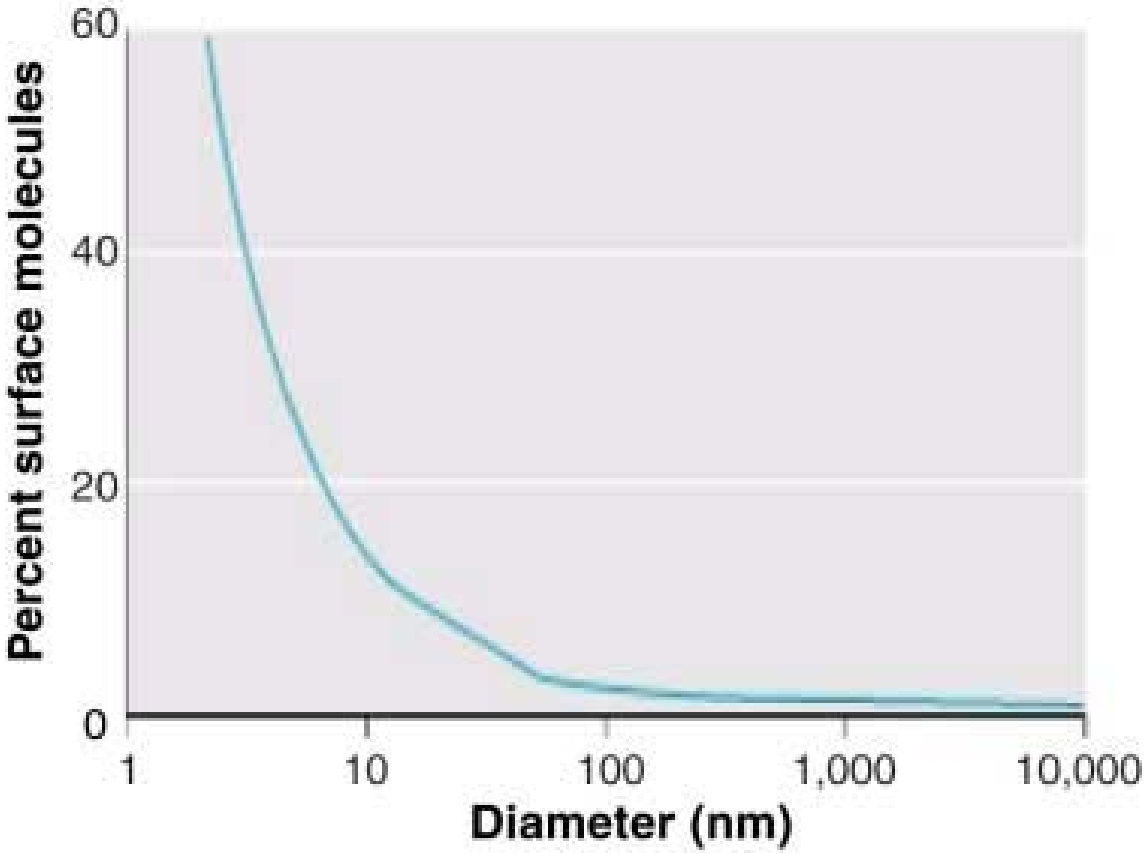

Figure 1.2: Showing relationship between QD size and percentage of surface expressed molecules. Below 100 nm size, the percentage of surface molecules increased exponentially. In a QD size of 30 nm, approximately 10% of surface molecules are expressed. Between QD size of 10 and 3 nm, the percentage of surface molecules increased to 20 and 50 respectively [Adapted from (Nel A. et al. 2006a, Oberdorster et al. 2005)]. Permission to reproduce this figure has been granted by Oberdorster.

The size of QDs influences wavelength of light and the wavelength has the ability to control its color as shown in figure 1.3. Because of their small size, different sized QDs can be used as multiple color labels simultaneously (Pathak et al. 2006a, Vanmaekelbergh and Liljeroth 2005, Yu et al. 2003). The graphic representation in figure 1.4 shows the linear correlation in change of size of QDs against color change of light (absorption).

Figure has been removed due to Copyright restrictions

Figure 1.3: Schematic representation of the changes in optical behavior of QDs depending on their size. Top: Electronic structure of QDs with 'blue shift' due to quantum confinement. Below: From left to right (blue to red) are ten distinct colors of QDs (Chan W. C. et al. 2002a, Mansur 2010).

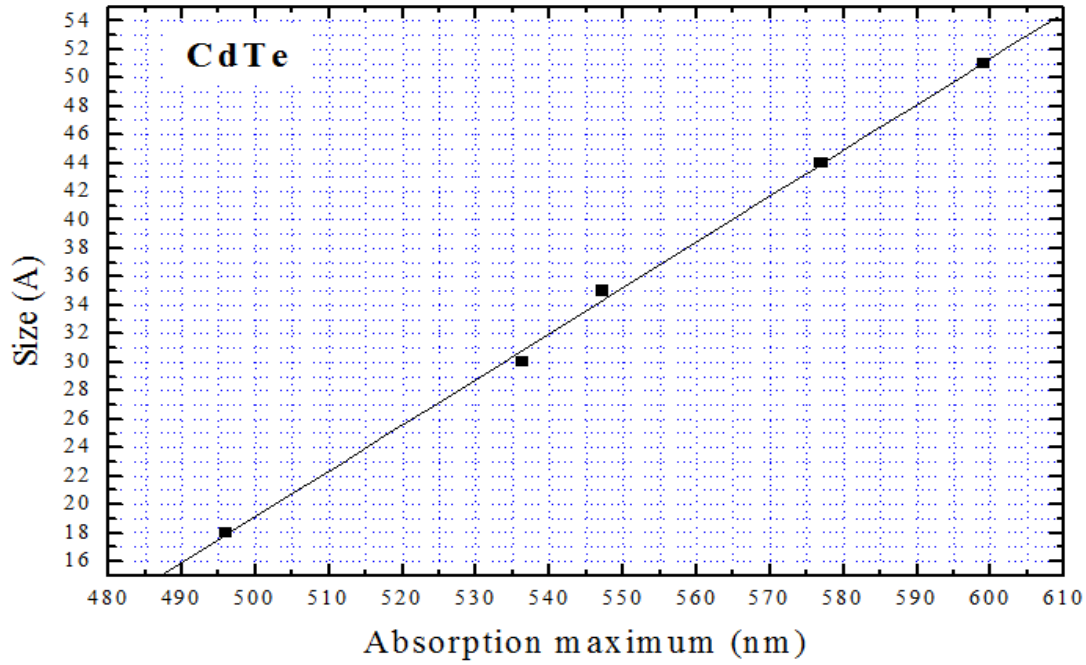

Figure 1.4: Graph showing sizing curves for CdTe nano-particles supplied by our collaborator Prof. Yurii K. Gunko group, Inorganic Chemistry, Trinity College Dublin.

The different properties of QDs like size, broad absorption and narrow emission spectrum, photostability, high fluorescence intensity and modification of surface made QDs with different functional applications in biology and medicine as shown in table 1.1, and are a break through in understanding and discovering the unknown aspects in biology and medicine in future.

Properties of QDs	**Functional applications of QDs in biology and medicine**
Size tunable	Multi color imaging (Chan W. C. et al. 2002a)
Broad absorption and narrow emission spectrum	Multi color imaging, *in vivo* imaging (Gao X. et al. 2005) and *in vitro* diagnosis
Photostable	*In vitro* diagnosis and drug delivery (Bisht et al. 2007, Chouhan and Bajpai 2009, Lai et al. 2003)
High fluorescence intensity	*In vivo* imaging, *in vitro* diagnosis (Rosenzweig et al. 2004, Zhang H. et al. 2009a) and drug delivery
Modification of surface	Hydrophilicity of QDs make them useful in biological applications (Chan W. C. and Nie 1998b, Zhang W. et al. 2009b), conjugation of QDs with drugs (Bisht et al. 2007, Chouhan and Bajpai 2009, Lai et al. 2003), proteins (Jaiswal et al. 2003) and antibodies (Goldman et al. 2002) etc

Table 1.1: Showing the different properties of QDs and their functional applications in biology and medicine.

1.3 Applications of QDs

QDs are excellent fluoropores with widespread recognition because of their exceptional photo-physical properties. They are being applied extremely to existing and emerging technologies, and have pivotal importance in many areas (Jamieson et al. 2007). There is lot of advancement and progress in biological imaging especially in the area of fluorescent semi-conductor nano-crystals because of its resistance to photo-bleaching (Bruchez M., Jr. et al. 1998a, Chan W. C. and Nie 1998b, Gao X. et al. 2004b), and this paved the way for the development in medical diagnostics and drug delivery using QDs. One of the most important criteria for the future development of QDs as efficient cellular delivery (Derfus et al. 2007, George et al. 2009, Park K. H. et al. 2010), labelling (Muller-Borer et al. 2007, Shah et al. 2006, Vazquez et al. 2009) and targeting agents (Pietrasanta et al. 2007, Wu X. et al. 2003a, Zhang H. et al. 2009a) is that their intracellular uptake into the cells has the ability to selectively detect one molecule, or a small number of molecules. The QD probes must be able to selectively access various sub-cellular compartments which need to be targeted in order to understand the dynamics of cellular organisation without causing a cyto-toxic effect during the time period required (Delehanty et al. 2006).

Currently methods having access to single molecule properties in living cells are limited due to the size of the probe or photo-bleaching of fluorescent biomarkers. QDs have a great potential as fluorescent probes thanks to their size ranging from approximately 2 to 5 nm and their enhanced photo-stability, whereby signal detection is not diminished even after exposure to the acidic cell environment (Dahan et al. 2003).

1.3.1 Bioimaging

Quantum Dots (QDs) have been widely touted as new replacements for traditional dyes for the imaging of living cells and tissues. Due to their extremely small size QDs can, *via* specific and non-specific pathways penetrate and label both the exterior and interior of numerous cell types (Dubertret Benoit et al. 2002b, Gao Xiaohu et al. 2004b, Goldman et al. 2002, Jaiswal et al. 2004, Pinaud et al. 2004, Rosenthal et al. 2002b, Wu Xingyong et al. 2003b). The applications of QDs in biological imaging as shown in figure 1.5.

Figure has been removed due to Copyright restrictions

Figure 1.5: Showing the applications of quantum dots as multimodal contrast agents in bio-imaging [Adapted from (Michalet et al. 2005)].

1.3.1.1 Fluorescent labeling of cell organelle, proteins and receptors

Labeling of cellular proteins with QDs has made rapid progress and attracted wide attention among cell biologists. Bio-functionalized QDs of different color or size have the ability to label cells. Cells labeled with these QDs give access to visualize all the organelle and different proteins of cells like nucleus/nuclear proteins, mitochondria, microtubules, actin filaments, endocytic compartments, mortalin and cyto-keratin etc as shown in table 1.2 under continuous illumination with multi-color imaging, which highlights the importance of these fluorophores over the conventional organic dyes which bleaches very easily (Medintz et al. 2005). It is very difficult for the larger QDs to enter into the cytoplasm of the cell crossing the cell membrane lipid bi-layer. This uptake will be accomplished by non-specific endocytosis, microinjection of QDs, conjugation of quantum dots to translocating proteins or cationic peptides, or membrane specific receptors where QDs often end up in cytoplasmic compartment of the cell (Ghasemi et al. 2009, Medintz et al. 2005). After entering into the cytoplasm of cell, QDs will disperse depending on their surface coating and pH stability. QDs will aggregate in the cytoplasm if they are capped with COOH-terminated groups, because of their poor stability in acidic environment of the cell, whereas protein-coated QDs will be dispersed in the cytoplasm of the cell (Medintz et al. 2005). Cell membrane receptors like glycine and erbB/HER and cell membrane protein biomarkers like *p*-glycoprotein, serotonin transport proteins, prostate-specific membrane antigen and Her2 proteins have been labeled with QDs enabling real-time tracking of biomarkers and imaging single molecules made QDs adventurous in recent times (Ghasemi et al. 2009, Medintz et al. 2005).

Cell organelle/ Proteins/ Receptors	**Functional properties of QDs**
Nucleus/nuclear proteins or antigens	Brightness and photostability of QDs, probes and localise nucleus and nuclear antigens (Chen and Gerion 2004, Wu X. et al. 2003a).
Mitochondria	QDs tracks and localises surrounding mitochondria (Derfus et al. 2004a).
Microtubules and actin filaments	Brightness and photostability of QDs, probes and localise microtubules and actin (Wu X. et al. 2003a).
Endocytic compartments	Vesicles which are formed on cell surface mediate both specific and non-specific uptake of foreign molecules (Hanaki et al. 2003).
Mortalin	Heat shock 70 protein present in normal and precancerous cells shows different staining pattern by immune-fluorescence labeling and is a reliable marker in normal Vs transformed cell (Kaul et al. 2003).
Cytokeratin	Cytoskeleton protein over-expressed in many skin cancer cells labelled with QDs (Sukhanova et al. 2004).
Serotonin transport proteins	Transporter of serotonin on cell surface. Serotonin linked QD probes recognised and labelled serotonin-specific neurotransmitters as well as inhibited serotonin transportation in a dose dependent manner and explored serotonin transport mechanism (Rosenthal et al. 2002a).
Prostate-specific membrane antigen	Normal and cancerous prostate cells express this protein on their surfaces (Gao X. et al. 2004a).
Her2	Brightness and photostability of QDs, probes and localise marker protein (Her2) over-expressed by breast cancer cell surface (Wu X. et al. 2003a).
Glycine receptor	Neurotransmitter receptor on surface of spinal nerve cells whose main function is inhibition. Larger diffusion co-efficient of QDs helps in tracking QDs and analysing the trajectories (Dahan et al. 2003).
erbB/HER	Cellular membrane receptor over-expressed in many cancers mediating cellular response to growth factors. QDs conjugated with EGF binds to the filopodium of cell. High photo-stability of QDs makes them enable to understand binding and internalization kinetics and this transduction mechanism is helpful in receptor-targeted therapeutics. (Lidke et al. 2004).
p-glycoprotein	QDs labelled membrane glycoproteins to study heat stress effect (Minet et al. 2004) which is a mediator of multidrug resistance in cancer cells (Jaiswal et al. 2003).

Table 1.2: Showing cell organelle, proteins and receptors in the cell labelled with QDs and their functional properties.

1.3.1.2 Fluorescence resonance energy transfer (FRET) analysis

Fluorescence resonance energy transfer (FRET) is very helpful in measuring protein conformational changes, monitoring protein interactions and assaying of enzyme activity. It works on the basis of transfer of fluorescence energy from a donor particle to an acceptor particle whenever the distance between the donor and the acceptor is smaller than a critical radius called as Forster radius (Jamieson et al. 2007). Reports by Kagan et al. showed that resonance energy transfer occurred between closely packed CdSe QD solids (Kagan et al. 1996a, Kagan et al. 1996b). To monitor intracellular interactions and binding events, researchers are using QDs of 1-10 nm range, as FRET is very sensitive to molecular rearrangements in the range of 1-10 nm which will correlate to the size of biological macromolecules such as DNA, proteins and receptors (Medintz et al. 2005). Because of long-term photo-stability, QDs are extremely useful in the area of biosensors in a method to create an ‘‘on/off’’ switching capability via FRET whereby non-radiative energy transfer occurs between the QDs as highly efficient donors in FRET when coupled with a variety of acceptors, such as organic fluorophores or dyes as well as other QDs or metallic nano-particles which is helpful in real-time and continuous monitoring (Bailey et al. 2004). Because of broad absorption spectrum and narrow emission spectrum with continuous size tunable properties, QDs have unique advantage to use as donor surfaces in FRET by self-assembling acceptor dye-labeled proteins without spectral overlap by having multiple acceptor dyes interact with a single QD-donor substantially improved FRET efficiency (Bailey et al. 2004, Medintz et al. 2005). This means fluorescence resonance energy transfer occurs between QD donor/acceptor and organic dye acceptor/donor (Greenham et al. 2001, Kotov et al. 2001).

1.3.1.3 Gene technology

Because of broad absorption and narrow emission spectrums, several QDs can be excited at the same wavelength of light. This property of QDs could be exploited in high-throughput screening and analysis of genes, proteins and peptides. By multiplexing several QDs within a polymer bead assigned with bio-recognition molecules as many as six colors with ten different intensity levels for each color and exposed to multiple molecules of genes or proteins, it could give information about location, abundance and distribution of 10^6 unique codes of different genes or proteins. But practically, 1000

different codes would be more than enough in standard terms for analyses as the present techniques using organic flourophores with polymer microspheres would be limited to give information about only 100 different codes (Azzazy et al. 2007, Bailey et al. 2004). This application of QDs is popularly called as fluorescent in situ hybridization (FISH) to study the expression of specific RNA (Liu et al. 2006, Sealfon et al. 2005), DNA transcripts (Travas-Sejdic et al. 2007, Wang T. H. et al. 2005, Zhang C. Y. and Hu 2010) and protein markers (Cho Y. H. et al. 2008, McDevitt et al. 2009, Zhukov et al. 2007). This technology facilitates the ultrasensitive simultaneous detection of multiple RNA, DNA and protein markers in cell and tissue culture as well as in histological sections.

1.3.1.4 Pathogen and toxin detection

Multiplexed QDs conjugated with antibodies would be helpful in immunoassays to detect pathogens and toxins. After a brief incubation period of QDs conjugated with antibodies, the unbound antibodies will be washed away leaving the amount of bound antibodies to QDs flourophores. The unique spectral properties and resistance to photo bleaching has made QDs possible for multiplexing in immunoassays (Bailey et al. 2004, Medintz et al. 2005).

1.3.1.5 Tumor biology investigation

Imaging of multiple targets inside or on the surface of live cells simultaneously have been made possible by characteristic narrow emission spectra of QDs which is a breakthrough in early detection and identification of malignant tumors based on multiple molecular markers. Using QDs as multiple color labels, it made possible in the analysis of tissue samples by consuming less time for analysis while increasing the number of biomarkers that needs to be examined (Bailey et al. 2004, Cho Y. H. et al. 2008, McDevitt et al. 2009, Zhukov et al. 2007).

1.3.1.6 Cell tracking

High photo-stability and the extraordinary brightness of QDs make them potential applicants in the long-term for the tracking the particles in the living cells (Ruan and Winter 2011). With these properties of QDs, Li et al. used QDs to detect the gene silencing effect by co-transfected with small interfering RNA (siRNA) using cationic

liposomes, based upon an assumption that the biological effect of siRNA has direct correlation with the fluorescence intensity of QDs loaded in cells (Li Y. et al. 2011). The main major limitation with QDs in interruption of particle tracking is because of intermittent loss of fluorescence known as blinking. With the introduction of a new class of quantum dot-based composite nano-particles which exhibit near-continuous, alternating-color fluorescence and at the same time are able to discriminate aggregation status by observing the changes in color even while moving across the focal plane. These materials will greatly enhance particle tracking in cell biology and biophysics (Ruan and Winter 2011).

1.3.1.7 *In vivo* animal imaging

The advantages of *in vivo* animal imaging with QDs over other molecular imaging modalities like single-photon emission computed tomography (SPECT), positron emission tomography (PET), magnetic resonance imaging (MRI) and X-ray computed tomography (CT) are due to their low cost and easy handling, no exposure of ionizing radiations, short acquisition times, and high sensitivity (Texier and Josser 2009). QDs have high-fluorescence photon flux due to high quantum yield in conjunction with high extinction coefficient. Long fluorescence lifetimes of QDs eliminated their auto-fluorescence by enabling time-gated imaging and improving the sensitivity of fluorescence detection *in vivo*. Because of their large surface to volume ratio, biocompatible QD conjugates are helpful in tumor targeting, metastatic tumor cell tracking, mapping of sentinel lymph nodes and tumor angiogenesis (Bentolila et al. 2009)

1.4 Intracellular uptake of QDs

Recent research on QDs shows that they are of much use as fluorescent labels in cellular and molecular live imaging applications in biology and biomedicine (Duan and Nie 2007, Prasad et al. 2010b, Xie et al. 2007). QDs can traverse through the epithelium of airway passages and vascular system and enter the cell organelle such as vesicles, lysosomes and endosomes because of their small size. This leads to aggregation of QDs as clusters inside living cells. This entrapment of QDs inside the cell organelle limits the interaction of QDs with the cytoplasm environment. As a result of this, little

information is known in terms of their interaction with other cell organelle and intracellular proteins inside living cells. To overcome this obstacle a study was done with cell-penetrating peptides like poly-arginine and TAT by conjugation with QDs. Even with the use of these conjugated QDs, the QDs were still getting entrapped inside the cell organelle like lysosomes, endosomes and vesicles thus limiting their use in cellular targeting and molecular diagnostics (Duan and Nie 2007, Ruan et al. 2007).

QDs research with phagocytic cells shows phagocytic behaviour of cells with QDs rapid ingestion and accumulation of QDs in intracellular and nuclear regions. Various studies with negatively charged QDs by surface coating have shown strong tropism towards core histones and histone-rich cell organelle. This shows that the surface charge of QDs will determine the cellular uptake and their location within the cell. This is due to negatively charged QDs attracted to positively charged histones of nucleus. This is the reason why the bulk of TGA-capped CdTe QDs in our studies shows their location in the cytoplasm, surrounding the nucleus (Conroy et al. 2008).

QDs larger than 50 nm were taken up by cells through endocytotic process regardless of their surface conjugation but little is known about the uptake of QDs of smaller size less than 10 nm. Recent research on the uptake of QDs has shown that the QDs cell nonspecific binding depends on characteristic of QDs surface. Before using QDs as fluorescent labels, the main important factors to be taken into consideration are their stability, biocompatibility, non-toxic effect, ability to target and bind specific proteins and receptor sites. In order to achieve the above factors, thicker coatings on the surface of QDs may cause disadvantages in their application of manipulating the cell functions by preventing efficient transfer of electrons, holes or heat to the cells or decreasing local electric fields associated with the QDs. The increased radius of the QDs due to increase in thickness of protective surface coating may damage the bio-molecular machinery of the cell nucleus while passing through nuclear membrane pores which hinders to transport larger molecules of size more than 20 nm (Gomez N. et al. 2005a).

In our experiment, QDs were found to be localised within cytoplasm and around the nucleus and are heterogeneously distributed without entering inside the nucleus. Research studies done by Ruan et al. showed that QDs after entering into the nucleus and were entrapped by cell organelle like lysosomes, endosomes and vesicles. The nuclear pore complex and selective transport system mechanism of nucleus could be the hindering factors for the QDs to enter into nucleus (Ruan et al. 2007). In conclusion

based on research regarding the uptake of QDs inside the cells by several other groups shows that several known processes are involved that includes nonspecific uptake by endocytosis, where the QDs most often end up in endocytic compartments, direct microinjection of QDs in nanoliters of dispersion but is a tedious process and only applies to limited number of cells, electroporation process which physically pushes QDs across the membrane with different charges on QDs and mediated/targeted uptake of QDs based on the surface functionalization or modification of QDs by conjugating with various biological ligands and promoters (Mansur 2010, Medintz et al. 2005). The QD conjugate and its movement inside the cytoplasm of the cell was shown in figure 1.6 with the representation of cell membrane of lipids and proteins bilayer along with specific receptor molecules by QD-conjugate approximation in (a), affinity QD-ligand–cell receptor interaction at interface in (b) and early endosome by endocytotic process in (c) (Mansur 2010).

Figure has been removed due to Copyright restrictions

Figure 1.6: Showing the representation of cell membrane with the lipids and proteins bilayer along with specific receptor molecules and the QD-conjugate approximation in (a); affinity ligand–cell receptor interaction at interface in (b); early endosome by endocytotic process in (c) (Adapted from Mansur 2010).

1.5 Mechanism of interaction of QDs with Biological tissues

With quantum confinement of QDs by shrinkage in size it creates discontinuous crystal planes which increases the number of structural defects and also disrupts the well structured electronic configuration of the material, by giving rise to altered electronic properties as shown in figure 1.7 (Oberdorster et al. 2005). This leads to formation of specific surface groups and finally functions as reactive sites. These surface groups on QDs may make them catalytically active or passive and change their solubility in water by making them hydrophobic or hydrophilic, lipophobic or lipophilic. The toxicity of QDs is due to interaction of electron donor or acceptor active sites which are activated physically or chemically by molecular O_2. The additional formation of ROS is

generated from superoxide radical formation through dismutation or Fenton chemistry by electron capture. Some of the QDs coated with metals like iron and vanadium and also organic coatings leads to the formation of quinines through redox-cycling and catalytic chemistry (Nel A. et al. 2006a).

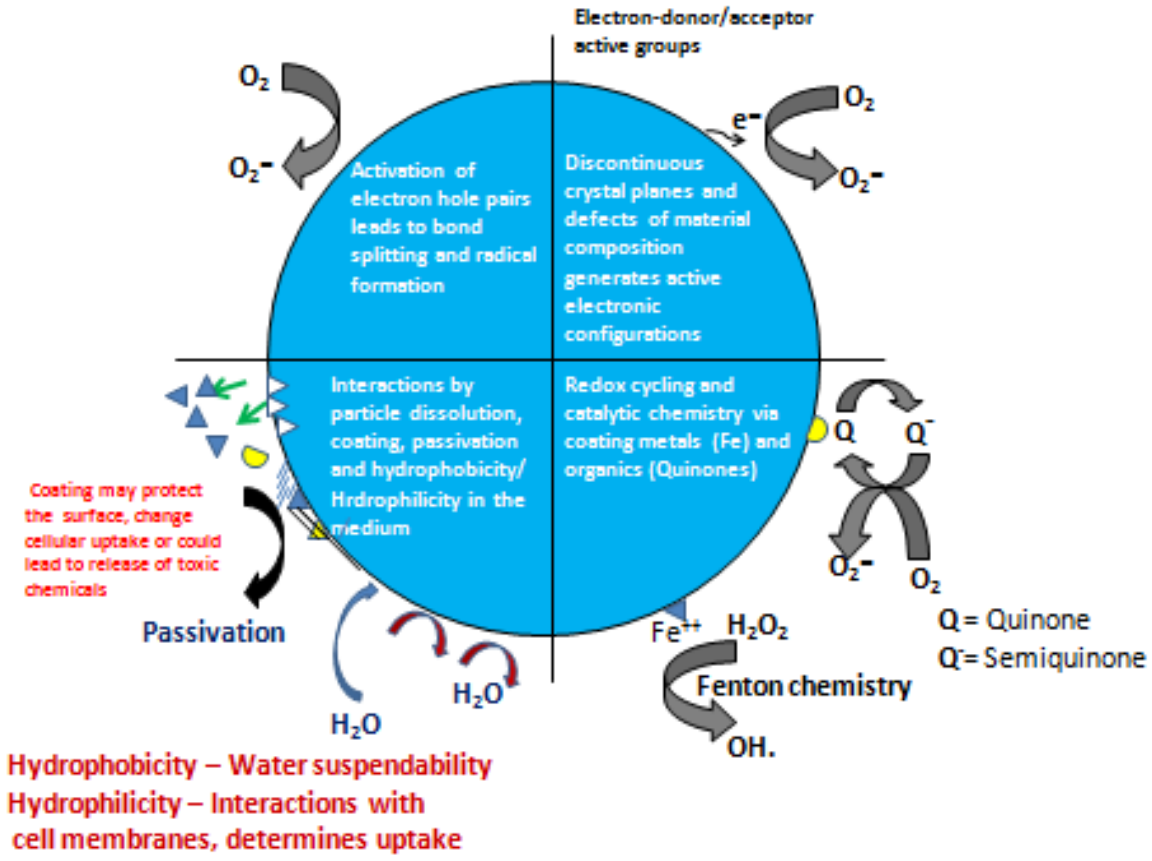

Figure 1.7: Showing schematic of mechanism of interaction of QD with biological tissues and illustrating the importance of composition of the material, electronic structure, bonded surface species of having metals, active or passive surface coatings and solubility along with the contribution of surface species and coatings and their interaction with other environmental factors such as activation of hole pairs.

1.6 Mechanism of cytotoxicity

There are four main different mechanisms that are leading to QDs cytotoxicity. The first mechanism is the release of toxic metals from the core of QDs. Second mechanism is the generation of reactive oxygen species (ROS). Third mechanism is the QDs aggregation on the surface of cell and the last mechanism is the cytotoxicity of surface-covering molecules of QDs (Li K. G. et al. 2009a). Of course the other physical characteristics of QDs like the hydrodynamic size, surface charge and concentration also play a key role in the cytotoxicity of QDs (Bhirde et al. 2011).

1.6.1 Cyto-toxic effect of Cadmium ions

Free Cd^{2+} plays a pivotal role in QD cytotoxicity at higher concentrations upon releasing into the internal environment of the cell. Cadmium metal is a potent immune-toxic pollutant to the internal environment of the cell and exhibits immune-toxicity, nephro-toxicity and hepato-toxicity. It also causes cytotoxicity with the substitution of physiological Zn along with induction of reactive oxygen species (ROS). Fragmentation of DNA is caused by cadmium ions, which is one of the hallmarks of apoptosis. Cadmium toxicity affects the cell by the induction of apoptosis. Apoptosis is a programmed cell death which involves activation of cell death machinery, Caspase-9, Apaf-1 and Cytochrome c. Some of the morphological features of the cell in apoptosis are chromatin margination along the nuclear membrane, nuclear condensation, budding and fragmentation as shown in figure 1.8. These morphological changes are due to Caspases, a family of cysteine proteases that carry out these complex biochemical events in the cell. Caspases family consists of initiator caspases like caspases-8, -9 and -12, whose main function is to activate downstream caspases and executor caspases like caspases-3, -6 and -7, whose main function is to degrade the cellular proteins (Kondoh M. et al. 2002a, Li K. G. et al. 2009a).

Previous research by Kondoh M. et al. has shown that induction of apoptosis is by cadmium ions, which activates Cytochrome *c* release from the mitochondria into the cytosol. By the release of Cytochrome *c* into the cytosol, Caspase-9 is activated, which then activates the Cytochrome *c*/Apaf-1 complex. In the mitochondrial-dependent pathway, Caspase-9 is an upstream caspase. Caspase-3 is a downstream caspase, which is then activated by the initiator Caspase-9. By the activation of downstream caspases,

such as caspase-3, we can conclude from this research that cadmium-induced apoptosis is thought to be activated by the mitochondrial dependent pathway (Kondoh M. et al. 2002a).

Cadmium ions (Cd^{2+}) have a higher binding affinity for sulfhydryl groups several times greater than its affinity for phosphate, chloride, carboxyl or amino groups. Metallothionein and Glutathione (GSH) compounds are rich in cysteine residues. Metallothionein (metal-binding protein) and intracellular GSH prevent the cell from cadmium toxicity. Metallothionein detoxifies cadmium by preventing Cd^{2+} ions reacting with target molecules by sequestering Cd^{2+} ions into an inert complex. Research studies have shown that metallothionein synthesis and defence mechanism occurs after GSH. GSH is the first line of defence against cadmium toxicity. GSH plays many key roles in protecting the cell against ROS and toxins, helps in protein and DNA synthesis, maintains integrity of cell membrane, regulates enzyme activities and also helps in maintenance of protein thiol groups in animal tissues and in the sulfhydryl group, it is the most abundant thiol compound. Oxidative stress in the cell is the first sign in the mechanism of cytotoxcity which shows GSH gets depleted. Recent research by K. G. Li *et al.* demonstrated that GSH depletion in CHL cells signalled the harmful effect of CdS QDs on the cellular antioxidant system. The experimental observation by Li and Rikans showed that the free cadmium ions released from the CdS QDs which do not possess a gelatine protective layer leads to reduction in GSH levels (Li K. G. et al. 2009a, Rikans and Yamano 2000b).

Cadmium ions disturb the lipid composition and thereby enhance lipid peroxidation and increases intracellular calcium concentration. Cadmium ions have high affinity to bind to thiol groups of proteins. This binding of cadmium ions with the essential proteins in the sulfhydryl group leads to inactivation of thiol proteins. This further causes cytoskeleton disorganisation and dysfunction of cell organelle like nuclei, mitochondria and endoplasmic reticulum. This inactivation of thiol group proteins by unwanted binding of cadmium ions also affects the intracellular redox state which finally induces oxidative stress in the cell. This oxidative stress in the cell manifests many harmful effects including mitochondrial dysfunction which causes increased mitochondrial membrane permeability. This leads to release of cytochrome *c* with onset of apoptosis (Rikans and Yamano 2000b).

1.6.2 Cytotoxic effect of Reactive Oxygen Species (ROS) by QDs

The increase of ROS levels in the cell leading to changes in cellular morphology and damage as shown in figure 1.8 and 1.9 are triggered by different pathways.

1. Due to release of Cd^{2+} ions from QDs inside the cell.

2. Due to damage of intracellular antioxidant system by QDs inside the cell- QD-induced cytotoxcity or cell death occurs due to the generation of ROS by QDs in the extracellular environment of the cell and also inside the cell. This ROS leads to damage of plasma membrane and intracellular organelle such as mitochondria and nucleus. As the mitochondria are very sensitive cell organelle and they get affected first as shown in figure 1.8 (Lovric et al. 2005a, Tsay and Michalet 2005).

Figure has been removed due to Copyright restrictions

Figure 1.8: Showing proposed mechanism of QD-induced cytotoxicity by naked QDs [Adapted from (Lovric et al. 2005a)]

3. Due to excitation, transfer of electron to oxygen takes place and this leads to formation of electron-hole pairs by QDs (Cho S. J. et al. 2007b, Tsay and Michalet 2005).

The raise of intracellular ROS levels by the above mechanisms finally leads to changes in cell morphology with enlargement of lysosomes and rounding of mitochondria (Cho S. J. et al. 2007b) along with damage of the DNA, proteins and membrane lipids. The studies done by K. G. Li *et al*. showed that by surface modification of CdSe or CdTe QDs, the cellular damage by the release of free cadmium ions from QDs can be significantly reduced. In the same study by K. G. Li *et al*. have shown a rise in ROS levels by 20-30% in cells treated with the CdS QDs when compared to the untreated controls and concluded that the CdS QDs promoted the intracellular ROS production. This difference of the increase of ROS levels when compared with controls is due to excitation of CdS QDs or by damage of intracellular antioxidant system by CdS QD

interaction inside the cell. It also concluded that the QDs produce ROS in the presence or absence of light (Li K. G. et al. 2009a). So the ligands on QD surface may be effective in preventing surface corrosion and release of cadmium ions. The surface modification of gelatine coating of TGA CdTe QDs in our research would be highly biocompatible and prevents release of toxic cadmium ions from the core of QDs and also reduces surface corrosion of QDs.

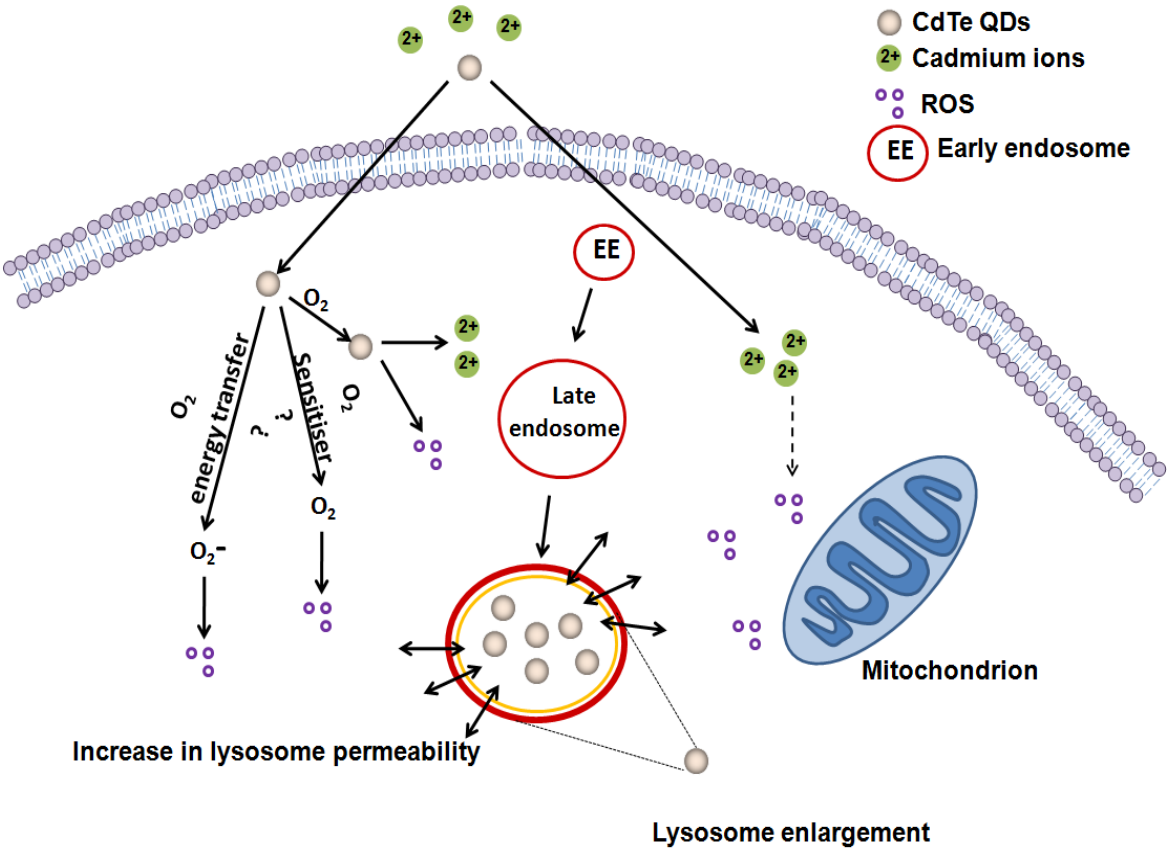

Figure 1.9: Showing schematic representation of the pathways involved in the cytotoxicity of CdTe QDs in live cells in vitro, highlighting the prominent changes in the morphology of cell, the chemical reactions and reactive oxygen species leading to the formation of ROS and also free Cd^{2+} ion release.

1.6.3 Cytotoxic effect of surface covering molecules of QDs

Hoshino et al. in their study investigating different surface covering molecules of QDs such as mercapto-undecanoic acid (MUA), cysteamine, and thioglycerol, trioctylphosphine oxide (TOPO) and zinc sulphide (ZnS) showed the effect of

cytotoxicity of these surface covering molecules. MUA caused severe cytotoxicity with damage of DNA of the cells. Cysteamine were less genotoxic. Thioglycerol was less toxic. TOPO was both cytotoxic and genotoxic compound. No significant cytotoxicity was observed with ZnS. It is prudent therefore that the surface-covered functional groups and bio-molecules covering the surface of QDs plays a pivotal role in the biological behaviour of whole QDs (Hoshino et al. 2004b).

The QDs in our study have a heavy metal core packed with cadmium telluride (CdTe) which is responsible for the fluorescence properties of QDs. An intermediate shell made of thioglycolic acid (TGA), which is non-emissive and also acts as a stabiliser. The outer protective layer is made of gelatine, which originates from collagen of animal bones and skin and is suitable in biological applications because of its biocompatibility by preventing the leakage of heavy metals from the core (Pathak et al. 2006a). This gelatine is a natural macromolecule which is non-toxic, inexpensive, biodegradable, less immunogenic and chemical modification is easy and also prevents non-specific binding possesses several functional groups on its surface for covalent modification by binding with different drugs and ligands (Balthasar et al. 2005, Coester et al. 2006). By conjugating the highly luminescent gelatinated QDs to proteins, peptides and other biological macromolecules to live cell cultures will reveal the mechanistic pathways of their transport inside the cell (Byrne S. J. et al. 2006). The quantum yield (QY) of the QDs can be enhanced by effectively capping the defects of heavy metal core of QDs with TGA acting as epitaxial-type shell because of large band gap. The surface layer of long chain biopolymer molecules of QDs has the ability to counteract the toxic effect of CdTe core (Byrne Stephen J et al. 2007a).

1.6.4 Cytotoxic effect of aggregation of QDs

A fundamental problem of QDs is that of aggregation and accumulation, which are particularly prevalent upon entrapment in organelles such as vesicles, endosomes and lysosomes inside living cells (Derfus et al. 2004a, c, Lee H. M. et al. 2009). If the physicochemical properties get changed, the number concentration of the QDs also changes. The size, size distribution, surface-to-volume ratio and the surface reactivity of QDs gets altered. These are the important parameters that play a pivotal role in the toxicity of QDs and get altered by aggregation. Therefore it is important to take these changes into consideration before assessing the cytotoxicity of QDs (Dhawan and

Sharma 2010, Teeguarden et al. 2007, Wick et al. 2007). It is understood that the QDs can traverse various barriers of the biological system of different cells because of their small size. Small size gives larger surface area and aggregation of QDs leads to decrease in total available surface area, which causes alteration in biological response. This finally leads to underestimation of cytotoxic potential of QDs which is important in drug delivery and also in assessment of threshold levels of their safety or toxicity (Dhawan and Sharma 2010). QDs after entering inside the cells because of their interaction with the macromolecules like proteins, the rate and extent of aggregation may alter (Balbus et al. 2007, Dhawan and Sharma 2010). This aggregation of QDs inside the cell may lead to change of hemostasis of the cell environment could finally lead to toxicity (Bhirde et al. 2011). There is possibility that QDs may show their toxic effects as aggregates by the release of toxic chemicals (Nel A. et al. 2006b).

1.7 Cytotoxicity of QDs *in-vitro*

Quantum Dots (QDs), though an attractive diagnostic and therapeutic tool, have the major disadvantage of being cytotoxic in nature, due to their cadmium components (Li K. G. et al. 2009b, Lovric et al. 2005a). One significant problem with QDs is their heavy metal composition (Kondoh Masuo et al. 2002b, Limaye and Shaikh 1999, Rikans and Yamano 2000a), which has given genuine cause for concern due to their potential cytotoxicity (Kondoh Masuo et al. 2002b, Nel Andre et al. 2006b, Rikans and Yamano 2000a). In an effort to combat this problem, much research has been conducted into the mechanisms that result in QDs acting as toxic agents once exposed to a cellular environment (Derfus et al. 2004b, E. Chang et al. 2006, Guo Guoning et al. 2007a, Hoshino et al. 2004c, Kirchner et al. 2005a, Lovrić et al. 2005, Wang Lin et al. 2008b) and ways of reducing their toxicological impact via non-toxic coatings (Byrne Stephen J et al. 2007a). The difference in size can also affect their uptake may lead to alterations in cellular activity and cytotoxicity (Gomez Natalia et al. 2005b, Osaki et al. 2004).

Due to inherent cytotoxicity and interference of QDs with the cellular process, it leads to cell death within hours of adding the QDs (Chan W. H. et al. 2006b, Lovric et al. 2005b). To counteract this problem, several investigations have been carried out by modifying the QDs where hepatocytes were exposed to mercaptoacetic acid coated CdSe QDs; it was shown that the cellular activity of hepatocytes was not affected and

thereby coating of QDs reduced the cytotoxicity (Derfus et al. 2004c). Another study on HeLa cells by capping of ZnS/CdSe QDs with dihydrolipoic acid showed that after one week the QDs have little effect on the cells and thereby coating helped in reducing the cytotoxicity (Jaiswal et al. 2003). This indicates that the modification of QDs by surface coatings with an effective molecule helps in reducing the cytotoxicity of QDs.

The following table 1.3 shows the study of toxicity of QDs by different authors with various sizes and types of QDs *in vitro,* co-incubated using numerous cell lines and observed cytotoxicity, the mechanism of uptake, pathways involved and also the significant findings observed.

Type of Quantum Dots	**Size of Quantum Dots**	**Cells, Tissue or Organism tested**	**Concentration of QDs used**	**Duration of treat-ment**	**Cytotoxicity observed**	**Mechanism of uptake**	**Pathways involved**	**Significant findings**	**References**
CdSe/ZnS-PEI QDs microencapsulated within PEG-terminated microcapsules of PSS and PAH	Free QDs is 14–16 nm and QDMC is 3–5µm.	Human dermal fibroblasts (HDF)	0.05–50 nM QDs or microencapsulated QDMCs	12-48h	Cytotoxicity is dose- and time-dependent and present in both free QDs and $CdCl_2$-treated cells. No significant change in metabolic activity was observed until 48 hr in cells treated with QDMC	Not reported	Not reported	Microencapsulation of the QDs decreased cytotoxicity, without compromise of luminescence which is a precursor of functionality	(Romoser et al. 2011)
CdTe and CdS/ZnS core-shell-shell (CSS) QDs	Not reported	Human embryonic kidney cells (HEK293 cells)	0, 18.75, 37.5, 75, 150 and 300 nM	24 h	CdTe QDs are cytotoxic for HEK293 and CSS-QDs showed less reduction in metabolic activity	Not reported	Not reported	Cd^{+2} released from CdTe QDs and nanoscale effect of QDs are the causes of cytotoxicity	(Su Y. et al. 2010)
CdTe, CdTe/CdS, CdTe/CdS/ZnS QDs were	Not reported	K562 and HEK293T human cell	0.2–3.0µM	0–48 h	Cells treated with CdTe and CdTe/ CdS QDs were mostly	Not reported	Not reported	ZnS shells may protect from release of Cd^{+2} and	(Su Y. Y. et al. 2009)

Type of Quantum Dots	Size of Quantum Dots	Cells, Tissue or Organism tested	Concentration of QDs used	Duration of treat-ment	Cytotoxicity observed	Mechanism of uptake	Pathways involved	Significant findings	References
synthesized in aqueous solution		lines			nonviable by 48 h for all concentrations tested. Cells treated with CdTeS/CdS/ZnS QDs showed no toxicity up to 48 h			resulting cytotoxicity. Other reports shows that residual organic solvents in non-aqueous QD preparations may have resulted in QD independent cytotoxicity	
CdSe/ZnS-PEG (EviTag T1 490 QDs).	1.4-2.5nm diameter	Caco-2 (human colon carcinoma) cell line	0.84–105μM	0–24 h	Low cytotoxicity induced cell detachment	Not reported	Not reported	Acid treatment by simulated gastric fluid increased the toxicity of PEG coated QDs, likely by inducing release of free Cd^{+2} by QDs degradation	(Wang L. et al. 2008a)

Type of Quantum Dots	Size of Quantum Dots	Cells, Tissue or Organism tested	Concentration of QDs used	Duration of treat-ment	Cytotoxicity observed	Mechanism of uptake	Pathways involved	Significant findings	References
CdSe	2.38 nm diameter	Primary rat Hippocampal neuron cells	1, 10, and 20nM	24 h	Cells treated with 1nM QDs for 24 h showed no decrease in cell viability. Cells treated with 10 and 20nM QDs for 24 h showed decrease in viability of 20 and 30% respectively.	Not reported	Not reported	CdSe QDs induced death of neuronal cells in a dose-dependent Manner and induce dysregulation of cytoplasmic calcium levels in neuronal cells	(Tang M. et al. 2008a)
CdSe/ZnS-Cys, CdTe-MPA, CdTe-Cys, CdTe-NAC	Not reported	MCF-7 (human breast cancer) cell line	10 µg/ml	1–24 h	Treatment of cells with all forms of CdTe QDs resulted in significant cell death at both 1 and 24 h. CdTe QDs are toxic and CdSe/ZnS QDs are not cytotoxic.	Not reported	Photo-oxidative pathways leading to reactive oxygen species	Release of free Cd^{+2} ions by CdTe QDs but not CdSe/ZnS QDs. CdTe QDs induce cell death via both Cd^{+2} ion dependent	(Cho S. J. et al. 2007b)

Type of Quantum Dots	Size of Quantum Dots	Cells, Tissue or Organism tested	Concentration of QDs used	Duration of treat-ment	Cytotoxicity observed	Mechanism of uptake	Pathways involved	Significant findings	References
					Cells treated with CdSe/ ZnS QDs were mostly viable after 24 h of exposure.		generatio n	and independent (ROS) mechanisms	
CdSe in PLA nano-particles, coated with F-68 (non-ionic), CTAB (-ve charge), or SDS (+ve charge)	159 nm-266 nm diameter	HepG2 (human hepatoma) cell line	0–400 ppm	12–72 h	All QDs tested induced some loss in cell viability, with > 80% viability upon treatment with F-68 QDs. This was in contrast to CTAB CdSe QDs, where viability was significantly decreased at low concentrations (10, 20, and 50 ppm) even at 12 h.	Not reported	Not reported	CdSe QDs modified with F-68 have low cytotoxicity based on observation of 80% or better cell viability up on treatment with QDs. Surface modification with non-ionic F-68 is less cytotoxic than modification with	(Guo G. N. et al. 2007b)

Type of Quantum Dots	Size of Quantum Dots	Cells, Tissue or Organism tested	Concentration of QDs used	Duration of treat-ment	Cytotoxicity observed	Mechanism of uptake	Pathways involved	Significant findings	References
								+ve charged CTAB.	
CdSe/ZnS QDs of two different sizes and shapes: QD-565 and QD-655 coated with PEG (neutral), PEG-amine (-ve charge), or polyacrylic acid (+ve charge).	4.6 nm-12 nm	Primary neonatal human epidermal keratinocytes (HEKs)	0, 0.2, 2.0 and 20nM	24 and 48 h	+ve QDs showed more cytotoxicity with 20nM concentration resulting in loss in viability by 24 h for both sizes of QDs. Treatment of HEKs with -ve charged QDs for both sizes at 20nM resulting in loss of cell viability at 48 h only. PEG-coated QDs had no effect on viability, except 20nM PEG-QD-655 resulted in some loss of viability	Non-selective endocytosis	Not reported	QDs with neutral surface coatings are less toxic to skin cells than QDs with +ve or -ve charged surface coatings. Positively charged QDs induced release of cytokines (IL-1b, IL-6, IL-8).	(Ryman-Rasmussen et al. 2007)

Type of Quantum Dots	Size of Quantum Dots	Cells, Tissue or Organism tested	Concentration of QDs used	Duration of treat-ment	Cytotoxicity observed	Mechanism of uptake	Pathways involved	Significant findings	References
					at 48 h.				
CdTe QDs	red (6 nm), yellow (4 nm), and green (2 nm) variants tested	HepG2 (human hepatoma) cell line	0–100 µM	48 h	50% reduction in viability activity at concentrations of 19.1, 4.8, and 3.0 µM for red, yellow, and green QDs respectively	Not reported	Not reported	Smaller QDs appeared to be more cytotoxic than larger QDs	(Zhang Y. et al. 2007)
CdSe/ZnS-peptide QDs	Not reported	HEK 293T/17 (human embryonic kidney) and COS-1 (African	15–250nM	1 h-acute, 24 h-chronic	Varying concentration of QDs at 1 h showed little or no cytotoxicity. At 24 h showed significant cell death at higher QDs concentrations (60–	Endocytosis	Not reported	There is difference between toxic effects following acute (1 h) and chronic (24 h) exposure of QDs Cell type-	(Delehanty et al. 2006)

Type of Quantum Dots	Size of Quantum Dots	Cells, Tissue or Organism tested	Concentration of QDs used	Duration of treat-ment	Cytotoxicity observed	Mechanism of uptake	Pathways involved	Significant findings	References
		green monkey kidney) cell lines			250nM)			dependent QD mediated cytotoxicity was observed.	
CdSe/ZnS QDs that were both PEG coated and silanized	8-10 nm diameter	Human HSF-42 (skin fibroblast) and IMR-90 (lung fibroblast) cell lines	0, 8, or 80nM (80nM ¼ 40 mg/ml at M.W. of 500 kDa, or approx. 5 3 1010 QD per mm3).	48 h	No decrease in cell numbers or increased apoptosis or necrosis at 48 h and slight increase in skin but not lung fibroblasts	Endocytosis and intracellular transport pathway	Transcript ion regulatory pathway	QDs were internalized into cells after 48 h of exposure. Nearly 0.2% of genes was significantly differentially expressed in QDs-treated skin fibroblasts vs controls.	(Zhang T. et al. 2006)
CdTe QDs	2.1 to 5.3nm	PC12 (rat pheochronoc	0.01–100 µg/ml	2-24 h	10µg/ml is cytotoxic	Not reported	Signal transducti	Distribution in the subcellular	(Lovric et al. 2005b)

Type of Quantum Dots	Size of Quantum Dots	Cells, Tissue or Organism tested	Concentration of QDs used	Duration of treat-ment	Cytotoxicity observed	Mechanism of uptake	Pathways involved	Significant findings	References
	radius	ytoma) and N9 (murine microglia) cell lines					on pathways of apoptosis and cell death	compartment of QDs depends on the size of QDs and QD-induced cytotoxicity can be altered by drugs	
MPA-coated CdTe	Not reported	Human breast cancer cells (MCF-7)	5 or 10 mg/ml	4-24 h	QDs lost protective coating and became naked causing injury to cells by damaging plasma membrane, mitochondrion, and nucleus and finally lead to cell death	Not reported	cellular damage mediated by Reactive oxygen species (ROS)	QD induced cytotoxicity by nonclassical apoptosis and its role in subcellular compartments was observed	(Lovric et al. 2005a)
CdSe/ZnS-MUA	Not reported	Vero and HeLa cell lines;	0–0.4 mg/ml	24 h	Toxicity observed at 0.2 mg/ml in Vero cells, 0.1 mg/ml in	Not reported	Glycolytic pathways	Attention is needed when MUA-QDs applied to living	(Shiohara et al. 2004)

Type of Quantum Dots	Size of Quantum Dots	Cells, Tissue or Organism tested	Concentration of QDs used	Duration of treat-ment	Cytotoxicity observed	Mechanism of uptake	Pathways involved	Significant findings	References
		primary human hepatocytes			HeLa cells and 0.1 mg/ml in hepatocytes			organisms even at low concentrations	
CdSe/ZnS-SSA	Not reported	EL-4 cells (mouse lymphocyte)	0.1–0.4 mg/ml	0–24 h	0.1 mg/ml showed altered cell growth; most cells are dead at 0.4 mg/ml.	Endocytosis	Not reported	QD-labeling was stable and did not affect either cell activation or function	(Hoshino et al. 2004a)
CdSe/ZnS conjugates: NH2, OH, OH/COOH, H2/OH, MUA, COOH	Not reported	WTK1 cells	1–2µM	12 h	2µM QD-COOH induced DNA damage at 2 h.	Not reported	Not reported	Properties of QDs are not related to those of QD-core materials but to molecules covering the surface of QDs	(Hoshino et al. 2004b)
CdSe-MAA, TOPO QDs	Not reported	Primary rat hepatocytes	62.5–1000 lg/ml	1–8 h	Concentration of 62.5 µg/ ml was cytotoxic under oxidative/	Not reported	Not reported	Surface oxidation by variety of pathways led to	(Derfus et al. 2004c)

Type of Quantum Dots	Size of Quantum Dots	Cells, Tissue or Organism tested	Concentration of QDs used	Duration of treat-ment	Cytotoxicity observed	Mechanism of uptake	Pathways involved	Significant findings	References
					photolytic conditions. No cytotoxicity was observed by addition of ZnS cap to QDs.			formation of reduced Cd on the QD surface and release of free Cd^{+2} correlated with cell death	
CdSe/ZnS	8-10nm	HeLa cells	10 pmol QDs per 10,000 cells (approx. 10nM)	10 days	10nM QD had minimal impact on cell survival.	Not reported	Not reported	Peptide-QD conjugate actively translocate to the cell nucleus.	(Chen and Gerion 2004)
CdSe/ZnS-DHLA	Not reported	Dictyostelim discoideum and HeLa cells	400–600nM	45–60 min	No effect on cell growth was observed	Endocyt-osis	Not reported	Labeling of cells with QDs did not interfere their growth or differentiation	(Jaiswal et al. 2003)
Avidin-conjugated CdSe/ZnS QDs	Not reported	HeLa cells	0.5–1.0 µM	15 min	No effect of cell growth or development noted.	cell membrane proteins depending on	Not reported	QD-antibody bio conjugates selectively label only those	(Jaiswal et al. 2003)

Type of Quantum Dots	Size of Quantum Dots	Cells, Tissue or Organism tested	Concentration of QDs used	Duration of treat-ment	Cytotoxicity observed	Mechanism of uptake	Pathways involved	Significant findings	References
						the QDs conjugated to antibodies		cells and sub-cellular regions that express the proteins of interest	
CdSe/ZnS-MUA QDs; QD-SSA complexes	Not reported	Vero cells	0.24 mg/ml	2 h	MUA/ SSA-QD complexes did not affect the viability of Vero cells.	Endocytosis	Not reported	MUA-QD/SSA complex is highly photo-stable endosome marker for long-life use	(Hanaki et al. 2003)

Table 1.3: Showing the study of toxicity of QDs by different authors with various sizes and types of QDs in vitro using numerous cell lines and observed cytotoxicity, the mechanism of uptake, pathways involved along with the significant findings observed.

1.8 Summary of advantages, disadvantages and drawbacks for QDs applications in Biology and Medicine

1.8.1 Advantages of QDs

1. Different size of the QDs shows different color enabling them to be used as multiple color labels simultaneously by simply using different sized QDs.
2. Optical properties like fluorescence, resistance to photo-bleaching.
3. Serve as vehicles for integration of diagnostic imaging and therapeutic drug delivery, a potentially transformative clinical paradigm.
4. High surface to volume ratios enables modification with surface functional groups.

1.8.2 Disadvantages of QDs:

1. Cyto-toxicity issues.
2. Cellular uptake mechanism not understood.

1.8.3 Drawbacks for QDs applications in Biology and Medicine

1.8.3.1 Cytotoxicity of QDs:

1. Cytotoxicity and the potential interference of QDs labelling with cellular processes.

2. At higher concentrations, effects on embryo development have been noticed (Dubertret B. et al. 2002a).

3. Effects on cell viability, morphology, function, or development over the duration of the experiments at QD concentrations needs to be optimized for labelling efficiency.

1.8.3.2 Surface modification and the stability of QDs:

1. The less protected the core or core/shell material is, the faster the appearance of signs of interference with cell viability or function (2), with release of

Cd^{2+} or Te^{2-} ion reported in both core and core-shell QDs (Derfus et al. 2004c, Kloepfer et al. 2003).

2. QDs are not completely innocuous, but a safe range likely exists in which they can accomplish their task without major interference with the processes under study.

3. QDs are more stable in powder form than in colloidal state (soluble form). But the powdered form needs to be handled very carefully as inhalation of QDs leads to pulmonary toxicity. So the powdered form is more hazardous. The advantage of powered form is that there is no aggregation of QDs. In colloidal state, QDs are less hazaradous to handle but there is more chance of aggregation of QDs.

4. Extensive scrutiny of cytotoxicity and stability of QDs will naturally be needed before QDs can be used in biological and medical procedures.

1.9 Fabricated QDs available by commercial process

There are so many fabricated QDs which are commercially available. The molecular probes (Invitrogen) from Life technologies (http://www.invitrogen.com), Cytodiagnostics (http://www.cytodiagnostics.com/), Ocean NanoTech (http://oceannanotech.com) and mkNANO (http://www.mknano.com) are supplying fabricated QDs in commercial process.

1.10 Gelatinated Cadmium Telluride Quantum Dots

The QDs used in our project are specifically made for our purpose to study the cytotoxicity of QDs *in vitro* which are fabricated and supplied with the coating of gelatine for cadmium telluride QDs capped with thioglycolic acid (TGA) from our collaborator Prof. Yurii K. Gunko group, Inorganic Chemistry, Trinity College Dublin.

In our project two different sized QDs of red and orange were coated with gelatine and were compared to red and orange non-gelatine coated QDs to investigate if there was any difference in the cellular activity on cells and their differential expression of genes.

The schematic structure of gelatinated and non-gelatinated Quantum Dots as shown in figure 1.10 for our study were prepared according to the published methods (Byrne S. J. et al. 2006). The characteristics of QDs in table 1.4 shows the coating on the QDs and the surface of core QDs, Photo-Luminescence (PL) emission peak and absorption peak wavelengths, the quantum yield, core size, hydrodynamic diameter and Zeta potential of QDs. The quantum yield is the efficiency at which the QD emits light relative to the absorbed light and at room temperature it was determined by comparing the nano-crystals integrated emission of the QDs with the emission of Rhodamine 6G in absolute ethanol which had a quantum efficiency of 95% (Byrne S. J. et al. 2006). The characteristics of the QDs such as quantum yield and the size can be controlled during their synthesis by varying certain conditions like adjusting the ratio of Cd:Te and Cd:TGA (Byrne S. J. et al. 2006). Using CdO as a precursor, high quality Cadmium Telluride (CdTe) QDs can been produced (Peng X. G. and Peng 2001).

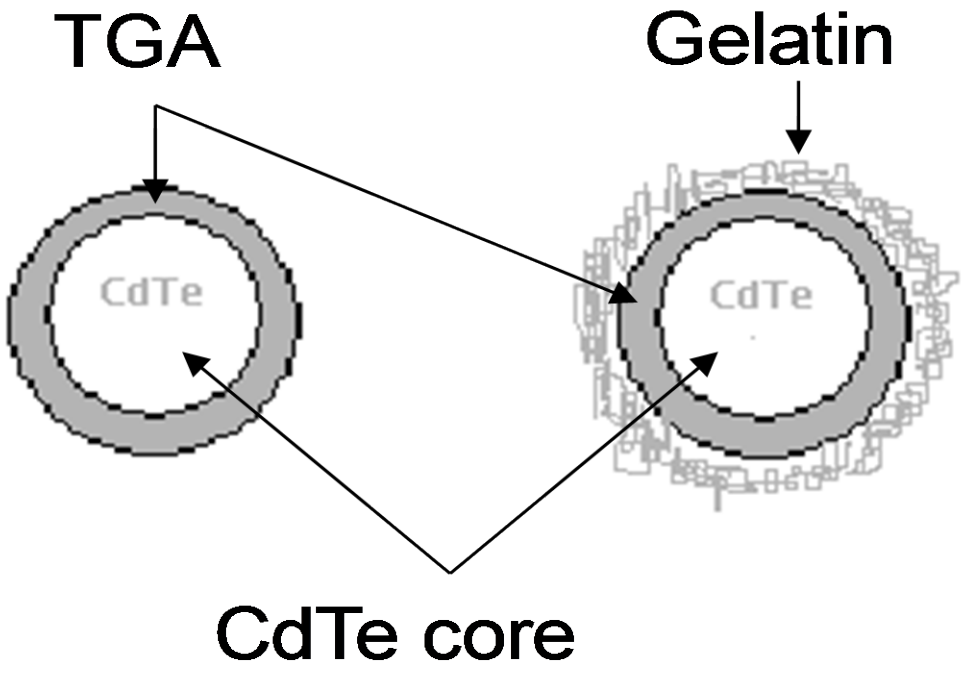

Figure 1.10: Showing schematic structure of gelatinated and non-gelatinated Quantum Dots (QDs) synthesised and supplied by Prof. Yurii K. Gunko group, Inorganic Chemistry, Trinity College Dublin.

QD type	Surface	Absor-bance peak (nm)	PL emission peak (nm)	Quantum Yield	Core size (nm) (+/- 0.1)	Hydro-dynamic diameter (nm)	Zeta potential (mV)
Red non-gel	TGA	586	608	30%	4.7	11.7	-30
Orange non-gel	TGA	515	546	23%	2.4	3.6	-27
Red gel	TGA-gelatine	579	610	34%	4.5	14.3	-29
Orange gel	TGA-gelatine	522	550	29%	2.6	5.3	-42

Table 1.4: Showing different characteristics of Quantum Dots (QDs) synthesised (various types of colours such as red and orange upon observation with naked eye) and supplied by Prof. Yurii K. Gunko group, Inorganic Chemistry, Trinity College Dublin.

1.11 Poly(dimethylsiloxane) (PDMS or silicone)

Poly(dimethylsiloxane) (PDMS or silicone) elastomers exhibit a broad range of beneficial properties that are exploited in biomaterials as shown in figure 1.11. Biomaterials, from breast implants to coronary stents, have evolved over time without a clear understanding of the properties that lead to optimal biocompatibility (Ratner et al. 2004).

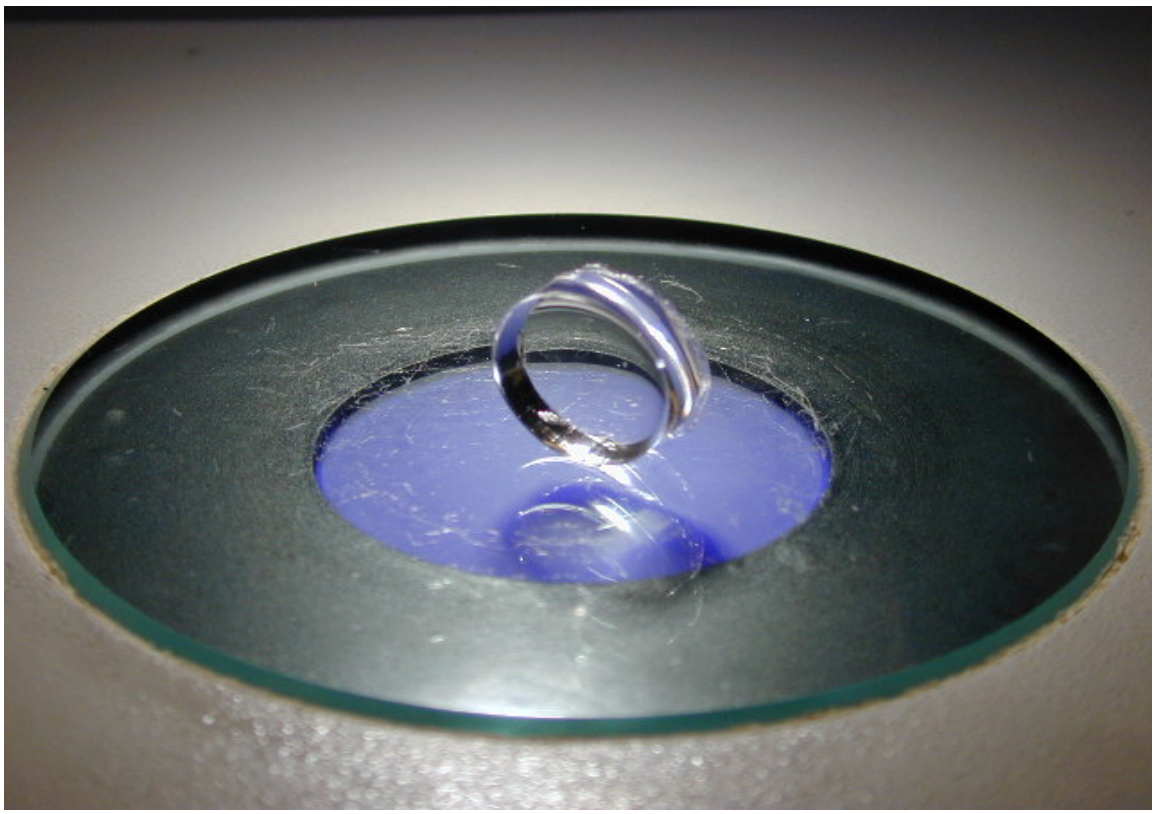

Figure 1.11: Showing the photographic image of PDMS or silicone sample (Adapted from Wikipedia).

Surface topography plays a significant role in biological processes such as cell attachment (Khorasani and Mirzadeh 2004, Kidambi et al. 2007, Lee J. N. et al. 2004, Toworfe et al. 2004), motility, proliferation (Kidambi et al. 2007, Li B. et al. 2006, Yim et al. 2005), differentiation (Liao et al. 2003), as well as regulation of gene expression (Kyriakides et al. 1999): these biological processes are important criteria for implant acceptance. It is well known that surface characteristics such as roughness, texture, surface free energy, surface charge and chemical composition all play key roles in cell adhesion and growth, and that the nature of a biomaterial surface governs the phenotypic response of interacting cells (Ratner et al. 2004). The roughness of the implant surface can have significant influence on the cellular behaviour (McLucas et al. 2006) and thus the foreign body reaction (Kao et al. 1994, Kyriakides et al. 1999, Rice et al. 1998) can be minimized by critical adjustment of the roughness (Mirzadeh et al. 2003).

Poly(dimethylsiloxane) (PDMS or silicone) is a versatile polymer because of its biological stability (Chang et al. 2007, Kheir et al. 1998) and low toxicity (Chang et al. 2007), the ease with which the hardness of silicone elastomers can be controlled, and its ability to be easily molded and shaped (Kheir et al. 1998). These properties make it suitable for a variety of applications such as breast implants (Backovic and Wolfram 2007), cochlear implants (Abbasi et al. 2006, Mirzadeh and Abbasi 2004), maxillofacial reconstruction (Kheir et al. 1998), artificial corneas(Klenkler et al. 2005), artificial skin**,** soft contact lenses (Nicolson and Vogt 2001), and coatings for pacemaker leads. In some cases, however, problems can arise at silicone elastomer interfaces. With breast implants, for example, the fibrous capsule that forms at the silicone interface can undergo contracture, which can lead to the need for revision surgery. The relationship between surface topography and wound healing – which could impact on the degree of contracture – has not been examined in detail.

The wound healing response at the external surface of a silicone implants leads to the formation of a fibrous capsule. Capsule formation can be either interrupted or unduly enhanced by infection, immune reaction, implant migration, or extrusion (Kheir et al. 1998). In the case of breast implants, the capsule can undergo significant contracture (shrinkage), a condition that can be painful and require revision operations (Barr et al. 2009).

Silicone breast implants are sold with smooth surfaces, or surfaces that are rough at the hundreds of microns scale. The rough surfaces are designed to facilitate tissue infiltration. However, the impact of silicone roughness at the sub-micron level on healing has not been examined in detail. Changing the roughness of PDMS at this length scale may modulate fibroblast growth and proliferation, which in turn may affect post-implantation fibrous capsule formation and could also facilitate tissue reconstruction procedures (Kidambi et al. 2007).

1.12 Poly(dimethylsiloxane) (PDMS or silicone) of nanosurface roughness

The chemical structure of PDMS elastomer before and after etching process along with polymerisation/depolymerisation by equilibration was shown in figure 1.12. The microscopic physical structure of PDMS or silicone (nano-roughness) was shown in

figure 1.13. The PDMS or silicone (nano-surface roughness) of varying surface roughnessess were supplied by our collaborator Prof. Michael A. Brook group, Department of Chemistry, McMaster University, Ontario, Canada. They have recently developed synthetic methodologies that introduce roughness on silicone elastomer surfaces of up to hundreds of nanometers without changing the chemical composition of the surface. We investigated these silicone samples and correlate the ability of 3T3 fibroblasts to adhere and proliferate on silicone surfaces (nano-surface roughness) with different surface topographies at the sub-micron scale as shown in table 1.4.

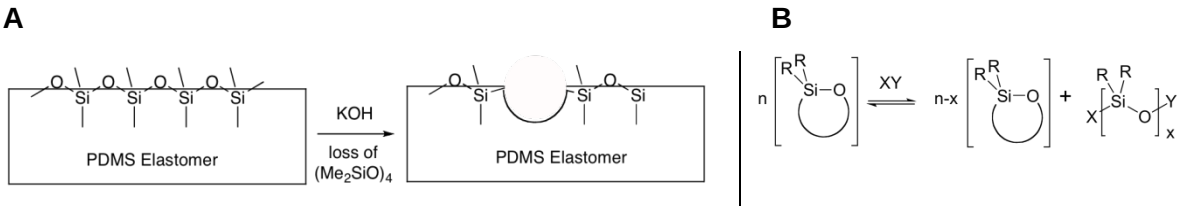

Figure 1.12: Showing chemical structure of PDMS or silicone elastomer samples. Elastomer etching process in (A) and silicone polymerization/depolymerization by equilibration in (B) provided by Prof. Michael A. Brook group, Department of Chemistry, McMaster University, Ontario, Canada (Prasad et al. 2010a).

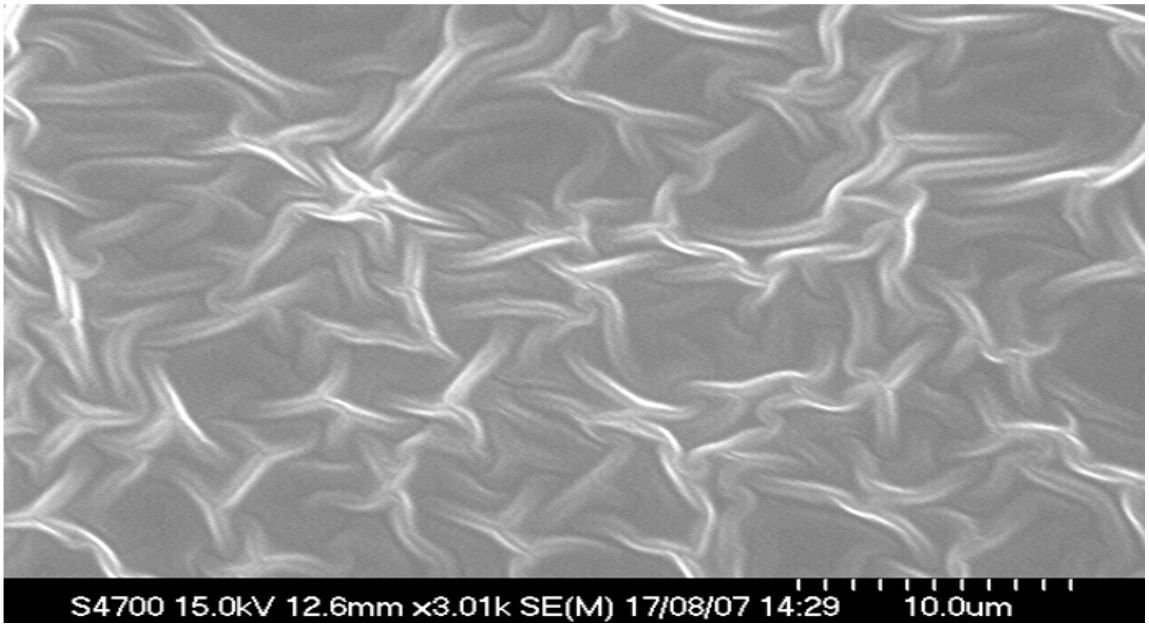

Figure 1.13: Showing the scanning electron microscopic (SEM) image of smooth PDMS or silicone (20nm roughness) sample.

Technique	Different surface roughness of PDMS by controlled etching			
	Smooth	**Bumpy**	**Very Rough**	**Very Rough**
Optical Profiler (Rq roughness)	20 nm	150 nm	300 nm	400 nm
Atomic Force Microscopy (Ra roughness)	88 nm	378 nm	604 nm	650 nm

Table 1.4: Showing varying roughness of PDMS or silicone nano-surfaces obtained by the optical profiler (Optical profiler data provided by Prof. Michael A. Brook group, Department of Chemistry, McMaster University, Ontario, Canada) and atomic force microscopy in nanometre scale.

CHAPTER 2: MATERIALS AND METHODS

2.1 Synthesis of Quantum Dots

2.1.1 Protocol for Synthesis of Cadmium Telluride (CdTe) Thioglycolic Acid (TGA) - capped Quantum Dots

Materials:

Aluminium Telluride (Al_2Te_3), Cadmium (Cd), Thioglycolic Acid (TGA), Millipore water, NaOH, H_2SO_4, Isopropanol, 50 ml tubes, syringe, round bottomed flasks, rubber stopper, stirrer, reflux apparatus, condenser, evaporator apparatus, gel chromatography apparatus, argon gas supply and centrifuge. All chemicals for QD synthesis were purchased from Sigma-Aldrich. Al_2Te_3 was purchased from Cerac Inc.

Method:

The whole synthesis is carried out in argon atmosphere with vigorous stirring continuously. Prepare the experimental setup as shown in figure 2.1. 100ml of Millipore water is degassed by bubbling argon. Aluminium Telluride (Al_2Te_3) in flask is placed under vacuum in order to ensure no air is present. Once in vacuum, argon is released into the flask. This argon bubbled Telluride is taken from the main flask in a smaller round bottomed flask carefully by switching out another round bottomed flask so as not to allow air to get in. The argon is still bubbling so as to ensure a constant argon vacuum. The Telluride is then measured and emptied into a three-necked round bottomed flask with a septum and valves and is deaerated by N_2 bubbling for approximately 30 minutes. We then work out how much Cadmium and Thioglycolic Acid (TGA) (stabiliser) we need for amount of Telluride used. The ratio of cadmium to telluride to thioglycolic acid is 1:0.25:1.4.

Cadmium and TGA are added to Millipore water and are placed in a three-necked round bottomed flask set up on reflux apparatus. Argon gas tap is switched off from aluminium telluride flask and now flows into flask containing Cd and TGA. At first this solution is a cloudy frothy milky colour which tells us that it is too acidic. Then 2 M NaOH solutions are added until the colour changes to clear/transparent and the pH reads 11. When appropriate, 0.3 gm of gelatine was added to the solution.

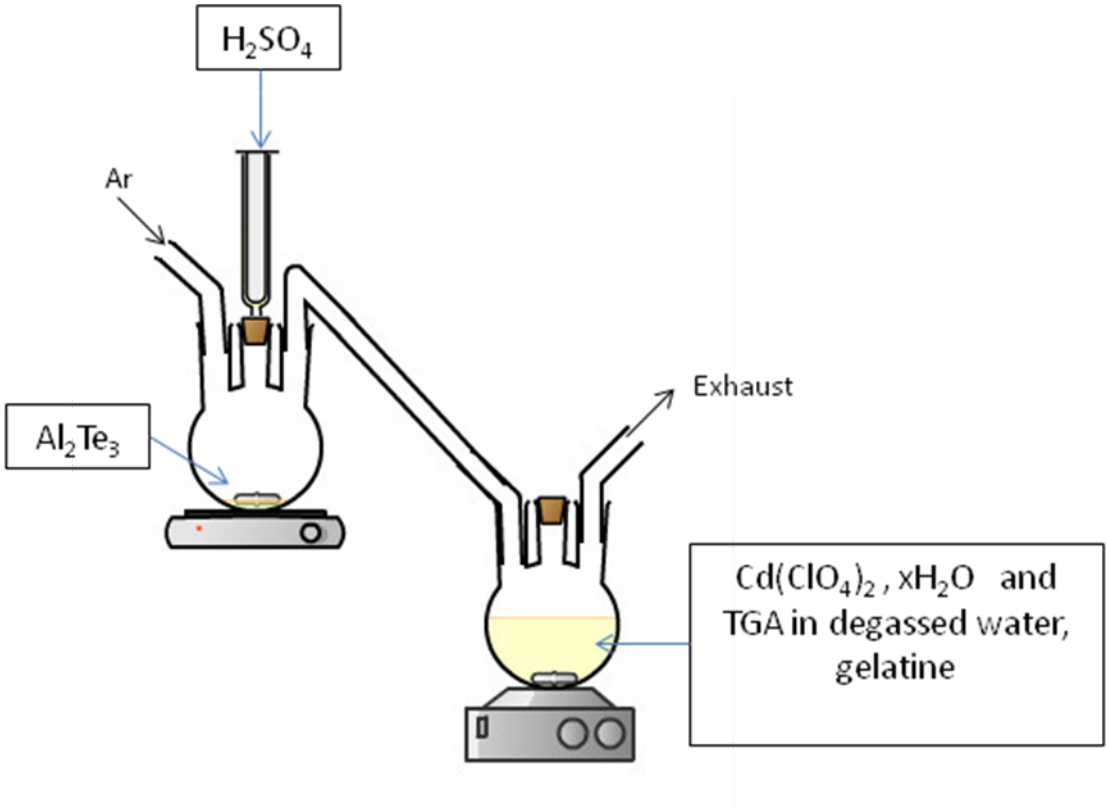

Figure 2.1: Schematic of the experimental set-up for the synthesis of thioglycolic acid-capped CdTe QDs coated with gelatine (Byrne Stephen J et al. 2007a) supplied by Prof. Yurii K. Gunko group, Inorganic Chemistry, Trinity College Dublin.

Under stirring, to a known weight of Al_2Te_3, 15ml of H_2SO_4 solution is slowly added to the telluride by drop-wise addition through a syringe placed into the rubber stopper to generate the H_2Te gas which bubbles into the Cd/ TGA or Cd/TGA/gelatine (pH 11) solution through a funnel under a slow argon flow. All telluride has been reacted with, so an excess of H_2SO_4 and a stirrer is used. Once all the telluride has been reacted with, the CdTe stabilised with TGA is then left on reflux for 100 minutes (time depending on size of particles required). The resulting non-luminescent solution was then heated under reflux. Once the QDs reached the desired size, the reflux was stopped. The flask is also attached to a condenser to ensure all H_2O is not evaporated. Samples are spectroscopically characterised at different time intervals to generate a range of different size distributions. The concentration of QDs was deduced from the UV-vis absorption spectrum, by applying the Brus equation to obtain the average diameter which was corrected for size distribution using the PL Full Width at Half Maximum

(FWHM). By deducting the extinction coefficient and finally applying the Beer's law, the concentration of QDs were calculated.

Partial evaporation of water to ensure a concentration of 10^{-4} takes place using an evaporator. Purification of sample must then take place to remove any residual reagents in solution when sample is to be used for biological application. The sample runs through gel chromatography apparatus to generate purified QDs sample. Centrifugation of solution to generate pellet of CdTe TGA stabilised QDs, pellet must be all red to be viable to use. Isopropanol was added to solution to ensure better aggregation of quantum dots during centrifugation. After isopropanol has been added, solution is centrifuged again to generate second fraction. This process was repeated until the isopropanol had no effect anymore. Fractions are stored at 4^{o}C. Concentration of each fraction was approximately 2 x 10^{-4} M and this was diluted down by dissolving in de-ionised sterile water for biological use (Byrne S. J. et al. 2006, Gaponik et al. 2002). The crude solutions were purified *via* size selective precipitation and individual fractions were characterised by UV-vis absorption and photoluminescence (PL) emission spectroscopy (λ_{ex} 425 nm). Prior to initiating cell culturing experiments, the QDs were further purified on a sephadex-G25 column. This enabled us to remove any residual un-reacted moieties that may have been present from the original crude solution. Two differently sized batches of QDs (for both gel and non-gel QDs) were synthesised to allow us to investigate if the additional parameter of QD size had any impact on cell response.

2.2 Optical and Physical Characterisation

2.2.1 UV-Vis absorption spectroscopy

A Shimadzu UV-1601 UV - Visible Spectrophotometer was used to measure QD and metallic nanoparticles absorption. Most of the scans were carried in the 300-700 nm range although this was extend in some special cases; required to scan up to 1100 nm while the presence of oligonucleotides was assessed by scanning down to 200 nm in order to measure the characteristic absorption peak at 260 nm.

2.2.2 Photo-luminiscence (PL) Spectroscopy

A Varian-Cary Eclipse Fluorescence Spectrophotometer was used to determine the photo-luminescence (PL) Spectra of the QDs. Photoluminescence measurements were performed at room temperature. The excitation wavelength was 480 nm and the emission was detected in the range 490-700 nm. The Quantum Yields (QY) were calculated from the PL spectra (wavelength emission or absorption) using Rhodamine B as a reference. The room-temperature PL quantum efficiency of TGA-capped CdTe QDs was estimated by comparing with Rhodamine-6G in ethanol, which is assumed to have PL QE of 95%.

2.2.3 Transmission Electron Microscopy (TEM)

A JEOL 3011 Transmission Electron Microscope (TEM) was used to determine the size distribution of the QDs and for imaging.

QDs type and colour	Surface	Absorbance peak (nm)	PL emission peak (nm)	Quantum Yield	Size(nm) (+/- 0.1)
Red non-gel	TGA	586	608	30%	4.7
Orange non-gel	TGA	515	546	23%	2.4
Red gel	TGA-gelatine	579	610	34%	4.5
Orange gel	TGA-gelatine	522	550	29%	2.6

Table 2.1: Showing different characteristics of Quantum Dots (QDs) synthesised (various types of colours such as red and orange upon observation with naked eye) and supplied by Prof. Yurii K. Gunko group, Inorganic Chemistry, Trinity College Dublin.

2.3 Cell Culture of undifferentiated PC12 cells with QDs

2.3.1 PC12 cell seeding and treatment with QDs for imaging and cellular activity

Materials

PC12 cells (cell line derived from a transplatable pheochromocytoma of the rat adrenal medulla) were used for this study (Greene and Tischler 1976). Dulbecco's Modification

of Eagle Medium (DMEM) supplemented with 10% heat inactivated horse serum, 5% fetal bovine serum, 1% penicillin-streptomycin, Hanks Balanced Salt Solution (HBSS), 1X Trypsin-EDTA solution, Poly-L-lysine (PLL) were purchased from Sigma-Aldrich. T-75 flasks, 5, 10 and 25 ml pippetes and 96-well flat tissue culture plates were purchased from Sarstedt. Nunc tissue culture– treated 48-well plates were purchased from Biosciences. Permonax four-well chamber slides were purchased from Lab-Tek (Nalgene Nunc International).

Methods

PC12 cells were cultured in medium (DMEM supplemented with 10% heat inactivated horse serum, 5% fetal bovine serum, 1% penicillin-streptomycin) @ 37 ^{o}C and 5% CO_2 atmosphere. All the tissue culture plates and chamber slides were treated with 0.001% Poly-L-Lysine (PLL) for 24 hours.

Chamber slides for imaging: Cells were seeded into four-well chambers at density of 10^5 cells/ cm^2. After 24 hours, QDs (10% of amount of Medium) of sizes ranging from ~ 4.5-4.7 nm (Red Gel, Red Non-gel) and ~2.4-2.6nm (Orange Gel and Orange Non-gel) were added to make final concentrations of QDs to $10^{(-9)}$ M and were incubated for 72 hours.

48- well plates for AlamarBlue Assay: PC12 cells were seeded at density of 10^5 cells/ cm^2 in three 48-well micro-plates (Nunc) as triplicates. After 24 h, QDs were added (10% of amount of Medium) to make final concentrations in the range of $10^{(-7)-(-9)}$ M and were incubated for 24, 48 and 72 hours. Three different types of controls, namely: positive, negative and background were used throughout the study. Positive controls had cells with culture medium but without treatment with QDs. Negative controls were treated with QDs with culture medium and no cells. Background controls were cells treated with QDs but without culture medium.

48- well plates for PicoGreen Assay: PC12 cells were seeded at density of 10^5 cells/ cm^2 in three 48-well micro-plates (Nunc) as triplicates. After 24 h, QDs were added (10% of amount of Medium) to make final concentrations in the range of $10^{(-7)-(-9)}$ M and were incubated for 24, 48 and 72 hours. Three different types of controls, namely: positive, negative and background were used throughout the study. Positive controls had cells with culture medium but without treatment with QDs. Negative controls were

treated with QDs with culture medium and no cells. Background controls were cells treated with QDs but without culture medium.

96- well microplates for Cell Proliferation ELISA BrdU: PC12 cells were grown in three 96-well microplates (Nunc) as triplicates. After 24 h, QDs were added (10% of amount of Medium) to make final concentrations in the range of $10^{(-7)-(-9)}$ M and were incubated for 24, 48 and 72 hours. Three different types of controls, namely: positive, negative and background were used throughout the study. Positive controls had cells with culture medium but without treatment with QDs. Negative controls were treated with QDs with culture medium and no cells. Background controls were cells treated with QDs but without culture medium.

2.4 Imaging of undifferentiated PC12 cells with QDs

2.4.1 Staining of cells and Confocal Microscopy

Materials

Rhodamine-Phalloidin and DAPI were purchased from Molecular Probes (Invitrogen) and Vector Laboratories respectively.

Methods

Cell Staining: Cells grown on 4 well Permonax Chamber slides in the presence of QDs and were washed with 1% phosphate-buffered saline (BSA/PBS). Cells were fixed with 4% paraformaldehyde for 15 minutes and then washed 3 times with PBS. Then cells were permeabilized with permeabilizing solution (5 min, 0° C). Actin filaments of cytoplasm were labelled with Rhodamine-Phalloidin, at 1:200 dilution with PBS for 15 minutes and again washed 3 times with PBS. Nuclei were labelled with Vectashield mounting medium with DAPI to preserve fluorescence and counterstained DNA with DAPI 1 µg/ml.

Confocal Microscopy: An LSM 510 (Carl Zeiss, Jena, Germany) Confocal Laser Scanning microscope was used to examine QDs inside PC12 cells and its morphology.

Cell Imaging was carried out using a LSM 510 Inverted Confocal Microscope which is equipped with the following excitation lasers: (a) Argon Laser Excitation -wavelengths

(λ_{Ex}) = 458 nm, 488 nm, 514 nm, (b) HeNe1 - λ_{Ex} = 543 nm and (c) Titanium Sapphire Tuneable Two-photon Laser tuneable from 710 nm to 1000 nm with a resulting excitation range of 355 nm to 500 nm. All confocal laser scanning was carried out at laser scan speed of 7 with the Photomultiplier Tube settings adjusted to eliminate noise and saturation with the aid of the range indicator setting in the LSM 510 software. For image optimisation scan averaging was carried out on 8 scans per image. Sequential acquisition was used to acquire the two colour images of the QDs in cells. For visualisation of the QDs, the samples were excited with the Argon 514 nm Laser and the microscope configuration was set up to capture the emitted fluorescence at 550 nm or 600 nm as desired. Differential Interference Contrast (DIC) or Nomarski Microscopy was used to visualise the cell morphology, and was carried out by using the HeNe1 488 nm laser with the Transmission Channel Detector selected and the DIC polariser and Nomarski prisms engaged. The two images were then over laid using the LSM 510 software. Sequential acquisition was also used to acquire three colour images. Rhodamine phalloidin was excited using the HeNe1 543 nm laser and the emitted fluorescence was acquired at 575 nm. DAPI stain was excited with laser light at 390 nm (from the Two Photon laser tuned to 780 nm) and emitted fluorescence was acquired at 458 nm. The three separate images were over laid using the LSM510 software to make up the three colour images.

2.5 AlamarBlue Assay of undifferentiated PC12 cells with QDs

2.5.1 Cell Viability by alamarBlue Assay

Materials

AlamarBlue reagent (Biosource International) was purchased from Biosciences UK.

Methods

After 24 hours of co-incubation with QDs, the medium was removed and the wells were washed with HBSS. AlamarBlue solution was prepared by adding alamarBlue and HBSS in the ratio of 1:10. 200 µl of alamarBlue solution was added to each well and the plates were incubated for 1 hour. 100 µl of reduced alamarBlue solution from each well

was dispensed in a clear tissue culture 96 well microplate. The Plate was analysed using a Wallac Victor Fluorescent Plate Reader. Absorbance was measured at lower wavelength of 550 nm and higher wavelength of 595 nm with a measurement time of 5.0 s. This was repeated with incubation periods of 48 hours and 72 hours.

2.6 PicoGreen Assay of undifferentiated PC12 cells with QDs

2.6.1 Quantification of DNA by PicoGreen Assay

Materials

Quant-iT PicoGreen DNA assay kit was purchased from Molecular Probes (Invitrogen).

Methods

After 24 hours of co-incubation with the QDs, the medium was removed and the wells were washed with HBSS. 200 µl of deionised double-distilled water was then added and the cells were lysed by freezing for 15 minutes at -80^{o}C and thawing for 15 minutes at room temperature repeated 3 times. According to the assay kit a standard curve was then constructed. Final concentrations of the standards were 1000, 500, 100, 50, 25, 10, 5, and 0 ng/µl. 100µl of lysed DNA solution of cells from each well were dispensed in a clear tissue culture 96-well plate. 100 µl of diluted PicoGreen solution were added to each of the test wells of 96-well plate. The Plate was analysed using a Wallac Victor Fluorescent Plate Reader by Fluorescence 485 nm/535 nm, 1.0 s protocol. Levels of DNA in each sample were calculated using the standard curve. This was repeated with incubation periods of 48 hours and 72 hours.

2.7 Cell Proliferation ELISA BrdU of undifferentiated PC12 cells with QDs

2.7.1 Cellular proliferation by Cell Proliferation ELISA BrdU (Colorimetric)

Materials

A BrdU cell proliferation kit was purchased from Roche Diagnostics.

Methods

10 µl of BrdU labelling solution was added to each well after 24 hours of adding QDs to PC12 cells and incubated @ 37^{o} C and 5% CO_2 atmosphere for 6 hours. The culture medium was removed and the cells denatured, and the anti-BrdU-POD added. This binds to the BrdU incorporated into cellular DNA. The level of incorporation is detected by means of a colorimetric substrate reaction. Quantification of the bound anti-BrdU-POD was accomplished by adding 100 µl TMB to each well and a further 20 minute incubation time at room temperature. 25 µl 0.1M H_2SO_4 was then added, incubated for 1 minute and shaken at 300 rpm to stop the reaction. The Plate was analysed using the Wallac Victor Fluorescent Plate Reader (450-550 nm) protocol and measured absorbance for 2 minutes at room temperature. This was repeated with incubation periods of 48 hours and 72 hours.

2.8 Cell Culture of differentiated PC12 cells with QDs

2.8.1 PC12 cell seeding and treatment with QDs for imaging and cellular activity after differentiation

Materials

PC12 cells (cancer cell line derived from a pheochromocytoma of the rat adrenal medulla) were used for this study. Dulbecco's Modification of Eagle Medium (DMEM) supplemented with 10% heat inactivated horse serum, 5% fetal bovine serum, 1% penicillin-streptomycin, Hanks Balanced Salt Solution (HBSS), 1X Trypsin-EDTA solution, Poly-L-lysine (PLL) were purchased from Sigma-Aldrich. T-75 flasks, 5, 10

and 25 ml pippetes and 96-well flat tissue culture plates were purchased from Sarstedt. Permonax four-well chamber slides were purchased from Lab-Tek (Nalgene Nunc International). Mouse Nerve Growth Factor (mNGF 2.5S Grade 2) was purchased from Alomone labs.

Methods

PC12 cells were cultured in medium (DMEM supplemented with 10% heat inactivated horse serum, 5% fetal bovine serum, 1% penicillin-streptomycin) @ 37 ^{o}C and 5% CO_2 atmosphere. All the tissue culture plates and chamber slides were treated with 0.001% Poly-L-Lysine (PLL) for 24 hours.

Chamber slides for imaging: Cells were seeded into four-well chambers at density of 1000 cells/ cm^2. After 24 h, QDs (10% of amount of Medium) of size ~ 4.5 nm (Red Gel, Red Non-gel) and ~2.5nm (Orange Gel and Orange Non-gel) were added to make final concentrations of QDs to $10^{(-9)}$ M. After 48 hours of seeding, the cells were treated with final concentration of 200 ng/ ml of Nerve Growth Factor (NGF) on every second day with 200 µl of fresh medium in each well and were incubated for 17 days.

96- well microplates for MTT Assay: PC12 cells of approximately 1000/well were seeded in a two flat 96-well micro-plates as triplicates. Three different types of controls, namely: positive, negative and background were used throughout the study. Positive control had cells with culture medium treated with NGF but not exposed to QDs. Negative control had QDs without cells. Background control had culture medium without cells. After 24 h, QDs (10% of amount of Medium) of size ~ 4.5 nm (Red Gel, Red Non-gel) and ~2.5nm (Orange Gel and Orange Non-gel) were added to make final concentrations of QDs to $10^{(-9)}$ M. After 48 hours of seeding, the cells were treated with final concentration of 200 ng/ ml of Nerve Growth Factor (NGF) on every second day (Pelzl et al. 2009) with 200 µl of fresh medium in each well and were incubated for 10 and 16 days after adding QDs.

96- well microplates for ApoTox-Glo^{TM} Triplex Assay: PC12 cells of approximately 1000/well were seeded in a three flat 96-well micro-plates as triplicates. Four different types of controls, namely: positive, untreated, Negative and Background controls were used throughout the study. Positive control had cells with culture medium treated with NGF and exposed to Staurosporine of 500nM final concentration for 16 hours to induce apoptosis. Untreated cells control had cells with culture medium, treated with NGF.

Optional test compound control (Negative control) had QDs without cells. No-Cell Control (Background) had only culture medium without cells. After 24 h, QDs (10% of amount of Medium) of size ~ 4.5 nm (Red Gel, Red Non-gel) and ~2.5nm (Orange Gel and Orange Non-gel) were added to make final concentrations of QDs to $10^{(-9)}$ M. After 48 hours of seeding, the cells were treated with final concentration of 200 ng/ ml of Nerve Growth Factor (NGF) on every second day (Pelzl et al. 2009) with 200 µl of fresh medium in each well and were incubated for 7, 12 and 17 days after adding QDs.

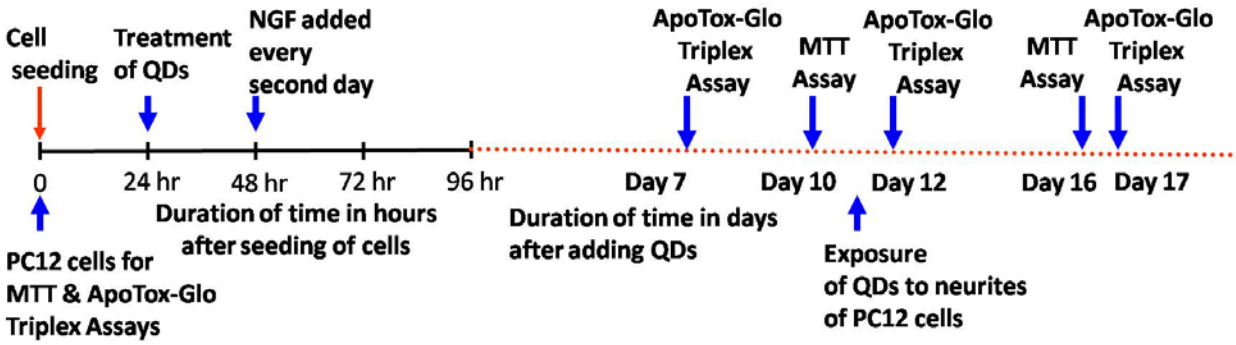

Figure 2.2: Chart showing timeline schematic representation of seeding of PC12 cells treated with QDs and NGF for measuring cellular activity of differentiated PC12 cells with MTT and ApoTox-Glo Triplex assays.

2.9 Imaging of differentiated PC12 cells with QDs

2.9.1 Staining of cells and Confocal Microscopy

Materials

Phalloidin-FITC and DAPI were purchased from Sigma-Aldrich and Vector Laboratories respectively.

Methods

Cell Staining: Cells grown on 4 well Permonax Chamber slides in the presence of QDs and were washed with 1% phosphate-buffered saline (BSA/PBS). Cells were fixed with 4% paraformaldehyde for 15 minutes and then washed 3 times with PBS. Then cells

were permeabilized with permeabilizing solution (5 min, 0° C). Actin filaments of cytoplasm were labelled with Phalloidin FITC, at 1:50 dilution with PBS for 20 minutes and again washed 3 times with PBS. Nuclei were labelled with Vectashield mounting medium with DAPI to preserve fluorescence and counterstained DNA with DAPI 1 µg/ml.

Confocal Microscopy: An LSM 510 (Carl Zeiss, Jena, Germany) Confocal Laser Scanning microscope was used to examine QDs inside PC12 cells and its morphology.

Cell Imaging was carried out using a LSM 510 Inverted Confocal Microscope which is equipped with the following excitation lasers: (a) Argon Laser Excitation -wavelengths (λ_{Ex}) = 458 nm, 488 nm, 514 nm, (b) HeNe1 - λ_{Ex} = 543 nm and (c) Titanium Sapphire Tuneable Two-photon Laser tuneable from 710 nm to 1000 nm with a resulting excitation range of 355 nm to 500 nm. All confocal laser scanning was carried out at laser scan speed of 7 with the Photomultiplier Tube settings adjusted to eliminate noise and saturation with the aid of the range indicator setting in the LSM 510 software. For image optimisation scan averaging was carried out on 8 scans per image. Sequential acquisition was used to acquire the two colour images of the QDs in cells. For visualisation of the QDs, the samples were excited with the Argon 514 nm Laser and the microscope configuration was set up to capture the emitted fluorescence at 550 nm or 600 nm as desired. Differential Interference Contrast (DIC) or Nomarski Microscopy was used to visualise the cell morphology, and was carried out by using the HeNe1 488 nm laser with the Transmission Channel Detector selected and the DIC polariser and Nomarski prisms engaged. The two images were then over laid using the LSM 510 software. Sequential acquisition was also used to acquire three colour images. Phalloidin FITC was excited using the HeNe1 488 nm laser and the emitted fluorescence was acquired at 518 nm. DAPI stain was excited with laser light at 390 nm (from the Two Photon laser tuned to 780 nm) and emitted fluorescence was acquired at 458 nm. The three separate images were over laid using the LSM510 software to make up the three colour images.

2.10 MTT assay of differentiated PC12 cells with QDs

2.10.1 Cell Proliferation by MTT Assay

Materials

MTT Reagent and stop solution was kindly received from Dr. Afshin Samali, Apoptosis Group of NCBES, NUI Galway.

Methods

After 10 days of exposure to QDs, old medium was removed from all the wells and added 100 µl of fresh medium. 10 µl of MTT reagent was then added to each well and incubated for 3 hours. To stop the reaction of the assay, 100 µl of stop solution was added to each well. 96-well plate was left on shaker overnight at speed 300 rpm and was then analysed using Perkin Elmer Victor$^{3}{}_{TM}$V Wallac plate reader at absorbance of 570 nm. This was repeated again for another 96 well plate with incubation period of 16 days after adding QDs (Pelzl et al. 2009). The yellow tetrazolium MTT (3-(4, 5-dimethylthiazolyl-2)-2, 5 diphenyltetrazolium bromide) is reduced by metabolically active cells, in part by the action of dehydrogenase enzymes, to generate reducing equivalents such as NADH and NADPH. The resulting intracellular purple formazan can be solubilized and quantified by spectrophotometry. The MTT Cell Proliferation Assay measures the cell proliferation rate and conversely, when metabolic events lead to apoptosis or necrosis, the reduction in cell viability.

2.11 APOTOX-Glo^{TM} Triplex assay of differentiated PC12 cells with QDs

2.11.1 Cytotoxicity, Viability and Apoptosis by APOTOX-Glo^{TM} Triplex Assay

Materials

APOTOX-Glo^{TM} Triplex assay kit to measure cytotoxicity, viability and apoptosis was purchased from Promega Corporation.

Methods

After 7 days of exposure to QDs, old medium was removed from all the wells and added 100 µl of fresh medium. 20 µl of Viability/Cytotoxicity reagent containing both GF-AFC and bis-AAF-R110 substrates was added to each well, and briefly mixed by orbital shaking at 300-500rpm for 30 seconds and then incubated at 37 ^{o}C for 30-180 minutes. Fluorescence was measured at 400_{Ex}/ 505_{Em} (Viability) and 485_{Ex}/ 520_{Em} (Cytotoxicity) by using PerSeptive Biosystems CYTOFLUOR® multi-well plate reader series 4000. After that 100 µl of Caspase-Glo 3/7 reagent was added to each well, and briefly mixed by orbital shaking at 300-500rpm for 30 seconds and then incubated at room temperature for 30-180 minutes. Luminiscence was measured using Perkin Elmer Victor$^{3}{}_{TM}$V Wallac plate reader by Luminiscence (1.0s) protocol which is proportional to the amount of caspase activity present. This was repeated again for another 96 well plates with incubation period of 12 and 17 days after adding QDs. It combines three assay chemistries to assess viability, cytotoxicity and caspase activation events within a single assay well. In the first part of the assay, it measures two protease activities simultaneously that is one is a marker of cell viability and the other is a marker of cytotoxicity. Peptide substrate (glycylphenylalanyl-aminofluorocoumarin; GF-AFC) enters intact cells where it is cleaved by the live-cell protease activity to generate a fluorescent signal proportional to the number of living cells. This live-cell protease becomes inactive upon loss of cell membrane integrity and leakage into the surrounding culture medium. Peptide substrate (bis-alanylalanyl-phenylalanyl-rhodamine 110; bis-AAF-R110) is used to measure dead-cell protease activity, which is released from cells that have lost membrane integrity. Bis-AAF-R110 is not cell-permeate, so no signal from this substrate is generated by intact, viable cells. The live- and dead-cell proteases produce different products, AFC and R110, which have different excitation and emission spectra, allowing them to be detected simultaneously. In the second part of the assay, the Caspase-Glo® 3/7 Reagent was added in an “add-mix-measure” format results in cell lysis, followed by caspase cleavage of the substrate and generation of a “glow-type” luminescent signal produced by luciferase.

2.12 Cell Culture of HPMEC-ST1.6R cells with QDs

2.12.1 HPMEC-ST1.6R cell seeding and treatment with QDs for imaging and cellular activity

Materials

HPMEC-ST1.6R cells [endothelial cell line derived by transfection of HPMEC with plasmids encoding the SV-40 large T-antigen (pSV3neo) and human telomerase (pC1.neo.hTERT) (Krump-Konvalinkova et al. 2001)] were kindly received from Ronald E. Unger, Institute of Pathology, Johannes Gutenberg University, Mainz, Germany, and were used for this study. Gelatinated (Byrne Stephen J et al. 2007a) and non-gelatinated (Byrne S. J. et al. 2006) Quantum Dots were prepared and characterised by Prof.Yurii K. Gun'ko group, CRANN and The School of Chemistry, Trinity College Dublin, Dublin, Ireland. To make HPMEC medium, Medium199 (Sigma-Aldrich), Fetal calf serum (Sigma-Aldrich), Glutamax Pen/Strep (all Life Technologies), ECGS (Becton Dickinson), heparin, gelatine, and Trypsin-EDTA (all Sigma-Aldrich) were purchased. Nunc tissue culture treated 48-well plates were purchased from Biosciences UK and 96-well flat tissue culture plates were purchased from Sarstedt. For RNA extraction and purification, 1.5 ml nuclease free tubes, nuclease free water and TRI Reagent were purchased from Ambion, RNeasy kit and DNase set were purchased from Qiagen, T75 and T175 flasks, chloroform and ethanol were purchased from Sigma–Aldrich, RNA 6000 Nano Kit was purchased from Agilent Technologies. For microarray Gene Expression analysis, Whole Human Genome kit 4x44K,, Quick-Amp Labeling Kit (one-color), Gene Expression Hybridization Kit, SureHyb Gasket Slides, Gene Expression Wash Pack and RNA spike in kit (one color) were purchased from Agilent Technologies.

Methods: HPMEC-ST1.6R cells were cultured in HPMEC medium [500 µl M199, 20% FCS, 2 mM Glutamax, Pen/Strep (100 U/100 µg/ml), heparin (50 µg/ml), ECGS (50 µg/ml)] in tissue culture flasks precoated with gelatine (0.2%) for several days until subconfluent @ 37 ^{o}C and a 5% CO_2 atmosphere.

48- well plates for AlamarBlue Assay: HPMEC-ST1.6R cells were seeded at density of 10^5 cells/cm^2 in three 48-well microplates as triplicates. After 24 h of incubation @

37 ^{o}C and a 5% CO_2 atmosphere, QDs were added (10% of amount of Medium) to make final concentrations of 10^{-9} M (see **note 1**) and were incubated @ 37 ^{o}C and a 5% CO_2 atmosphere for 24, 48 or 72 hours. Three different types of controls, namely positive, negative and background were used throughout the study. Positive control wells contained cells in culture medium without addition of QDs. Negative controls wells contained QDs with culture medium but no cells. Background control wells were cells treated with QDs but without culture medium.

48- well plates for PicoGreen Assay: HPMEC-ST1.6R cells were seeded at density of 10^5 cells/cm^2 in three 48-well microplates as triplicates. After 24 h of incubation @ 37 ^{o}C and a 5% CO_2 atmosphere, QDs were added (10% of amount of Medium) to make final concentrations of 10^{-9} M and were incubated @ 37 ^{o}C and a 5% CO_2 atmosphere for 24, 48 or 72 hours. Three different types of controls, namely positive, negative and background were used throughout the study. Positive control wells contained cells in culture medium without addition of QDs. Negative controls wells contained QDs with culture medium but no cells. Background control wells were cells treated with QDs but without culture medium.

2.13 Imaging of HPMEC-ST1.6R cells with QDs

2.13.1 Confocal Microscopy

Methods

Confocal Microscopy: An LSM 510 (Carl Zeiss, Jena, Germany) Confocal Laser Scanning microscope was used to examine QDs inside HPMEC-ST1.6R cells and its morphology.

Cell Imaging was carried out using a LSM 510 Inverted Confocal Microscope which is equipped with the following excitation lasers: (a) Argon Laser Excitation -wavelengths (λ_{Ex}) = 458 nm, 488 nm, 514 nm, (b) HeNe1 - λ_{Ex} = 543 nm and (c) Titanium Sapphire Tuneable Two-photon Laser tuneable from 710 nm to 1000 nm with a resulting excitation range of 355 nm to 500 nm. All confocal laser scanning was carried out at laser scan speed of 7 with the Photomultiplier Tube settings adjusted to eliminate noise and saturation with the aid of the range indicator setting in the LSM 510 software. For

image optimisation scan averaging was carried out on 8 scans per image. Sequential acquisition was used to acquire the two colour images of the QDs in cells. For visualisation of the QDs, the samples were excited with the Argon 514 nm Laser and the microscope configuration was set up to capture the emitted fluorescence at 550 nm or 600 nm as desired. Differential Interference Contrast (DIC) or Nomarski Microscopy was used to visualise the cell morphology, and was carried out by using the HeNe1 488 nm laser with the Transmission Channel Detector selected and the DIC polariser and Nomarski prisms engaged. The two images were then over laid using the LSM 510 software. Sequential acquisition was also used to acquire three colour images.

2.14 AlamarBlue Assay of HPMEC-ST1.6R cells with QDs

2.14.1 Cell viability by alamarBlue Assay

Materials

AlamarBlue reagent (Biosource International) was purchased from Biosciences UK.

Methods

After 24 hours of co-incubation with QDs, the medium was removed and the wells were washed with HBSS. AlamarBlue solution was prepared by adding alamarBlue and Hanks balances salt solution (HBSS) in the ratio of 1:10. Two hundred microliters of alamarBlue solution was added to each well and the plates were incubated for 1 hour. One hundred microliters of reduced alamarBlue solution from each well was removed and dispensed in a clear tissue culture 96 well microplate. The plate was analysed using a Perkin Elmer Victor Multilabel plate Reader, where absorbance was measured at lower wavelength of 550 nm and higher wavelength of 595 nm with a measurement time of 5.0 s. This process was repeated for cells with incubation periods of 48 hours and 72 hours.

2.15 PicoGreen Assay of HPMEC-ST1.6R cells with QDs

2.15.1 Quantification of DNA by PicoGreen Assay

Materials

Quant-iT PicoGreen DNA assay kit was purchased from Molecular Probes (Invitrogen).

Methods

After 24 hours of co-incubation with the QDs, the medium was removed and the wells were washed with HBSS. Then 200 µl of sterile deionised double-distilled water was added and the cells were lysed by subjecting them to 3 cycles of freezing for 15 minutes at -80^{o} C and thawing for 15 minutes at room temperature. Prepare first three of four solutions necessary for the assay according to the kit instructions in the following procedure:

PicoGreen kit ➞ Quant-iT$_{TM}$ dsDNA High-Sensitivity Assay Kit (Invitrogen)

A. Solution 1 ➞ Preparation of 1 X TE buffer 8.075 ml distilled water + 425 µl 20 X TE buffer (in kit)
B. Solution 2 ➞ Preparation of 2 mg/ml 588 µl 1 X TE buffer (from solution 1) + 12 µl 100 mg/ml DNA standard (in kit).
C. Solution 3 ➞ Preparation 50 ng/ml DNA stock 586 µl 1 X TE buffer (from solution 1) + 15 µl 2 mg/ml DNA (from solution 2).
D. Solution 4 ➞ Preparation Pico Green ➞ **Make up at the last minute** 5.174 ml 1 X TE buffer (from solution 1) + 26 µl concentrated PicoGreen (in kit).

A standard curve was then constructed, following the assay kit instructions as shown in table 2.2. Final concentrations of the standards were 1000, 500, 100, 50, 25, 10, 5, and 0 ng/µl. Lysed cell solution of 100µl from each well were dispensed in a clear tissue culture 96-well microplate.

	DNA from Soln. 2					DNA from Soln. 3		
Constituents	**1000**	**500**	**100**	**50**	**0**	**25**	**10**	**5**
DNA (µl)/buffer(µl)	100/0	50/50	10/90	5/95	0/100	100/0	40/60	20/80
DNA (µl)/buffer (µl)	100/0	50/50	10/90	5/95	0/100	100/0	40/60	20/80
DNA (µl)/buffer (µl)	100/0	50/50	10/90	5/95	0/100	100/0	40/60	20/80

Table 2.2: Calibration curve for PicoGreen assay

Then 100 µl of diluted PicoGreen solution were added to each of the test wells of 96-well plate. The plate was analysed using a Perkin Elmer Victor Multilabel Plate Reader by Fluorescence (excitation at 485 nm and emission at 535 nm, with a read time of 1.0 s). Levels of DNA in each sample were calculated using the standard curve. This process was repeated for cells with incubation periods of 48 hours and 72 hours.

2.16 Cell Culture of HPMEC-ST1.6R cells with QDs for RNA extraction

2.16.1 HPMEC-ST1.6R cell seeding and treatment with QDs for RNA extraction

Five sets of confluent cell cultures of HPMEC-ST1.6R cells in T75 flasks, each set comprising of five replicates, were prepared in order to obtain the required amount of RNA from each replicate (minimum 1000 nanograms). HPMEC-ST1.6R cells in each replicate of T75 flask were treated with red gel (set A), red non-gel (set B), orange gel (set C) and orange non-gel (set D) QDs with concentrations of 10^{-9} M for 72 hours along with untreated controls (set E). Extraction of total RNA from the treated and non-treated cultured cells was performed according to the following procedure.

2.16.2 Procedure of RNA extraction

- **Extraction of Total RNA:** After the culture, washed cells by the medium Hanks balanced Salt solution.

Extraction:

1. Homogenization of cells by 1 mL Trizol onto the scaffold by a tissue ruptor and by pipetting for cells onto the TCP. Stored at -80^{o}C
2. Stored homogenate for 5 minutes at RT (complete dissociation of nucleoprotein complexes)
3. Heated at 37°C for 10 minutes.
4. Vortexed for 15s.

Phase Separation:

5. Added 200 µl of Chloroform per 1 ml of Trizol
6. Shaked vigorously for 15 seconds by inversion
7. Incubated for 15 minutes at RT
8. Centrifuged at 12000 g max (tr/min) for 15 minutes at 4°C
9. Following the centrifugation, 3 phases: - a lower red phenol-chloroform phase, an interphase, an aqueous phase (translucent). Removed clear upper aqueous phase (~ 650µl) and added in a fresh tube
10. Slowly added 1 volume of 70% ethanol (in 3 equal aliquots) mixing by inversion.
11. Applied 700µl sample from step8 to RNeasy column, centrifuged for 15s at 8000g and dicarded flow-through. Repeated for remaining sample.
12. Added 350 µl of RW1 buffer to center of column, centrifuged for 15s at 8000g, discarded flow-through.
13. Added 10µl DNase stock solution to 70 µl Buffer RDD and added the DNase incubation mix directly onto the RNeasy column. Incubated at RT for 15 min.
14. Added 350 µl of RW1 buffer to center of column, centrifuged for 15s at 8000g, discard flow-through.
15. Transferred column to new 2ml collection tube. Added 500 µl RPE to center of column, centrifuged for 15s at 8000 g, discarded flow-through.

16. Added 500 µl of RPE buffer to center of column, centrifuged for 15s at 8000g, discard flow-through, centrifuged for a further 2 minutes at 8000g.
17. Transferred column to new 1.5 ml tube, added 20µl RNase-free water onto the column, incubated at RT for 1 min, centrifuged for 1 minute at 8000g.
18. Added a further 20µl RNase-free water onto the column, incubated at RT for 1 min, centrifuged for 1 minute at 8000g.
19. Taken back the 20µl of eluate and added again onto the column, incubated at RT for 1 min, centrifuged for 1 minute at 8000g.
20. Split up in 3 the eluate
21. Determined the concentration at the nanodrop and freezed at -80°C.

2.16.3 RNA Quantification and Purity determination

- **Quantification:** Dilution of RNA 1/50 or 1/100 in water RNase Free. Measured the absorbance at 260 nm. (Calibration of the spectrometer with water)
    1. 1 unit of A_{260} = 40 ng/µl of RNA
    2. Concentration of RNA sample = 40 * A260 * dilution factor = x ng/µl
    3. Quantity of RNA = concentration * volume of sample in µl = ng
- **Purity:** Ratio between A260 and A280.
    1. If the ratio A260/A280 is superior at 1.8-1.9 obtaining of a pure RNA (max of the ratio 2.2).
    2. The ratio of reading at A260/A280 provides an estimate of the purity of RNA with respect to contaminants that absorb in the UV, such as protein. It's influenced by the pH. Since water is not buffered, the pH and the resulting A260/A280 ratio can vary greatly. But the extinction coefficient is calculated in water, so for the concentration it's better to calculate in water.

Samples are considered 100% pure when they exhibit a ratio of A_{260}/A_{280} greater than or equal 2.0. RNA Quantity was determined for all the 25 samples as listed in table 2.3.

RNA quantity was good 100% pure for all the samples. All the samples are quiet enough to go for testing the RNA integrity or quality.

A_{260}/A_{280}	RNA Purity (%)
2.00	100
1.98	90
1.97	80
1.94	70
1.91	60
1.87	50
1.81	40
1.73	30
1.59	20
1.32	10

Table 2.3: Correlation between A_{260}/A_{280} and RNA purity

2.16.4 Procedure for the determination of RNA integrity or Quality

- **Preparation of the RNA Ladder:** For proper handling of the ladder, following steps are necessary. After reagent kit arrival, pipette the ladder in RNase-free vial. Heat denatured it for 2 minutes at 70°C. Immediately cooled down the vial on ice. Prepared aliquots in RNase-free vials with the required amount for a typical daily use. Stored aliquots at -70°C. Before use, thawed ladder aliquots and kept them on ice (to avoid extensive warming upon thawing process).

- **Agilent RNA 6000 Nano Assay Protocol:**

  Decontamination of the Electrodes: To avoid decomposition of RNA sample, we have to follow this electrode decontamination procedure on a daily basis before running any RNA Nano assays.

1. Slowly filled one of the wells of an electrode cleaner with 350 µl RNaseZAP.
2. Opened the lid and placed electrode cleaner in the Agilent 2100 bioanalyzer.
3. Closed the lid and leave it closed for about 1 minute.
4. Opened the lid and remove the electrode cleaner. Labeled the electrode cleaner and kept it for future use.
5. Slowly filled one of the wells of another electrode cleaner with 350 µl RNase-free water.
6. Placed electrode cleaner in the Agilent 2100 bioanalyzer.
7. Closed the lid and leave it closed for about 10 seconds.
8. Opened the lid and remove the electrode cleaner. Label it and keep it for further use. Waited another 10 seconds for the water on the electrodes to evaporate before closing the lid.

Preparation of the Gel

1. Allowed all reagents to equilibrate to room temperature for 30 minutes before use.
2. Placed 550 µl of Agilent RNA 6000 Nano gel matrix (red) into the top receptacle of a spin filter.
3. Placed the spin filter in a microcentrifuge and spinned for 10 minutes at 1500 g ± 20 % (for Eppendorf microcentrifuge, this corresponds to 4000 rpm).
4. Aliquoted 65 µl filtered gel into 0.5 ml RNase-free microfuge tubes that are included in the kit. Stored the aliquots at 4 °C and use them within one month of preparation.

Preparation of the Gel-Dye Mix

1. Allowed all reagents to equilibrate to room temperature for 30 minutes before use. Protected the dye concentrate from light while bringing it to room temperature.
2. Vortexed RNA 6000 Nano dye concentrate (blue) for 10 seconds and spinned down.

3. Added 1 µl of RNA 6000 Nano dye concentrate (blue) to a 65 µl aliquot of filtered gel
4. Capped the tube, vortexed thoroughly and visually inspected proper mixing of gel and dye. Stored the dye concentrate at 4 °C in the dark again.
5. Spinned tube for 10 minutes at room temperature at 13000 g (for Eppendorf microcentrifuge, this corresponds to 14000 rpm). Use prepared gel-dye mix within one day.

NOTE A larger volume of gel-dye mix can be prepared in multiples of the 65+1 ratio, if more than one chip will be used within one day. Always re-spin the gel-dye mix at 13000 g for 10 minutes before each use.

Loading of Gel-Dye Mix

1. Allowed the gel-dye mix to equilibrate to room temperature for 30 minutes before use and protected the gel-dye mix from light during this time.
2. Taken a new RNA Nano chip out of its sealed bag.
3. Placed the chip on the chip priming station.
4. Pipetted 9.0 µl of the gel-dye mix at the bottom of the well marked and dispense the gel-dye mix.
5. The timer was set to 30 seconds, make sure that the plunger is positioned at 1 ml and then close the chip priming station. The lock of the latch will click when the Priming Station is closed correctly.
6. Pressed the plunger of the syringe down until it is held by the clip.
7. Waited for exactly 30 seconds and then released the plunger with the clip release mechanism.
8. Visually inspected that the plunger moves back at least to the 0.3 ml mark.
9. Waited for 5 seconds, then slowly pull back the plunger to the 1 ml position.

10. Opened the chip priming station.
11. Pipetted 9.0 µl of the gel-dye mix in each of the wells marked.

Loading of RNA 6000 Nano Marker

1. Pipetted 5 µl of the RNA 6000 Nano marker (green) into the well marked with the ladder symbol and each of the 12 sample wells.

NOTE Do not leave any wells empty or the chip will not run properly. Unused wells must be filled with 5 µl of the RNA 6000 Nano marker (green) plus 1 µl of the buffer in which the samples are diluted.

Loading of Ladder and Samples

1. Before use, thawed ladder aliquots and kept them on ice (avoid extensive warming upon thawing process)
2. To minimize secondary structure, heat denatured (70 °C, 2 minutes) the samples before loading on the chip.
3. Pipetted 1 µl of the RNA ladder into the well marked with the ladder symbol.
4. Pipetted 1 µl of each sample into each of the 12 sample wells.
5. Set the timer to 60 seconds.
6. Placed the chip horizontally in the adapter of the IKA vortex mixer.
7. Vortexed for 60 seconds at 2400 rpm.

Inserting a Chip in the Agilent 2100 Bioanalyzer

1. Opened the lid of the Agilent 2100 bioanalyzer.
2. Checked that the electrode cartridge is inserted properly and the chip selector is in position.
3. Placed the chip carefully into the receptacle. The chip fits only one way.
4. Carefully closed the lid. The electrodes in the cartridge fit into the wells of the chip.

5. The 2100 expert software screen shows that you have inserted a chip and closed the lid by displaying the chip icon at the top left of the Instrument context and started the chip run.

According to the recommended practices, the RNA Integrity Number (RIN) of the extracted total RNA should be above 7.5 on a maximum scale range of 10 to be suitable for labelling and amplification for use with with one colour microarray kit. The RNA Integrity Number (RIN) in all the set of samples (treated with red gel and non-gel QDs, orange gel and non-gel QDs and untreated controls) measured above 9.0 were taken for the next step, i.e Quick Amplification and labelling. Only 3 samples from each set were used for Quick Amplification and labelling.

2.17 One-Color Microarray-Based Gene Expression Analysis (Quick Amp Labelling)

Agilent's Quick Amp Labelling Kit generates fluorescent cRNA (complimentary RNA) with a sample input 200 ng of total RNA for one-color processing. The method uses T7 RNA polymerase, which simultaneously amplifies target material and incorporates cyanine 3-labeled CTP. Amplification is typically at least a 100-fold from total RNA to cRNA with the use of this kit.

2.17.1 Sample Preparation

- **Step 1. Preparation of One-Color Spike Mix:** Prepared the Agilent One-Color Spike-Mix dilution appropriate for 1000 ng of total RNA starting sample:
    1. Mixed the thawed Agilent One-Color Spike-Mix concentrate vigorously on a vortex mixer.
    2. Heated at 37°C in a circulating water bath for 5 minutes.
    3. Mixed the Agilent One-Color Spike-Mix tube vigorously again on a vortex mixer.
    4. Spun briefly in a centrifuge to separate contents to the bottom of the tube.

5. Added 2 µl of Agilent One-Color Spike-Mix stock to 38 µl of Dilution Buffer provided in the kit (1:20).
6. Mixed thoroughly on a vortex mixer and spun down quickly to collect all of the liquid at the bottom of the tube. This tube contains the First Dilution.
7. Added 2 µl of First Dilution to 48 µl of Dilution Buffer for the Second Dilution (1:25).
8. Mixed thoroughly on a vortex mixer and spun down quickly to collect all of the liquid at the bottom of the tube. This tube contains the Second Dilution.
9. Added 8 µl of Second Dilution to 32 µl of Dilution Buffer for the Third Dilution (1:5).
10. Mixed thoroughly on a vortex mixer and spun down quickly to collect all of the liquid at the bottom of the tube. This tube contains the Third Dilution (now at a 5000-fold final dilution).
11. Added 5 µl of Third Dilution to 1000 ng of sample total RNA and continue with cyanine 3 labeling using the Agilent Low Input Linear Amplification Kit protocol as specified.

- **Step 2. Preparation of labeling reaction:**

1. Added 1000 ng of total RNA to a 1.5-ml microcentrifuge tube of 5.3 µl
2. Added 1.2 µl of T7 Promoter Primer (from the Agilent Quick Amp Kit, One-Color).
3. Added the appropriate volume of diluted Spike-Mix of 5.0 µl
4. Denatured the primer and the template by incubating the reaction at 65°C in a circulating water bath for 10 minutes.
5. Placed the reactions on ice and incubated for 5 minutes.
6. Immediately prior to use, gently mixed the components as listed in table 2.4 for the cDNA Master Mix by adding in the order indicated, and kept on ice.

Component	**Volume (µl) per reaction**	**Volume (µl) per 4.5 reactions**
5X First Strand Buffer	4	18
0.1 M DTT	2	9
10 mM dNTP mix	1	4.5
MMLV-RT	1	4.5
RNaseOUT	0.5	2.3
Total Volume	***8.5***	***38.3***

Table 2.4 cDNA Master Mix

7. Prewarmed the 5X first strand buffer at 80°C for 3 to 4 minutes to ensure adequate resuspensions of the buffer components. For optimal resuspension, briefly mixed on a vortex mixer and spun the tube in a microcentrifuge to drive down the contents from the tube walls. Kept at room temperature until needed.

   MMLV-RT and RNaseOUT are enzymes, which need to be kept on ice and are to be added to the cDNA Master Mix just before starting the reactions.

8. Briefly spun each sample tube in a microcentrifuge to drive down the contents from the tube walls and the lid. Returned the tubes to ice.
9. Added 8.5 µl of cDNA Master Mix to each sample tube and mixed by pipetting up and down.
10. Incubated samples at 40°C in a circulating water bath for 2 hours.
11. Moved samples to a 65°C circulating water bath and incubated for 15 minutes.
12. Moved samples to ice. Incubated for 5 minutes.
13. Spun samples briefly in a microcentrifuge to drive down tube contents from the tube walls and lid.

14. Immediately prior to use, gently mixed the components listed in the order indicated for the Transcription Master Mix as listed in table 2.5 by pipetting at room temperature.
15. Prewarmed the 50% PEG solution at 40°C for 1 minute. For optimal resuspension, briefly mixed on a vortex mixer and spun the tube in a microcentrifuge to drive down the contents from the tube walls. Careful pipetting is required to ensure accurate volume. Kept at room temperature until needed.

    RNaseOUT, inorganic pyrophosphatase, and T7 RNA polymerase are enzymes, which was kept on ice and added to the Transcription Master Mix just before starting the reactions.

Component	**Volume (µL) per reaction**	**Volume (µL) per 4.5 reactions**
Nuclease-free water	15.3	68.9
4X Transcription Buffer	20	90
0.1 M DTT	6	27
NTP mix	8	36
50% PEG	6.4	28.8
RNaseOUT	0.5	2.3
Inorganic pyrophosphatase	0.6	2.7
T7 RNA Polymerase	0.8	3.6
Cyanine 3-CTP	2.4	10.8
Total Volume	60	270

Table 2.5 Transcription Master Mix

16. Added 60 µL of Transcription Master Mix to each sample tube. Gently mixed by pipetting.
17. Incubated samples in a circulating water bath at 40°C for 2 hours.

- **Step 3. Purification of the labeled/amplified RNA:**

1. Added 20 µl of nuclease-free water to your cRNA sample, for a total volume of 100 µl.
2. Added 350 µl of Buffer RLT and mix well by pipetting.
3. Added 250 µl of ethanol (96% to 100% purity) and mix thoroughly by pipetting. Do not centrifuge.
4. Transferred the 700 µl of the cRNA sample to an RNeasy mini column in a 2 ml collection tube. Centrifuge the sample at 4°C for 30 seconds at 13,000 rpm. Discarded the flow-through and collection tube.
5. Transferred the RNeasy column to a new collection tube and added 500 µl of buffer RPE (containing ethanol) to the column. Centrifuged the sample at 4°C for 30 seconds at 13,000 rpm. Discarded the flow-through. Re-used the collection tube.
6. Added another 500 µl of buffer RPE to the column. Centrifuged the sample at 4°C for 60 seconds at 13,000 rpm. Discarded the flow-through and the collection tube.
7. Transferred the RNeasy column to a new 1.5 ml collection tube and centrifuged the sample at 4°C for 30 seconds at 13,000 rpm to remove any remaining traces of buffer RPE. Discarded this collection tube and used a fresh tube to elute the cleaned cRNA sample.
8. Eluted the cleaned cRNA sample by transferring the RNeasy column to a new 1.5 ml collection tube. Added 30 µl RNase-free water directly onto the RNeasy filter membrane. Waited 60 seconds, then centrifuged at 4°C for 30 seconds at 13,000 rpm.
9. Maintained the cRNA sample-containing flow-through on ice. Discarded the RNeasy column.

- **Step 4. Quantification of the cRNA:** Quantitated cRNA using NanoDrop ND-1000 UV-VIS Spectrophotometer version 3.2.1. and recorded the following values:

    - Cyanine 3 dye concentration (picomolar/µl)

- RNA absorbance ratio (260 nm/280 nm)
- cRNA concentration (ng/µl)

1. Determined the yield and specific activity of each reaction as follows:
   - Used the concentration of cRNA (ng/µl) to determine the µg cRNA yield as follows:

     (Concentration of cRNA) * 30 µl (elution volume) / 1000 = µg of cRNA.
   - Used the concentrations of cRNA (ng/µl) and cyanine 3 (picomolar/µl) to determine the specific activity as follows:

     (Concentration of Cy3) / (Concentration of cRNA) * 1000 = picomolar Cy3 per µg cRNA
2. Examined the yield and specific activity results.

The yield and specific activity of all the samples of cRNA should be < 1.65 µg and 9.0 picomolar Cy3 per µg cRNA respectively in order to proceed with microarray hybridisation. All the samples of each set were above those values and proceeded for next step, i.e hybridisation.

2.17.2 Hybridization

- **Step 1. Preparation of 10X Blocking Agent:**

1. Added 500 µl of nuclease-free water to the vial containing lyophilized 10X Blocking Agent supplied with the Agilent Gene Expression Hybridization Kit.
2. Mixed by gently vortexing. As the pellet does not go into solution completely, so heated the mix for 5 minutes at 37°C.
3. Drived down any material adhering to the tube walls or cap by centrifuging for 10 seconds.

- **Step 2. Preparation of hybridization samples:**

1. Equilibrated water bath to 60°C.

2. For each microarray, added each of the components 1.65 µg of cyanine 3-labeled, linearly amplified cRNA, 11 µl of 10X Blocking Agent, Nuclease-free water bringing volume to 52.8 µl, 2.2 µl of 25X Fragmentation Buffer to a 1.5 ml nuclease-free microfuge tube for 4x44K microarray formats according to the Agilent protocol.
3. Mixed well but gently on a vortex mixer.
4. Incubated at 60°C for exactly 30 minutes to fragment RNA.
5. Added 55 µl of 2x GEx Hybridization Buffer HI-RPM to the 4x44K array format to stop the fragmentation reaction.
6. Mixed well by careful pipetting. Take care to avoid introducing bubbles. Do not mix on a vortex mixer; mixing on a vortex mixer introduces bubbles.
7. Spun for 1 minute at room temperature at 13,000 rpm in a microcentrifuge to drive the sample off the walls and lid and to aid in bubble reduction.
8. Placed sample on ice and loaded onto the array as soon as possible.

- **Step 3. Preparation of hybridization assembly:**

1. Loaded a clean gasket slide into the Agilent SureHyb chamber base with the label facing up and aligned with the rectangular section of the chamber base. Ensured that the gasket slide is flush with the chamber base and is not ajar.
2. Slowly dispensed the 100 µl volume of hybridization sample onto the gasket well in a “drag and dispense” manner.
3. Slowly placed an array “active side” down onto the SureHyb gasket slide, so that the “Agilent”-labeled barcode is facing down and the numeric barcode is facing up. Verified that the sandwich-pair is properly aligned.
4. Placed the SureHyb chamber cover onto the sandwiched slides and slided the clamp assembly onto both pieces.
5. Hand-tightened the clamp onto the chamber.

6. Vertically rotated the assembled chamber to wet the gasket and assess the mobility of the bubbles.
7. Placed assembled slide chamber in rotisserie in a hybridization oven set to 65°C and setup hybridization rotator to rotate at 10 rpm when using 2x GEx Hybridization Buffer HI-RPM.
8. Hybridized at 65°C for 17 hours.

2.17.3 Microarray Wash

- **Step 1. Addition of Triton X-102 to Gene Expression wash buffers:** The addition of 0.005% Triton X-102 to the Gene Expression wash buffers reduces the possibility of array wash artifacts. Added the Triton X-102 to Gene Expression wash buffer 1 and 2 when the cubitainer of wash buffer is first opened. Do this step to *both* Gene Expression wash buffer 1 and 2 before use.

- **Step 2. Prewarming of Gene Expression Wash Buffer 2:** Warmed the Gene Expression Wash Buffer 2 to 37°C as follows:

  1. Dispensed 1000 ml of Gene Expression Wash Buffer 2 directly into a sterile 1000-ml bottle.
  2. Tightly capped the 1000-ml bottle and placed in a 37°C water bath the night before washing arrays.

- **Step 3. Preparation of equipment:**

  Milli-Q water wash

  1. Run copious amounts of Milli-Q water through the staining dish.
  2. Emptied out the water collected in the dish.
  3. Repeated steps 1 and 2 at least 5 times, as it is necessary to remove any traces of contaminating material. Wash all dishes, racks, and stir bars with Milli-Q water.
  4. Discarded the Milli-Q water.

- **Step 4. Washing of microarray slides:**

1. Completely filled slide-staining dish #1 with Gene Expression Wash Buffer 1 at room temperature.
2. Placed a slide rack into slide-staining dish #2. Add a magnetic stir bar. Filled slide-staining dish #2 with enough Gene Expression Wash Buffer 1 at room temperature to cover the slide rack. Placed this dish on a magnetic stir plate.
3. Placed the empty dish #3 on the stir plate and added a magnetic stir bar.
4. Removed one hybridization chamber from incubator and recorded time. Recorded whether bubbles formed during hybridization and if all bubbles are rotating freely.
5. Prepared the hybridization chamber disassembly.
    a. Placed the hybridization chamber assembly on a flat surface and loosen the thumbscrew, turning counterclockwise.
    b. Slide off the clamp assembly and removed the chamber cover.
    c. With gloved fingers, removed the array-gasket sandwich from the chamber base by grabbing the slides from their ends. Kept the microarray slide numeric barcode facing up and quickly transferred the sandwich to slide-staining dish #1.
    d. Without letting go of the slides, submerged the array-gasket sandwich into slide-staining dish #1 containing Gene Expression Wash Buffer 1.
6. With the sandwich completely submerged in Gene Expression Wash Buffer 1, pry the sandwich opened from the barcode end only:
    a. Slipped one of the blunt ends of the forceps between the slides.
    b. Gently turned the forceps upwards or downwards to separate the slides.
    c. Let the gasket slide dropped to the bottom of the staining dish.
    d. Removed the microarray slide and placed into slide rack in the slide-staining dish #2 containing Gene Expression Wash Buffer 1 at room temperature. Minimized exposure of the slide to air.

Touched only the barcode portion of the microarray slide or its edges.

7. Repeated steps step 4 through step 6 for up to 3 additional slides in the group.
8. When all slides in the group are placed into the slide rack in slide-staining dish #2, stir using setting 4 for 1 minute.
9. During this wash step, removed Gene Expression Wash Buffer 2 from the 37°C water bath and poured into the slide-staining dish #3.
10. Transferred slide rack to slide-staining dish #3 containing Gene Expression Wash Buffer 2 at elevated temperature. Stirred using setting 4 for 1 minute.
11. Slowly removed the slide rack minimizing droplets on the slides. It took 5 to 10 seconds to remove the slide rack.
12. Discarded used Gene Expression Wash Buffer 1 and Gene Expression Wash Buffer 2.
13. Repeat step 1 through step 12 for the next group of eight slides using fresh Gene Expression Wash Buffer 1 and Gene Expression Wash Buffer 2 pre-warmed to 37°C.
14. Scanned slides immediately to minimize the impact of environmental oxidants on signal intensities.

2.17.4 Scanning and Feature Extraction

- **Step 1. Scanning of slides**

Agilent Scanner Settings

1. Assemble dthe slides into an appropriate slide holder. Placed the slides into the slide holder such that the numeric barcode side is visible.
2. Placed assembled slide holders into scanner carousel.
3. Verified scan settings for one-color scans.

Scan Settings: Scan Area of 61 x 21.6 mm, Scan resolution of 5µm, Single Pass 5µm scanning mode, selected eXtended Dynamic range, Green Dye channel and Green PMT of XDR Hi 100% XDR Lo 10% were set.

4. Selected settings for the automatic file naming
    a. Prefix 1 was set to Instrument Serial Number
    b. Prefix 2 was set to Array Barcode
5. Verified that the Scanner status in the main window says Scanner Ready.
6. Clicked **Scan Slot *m-n*** on the Scan Control main window where the letter ***m*** represents the Start slot where the first slide is located and the letter ***n*** represents the End slot where the last slide is located.

- **Step 2. Extracted data using Agilent Feature Extraction Software**

1. Opened the Agilent Feature Extraction (FE) software version 9.5.3 and follow the feature Extraction protocols for gene expression.
2. Added the images (.tif) to be extracted to the FE Project.
    A. Clicked Add New Extraction Set(s) icon on the toolbar or right-click the Project Explorer and select Add Extraction.
    B. Browsed to the location of the .tif files, select the .tif file(s) and clicked Open. To select multiple files, used the Shift or Ctrl key when selecting.
3. Checked the Extraction Set Configuration.
    A. Selected the **Extraction Set Configuration** tab.
    B. Verified that the correct grid template is assigned to each extraction set in the **Grid Name** column. To assign a different grid template to an extraction set, select one from the pull down menu.
    C. If a protocol is not available to select from the pull down menu, you must import it to the FE Protocol Browser. To import, right-click **FE Protocol Browser**, select **Import**. Browse for the FE

protocol (.xml) and click **Open** to load the protocol into the FE database.

D. Saved the FE Project (.fep) by selecting **File > Save As** and browse for desired location.

E. Verified that the icons for the image files in the FE Project Window no longer have a red X through them. A red X through the icon indicates that an extraction protocol was not selected. If needed, reselect the extraction protocol for that image file.

F. Selected **Project > Start Extracting**.

G. After the extraction is completed successfully, viewed the QC report for each extraction set by double-clicking the QC Report link in the **Summary Report** tab. Determined whether the grid has been properly placed by inspecting Spot Finding at the Four Corners of the Array.

2.17.5 Microarray data analysis

Data extraction of the microarray images was performed using the "Feature Extraction" (FE) software (Agilent, v9.1) resulting in an analysable spreadsheet with signal and background fluorescent intensities, as well as annotation information. The 15 data files were imported into GeneSpring GX v11 (Agilent) and normalised using default settings, for scaling and to reduce technical variability. All samples included in downstream analysis were required to pass the QC Metrics produced by FE. Principal Components Analysis was performed to cluster all samples based on the major sources of variability. The global gene list was filtered to remove non-expressed genes flagged as absent by FE.

To detect differentially expressed genes in all conditions examined, a Welch One-way ANOVA, using Benjamini and Hochberg multiple testing correction with an adjusted p-value <0.05, was used. To visualise the data, a Hierarchical Cluster was created, using Pearson clustering on conditions and differentially expressed genes. To determine the specific condition pair(s) where statistical differences occur, a Student-Newman-Keuls post-hoc test was performed. Finally, a >1.5 fold change cut off was applied to the resulting genelists.

Pathway analysis was performed to determine what pathways may be involved and to link differentially expressed genes, by mapping known direct interactions. Further functional analysis was performed using the DAVID (Database for Annotation, Visualisation and Integrated Discovery) suite of tools (Barton et al. 2008, Huang et al. 2009a, b), to find overrepresented annotation terms, which can be used to group genes into gene families, and to find significant themes within the data.

2.18 Surface property characterisation of nano-surface roughness of PDMS [Poly(dimethyl siloxane)] or Silicone

2.18.1 Fourier Transform Infrared Spectroscopy (FTIR)

PDMS samples were characterized for chemical composition by Fourier Transform Infrared Spectroscopy FTIR-8300 system (Shimadzu).

2.18.2 Scanning Electron Microscopy (SEM)

Surface topography of gold coated PDMS samples were analysed by scanning electron microscopy (SEM) using a Hitachi S-4700 instrument.

2.18.3 Atomic Force Microscopy (AFM)

The PDMS samples were also analyzed by atomic force microscopy (AFM) using a Digital Instruments Dimension 3100 in tapping mode in air with scanning size of 100x100 μm area.

2.19 Cell culture of NIH-3T3 fibroblast cells on nano-surface roughness of PDMS [Poly(dimethyl siloxane)] or Silicone

2.19.1 NIH -3T3 fibroblasts cell seeding and treatment on PDMS nano-surfaces for imaging and cellular activity

Materials

NIH-3T3 (mouse) fibroblasts were used for this study. Dulbecco's Modification of Eagle Medium (DMEM) supplemented with 10% fetal bovine serum, 1% penicillin-streptomycin, Hanks Balanced Salt Solution (HBSS), 10X Trypsin-EDTA solution, Poly-L-lysine (PLL) were purchased from Sigma-Aldrich. T-75 flasks, 5, 10 and 25 ml pipettes and 96-well flat tissue culture plates were purchased from Sarstedt. 24-well plates were purchased from Biosciences. PDMS or silicone samples were supplied by our collaborator Prof. Michael A. Brook group, Department of Chemistry, McMaster University, Ontario, Canada.

Methods

NIH-3T3 (mouse) fibroblasts were cultured in DMEM supplemented with 10% fetal bovine serum and 1% penicillin-streptomycin and kept in an incubator at 37 °C and 5% CO_2 atmosphere.

24- well plate for PicoGreen Assay: The PDMS samples of smooth, bumpy (~378nm) and very rough samples (~604nm and ~650 nm) were sterilized by treating with 70% ethanol for 20 min followed by successive washes 4 times with sterile PBS. Sterilized PDMS samples were kept in sterile 24 well plates, seeded with approximately 50 µl of a suspension of NIH-3T3 fibroblasts at a density of 40,000 cells/ cm^2 as triplicates. This was just enough to cover the PDMS samples so that the cells could not flow off of the PDMS sample surface. The cells were kept in an incubator for 1 h so that they became fixed on the PDMS surface and then DMEM was added to give a final volume of 800 µl in each well, and again the plates were placed in an incubator at 37 °C under 5% CO_2 for 24 h. DNA was quantified according to the calibration curve by PicoGreen assay.

2.1 Imaging of NIH-3T3 fibroblast cells on PDMS

2.1.1 Microscopy

Methods

Microscopy: Olympus IX71 Inverted Fluorescent Microscope with Olympus Cell P Software for live cell imaging of NIH-3T3 fibroblasts on PDMS samples after 24 hours of seeding of cells.

2.2 Cellular activity of NIH-3T3 fibroblast cells on PDMS

2.2.1 Quantification of DNA by PicoGreen Assay

Materials

Quant-iT PicoGreen DNA assay kit was purchased from Molecular Probes (Invitrogen).

Methods

After 24 hours of co-incubation of NIH-3T3 fibroblasts on PDMS samples, the medium was removed and the wells were washed with HBSS. Then 200 µl of sterile deionised double-distilled water was added and the cells were lysed by subjecting them to 3 cycles of freezing for 15 minutes at -80^{o} C and thawing for 15 minutes at room temperature. Prepare first three of four solutions necessary for the assay according to the kit instructions in the following procedure:

PicoGreen kit ➞ Quant-iT$_{TM}$ dsDNA High-Sensitivity Assay Kit (Invitrogen)

A. Solution 1 ➞ Preparation of 1 X TE buffer 8.075 ml distilled water + 425 µl 20 X TE buffer (in kit)
B. Solution 2 ➞ Preparation of 2 mg/ml 588 µl 1 X TE buffer (from solution 1) + 12 µl 100 mg/ml DNA standard (in kit).
C. Solution 3 ➞ Preparation 50 ng/ml DNA stock 586 µl 1 X TE buffer (from solution 1) + 15 µl 2 mg/ml DNA (from solution 2).

D. Solution 4 ➞ Preparation PicoGreen ➞ **Make up at the last minute**

5.174 ml 1 X TE buffer (from solution 1) + 26 µl concentrated PicoGreen (in kit).

A standard curve was then constructed, following the assay kit instructions as listed in table 2.6. Final concentrations of the standards were 1000, 500, 100, 50, 25, 10, 5, and 0 ng/µl. Lysed cell solution of 100µl from each well were dispensed in a clear tissue culture 96-well microplate.

	DNA from Soln. 2					**DNA from Soln. 3**		
Constituents	**1000**	**500**	**100**	**50**	**0**	**25**	**10**	**5**
DNA (µl)/buffer(µl)	100/0	50/50	10/90	5/95	0/100	100/0	40/60	20/80
DNA (µl)/buffer (µl)	100/0	50/50	10/90	5/95	0/100	100/0	40/60	20/80
DNA (µl)/buffer (µl)	100/0	50/50	10/90	5/95	0/100	100/0	40/60	20/80

Table 2.6: Calibration curve for PicoGreen assay

Then 100 µl of diluted PicoGreen solution were added to each of the test wells of 96-well plate. The plate was analysed using a Perkin Elmer Victor Multilabel Plate Reader by Fluorescence (excitation at 485 nm and emission at 535 nm, with a read time of 1.0 s). Levels of DNA in each sample were calculated using the standard curve.

2.3 Analysis of data

2.3.1 Statistical Analysis

All results were analysed using Minitab one-way analysis of variance (ANOVA) with Tukey's, family error rate of one-way multiple comparisons. A ρ value of less than 0.05 for the ANOVA was considered significant. Error was expressed as standard deviation.

CHAPTER 3: EFFECT OF QDS ON UNDIFFERENTIATED PC12 CELLS

3.1 Background and aims

The unique and tuneable photonic properties of Quantum Dots (QDs) have made them potentially useful tools for imaging biological entities. However, QDs though attractive diagnostic and therapeutic tools, have a major disadvantage due to their inherent cytotoxic nature. Our studies are focussed on the analysis of PC12 cells which have the ability to be differentiated into neurons upon treatment with nerve growth factors (NGF). The application of QDs to neuroscience specific fields is currently emerging (Cui et al. 2007, Jan et al. 2008, Lopez et al. 2003, Rajan et al. 2008, Tang M. L. et al. 2008b, Tang M. L. et al. 2008c) and various groups have investigated the specific labelling of neurons with QDs. While QDs have been investigated with a large variety of cell lines and types; more recently, in search of new neurotherapeutic and neuroprosthetic strategies, QDs have been explored to manipulate and create active cellular interfaces with nerve cells (Gomez Natalia et al. 2005b, Jan et al. 2008). However, the application of such entities to neuron cell imaging is limited and while QDs have been used for cell labelling experiments, little work has been undertaken into measuring the ranges of neuron cell response over long time scales upon their perturbation by the QDs. There are a number of studies which have investigated the toxicity of QDs for 24 hour co-incubations and demonstrated that increasing concentrations increase cell toxicity significantly (Amane Shiohara et al. 2004, Cho Sung Ju et al. 2007a, J. Lovrić et al. 2005, Tan et al. 2007, Tang M. L. et al. 2008c). Although shorter incubation periods have been used by some groups to investigate the toxicity (E. Chang et al. 2006, J. Lovrić et al. 2005), long term exposure is more reliable. The purpose of our study was to explore the potential for labelling of undifferentiated Pheochromocytoma 12 (PC12) cells with gelatinised and non-gelatinised TGA capped CdTe QDs with longer incubation periods. We have investigated the cellular interaction, uptake and resultant toxic influence of CdTe QDs (gelatinised and non-gelatinised Thioglycolic acid (TGA) capped) by serial co-incubations of 24, 48 and 72 hours and analysed the effect of three factors namely concentration, co-incubation time and surface modification in parallel. In conjunction to their analysis by confocal microscopy, the QD – cell interplay was explored as the QD concentrations were varied over extended (up to 72 hours) co-incubation times. Coupled to this investigation, cell

viability, DNA quantification and cell proliferation assays were also performed to compare and contrast the various factors leading to cell stress and ultimately death.

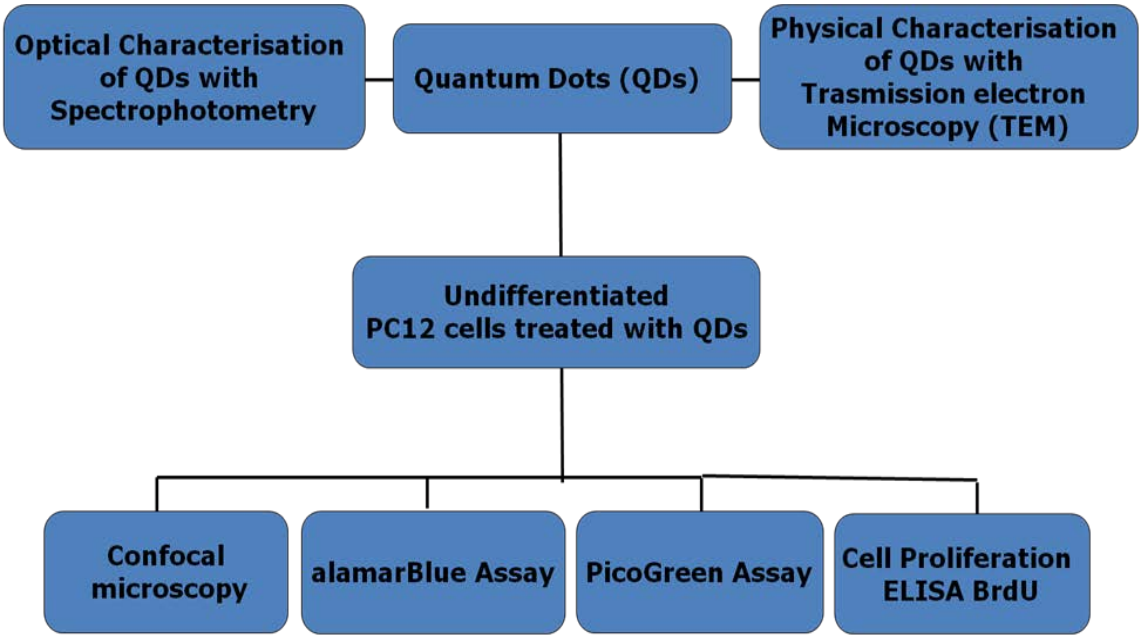

Figure 3.1: Flow chart showing experimental design of undifferentiated PC12 cells treated with QDs.

3.2 Results

3.2.1 Optical and Physical Characteristics of Quantum Dots

3.2.1.1 Optical characteristics of QDs:

Two differently sized batches of QDs (for both gel and non-gel QDs) were synthesised to allow us to investigate if the additional parameter of QD size had any impact on cell response. Figures 3.2, 3.3, 3.4 and 3.5 below shows the typical absorption and emission profiles indicative of aqueous CdTe QDs. Samples showed a well-resolved absorption maximum which can be seen in Figures 3.2, 3.3, 3.4 and 3.5 below displaying the UV-vis spectra, indicating a narrow size distribution of the TGA-capped CdTe QDs. Longer wavelengths were also achieved with increasing size of nanocrystals with our red gel QDs of ~4.5 nm having a wavelength of ~580 nm and our orange gel QDs of ~2.5 nm

having a wavelength of ~520 nm. This longer wavelength is as a result of quantum confinement, an increasing number of atoms are present resulting in longer wavelength.

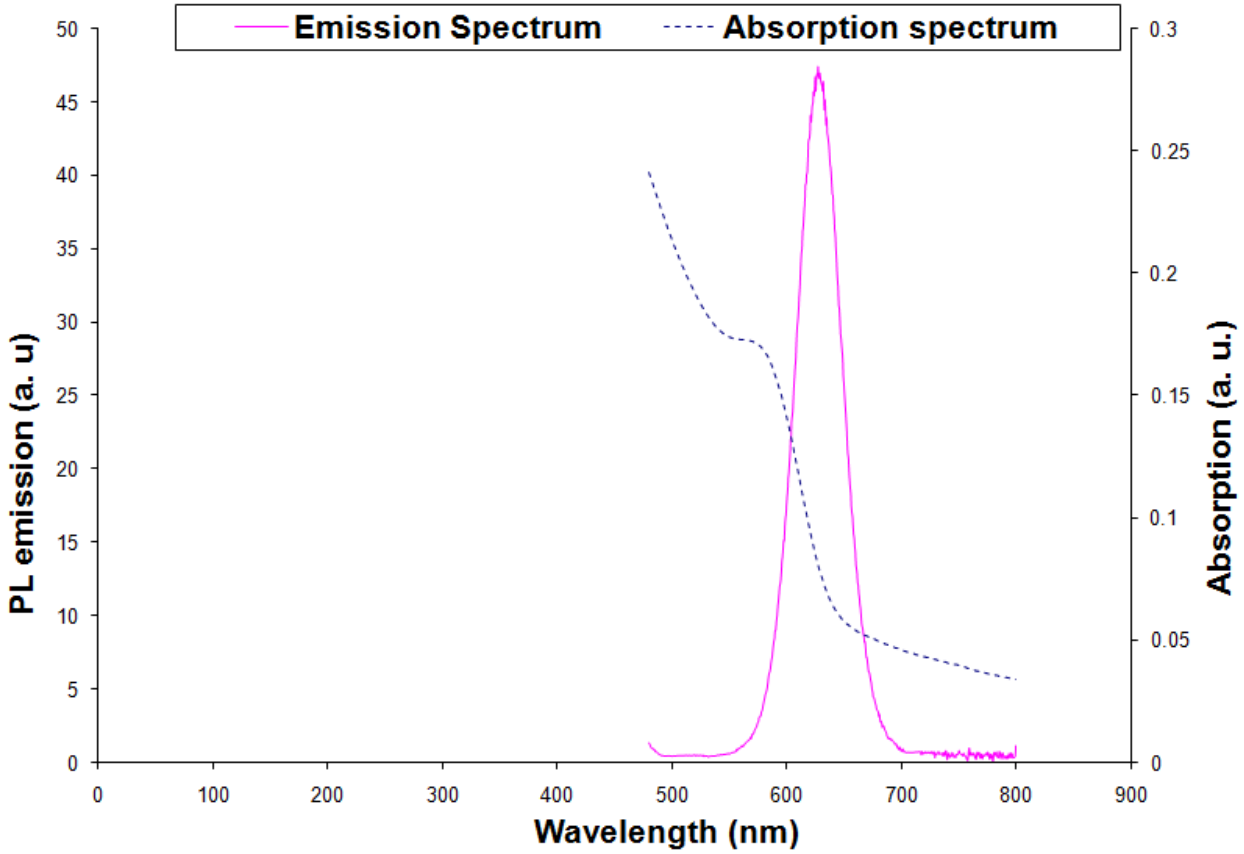

Figure 3.2: Absorption and fluorescence emission spectra (λ_{ex} 450 nm) of the Red Gel (~4.5nm size) QDs synthesised by Stephen Byrne and Valerie Gerard, Inorganic Chemistry, TCD

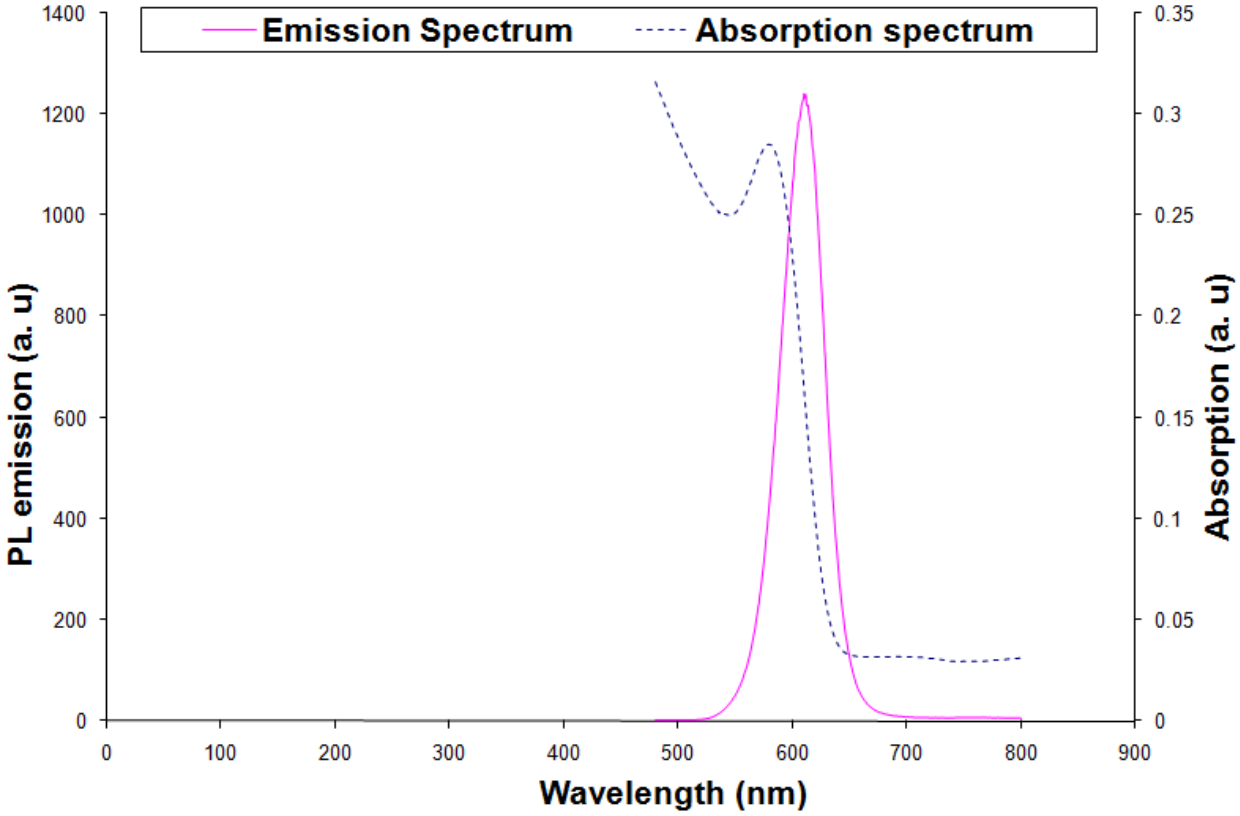

Figure 3.3: Absorption and fluorescence emission spectra (λ_{ex} 450 nm) of the Red Non-gel (~4.5nm size) QDs synthesised by Stephen Byrne and Valerie Gerard, Inorganic Chemistry, TCD

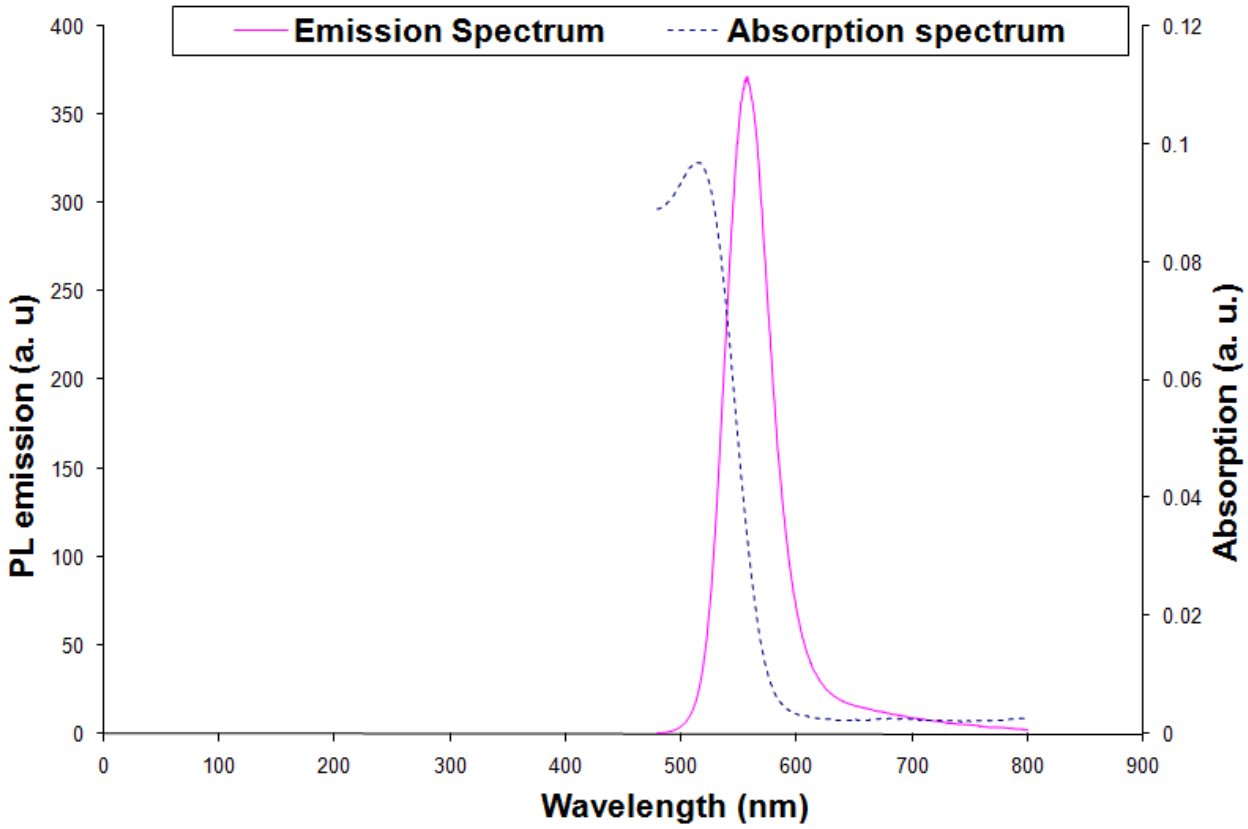

Figure 3.4: Absorption and fluorescence emission spectra (λ_{ex} 450 nm) of the Orange Gel (~2.5nm size) QDs synthesised by Stephen Byrne and Valerie Gerard, Inorganic Chemistry, TCD

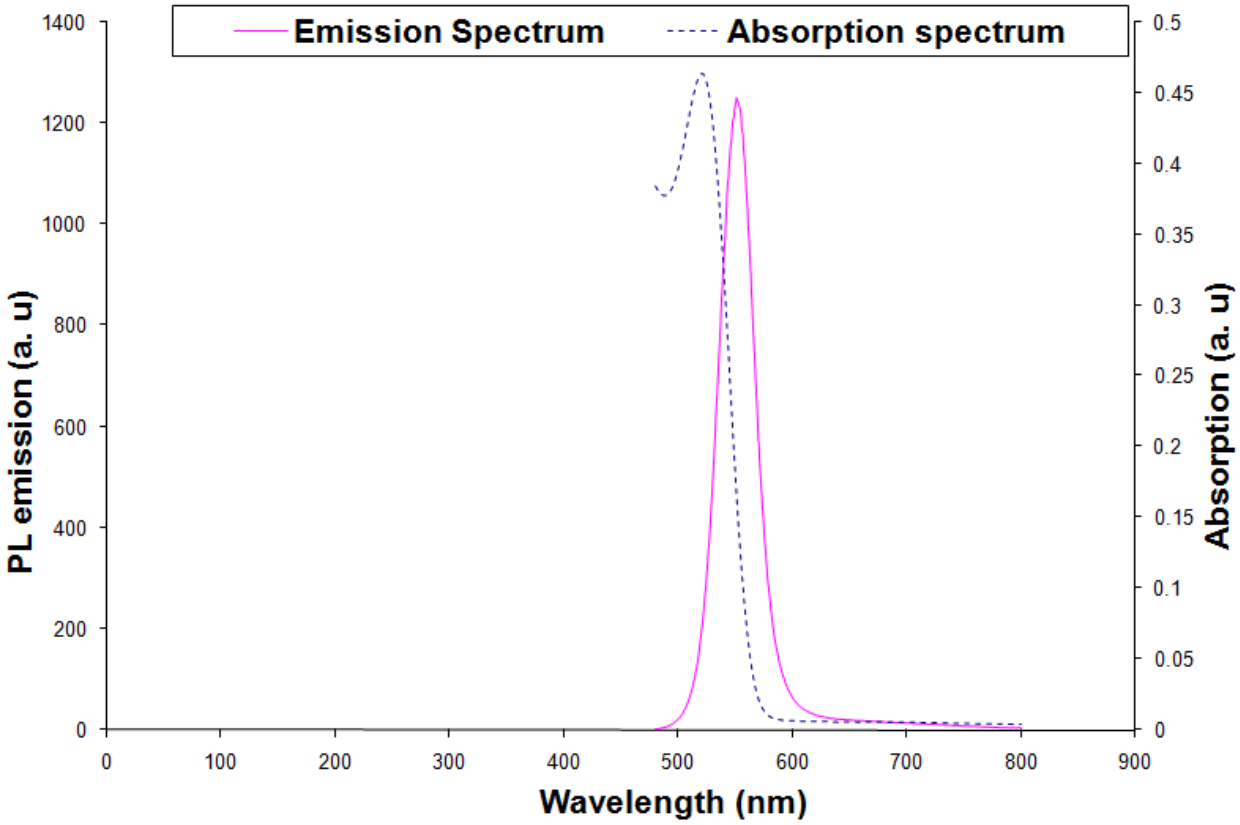

Figure 3.5: Absorption and fluorescence emission spectra (λ_{ex} 450 nm) of the Orange Non-gel (~2.5nm size) QDs synthesised by Stephen Byrne and Valerie Gerard, Inorganic Chemistry, TCD

Figure 3.6 shows the typical absorption and emission profiles indicative of aqueous CdTe QDs. As there are no differences in the spectral characteristics of gel and non-gel QDs, one spectrum indicative of each size is shown for clarity. The spectra shown in Figure 6 highlight the well resolved emission and absorption characteristics of the QDs. Narrow emission spectra (<40 nm full with half maximum [FWHM]) indicate <5% particle size distributions throughout. Gelatine was introduced during the synthesis of the QDs and its presence while altering QD growth rates and QYs (Byrne Stephen J et al. 2007a), does not significantly alter the size distribution of the QDs and acts primarily as a co-capping agent.

Quantum yields (QYs) for the solutions (measured against Rhodamine 6G) were ~25 % for the non-gel and ~35 % for the gel QDs. As the presence of uncapped surface atoms

provides alternate pathways for the non-radiative recombination of photons, the difference in QYs indicate the highly effective capping qualities of the gelatine.

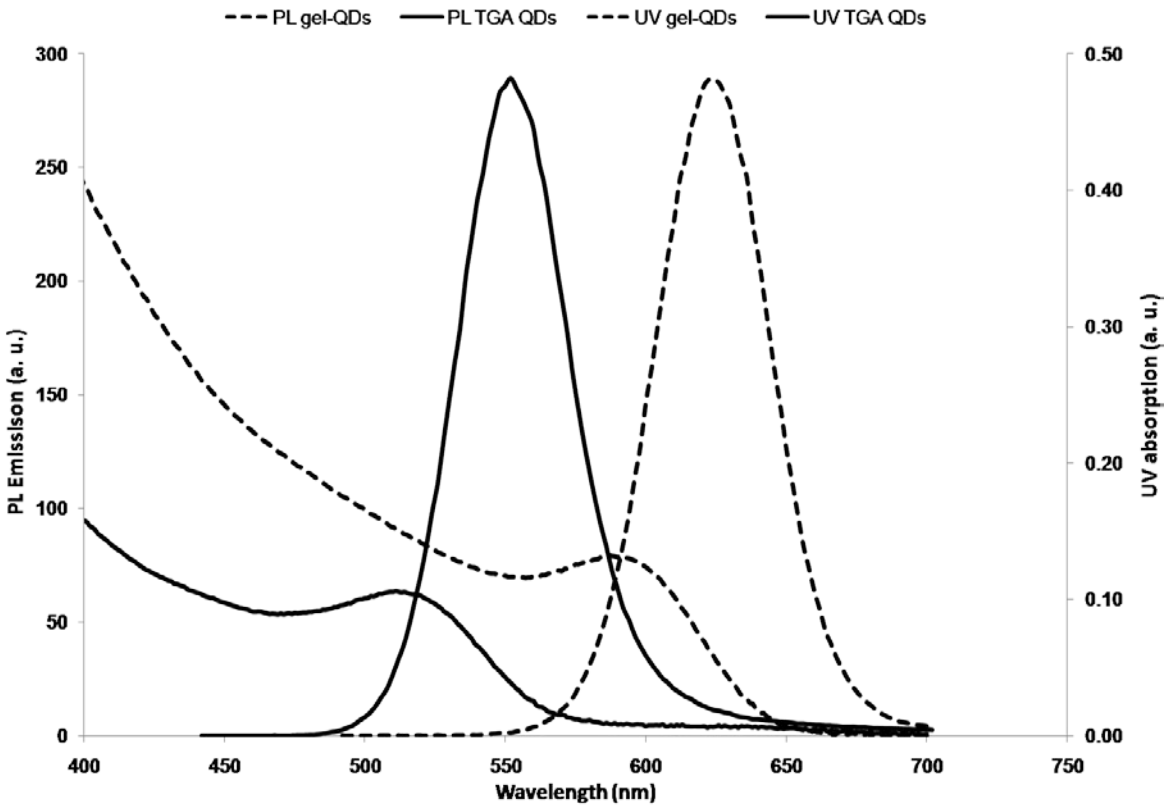

Figure 3.6: UV-vis absorption and fluorescence emission spectra (λ_{ex} 450 nm) of the differently sized (~ 2.5 nm – solid line & ~ 4.5 nm – dashed line) QDs synthesised and measured by Stephen Byrne and Valerie Gerard, Inorganic Chemistry, TCD.

3.2.1.2 Structure and Morphology of QDs

Transmission electron microscope (TEM) images were taken to examine the structure and morphology of QDs (Figure 3.7).

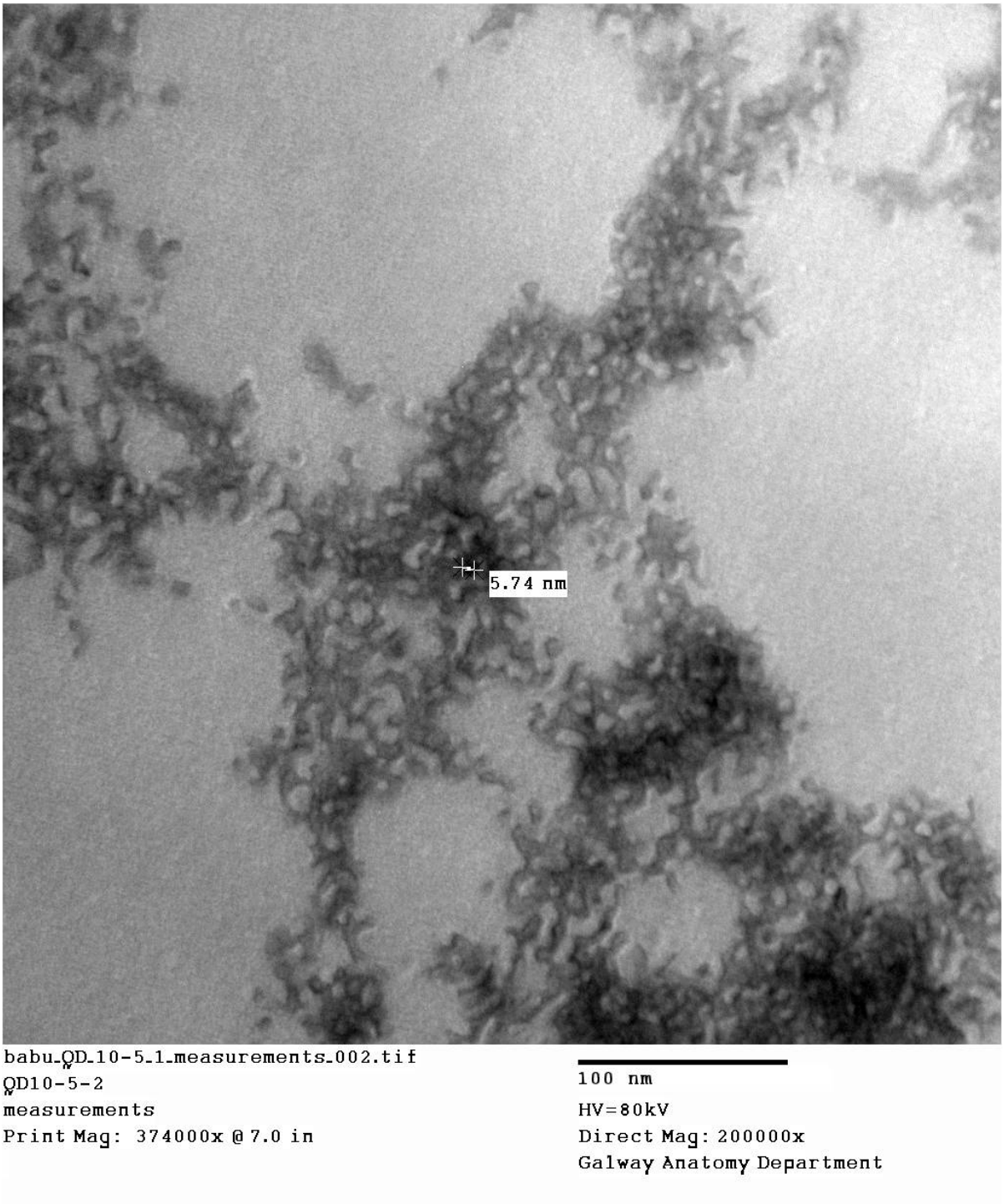

Figure 3.7: TEM image of aggregated TGA capped CdTe QDs.

Lattice spacings are in agreement with those expected for the (111) plane of cubic zinc blend CdTe (Tang Z. et al. 2004). We have previously shown that although the presence of gelatine during the synthesis of the QDs can influence the rate of QD growth and QY (Byrne Stephen J et al. 2007a), it does not seem to alter the physical structure of the QDs. Consequently, as can be seen from the resulting QY's, the gelatine must act solely

as a co-capping agent for the protection of the QD surface and the reduction of non-radiative transitions. The incorporation of gelatine during the QD synthesis results in smaller QDs being produced under the same conditions compared to non-gel QDs but does not seem to alter or influence the size distribution with the particle ensemble. Following size selective purification, size distributions for spectroscopically similar gel and non gel samples were comparable with the only noticeable difference being their respective QYs.

The influence of this additional exterior coating upon uptake and any induced toxicity were some of the properties we wished to explore with the PC12 cells.

Our next aim was to analyse the effect of the QDs on cell behaviour and morphology also to then investigate any alterations to cell proliferation, viability and DNA quantification using pre-determined assays over extended co-incubation times.

3.2.2 Uptake of QDs and their effect on cell morphology of undifferentiated PC12 cells

3.2.2.1 Confocal imaging of undifferentiated PC12 cells

Stock gel and non-gel QD solutions (10^{-4} M) (Yu et al. 2003) were diluted to a range of concentrations ($10^{(-7)-(-9)}$ M) and incubated with the cells as described in the experimental section. Confocal images were taken to visually inspect QD uptake, localisation and cell morphology following incubation (Figures 3.8/3.9/3.10).

In figure 3.8, panels A and B show PC12 cells following 72 hours of co-incubation with 10^{-7} M and 10^{-9} M concentrations of QDs respectively. In panel A, the cells were seen to be rounded and floating in the nutrient rich medium. This contrasts the morphology of the cells in panel B and the control cells (panel C), which were attached to the culture plate and polygonal in shape. It can be noted that as QD concentrations were reduced, the effect on the cell morphology was eliminated and the cells were morphologically identical to the control cells (Figure 3.8, panels B and C). Although some earlier studies (Tan et al. 2007, Tang M. L. et al. 2008c) have shown similar concentration dependence, there is no study investigating the effect on cell morphology at the extended time periods of 48 and 72 hours (J. Lovrić et al. 2005). Green fluorescence in the PC12 cells is due to QDs localisation in the cytoplasm.

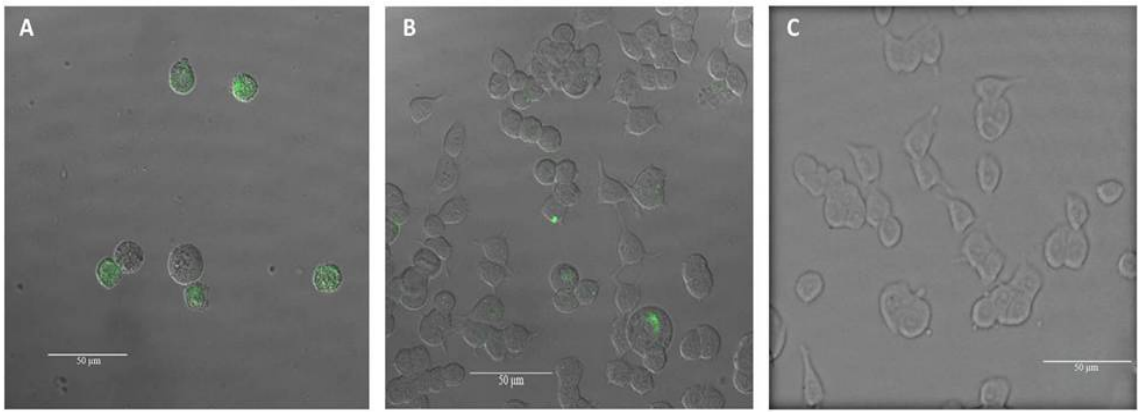

Figure 3.8: Overlay of fluorescent confocal images and corresponding differential interference contrast (DIC) images of PC12 cells exposed to a 10^{-7} M concentration of QDs (A), 10^{-9} M concentration of QDs (B) and a control sample with no QDs (C) following 72 hours of co-incubation. Scale bar = 50 µm.

Figure 3.9 shows the fluorescent image (panel A) and overlaid corresponding differential interference contrast (DIC) image (panel B) of the PC12 cells treated with a 10^{-9} M concentration of QDs following 72 hours of co-incubation. The QDs are found to be located within the cytoplasm of PC12 cells.

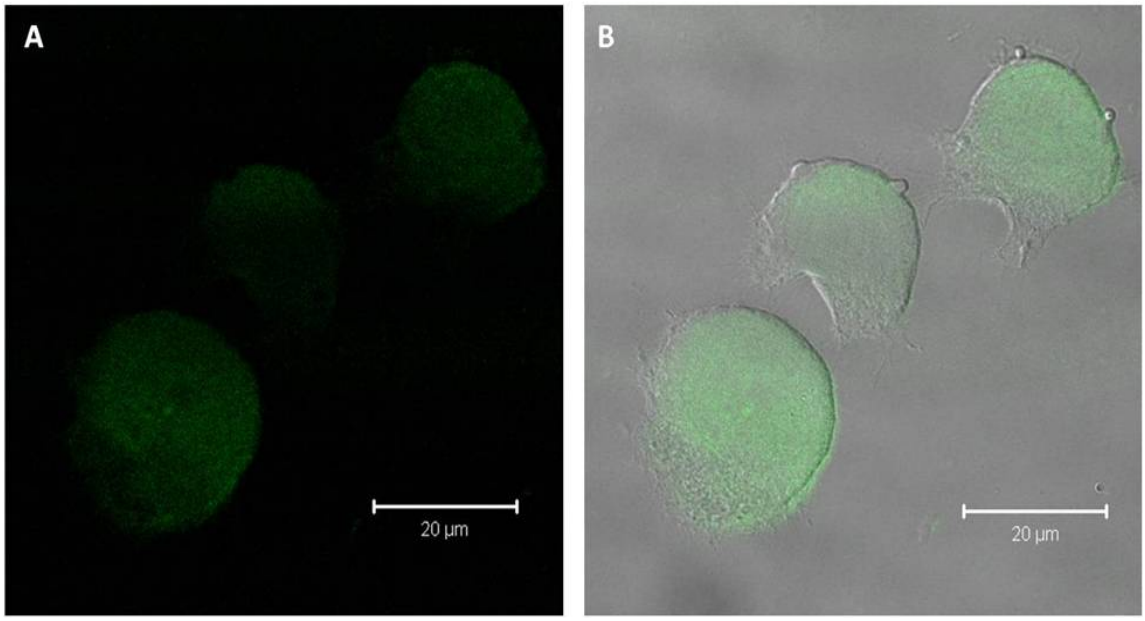

Figure 3.9: Fluorescent confocal image of PC12 cells exposed to a 10^{-9} M concentration of QDs (A) and corresponding differential interference contrast (DIC) image (B) with A overlaid following 72 hours of co-incubation [scale bar = 20 µm].

To enhance visualization, the nucleus and cellular membrane have been actin stained with blue and red colour respectively (Figure 3.10). The QDs (green luminescence) are visualized predominantly in the cytoplasm and their presence even after a 72 hour co-incubation in this region, does not seem to significantly perturb the cells. The cell morphology does not change when evaluated against the controls.

These initial observations illustrate the effect of changing QD concentration on cell survival and morphology and to further investigate cell behaviour, several assays were used to study the effect on cell proliferation, growth and metabolic activity.

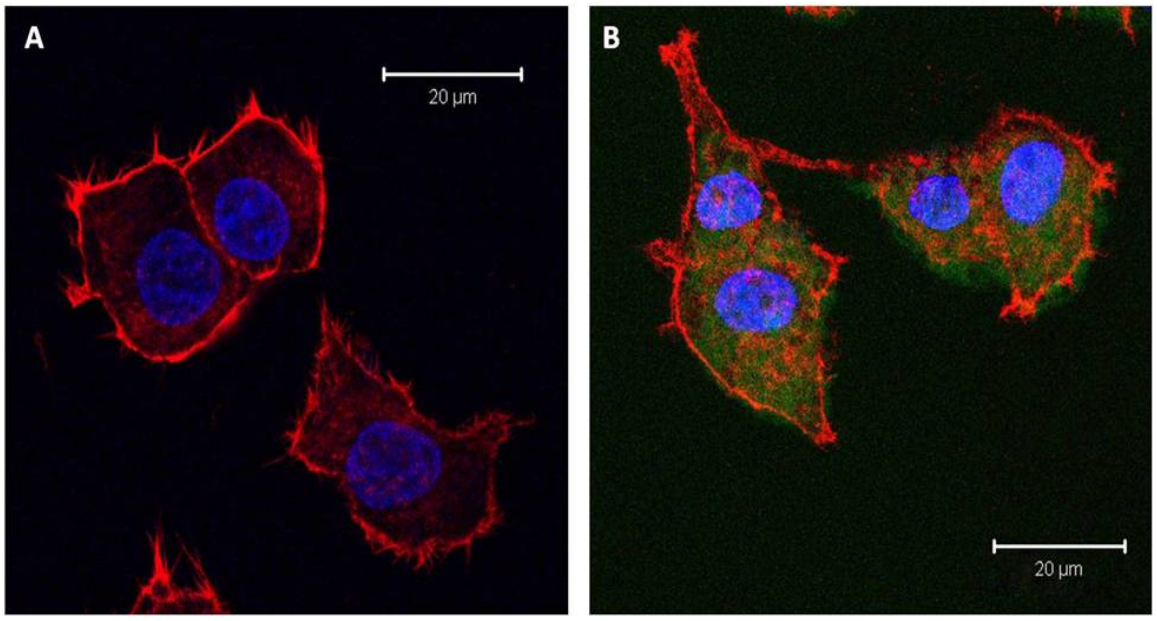

Figure 3.10: Fluorescent confocal images to illustrate the morphology of the actin stained PC12 cells with no QDs (A) as a control and PC12 cells exposed to the QDs (B) [conc. 10^{-9} M] following 72 hours of co-incubation. [Scale bar = 20 µm].

3.2.3 Effect of QDs on cellular activity of undifferentiated PC12 cells

The consequence of co-incubating classical molecules on the cell viability can be reliably predicted using single assays (Monteiro-Riviere et al. 2009), however, the dynamics of nanomaterials are not as comprehensively understood and hence drawing conclusions from single cell viability assays can be misleading. As such additional assays are required to give a more comprehensive analysis when determining nanoparticle toxicity for risk assessment (Monteiro-Riviere et al. 2009).

Consequently, alamarBlue (metabolic activity), PicoGreen (total DNA quantification) and ELISA BrdU (colorimetric assay for quantification of proliferating DNA) assays were run to analyse the effect of different QD concentrations, type and size following 24, 48 and 72 hour co-incubations with the PC12 cells.

The red/orange labels serve to differentiate the various QDs by size [~ 2.5 nm (orange) and ~ 4.5 nm (red)] and were used to investigate if the measured cell responses were in any way size dependant. The gel / non-gel label refers to the presence of gelatine during the synthesis of the QDs and these different QDs were analysed to investigate the influence that gelatine imparts on the QD induced cell toxicity.

The changes in luminescence intensity measured in response to the introduction of QDs to the cell cultures throughout all of our experiments can be solely attributed to direct interactions of the staining dyes upon entering the cells. Energy transfer to the dyes can be ruled out *via* a number of routes. Firstly, the dyes and QDs enter different regions of the cells and as such cannot interact directly on the scale required for FRET or other energy transfer phenomena. Secondly, the intensity (arbitrary units) of the dye emission is of the order of $\sim 10^3$ while the QDs display $\sim 10^2$. Thus, any energy transferred to the dye would be of an order of magnitude lower and would have a minimal effect on the emission intensity. Negative and background controls in our experiments also substantiate this fact.

3.2.3.1 AlamarBlue Assay

Viability of the PC12 cells, for different concentrations, sizes and types of QDs was investigated with an alamarBlue assay and the results graphed in Figure 3.11. This is a non-destructive assay and allows for the cells to be further utilised following analysis.

The graph shown in Figure 3.11 illustrates the alamarBlue response (percentage of reduced alamarBlue) for the PC12 cells following 24, 48 and 72 hour co-incubations with the QDs.

As seen in Figures 3.11 and 3.12 at 10^{-7} M QD concentrations the toxicity is extremely high at all incubation times, and approached the levels of negative controls after only 48 hours. We can see the influence of the gelatine coating up to 24 hours as cell viability responses are significantly higher for the gel QDs compared to their non-gel counterparts. Notably, all responses are lower than the controls indicating that at this

concentration the presence of any foreign entities generate a detrimental environment for the cells and result in high levels of cell death.

At 10^{-8} M QD concentrations, we can now see a shift with respect to viability response. Initially after 24 hours, responses are comparable (note: orange non-gel QDs do show a slightly decreased response) between QD types and also to controls. This indicates that over this short incubation period, the cells are not significantly perturbed by the QDs at this concentration.

At 48 and 72 hours, the cell responses now mimic those seen for 10^{-7}M concentrations and have dropped in comparison to controls; however, significant differences are noted between the two QD types. Responses for the gel QDs are considerably higher than those of the non-gel QDs and of note; the red QDs (whether gel or non-gel) are seemingly less toxic than the smaller orange QDs. This may be attributed to the fact that smaller QDs have been shown to penetrate further into cells than their larger counterparts. As nuclear pores are very small (J. Lovrić et al. 2005), nuclear staining of small "green" QDs and cytoplasmic localisation of larger "red" has demonstrated the size dependant nature of QD uptake. (Nabiev et al. 2007) Consequently, the smaller QDs may initiate deleterious cell reactions at far quicker rates than the larger ones.

Analysis of these responses at 48 and 72 hours reinforce the importance of the QD surface environment and the protective nature of the gelatine at this concentration. While the surface gelatine coating helps to reduce the toxicological impact of the QDs at 10^{-8} M concentrations, at 10^{-9} M we see the least amount of differences between QD types. Unlike previous concentrations, where alamarBlue responses decrease when comparing gel and non-gel QDs up to 72 hours, there is a certain amount of consistency when analysing the co-incubated QDs at 10^{-9} M concentrations. There are no significant changes in cell response, across the total incubation period. We can also see that final 72 hour cell responses are actually comparable to those recorded for gel QDs at 10^{-8} M. Throughout; all QDs types elicit responses below the levels of negative controls, however responses for gel QDs are far higher than non-gel QDs, indicating that even though their presence results in a certain level of toxicity, they are far less detrimental than their non-gel counterparts.

These results have been focussed on cell respiratory responses. Our next objective was to find out if the impact of the QDs remains the same for other cellular activities.

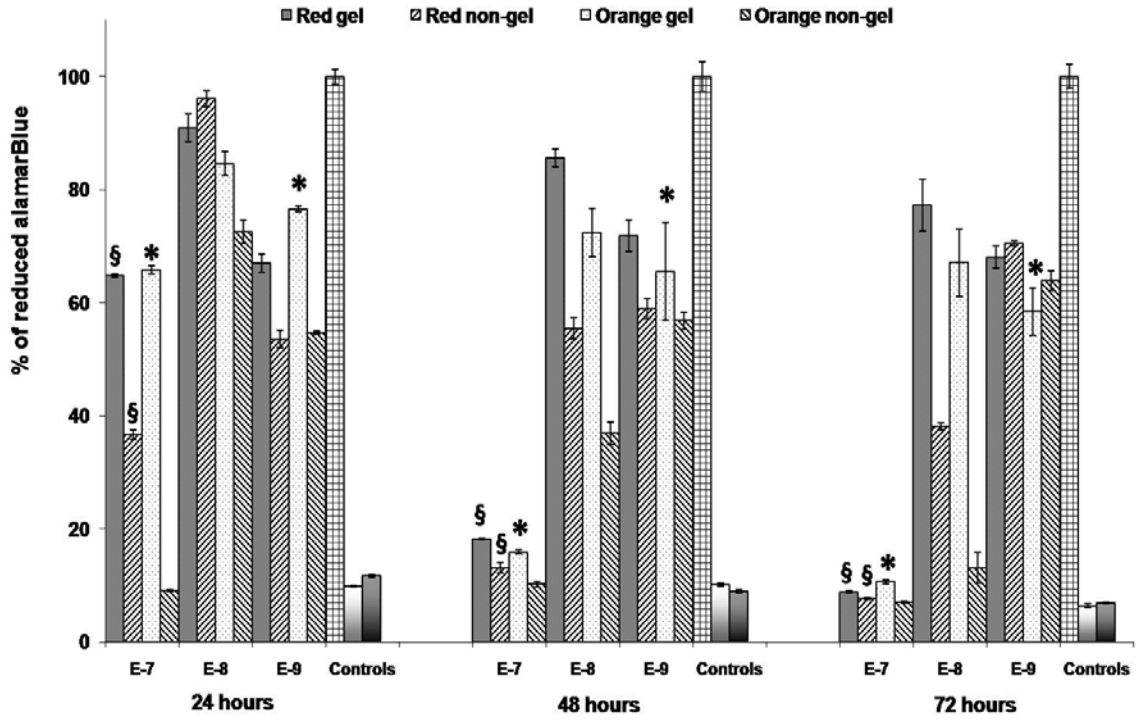

Figure 3.11: AlamarBlue assay at 24, 48 and 72 hours showing the viability of PC12 cells after treatment with varying concentrations [$10^{[(-7) - (-9)]}$ M] of the gel and non-gel QDs. From left to right, controls [positive, negative, background] are also shown. § denotes examples of statistical significance due to effect of gelatine, * denotes examples of statistical significance due to effect of concentration using a one- way ANOVA ($p< 0.05$) by Tukey's mean comparison.

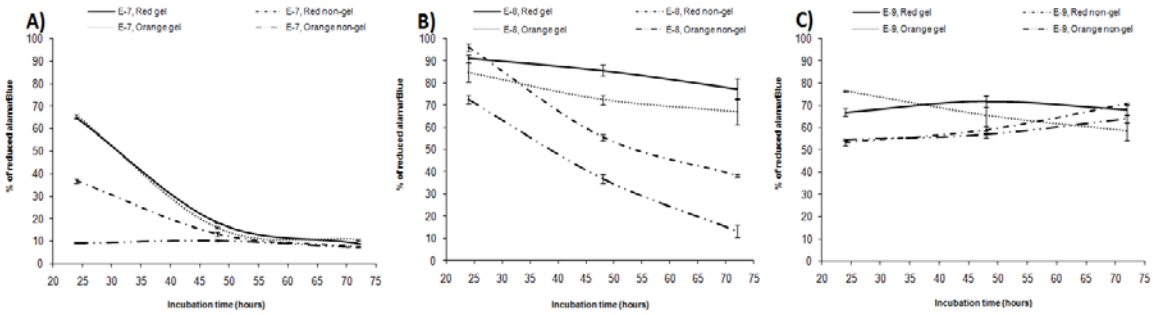

Figure 3.12: Graphical representation of the histogram results obtained from the alamarBlue assay. (A, B, C) represent the % reduced alamarBlue against incubation time for both gel and non-gel QD concentrations of E^{-7}, E^{-8}, E^{-9} respectively.

3.2.3.2 PicoGreen Assay

PicoGreen kit Quant-iT^{TM} dsDNA High-Sensitivity Assay Kit (Invitrogen) was used to quantify the amount of double stranded (ds) DNA in ng / µl.

The graph shown in Figures 3.13 and 3.14 illustrates the total amount of DNA present (ng / µl) in live PC12 cells after 24, 48 and 72 hours of co-incubation with both the gel and non-gel QDs. This assay allows us to directly relate the impact of the QDs on the overall cell population.

At 10^{-7} M QD concentrations, the histograms for the two QD types trend somewhat similarly to those seen for alamarBlue. Once again, responses never reach that of the control samples indicating the negative effect that the QDs have on this system. However, higher responses are once again recorded for the gel QDs after 24 hours and unlike the alamarBlue assay, the gel QDs show significantly higher results after 48 hours compared to the non-gel QDs. As before after 72 hours, both QD types elicit response similar to negative controls.

These data indicate that this assay seems to be more robust than the alamarBlue. This is an extremely sensitive assay to DNA concentrations and unlike the responses seen previously; there is an apparent shift in cell survival to longer co-incubation times. For example, responses for gel and non-gel QDs were comparable after only 48 hours with alamarBlue, while for PicoGreen this now occurs at 72 hours and this apparent shift continues as the concentrations are reduced.

As the QD concentrations are reduced to 10^{-8} M, we can see that after 24 hours DNA responses are approaching comparability with positive controls. Small differences once again favouring the gel QDs can be seen and these continue up to 48 hours. Notably, as recorded before, the orange non-gel QDs begin to show the lowest response indicating their increased impact on cell survival.

Only at 72 hours do we see responses drop below positive controls and significant differences can be seen between the two QD types with once again the gel QDs producing higher responses. Thus, comparing the two assays at this 10^{-8} M QD concentration, the shift to longer co-incubation times is clear indicating of increased cell survival rates and their ability to replicate for longer even in the presence of these toxic entities.

Similarly to the alamarBlue, there is a sense of consistency throughout the PicoGreen assay over all time points at 10^{-9} M QD concentrations. DNA responses are comparable

to positive controls and do not drop significantly even after 72 hours of co-incubation. This highlights the robustness of this cellular process to toxic influences at this concentration and also emphasizes the hormetic effect (Calabrese and Baldwin 2002, Jan et al. 2008).

These results further corroborate those from the alamarBlue assay verifying that the nature of the QD surface (gel or non-gel) greatly influences their behaviour and the resulting viability of the cells.

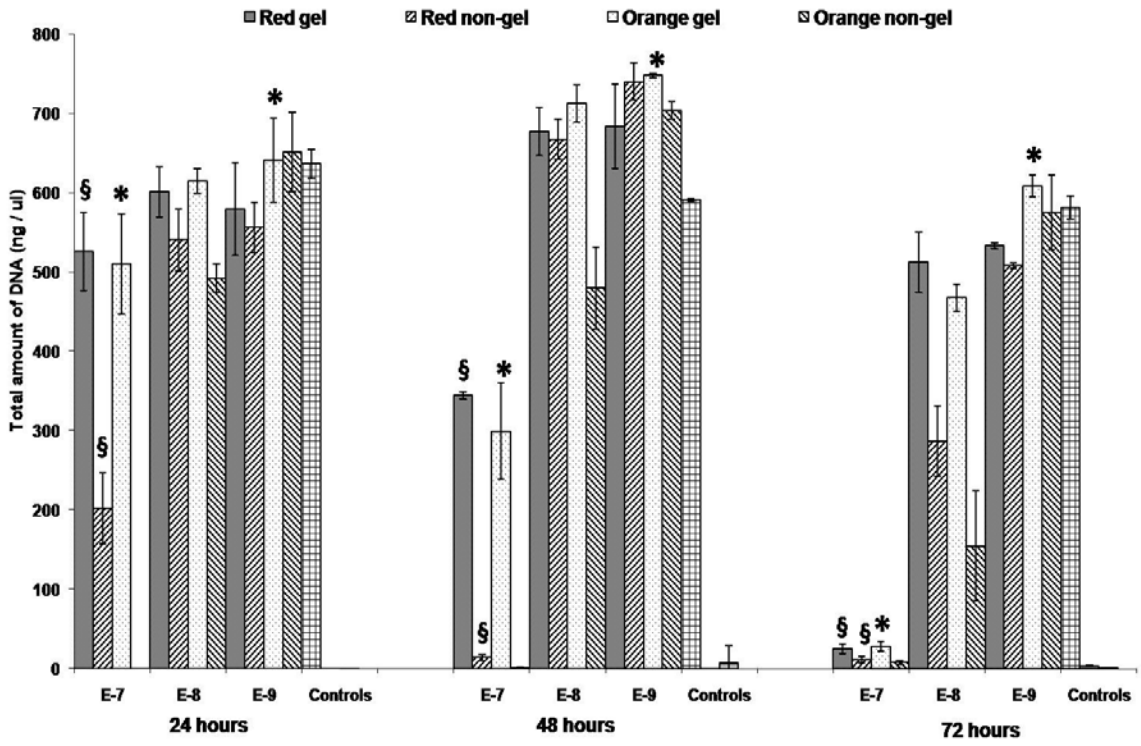

Figure 3.13: PicoGreen assay at 24, 48 and 72 hours illustrating the amount of DNA (ng/µl) measured from PC12 neurons following co-incubation with varying concentrations $10^{-7-(-9)}$ M of the gel and non-gel QDs. From left to right, controls [positive, negative, background] are also shown. § denotes examples of statistical significance due to effect of gelatine, * denotes examples of statistical significance due to effect of concentration using a one- way ANOVA ($p< 0.05$) by Tukey's mean comparison.

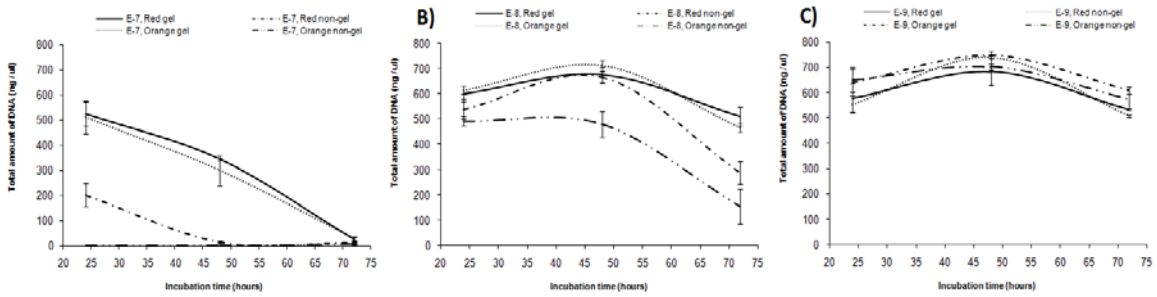

Figure 3.14: Graphical representation of the histogram results obtained from the PicoGreen assay. (A, B, C) represent the total amount of DNA (ng/µl) against incubation time for both gel and non-gel QD concentrations of E^{-7}, E^{-8}, E^{-9} respectively.

3.2.3.3 Proliferation ELISA BrdU

A Colorimetric Immunoassay was measured for the quantification of cell proliferation. This was based on the measurement of BrdU incorporation during DNA synthesis for the PC12 cells treated with different concentrations of gel and non-gel QDs. This cell proliferation allows us to extrapolate the healthy nature of the cells following co-incubation times of up to 72 hours. This assay is somewhat different from those previously examined as those cellular processes may still occur in cells that are not proliferating.

The graph shown in figures 3.15 and 3.16 illustrates the measured response for cell proliferation upon co-incubation with the QDs after 24, 48 and 72 hours. Notably, negative and background control responses are significantly higher than those seen for alamarBlue and PicoGreen.

Initially after 24 hours at 10^{-7} M QD concentrations, we can see a distinction between the less toxic gel and non-gel QDs however this levels off approaching negative controls at 48 and 72 hours. As the concentration drops to 10^{-8} M, we can once again see the significant influence of the gelatine capping. At 24 and 48 hours the non-gel QDs are substantially more toxic approaching negative controls, while gel QDs maintain parity with positive controls. Little distinction is recorded at 72 hours illustrating the negative impact that prolonged co-incubation with the QDs has on cell proliferation at this concentration.

Similarly to previous assays, little distinction can be made between QD types as the concentration is reduced to 10^{-9} M. After 24 hours, all QDs elicit responses in line with positive controls while after 48 and 72 hours, the red gel QDs once again showed the

least detrimental effect on cell responses. Overall we can see a general trend towards a drop in cell proliferation with incubation time and the drop in responses for positive controls highlights the delicate nature of maintaining cell proliferation over extended co-incubation times. This also illustrates the extremely sensitive nature of this assay to external perturbation. Even though cell activity decreased during this assay application the results do show a similarity to those previously determined, albeit on a reduced scale.

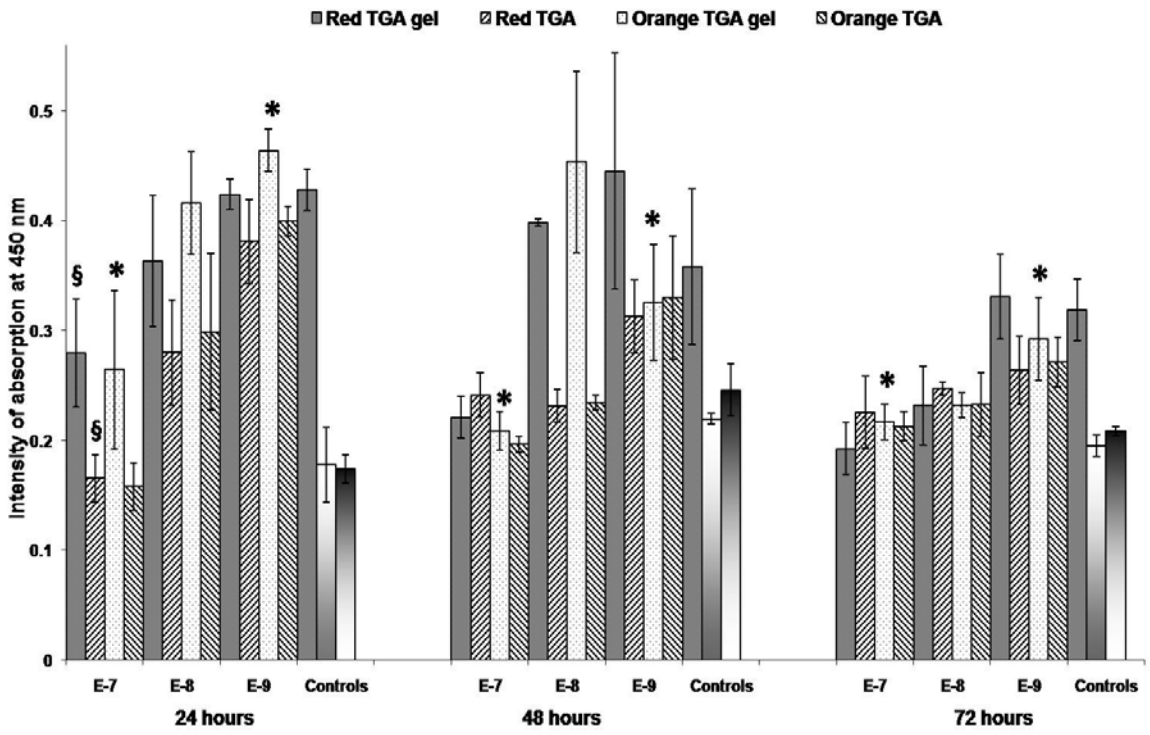

Figure 3.15: ELISA BrdU assay at 24, 48 and 72 hours illustrating (by intensity of absorption at 450 nm) the amount of cell proliferation following co-incubation with varying concentrations $10^{-7-(-9)}$ M of the gel and non-gel QDs. From left to right, controls [positive, negative, background] are also shown. . § denotes examples of statistical significance due to effect of gelatine, * denotes examples of statistical significance due to effect of concentration using a one- way ANOVA ($p < 0.05$) by Tukey's mean comparison.

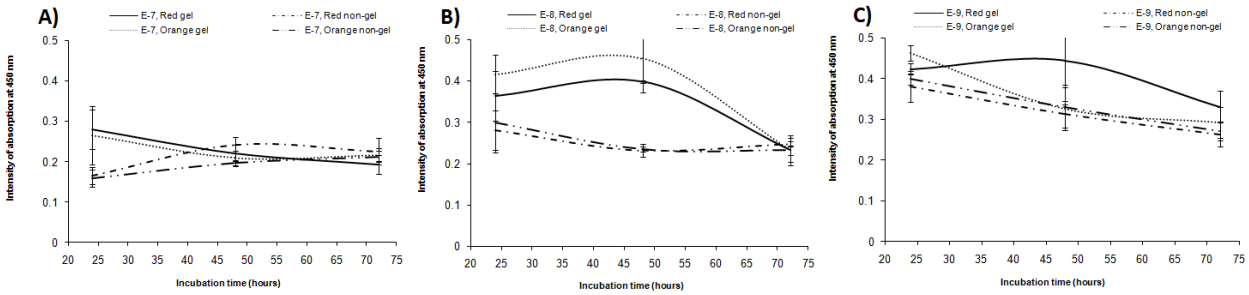

Figure 3.16: **Graphical representation of the histogram results obtained from the ELISA BrdU. (A, B, C) represent the intensity of absorption (measured at 450 nm) against incubation time for both gel and non-gel QD concentrations of E^{-7}, E^{-8}, E^{-9} respectively.**

3.3 Discussion

As QDs are essentially a combination of toxic materials, their negative impact on cell health is to be expected, however as cell response seems to level off we can postulate as to the reasons for the induced QD toxicity. The PC12 cells themselves can react to the presence of a foreign object, which may be the reason that overall QD cell responses are lower than the controls even after only 24 hours at low (10^{-9} M) concentrations. From our data it is also notable that at 10^{-9} M QD concentrations, the protective effect of gelatine coating was not obvious, with the sole exception of orange QDs at 24 hours. Thus, it can be argued that increases in cell viability at lower QD concentrations make it difficult for the protective effect of gelatine to be seen. CdTe QDs exert cytotoxicity characterised by decreases in the metabolic activity. The most common pathways involved in the toxicity of QDs are related to Reactive Oxygen Species (ROS). These free radicals act by activating different apoptotic pathways such as caspase-9-, caspase-3 and JNK (Chan Wen-Hsiung et al. 2006a). Some studies have shown involvement of MAPK pathways *via* over-expression of TNF-α CxCl8 (Lee H-M 2009) or AP-1 and PTK pathways mediated by MMP2 and 9 over-expression (Wan R 2008). Although there are different pathways involved, there is no obvious predilection for particular pathways in a particular cell line. A recent study with PC-12 cells has also shown involvement of reactive oxygen species (ROS) (J. Lovrić et al. 2005), where the authors have shown interactions of QDs with sub-cellular components and the detrimental effect

of uncapped versus capped QDs (Lovrić et al. 2005). This may indicate that the concentration of the leached atoms or reactive oxygen species even from non-gel QDs is so low at 10^{-9} M as to minimally impact the cells beyond the toxicity induced by their very presence.

Throughout the assay, we can see a progressive increase in cell viability for gel compared to non-gel QDs, indicating that the gelatine must act as an effective barrier towards these processes occurring. While it does not prevent the resulting negative impact on the cells, the gelatine seems to effectively slow down the adverse effects of the QDs on cell viability, allowing for longer cell survival, thus enhancing imaging and analysis over elongated co-incubation times.

The QD surface must be protected from the harsh intracellular environment if the cells are going to survive long enough to enable useful information about their behaviour and response to be gathered. The presence of gelatine on the QD surface clearly helps to reduce the impact of low intra-cellular pH ranges and the interactions of the various proteins present from breaking down the surface structure and releasing the "naked" toxic core atoms. Overall however the gelatine helps to nullify the toxic effects induced by the QDs; however the localisation of the QDs and their final destination must also play a role as there are variations in the impact that the different QD sizes and types have on each distinct cell response. This is quite significant and will require further investigation to fully determine and understand how changes in QD type, structure, surface functionality and concentration may impinge on the various cellular processes that occur during co-incubation.

3.1 Conclusion

In conclusion, we have co-incubated and analysed undifferentiated PC12 cells over extended incubation times (up to 72 hours) with both gelatinised (gel) and non-gelatinised (non-gel) thioglycolic acid capped CdTe QDs. We have visually inspected QD localisation, cell morphology and behaviour at a range of QD concentrations (10^{-7} – 10^{-9} M). The presence of the QDs at 10^{-7} M resulted in the death of all cells while at

concentrations of 10^{-9} M, the QDs were up taken primarily in the cytoplasm of the PC12s and did not initiate any detrimental effects.

Utilising alamarBlue (cell viability), Picogreen (DNA quantification) and ELISA BrdU (quantification of cell proliferation) assays we have measured and analysed cell response to co-incubations up to 72 hours with both gel and non-gel QDs. We have noted that throughout all our experiments, cell response varied in proportion to QD size, composition and concentration.

QD size significantly impacted measured responses. For the alamarBlue and PicoGreen assays at 10^{-7} & $^{-8}$ M QD concentrations, the orange non-gel QDs consistently produced lower cell responses. This indicates that the increased cellular penetration of these smaller QDs resulted in enhanced adverse effects compared to their larger red counterparts. Notably, these effects were significantly nullified by the gelatine coating with similarly sized gel QDs producing higher response throughout.

Increased QD concentrations also lead to a decrease in all measured cell responses. Notably however, it is evident at all time points that the gelatine coating has a protective effect as cell viability and survival rates are significantly higher for gel compared to non-gel QDs. Elongation of co-incubation times (up to 72 hours) also highlighted the importance and the significance of the gelatine for QD surface protection. The assays have shown that the gel QDs were consistently less toxic than their non-coated counterparts at concentrations up to 10^{-9} M. The presence of gelatine enables enhanced cell survival and proliferation at 10^{-8} M compared to non-gel QDs, while its influence is negated at 10^{-9} M concentrations over the longer co-incubation times. Thus, the 10^{-8} M QD concentration appears to act as a threshold for the initiation of deleterious effects. At 10^{-9} M concentrations, there appears to be a transition between the influences of QD surface structure (gel or non-gel) and QD concentration. The protective nature of the gelatine is countered by the drop in QD concentration and little variance was noted between the two QD types indicating that at this concentration the cells were unperturbed by the presence of either QD type.

CHAPTER 4: EFFECT OF QDS ON DIFFERENTIATED PC12 CELLS

4.1 Background and aims

Quantum Dots (QDs) has a major hindrance to use it in biological applications directly without modification because of inherent cytotoxicity. Previously, we have investigated the cytotoxicity of QDs by analysing the outcome of co-incubating a range of concentrations of various types of QDs with non-differentiated PC12 cells (Prasad et al. 2010b). In this chapter, we have studied the viability, cyto-toxicity and apoptosis (caspase activation) and localization of Gelatinised and non-gelatinised QDs by varying their concentrations to prevent cytotoxicity in the long term in differentiated PC12 cells. When treated with nerve growth factor (NGF), PC12 cells become differentiated and have functional properties enabling them to behave in a manner similar to neuronal cells (Greene et al. 1987). Their phenotype may not be similar to primary nerve cells as their origin is from tumour cells, however, in the presence of NGF they have the ability to produce neurites, synthesise neurotransmitters and receptors and exhibit the electrical activity which are characteristic of neurons (Radio et al. 2010). Although many cytotoxicity studies of QDs have been done with PC12 cells, in this study we clearly analysed the viability, cytotoxicity and apoptosis at different time periods and discussed the effect of exposure of QDs on PC12 cells before and after the neurites were grown. The apoptotic process involved in the cell death machinery and also the intrinsic behaviour of QDs upon uptake by the cells have been analysed. To make them as more potent neuroprosthetic and neurotherapeutic agents, CdTe QDs (gelatinised and non-gelatinised Thioglycolic acid (TGA) capped) have been investigated in this study with differentiated pheochromocytoma 12 (PC12) cells. The QD – cell interactions were investigated by MTT and APOTOX-Glo Triplex assays and also from confocal microscopic images to probe how individual cell functions (Cytotoxicity, Viability and Apoptosis) were affected by exposing the QDs to extended (up to 17 days) co-incubation times. In the same experiment, differentiated PC12 cells were also exposed to QDs after the neurites were grown for 10 days.

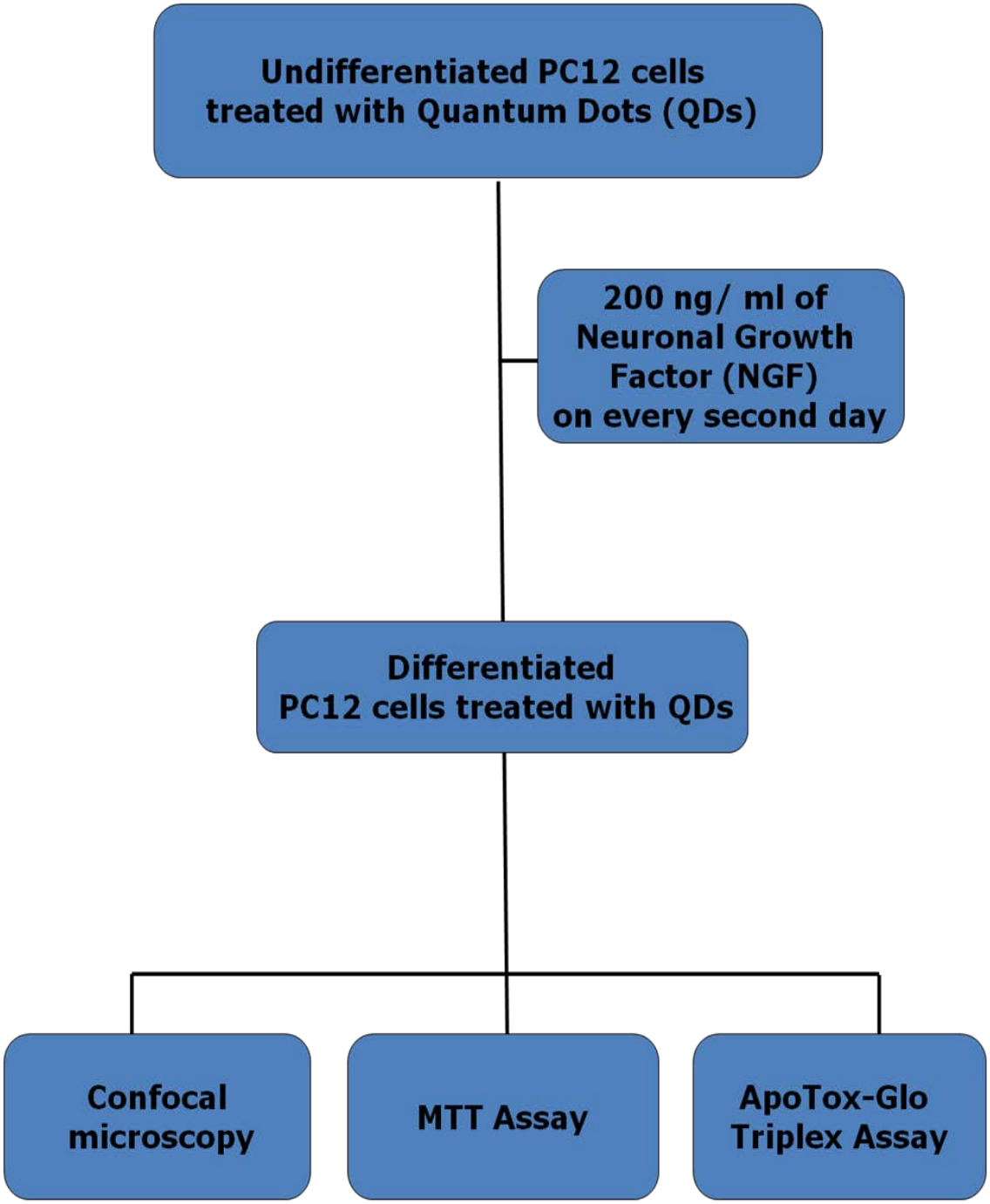

Figure 4.1: Flow chart showing experimental design of differentiated PC12 cells treated with QDs.

4.2 Results

4.2.1 Uptake of QDs and their effect on cell morphology of differentiated PC12 cells

4.2.1.1 Confocal imaging of differentiated PC12 cells

Confocal images were taken to visually inspect QD uptake, localisation and cell morphology following QDs exposure before and after the differentiation of PC12 cells (Figures 4.2, 4.3 and 4.4).

As seen in figure 4.2, the QDs were found to be located within the cytoplasm of differentiated PC12 cells in all the images. The cells exposed to gel QDs (red and orange) (panels A and C respectively) exhibited a similar morphology and neurite growth to the control (no treatment of QDs) in panel E. The cells exposed to non-gel QDs (panels B and D respectively) appeared rounded with partial inhibition of neurite growth (red non-gel) or no neurite growth (orange non-gel). This was attributed to the enhanced cytotoxicity of the smaller orange QDs relative to their larger red counterparts. These cellular morphologies indicated that the presence of gelatine provides a protective surface coating for the QDs and prevents the initiation of deleterious effects on the morphology and cellular activity of differentiated PC12 cells.

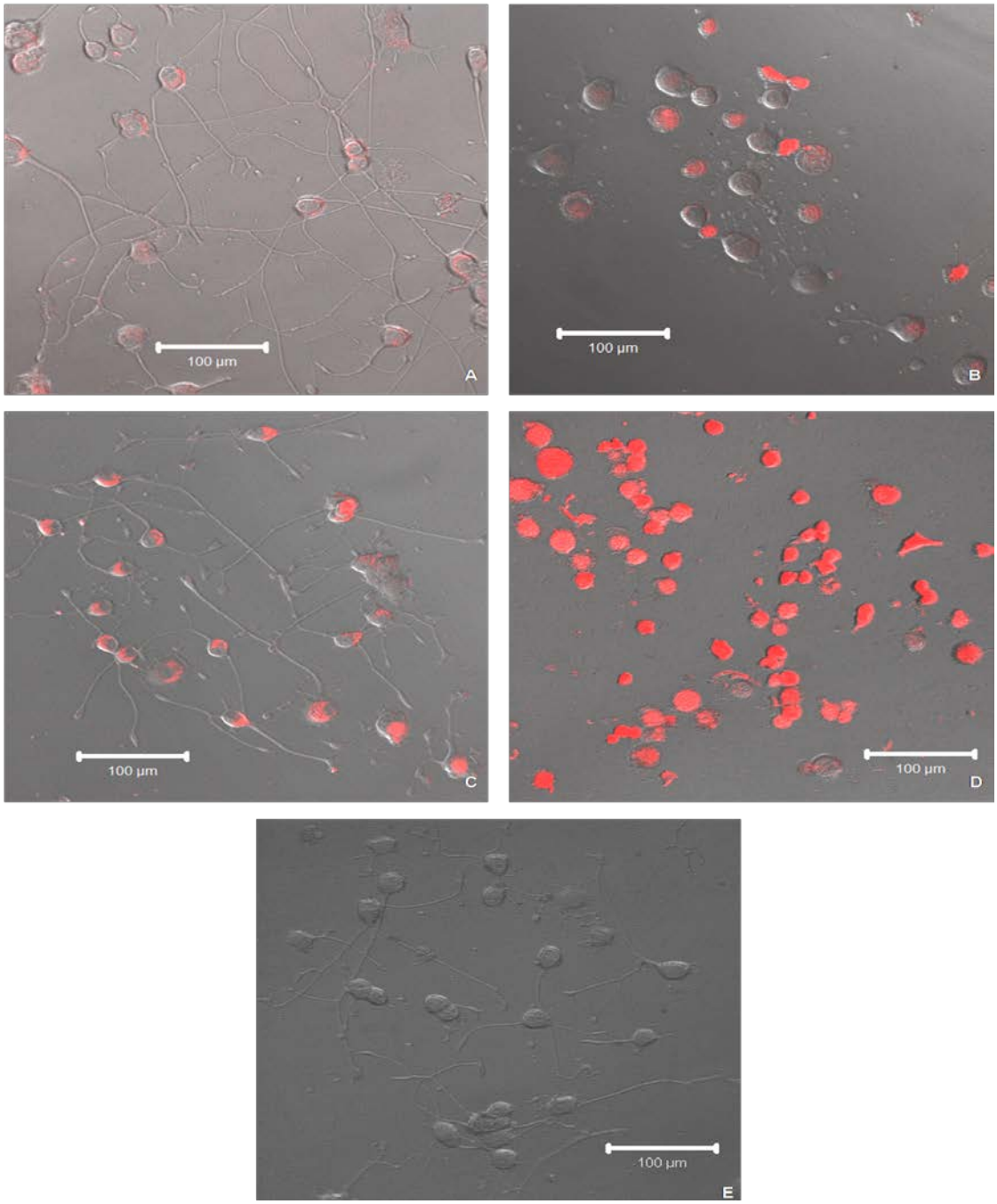

Figure 4.2: Overlaid differential interference contrast (DIC) images with corresponding fluorescent confocal images of differentiated PC12 cells exposed to 10^{-9} M concentrations of QDs showing Red Gel QDs in (A), Red Non-Gel QDs in (B), Orange Gel QDs in (C), Orange Non-Gel QDs in (D) and Control in (E) without exposure to QDs following 14 days of co-incubation [scale bar = 100 µm].

In figure 4.3, the nucleus was stained with DAPI (blue) and the cytoplasm was actin stained (green). The gel QDs (red luminescence) in panel A are visible predominantly in the cytoplasm and their presence, even after 17 days of co-incubation, did not seem to significantly perturb the cells. The QDs were also parsimoniously distributed in the neurites. The cell morphology did not change compared to the controls in panel B.

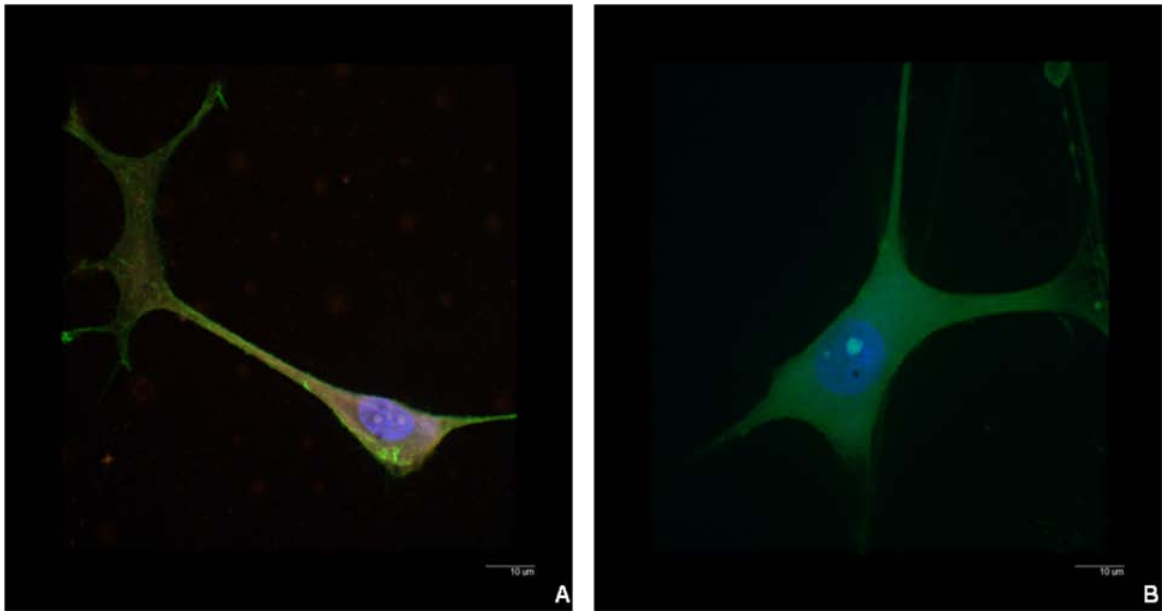

Figure 4.3: Overlaid fluorescent confocal images to illustrate the morphology of the actin stained differentiated PC12 cells exposed to the Red gelatinised QDs (A) and differentiated PC12 cells without exposure to QDs as a control (B) following 17 days of co-incubation. [Scale bar = 10 µm].

Figure 4.4 shows the overlaid differential interference contrast (DIC) images with corresponding fluorescent images of the differentiated PC12 cells treated with NGF for 6 days prior to exposure to 10^{-9} M concentrations of the QDs. Red gel QDs are shown in panel A, red non-gel QDs in panel B, orange gel QDs in panel C and orange non-gel QDs in panel D following 7 days of co-incubation. The QDs were found to be located within the cytoplasm of differentiated PC12 cells in all the images. The cells exposed to red and orange gel QDs (panels A and C respectively) showed similar morphology and neurite growth compared to the control (no treatment of QDs) in panel E. There was evidence of slight neurite degeneration in the cells exposed to orange gel QDs more so than in the cells exposed to red gel QDs, illustrating that the red gel QDs are more cyto-protective than the orange gel QDs. The cells exposed to red non-gel and orange non-

gel QDs (panels B and D respectively) appeared rounded with partial degeneration and full degeneration (fragmentation) of neurites respectively, which suggests that orange non-gel QDs are more cytotoxic than red non-gel QDs.

These initial observations using confocal microscopy illustrate the effect of exposure of QDs before and after the differentiation of PC12 cells on cell survival and morphology. In order to further investigate the cell behaviour, several assays were used to study the effect on cell proliferation, cytotoxicity, viability and apoptosis.

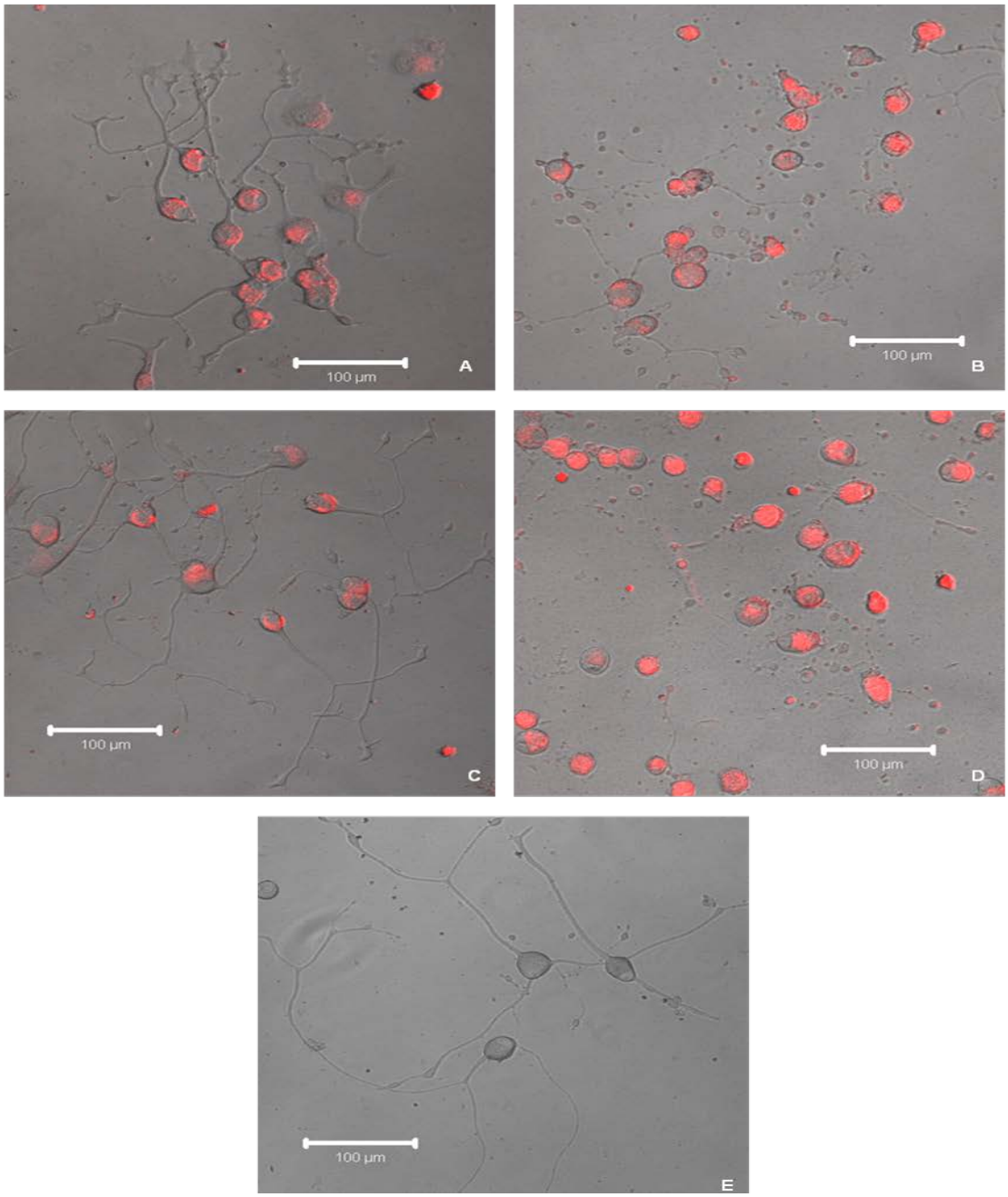

Figure 4.4: Differential interference contrast (DIC) images of differentiated PC12 with overlaid corresponding fluorescent confocal images, treated with NGF for 6 days prior to exposure to 10^{-9} M concentrations of QDs showing Red Gel QDs in (A), Red Non-Gel QDs in (B), Orange Gel QDs in (C), Orange Non-Gel QDs in (D) and Control in (E) without exposure to QDs following 7 days of co-incubation [scale bar = 100 µm].

4.2.2 Effect of QDs on cellular activity of differentiated PC12 cells

Results were analysed using a one-way ANOVA analysis by Tukey's mean comparison, where results with a p-value of less than 0.05 were reported as statistically significant and their occurrence can be deemed to be due to interactions in the system under investigation and chance variation can be eliminated. MTT (cell proliferation) and APOTOX Triplex (cytotoxicity, viability and apoptosis) assays were run to analyze the effect of different QD types and size following exposure of QDs before and after the differentiation of PC12 cells.

4.2.2.1 MTT Assay

The graph in figure 4.5 depicts the results of an MTT assay for PC12 cells treated with NGF and exposed to QDs after periods of 10 and 16 days. After 10 and 16 days, the proliferation of cells exposed to red gel QDs was the same as the positive controls whereas the proliferation of cells exposed to smaller (orange) gel QDs was significantly reduced. This clearly showed that smaller orange gel QDs are significantly more toxic than larger red gel QDs towards differentiated PC12 cells. Similarly, smaller orange non-gel QDs appeared to be significantly more cytotoxic than larger red non-gel QDs as co-incubation periods were prolonged. Overall, gel QDs was found to be less cytotoxic than their non-gel counterparts. The absorption of MTT, and therefore cell proliferation, further decreased when the co-incubation time was extended up to 16 days. Gel and non-gel QDs exhibited the same trend with regards to the impact of particle size on cytotoxicity. Even after prolonged exposure time, smaller QDs had a higher adverse effect on cell proliferation compared to their larger counterparts. As observed from the results displayed above, the gelatine layer on the surface of the gel QDs regardless of size proved to effectively reduce their cytotoxicity. This suggests that cell toxicity of QDs is due to the leakage of cadmium ions or from reactive oxygen species as we discussed in our previous paper with non-differentiated PC12 cells (Prasad et al., 2010).

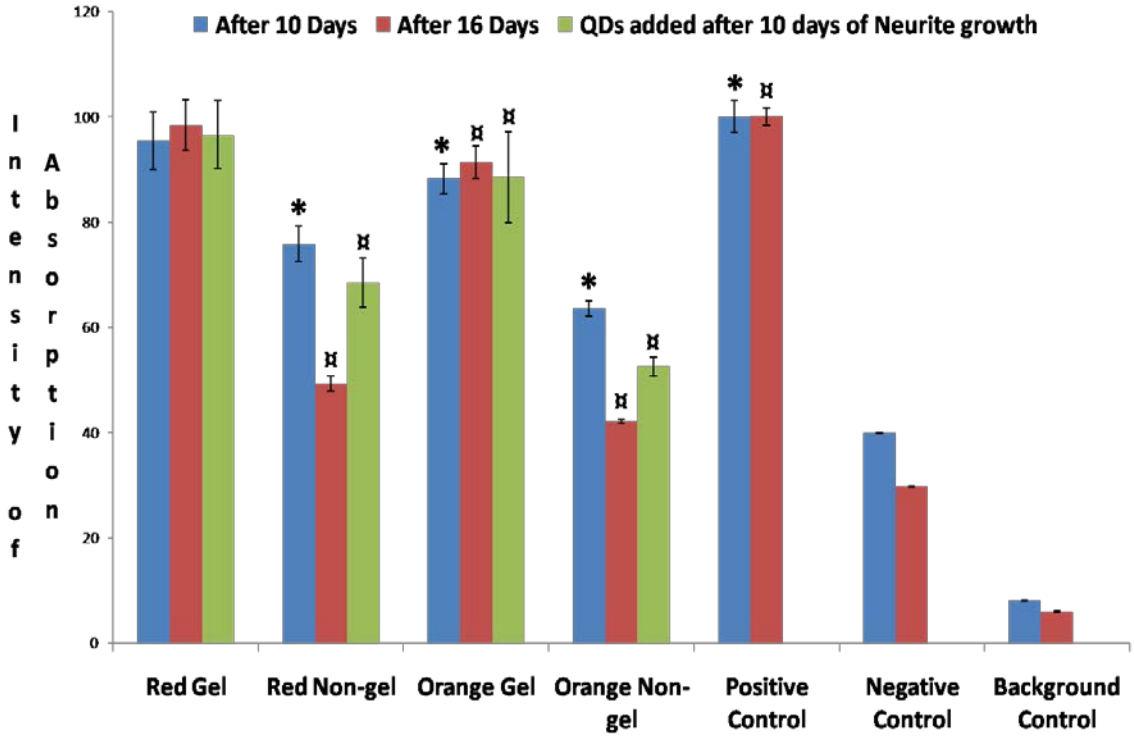

Figure 4.5: MTT assay after 10 and 16 days showing the rate of proliferation of differentiated PC12 cells after exposure to concentrations [$10^{(-9)}$ M] of the gel and non-gel QDs. Positive Control are differentiated PC12 cells without exposure to QDs and also the graph shows differentiated PC12 cells which were exposed with Red and Orange QDs of gel and non-gel types after neurites were grown for 10 days. Symbols * and ¤ denotes examples of statistical significance in comparison with positive controls using a one- way ANOVA ($p< 0.05$) by Tukey's mean comparison.

4.2.2.2 ApoTox-Glo™ Triplex Assay

The graph in figure 4.6 depicts the results of an APOTOX- Glo Triplex assay showing the cytotoxicity of PC12 cells treated with NGF and exposed to red and orange QDs of gel and non-gel types along with controls. The cells were also similarly treated after the neurites were grown for 10 days. After periods of 7, 12 and 17 days, the cytotoxicity of red gel QDs was comparable to the untreated cell controls but in the case of smaller gel QDs the cytotoxicity increased significantly. This clearly showed that smaller orange gel QDs are significantly more toxic than the larger red gel QDs. The smaller orange non-gel QDs also exhibited significantly more cytotoxicity than the larger red non-gel QDs as co-incubation periods were prolonged, and non-gel QDs were more cytotoxic than gel ones. Cytotoxicity levels increased as the co-incubation periods were prolonged

up to 17 days. Gel and non-gel QDs exhibited the same trend with regards to the impact of particle size on cytotoxicity, with the smaller ones being more toxic. Furthermore, the cells exposed to non-gel QDs were found to be more affected than those exposed to gel QDs. We found the same trend of cytotoxicity after neurites were grown for 10 days prior to QD exposure. This shows that there is absolutely no inhibition of cellular interactions with QDs after the cells were grown with neurites.

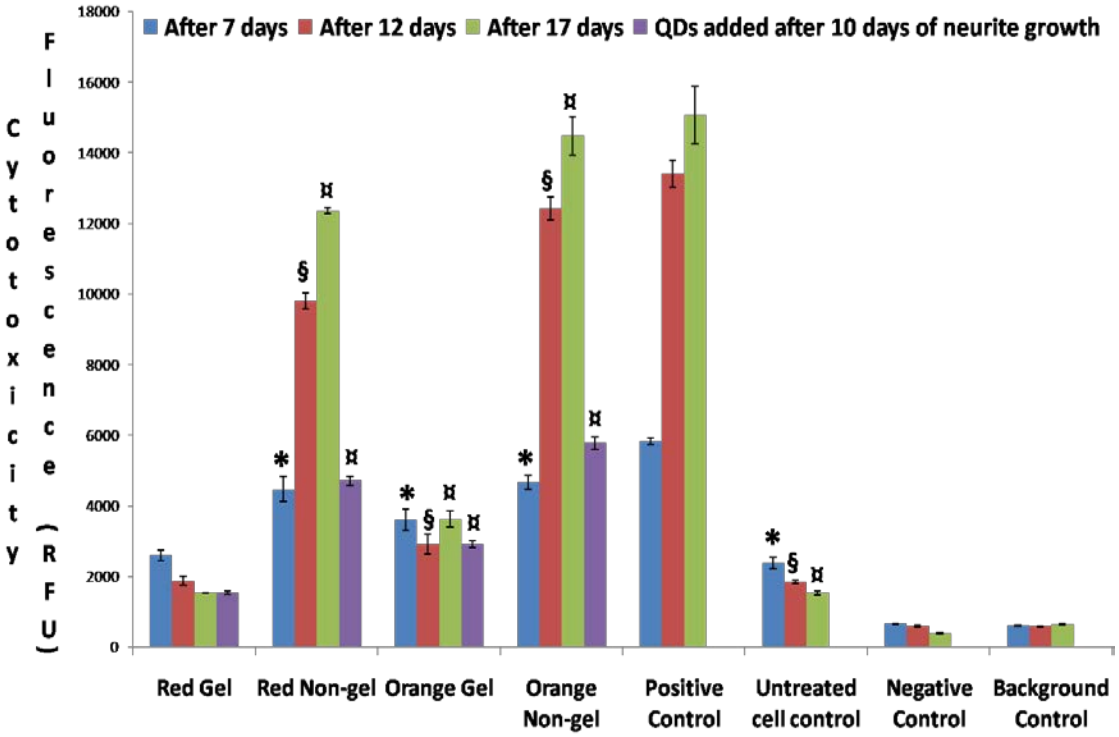

Figure 4.6: ***APOTOX GLO Triplex assay above showing the graph of cytotoxicity of differentiated PC12 cells after 7, 12 and 17 days treated with red and orange QDs of gel and non-gel types along with controls and also the cells were treated with Red and Orange QDs of gel and non-gel types after neurites were grown for 10 days. Symbols *, § and ¤ denotes examples of statistical significance in comparison with untreated cell controls using a one- way ANOVA (p< 0.05) by Tukey's mean comparison.***

The graph in figure 4.7 depicts the results of an APOTOX Triplex assay showing the viability of PC12 cells treated with NGF and exposed to red and orange QDs of gel and non-gel types along with controls and the viability of cells treated with red and orange QDs of gel and non-gel types after neurites had been grown for 10 days. After periods of 7, 12 and 17 days, the viability of cells exposed to red gel QDs was the same as that

of untreated cell controls, however the viability of cells exposed to the smaller orange gel QDs decreased significantly. Similar to previous assays, cells exposed to the smaller orange QDs were significantly less viable than cells exposed to the larger red QDs (both gel and non-gel) as co-incubation periods were prolonged. Viability levels decreased as the co-incubation periods were prolonged up to 17 days, and retained the same trend with regards to gel/non-gel and size influence. The cells exposed to gel QDs were found to be more viable than the ones exposed to non-gel QDs and were equally viable as untreated controls (negative controls). We found the same trend of cellular viability after neurites were grown for 10 days and cells were subsequently treated with QDs. This also shows that there is absolutely no inhibition of cellular interactions with gel QDs after the cells were grown with neurites.

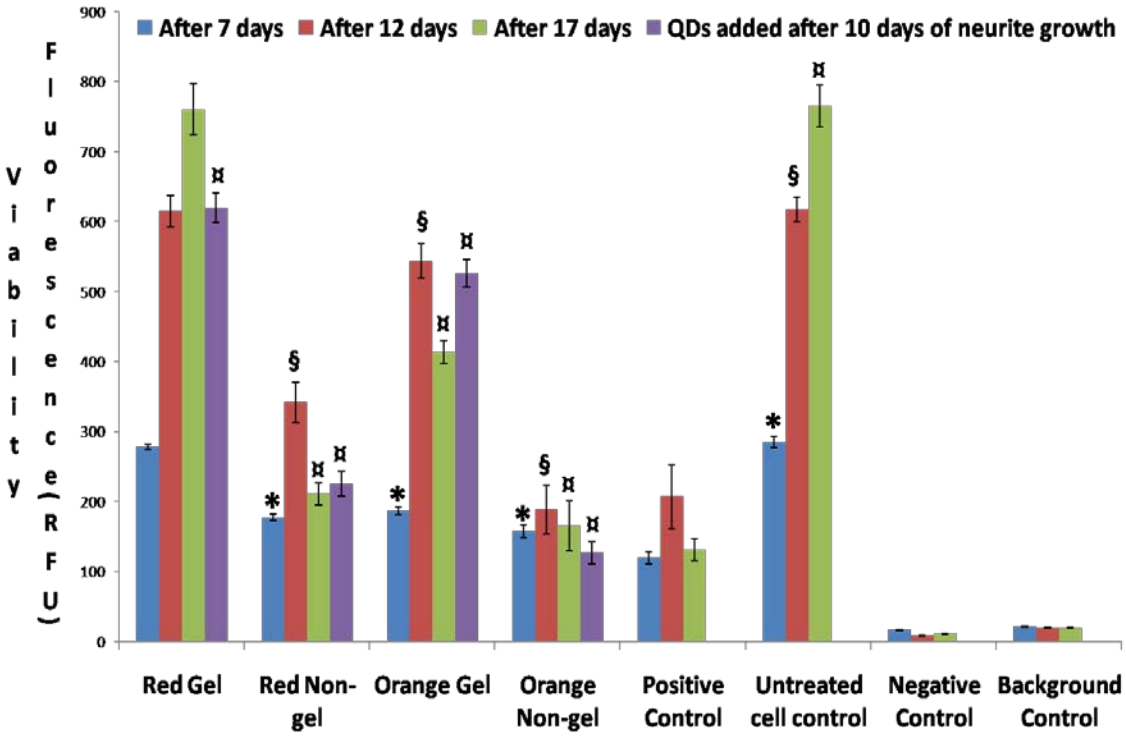

Figure 4.7: APOTOX GLO Triplex assay above showing the graph of viability of differentiated PC12 cells after 7, 12 and 17 days treated with red and orange QDs of gel and non-gel types along with controls and also the cells were treated with Red and Orange QDs of gel and non-gel types after neurites were grown for 10 days. Symbols *, § and ¤ denotes examples of statistical significance in comparison with untreated cell controls using a one- way ANOVA ($p< 0.05$) by Tukey's mean comparison.

The graph in figure 4.8 depicts the results of an APOTOX Triplex assay showing the apoptosis of PC12 cells treated with NGF and exposed to red and orange QDs of gel and non-gel types along with controls and also the apoptosis of cells which were treated with red and orange gel and non-gel QD types after neurites had been grown for 10 days. After periods of 7, 12 and 17 days, the apoptotic activity of cells exposed to red gel QDs was the same as that of untreated cell controls, whereas the apoptotic activity of cells exposed to smaller orange gel QDs was significantly increased. This illustrated that smaller orange QDs were significantly more cytotoxic than the larger red QDs for both gel and non-gel QDs as co-incubation periods were prolonged. Overall, non-gel QDs induced more apoptosis than gel QDs. Apoptotic activity levels increased with both gel and non-gel QDs as the co-incubation periods were prolonged up to 17 days and retained the same trend with regards to gel/non-gel and size influence. The cells exposed to non-gel QDs were found to undergo more cell death than the cells exposed to gel QDs. We found the same trend of cell death after neurites were grown for 10 days and subsequent treatment of the cells with QDs. This shows that there is absolutely no inhibition of cellular interactions with gel QDs after the cells were grown with neurites.

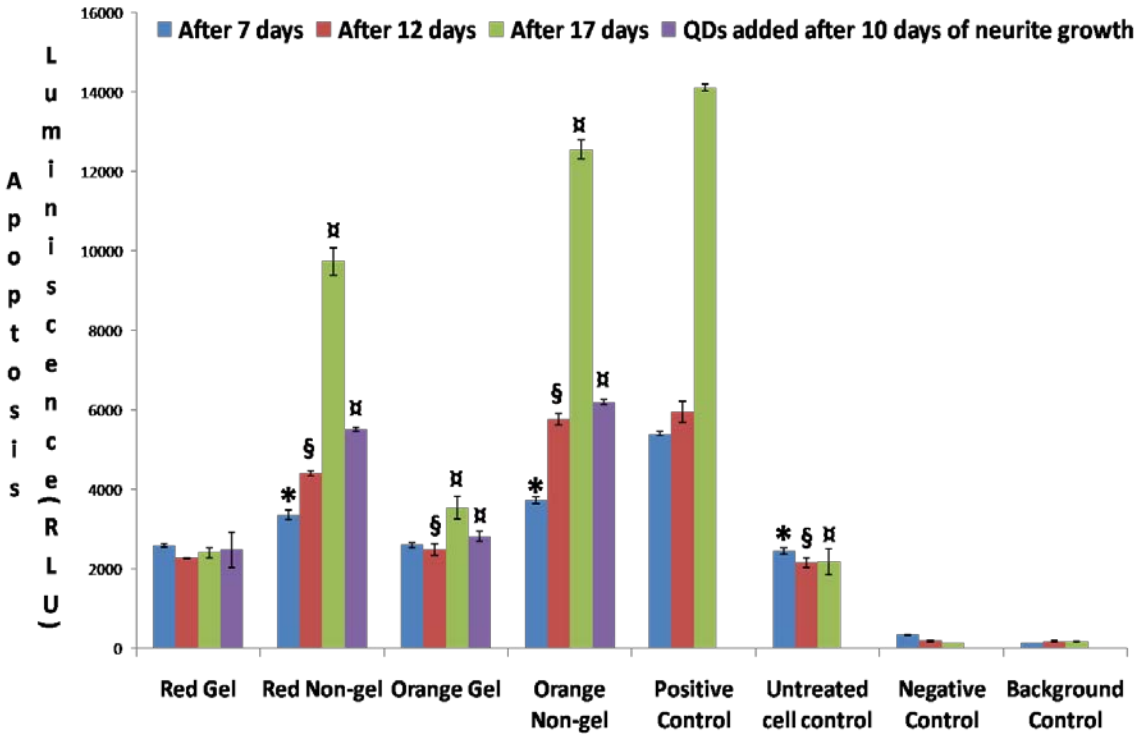

Figure 4.8: APOTOX GLO Triplex assay above showing the graph of apoptosis of differentiated PC12 cells after 7, 12 and 17 days treated with red and orange QDs of gel and non-gel types along with controls and also the cells were treated with Red and Orange QDs of gel and non-gel types after neurites were grown for 10 days. Symbols *, § and ¤ denotes examples of statistical significance in comparison with untreated cell controls using a one- way ANOVA ($p< 0.05$) by Tukey's mean comparison.

4.3 Discussion

The present study is aimed at defining the effect of gelatinated CdTe QDs on differentiated PC12 cells. The cellular uptake of QDs is mediated by proteins such as clathrins, which are coated to membrane vesicles on the cell surface at the entry (Byrne Stephen J et al. 2007a; Dawson et al., 2009; Watson et al., 2005). Non-specific binding occurred less frequently for PC12 cells (Vu et al., 2005) when compared to other cells like neuroblastoma cells as studied by Gomez et al. (Gomez et al., 2005). Confocal microscopy has been used to identify the localisation of the particles after cellular uptake, as shown in figure 4.2 and 4.3. Similarly to previously reported non-

differentiated PC12 cells (Prasad et al., 2010), gel QDs were mostly found in the cytoplasm, which became largely illuminated. This may be easily explained by the nature of the nanoparticles (QDs). The TGA-capped CdTe QDs used in this study were negatively charged thanks to the de-protonated carboxylic groups of the TGA molecules and they exhibit an average zeta potential of -40 mV. It has been shown in previous studies that negatively charged QDs have a strong tropism to core histones and histone-rich cell organelles (Conroy et al., 2008). This research has suggested that the surface charge of these nanoparticles may ultimately determine their cellular uptake and therefore their location within the cell. It has been suggested that the negatively charged QDs are drawn towards the nucleus due to molecular interactions with positively charged histones. This may explain why the majority of TGA-capped CdTe QDs reside in the cytoplasm (J. Lovrić et al., 2005), surrounding the nucleus as opposed to the neurites.

Macromolecules, such as proteins and RNA, responsible for genome structure and function must be transported by selective, energy-dependent mechanisms from the cytoplasm to the nucleus. The karyopherin family of proteins maintain this process of selective import and export into the nucleus and cytoplasm. The nuclear localisation signals, nuclear transport receptors and the proteins in the nuclear pore complex ensure that no unwanted molecules are transported into the nucleus (Cooper, 2007). This selective transport system could be the reason why QDs are not localised within the nucleus. A second reason why QDs seem to localise only in the cytoplasm could be due to entrapment within cell organelles such as endosomes, lysosomes and vesicles. However, examination of images of differentiated PC12 cells (Figures 4.2 and 4.3), shows some localisation of QDs within the neurites. This would mean that not all the QDs are accumulated within these cell organelles, but still are not observed within the nucleus (Byrne Stephen J et al. 2007a; Ruan et al., 2007).

Figure 4.4 displays a comparison of the morphological changes induced by exposure of cells to QDs of different sizes and structure. The degeneration of neurites observable mostly in the case of non-gel QDs was attributed to neuronal cell death and direct axonal toxicity, as evidenced by the study of Sanjeev Kumar Mahto et al., with differentiated PC12 cells inside microfluidic devices (Mahto et al., 2010). Another study also showed that the degeneration of neurites was due to autophagosomes or lysosomes produced in the cell cytoplasm and in the neurites, which traverse in both

anterograde and retrograde directions to destroy the already impaired mitochondria due to the toxicity of QDs (Yang et al., 2008).

Although observation of the cell morpology gave a rather clear idea of the trend in cytotoxicity among the different types of QDs, quantitative assays of the metabolic activity could provide a better understanding of the mechanisms involved. The MTT proliferation assay was designed to probe the activity of reductase enzymes as a measure of cell viability and proliferation. The results shown in Figure 4 indicated that gel QDs (both red and orange) did not significantly affect cell proliferation as compared to untreated control cell cultures. Non-gel QDs, however, caused a reduction of about 50% in cell proliferation. Interestingly, whether the cell differentiation occurred simultaneously or prior to QD treatment did not change the outcome of the assay. The MTT assay correlated well with the viability part of the APOTOX GLO Triplex assay (Figure 4.7), although the latter gave more subtle results, showing a discrepancy between red and orange QDs. This assay essentially assessed the cell membrane integrity and is therefore more sensitive than MTT which measures the enzyme level. Orange QDs are smaller in size and appeared to be slightly more cytotoxic then their larger red counterparts. It was previously reported by Lovric et al. (J. Lovrić et al., 2005) that QD cytotoxicity was inversely related to their size due to the fact that smaller particles may enter cells more readily thus interfering to a higher degree with the cell machinery. As expected, the cytotoxicity part of the APOTOX GLO Triplex assay produced similar results (Figure 4.6); gel QDs appeared to be much less cytotoxic than non-gel QDs, and orange (smaller) ones were more cytotoxic than red (larger) ones.

A recent study on the toxicity of QDs with PC12 cells has shown involvement of reactive oxygen species (ROS) (J. Lovrić et al., 2005) and the most common pathways involved in relation to toxicity of QDs with ROS has been discussed previously (Prasad et al., 2010). In the cell, mitochondria are cellular factories for the production of Adenosine Triphosphate (ATP) and are also a prime source of ROS production. In addition, they help to regulate the cytoplasmic calcium levels, pH and apoptosis. Abnormally increased levels of ROS (oxidative stress) during ischemia make it difficult for the neuronal cells to survive due to overwhelming multiple buffering mechanisms of ROS (Foster et al., 2006). Oxidative stress is a state in which glutathione (GSH) is depleted with accumulation of oxidized glutathione (GSSG) (Halliwell, 1999; Nel et al., 2006). Lower levels of ROS are easily neutralized by generation of GSH and

antioxidant enzymes. Protective or injury responses in the cells are characterized by the drop in GSH/GSSG ratio (Bell, 2003; Halliwell, 1999; Nel, 2005; Nel et al., 2006; Xiao et al., 2003). At lower oxidative stress, cellular redox hemostasis occurs, intermediate oxidative stress leads to inflammation and higher oxidative stress leads to cytotoxicity which finally leads to apoptosis (Halliwell, 1999; Nel et al., 2006).

Apoptosis is one form of cell death which involves the cell death machinery, Caspase-9, Apaf-1 and Cytochrome c. Chromatin margination along the nuclear membrane, nuclear condensation, budding and fragmentation are some of the features of apoptosis which can be seen in the cell morphology. DNA fragmentation, which is one of the hallmarks of apoptosis is thought to be induced by cadmium. Cadmium toxicity is thought to affect the cells by the production of ROS and can induce apoptosis through a mitochondrial caspase dependent pathway (Oh and Lim, 2006). Caspases, a family of cysteine proteases, carry out these complex biochemical events which cause cell morphology changes. Caspases are made up of initiator caspases such as caspases-8, -9 and -12, whose function is to activate downstream caspases, and executor caspases, such as caspases-3, -6 and -7, their function being to degrade cellular protein (Kondoh et al., 2002; Li et al., 2009).

In previous research on human neuroblastoma cells, Chan et al. described the apoptotic chain of events induced by CdSe QDs through the mitochondrial release of cytochrome c and activation of caspase-9 and caspase-3 (W H Chan et al., 2006). The trigger is the intracellular degradation of QDs, which leads to the release of free cadmium ions (Cd^{+2}) inside the cytoplasm. These free cadmium ions inside the cells are responsible for the formation of ROS, leading to oxidation of the phospholipid Cardiolipin, which helps in associating the cytocrome c with inner mitochondrial membrane (Shidoji et al., 1999). Due to oxidation of cardiolipin, cytochrome c is released, an important event in apoptotic signaling (Newmeyer and Ferguson-Miller, 2003). Release of cytochrome c is also due to ROS-induced changes in the conformation of the adenine nucleotide translocase, a protein which is involved in the formation of the mitochondrial permeability transition pore (McStay et al., 2002), and the voltage-dependent anion channel-selective permeabilization of the mitochondrial outer membrane (Madesh and Hajnoczky, 2001). It is thought that this release of Cytochrome c into the cytosol leads to Caspase-9 activation by Cytochrome c/Apaf-1 complex. Caspase-9 is the upstream caspase in the mitochondria-dependent apoptosis pathway and activates Caspase-3. In

our study, the apoptosis assay, while confirming the general trend among the various types of QDs, provided valuable information about the mechanisms involved in cell death upon QD treatment (Figure 4.8). The assay itself is based on the measurement of the activity of caspase 3/7 as an indicator of apoptosis. Therefore it can be concluded that QDs, in particular non-gel types, cause cell death via cadmium-induced mitochondrial release of cytochrome c and activation of caspase-9 and caspase-3 leading to apoptosis (Kondoh et al., 2002).

Long term exposure (up to 17 days) of PC12 cells to QDs both before and after undergoing differentiation displayed dramatic differences between non-gel and gel QDs. While the former exhibited a dramatic increase in cytototoxicity as measured by MTT and APOTOX GLO Triplex assays (Figures 4.5 to 4.8), the latter remained at a comparable level of toxicity as after 7 and 12 days of incubation. It was therefore concluded that the gelatine coating durably stabilized the QDs and created virtually no interference with cell functions over significant periods of time.

The results presented here are consistent with our published findings on non-differentiated PC12 cells (Prasad et al., 2010). Differentiated PC12 cells mimic neuronal cells behaviour, thus providing a model for QD interaction with neurons. The accumulation of nanoparticles in neurites was minor compared to the rest of the cytoplasm and did not appear to disturb the cell functions any further, even over extended periods of time (up to 17 days). In addition, we found that QDs did not affect differentiation itself, as proved by the growth of neurites in their presence.

4.4 Conclusion

There is clear evidence from MTT and APOTOX-Glo Triplex assay (Cytotoxicity, Viability and Apoptosis) and also from microscopic images that the gelatine-coating helps to reduce the toxicity of CdTe QDs and assists in protecting the cells themselves. This was observed indiscriminately when neurites were grown prior to or after exposure to QDs. The difference in toxicity and resulting cell death between the orange and red gel QDs is due to the smaller size of the orange QDs. By preventing leakage of cadmium ions from the QD core and providing a biocompatible interface, the gelatine

coating helps to delay caspase activation events that eventually lead to apoptosis. Gel QDs were shown neither to inhibit cell differentiation nor to be any more cytotoxic towards neuron-like differentiated cells than non-differentiated ones. This provided a good indication that these particles can remain in healthy and sensitive tissue for several days without damaging it, which opens applications in diagnostics and targeted drug delivery. This is an important starting point that can be used for development of other non-toxic nanoparticle-gelatine composites, which might have a range of potential biomedical applications such as controlled drug delivery, *in vivo* and *in vitro* diagnostics and anticancer therapy.

CHAPTER 5: EFFECT OF QDS ON HPMEC-ST1.6R CELLS

THE RESULTS OF THE EFFECT OF QDS ON HPMEC-ST1.6R CELLS HAS BEEN REMOVED DUE TO CONFIDENTIALITY FOR PUBLICATION

CHAPTER 6: EFFECT OF NANO-SURFACE ROUGHNESS OF SILICONES (PDMS) ON CELLULAR ACTIVITY OF NIH-3T3 CELLS

6.1 Background and aims

Poly(dimethylsiloxane) (PDMS or silicone) exhibit a broad range of beneficial properties that are exploited in biomaterials. Silicone is a versatile polymer because of its biological stability (Chang et al. 2007, Kheir et al. 1998) and low toxicity (Chang et al. 2007), the ease with which the hardness of silicone elastomers can be controlled, and its ability to be easily molded and shaped (Kheir et al. 1998). These properties make it suitable for a variety of applications such as breast implants (Backovic and Wolfram 2007), cochlear implants (Abbasi et al. 2006, Mirzadeh and Abbasi 2004), maxillofacial reconstruction (Kheir et al. 1998), artificial corneas (Klenkler et al. 2005), artificial skin, soft contact lenses (Nicolson and Vogt 2001), and coatings for pacemaker leads. The wound healing response at the external surface of a silicone implants leads to the formation of a fibrous capsule. Capsule formation can be either interrupted or unduly enhanced by infection, immune reaction, implant migration, or extrusion (Kheir et al. 1998). In some cases, however, problems can arise at silicone elastomer interfaces. With breast implants, for example, the fibrous capsule that forms at the silicone interface can undergo contracture, which can lead to the need for revision surgery (Barr et al. 2009). Surface topography plays a significant role in biological processes such as cell attachment (Khorasani and Mirzadeh 2004, Kidambi et al. 2007, Lee J. N. et al. 2004, Toworfe et al. 2004), motility, proliferation (Kidambi et al. 2007, Li B. et al. 2006, Yim et al. 2005), differentiation (Liao et al. 2003), as well as regulation of gene expression (Kyriakides et al. 1999): these biological processes are important criteria for implant acceptance. The roughness of the implant surface can have significant influence on the cellular behaviour (McLucas et al. 2006) and thus the foreign body reaction (Kao et al. 1994, Kyriakides et al. 1999, Rice et al. 1998) can be minimized by critical adjustment of the roughness (Mirzadeh et al. 2003). The relationship between surface topography (nanosurface roughnesses) and wound healing – which could impact on the degree of contracture – has not been examined in detail. To address this, silicone elastomer samples with rms surface roughnesses varying from ~88 nm to ~650 nm were examined with characterisation of silicone samples by Fourier Transform Infrared Spectrophotometry (FTIR), Scanning Electron Microscopy (SEM) and Atomic Force

Microscopy (AFM). We also measured the growth of NIH-3T3 fibroblasts on these surfaces for 24 hours by quantification of total amount of DNA by PicoGreen assay.

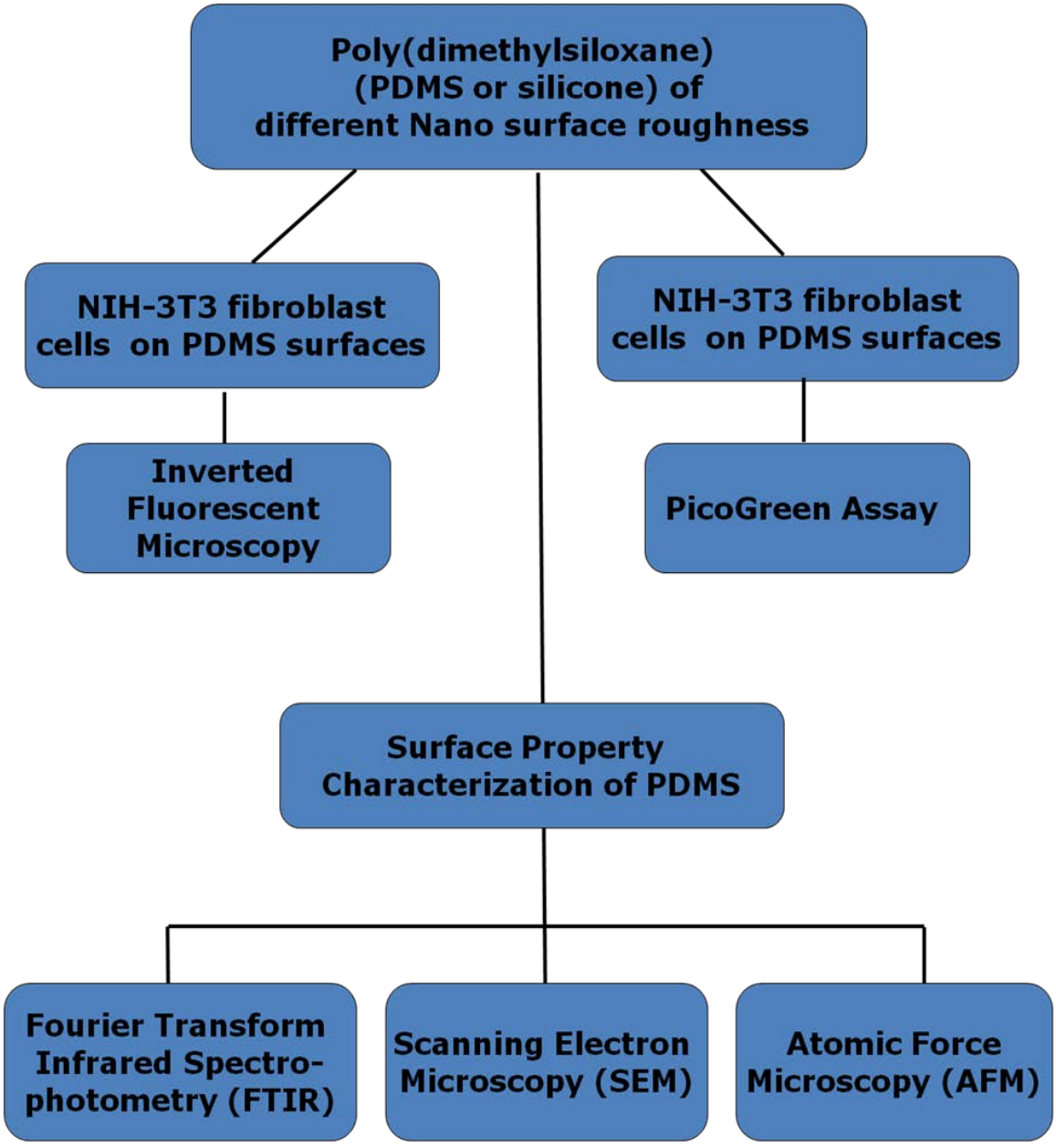

Figure 6.1: Flow chart showing experimental design of PDMS surface characterisation and growth of NIH-3T3 fibroblasts on PDMS nano-rough surfaces.

6.2 Results

6.2.1 Surface Property Characterization of Silicone or PDMS

6.2.1.1 Fourier Transform Infrared Spectrophotometry (FTIR)

FTIR spectra of the PDMS samples of different roughness as shown in figure 6.2, demonstrated that chemical etching did not affect the surface chemical composition, which remained that of pure poly(dimethylsiloxane).

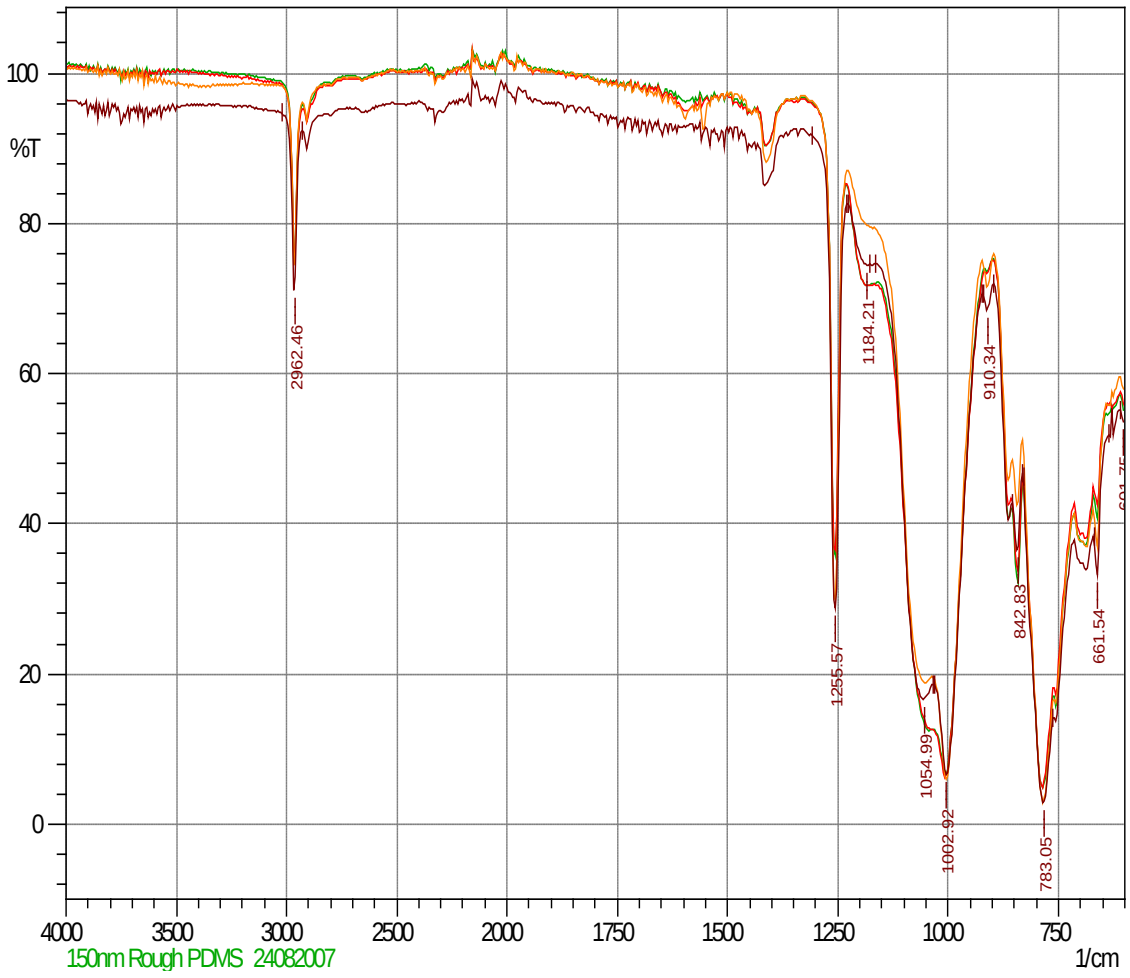

Figure 6.2: Overlay of FTIR spectra from ~88nm smooth PDMS (dark brown spectrum), ~378nm bumpy PDMS (green spectrum) and ~604nm (red spectrum) and ~650nm (orange spectrum) very rough PDMS.

6.2.1.2 Scanning Electron Microscopy (SEM)

Surface roughnesses of the PDMS samples were investigated by SEM. AFM and optical profilometry. SEM demonstrated qualitatively that the PDMS surfaces exhibited different degrees of roughness as shown in figure 6.3.

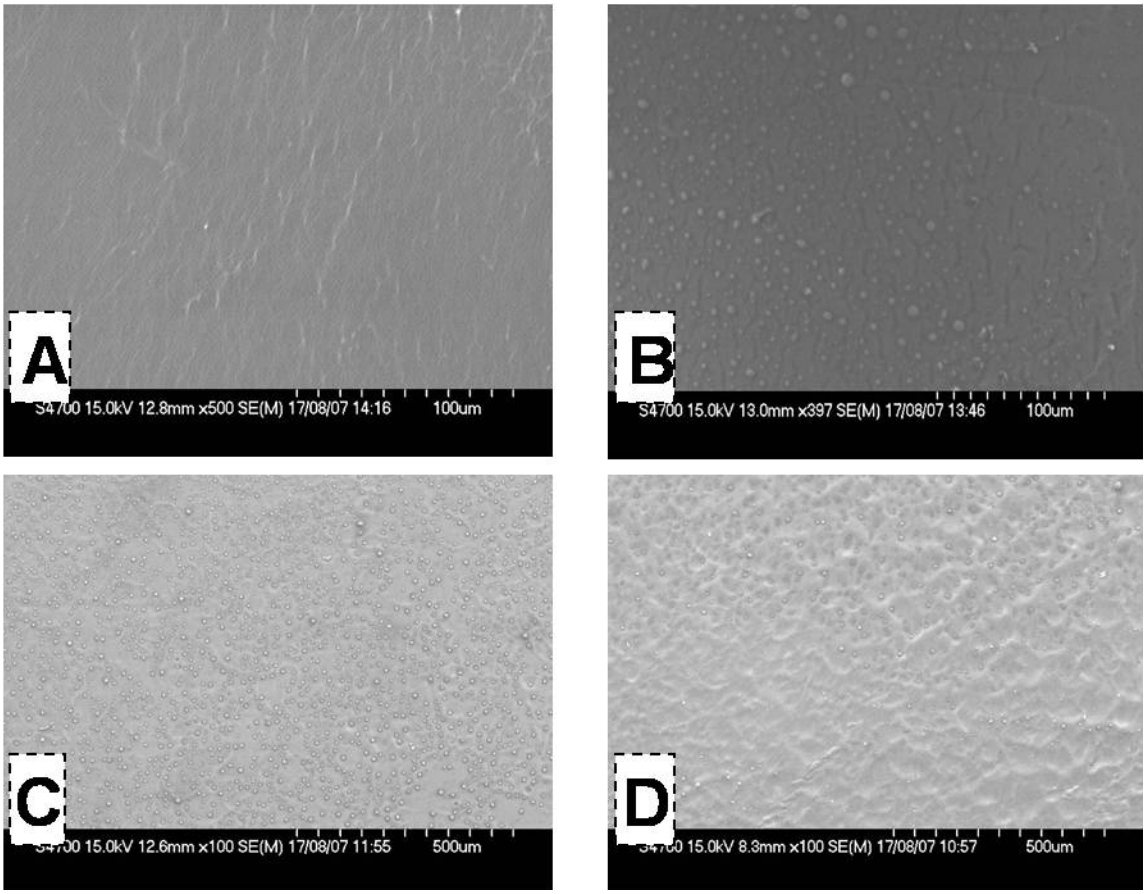

Figure 6.3: SEM pictures showing (A) smooth (B) bumpy, (C & D) very rough PDMS surfaces.

6.2.1.3 Atomic Force Microscopy (AFM)

Surface roughnesses of the PDMS samples were investigated by AFM. The different degrees of roughness of samples were quantified using AFM: the four surfaces exhibited root mean square roughness of ~88nm, ~378nm, ~604nm, and ~650nm, respectively, as shown in figure 6.4.

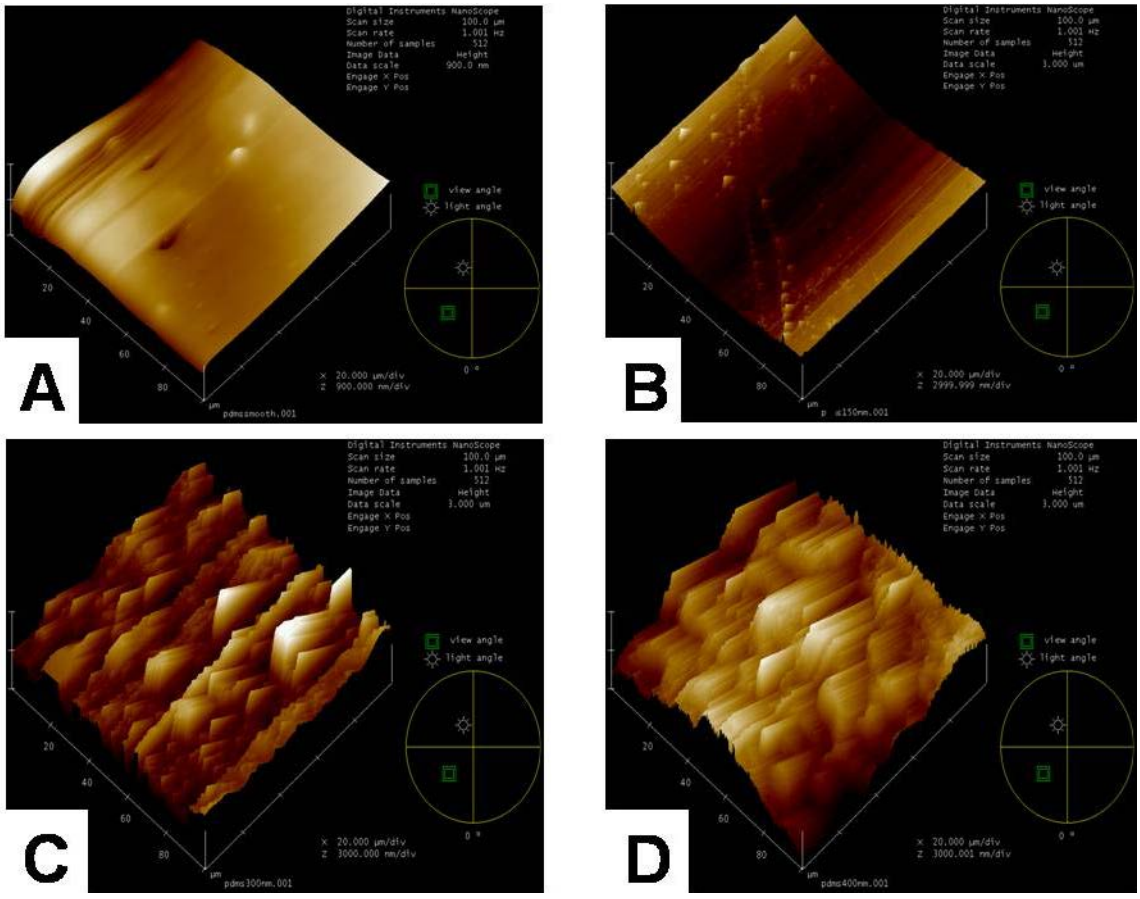

Figure 6.4: 3D AFM pictures showing (a) smooth, (b) bumpy, (c & d) very rough PDMS surfaces.

6.2.2 Imaging of NIH-3T3 fibroblast cells on PDMS

6.2.2.1 Microscopy

Imaging of NIH-3T3 fibroblasts on PDMS samples was done after 24 hours of seeding of cells and the morphology of cells on different surfaces was examined microscopically. Morphologically, the cells readily distinguished between the PDMS surfaces of different roughnesses. The growth on tissue culture plastic (TCP) was used as a control. As shown in figure 4, after 24 hours very significant differences were observed in the degree of proliferation and the appearance of the cells. 3T3 cells on TCP were adherent after 24 hours, proliferating although not to confluence, and exhibited their normal elongated (high aspect ratio) shape as shown in panel A of figure 4. Flat, smooth silicone surfaces were far more productive for cell growth than TCP: dense, near confluent cell layers were produced as shown in panel C of figure 4. By contrast, very

rough PDMS surfaces with the same chemical structure exhibited only a few adhering and rounded up cells as shown in panel B of figure 6.5.

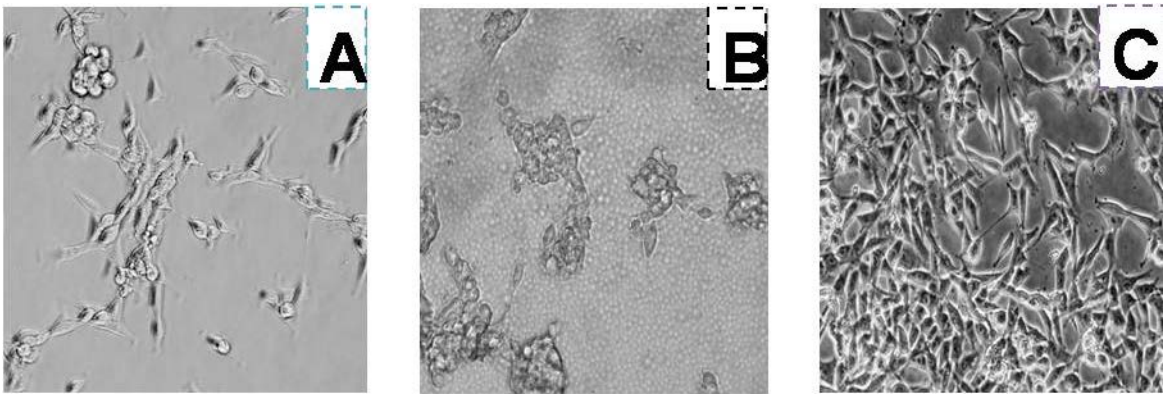

Figure 6.5: (A) 3T3 fibroblasts on TCP; (B) 3T3 cells clumped on a very rough PDMS surface; (C) dense 3T3 cells on smooth PDMS. In all cases, photos were taken 24 hours after seeding.

6.2.3 Cellular activity of NIH-3T3 fibroblast cells on PDMS

6.2.3.1 Quantification of DNA by PicoGreen Assay

The efficiency of cell proliferation was determined using a PicoGreen®Assay that determines the amount of fibroblast cellular DNA on different surfaces. The selectivity of the 3T3 cells for smoother surfaces was further demonstrated by the use of the PicoGreen® assay, which is a more objective method to quantify cellular proliferation by measuring the DNA produced. As shown in Figure 6.6, the fibroblast growth decreased with an increase in surface roughness. Smooth (~88nm rms roughness) PDMS elastomers had significantly higher and statistically different ($p<0.05$) amounts of fibroblast DNA per unit area than the 'bumpy' (~378nm) and very rough (~604nm and~650nm) PDMS samples. The smooth silicone surface exhibited far more cells at 24 hours than the TCP, which is normally considered the gold standard for tissue culture.

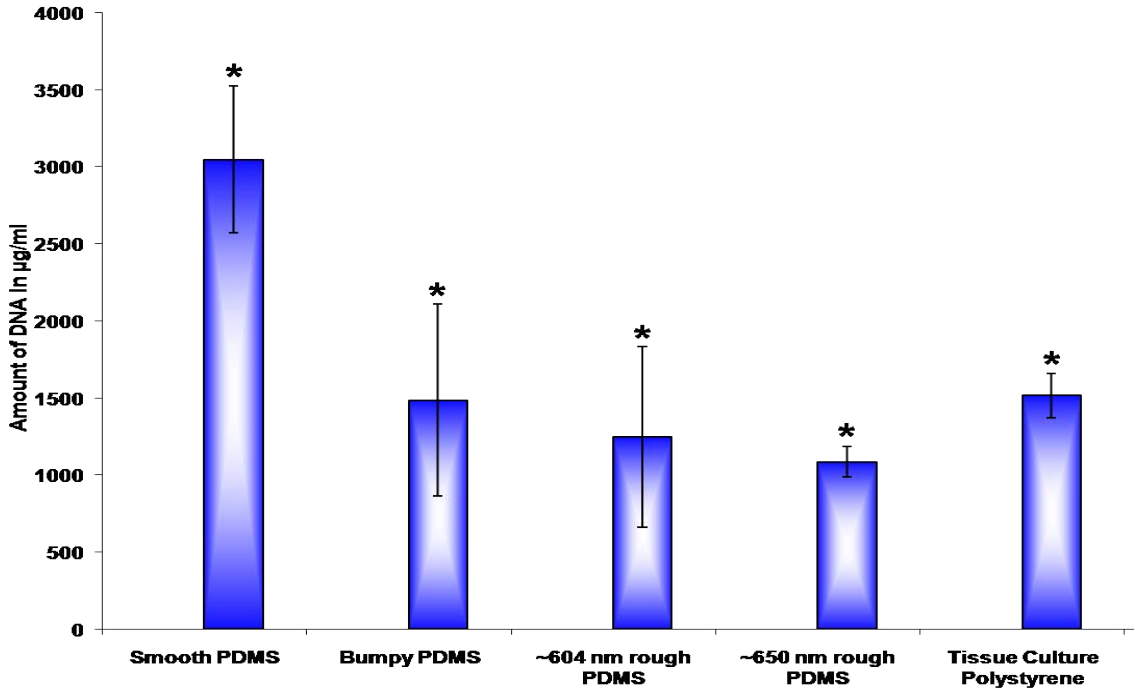

Figure 6.6: PicoGreen Assay results showing the amount of DNA on silicone surfaces in microgram per millilitre (* denotes statistical significance using a one- way ANOVA (p< 0.05) by Tukey's mean comparison when compared with smooth PDMS).

6.3 Discussion

A key step in wound healing is the proliferation of fibroblasts, and the generation of ECM, including collagen. In the case of some implants, notably breast implants, excessive production of collagen, particularly when the fibres are well oriented, leads to 'contracture', which can be painful and, in many cases, requires a surgical revision (Parker et al. 2002).

A variety of factors associated with a given surface can affect cellular compatibility. For example, low cell growth has been associated with hydrophobic surfaces such as silicones (Ai et al. 2002, Patel et al. 2006). However, the rough, bumpy and smooth surfaces described above are comprised of the same silicone of the same low surface energy. Thus, the distinction observed in the ability of cells to proliferate can be associated with roughness alone.

While some investigations have suggested that the topography of the silicone surface does not have a significant effect on contracture (Poeppl et al. 2007), more studies suggest that a correlation exists (Barnsley et al. 2006, Wong C. H. et al. 2006). These studies have compared 'smooth surfaces', prepared by dip coating with uncured silicone elastomers, to multi-micron scale rough surfaces, prepared either by moulding operations or by exposing the uncured silicone surface to salt, which is washed away after cure (Barr et al. 2009). The additional effect of softness of the material has been reviewed (Wong J. Y. et al. 2004). On smooth surfaces, fibroblasts more easily orient, leading to collagen fibres that can effectively contract. Deep, oriented multi-micron wide grooves lead to contact guidance of cellular growth along the groove (denBraber et al. 1996). The response of fibroblasts to oriented grooves was found to be better than to randomly oriented rough surfaces: thicker capsules formed in the former case, although when implanted the thinner capsules that were associated with random rough surfaces led to greater inflammatory responses (Parker et al. 2002). Therefore, in addition to the benefits that could arise from tissue ingrowths on rough surfaces, which can be important for holding the implant in place, particularly with reconstruction patients post-mastectomy, rough surfaces at the micron scale length may be associated with reduced contracture (Barnsley et al. 2006, Wong C. H. et al. 2006).

While the effects on cellular growth of both smooth and very rough silicone implant surfaces have been examined (Schumacher et al. 2007) and very little is known about the effects on cellular adhesion and proliferation of silicone surface roughness at the sub-micron scale. On silicon (the rigid element), slightly rougher surfaces (>70 nm) and very smooth (<10 nm) surfaces were detrimental to cell adhesion when compared with intermediate surfaces (20-50 nm) (Fan et al. 2002). One report suggests that nanotexturing may affect contracture (Barr et al. 2009). In the work above, we compared smooth surfaces with intermediate (bumpy) and very rough surfaces on the hundreds of nm scale. Smooth surfaces were associated with extremely efficient fibroblast proliferation, much better even than TCP.

The decrease in cellular compatibility of rougher silicone elastomer surfaces at the nm scale may be beneficial in a practical sense. The initial steps of the wound healing process involve protein adsorption on the silicone surface followed by cellular adsorption, particularly by fibroblasts. Since the ultimate outcome of over proliferation of fibroblasts can be thick and contracted capsule, surfaces that are less attractive to

such surfaces may be beneficial in silicone-based implantable devices as they may lead to lower rates of contraction. Further research on in vivo responses to such surfaces will address this question.

6.4 Conclusion

Controlled levels of surface roughness introduced on PDMS elastomer samples were measured by SEM and AFM. The PicoGreen Assay demonstrated that fibroblast growth decreased with increases in surface roughness. Relatively smooth (~88nm) PDMS samples had *ca.* twice as much fibroblast DNA per unit area than the ‘bumpy' (~378nm) and very rough (~604nm and~650nm) PDMS samples. While the PDMS sample with roughness of ~650 nm had significantly fewer fibroblasts at 24 hours than the TCP control and fibroblasts on the smooth silicone surprisingly reached confluence much more rapidly than on TCP is the gold standard for cell culture. Smooth PDMS surfaces supported 3T3 fibroblast cell growth better than both TCP and rougher silicone surfaces. The decreased ability of fibroblasts to proliferate on the rougher surfaces may be beneficial for in vivo applications, as it could lead to lower levels of capsular contracture than on smoother surfaces. Thus, increasing the surface roughness at the submicron scale scale (Nanosurface roughness) could be a strategy worthy of consideration to help mitigate fibroblast growth and control fibrous capsule formation on silicone elastomer implants.

CHAPTER 7: FINAL CONCLUSIONS AND FUTURE DIRECTIONS

7.1 Summary of experiments

The first aim of our study was to explore the potential for labelling of undifferentiated Pheochromocytoma 12 (PC12) cells with gelatinised and non-gelatinised TGA capped CdTe QDs with longer incubation periods (chapter 3). We have investigated the cellular interaction, uptake and resultant toxic influence of CdTe QDs (gelatinised and non-gelatinised Thioglycolic acid (TGA) capped) by serial co-incubations of 24, 48 and 72 hours and analysed the effect of three factors namely concentration, co-incubation time and surface modification in parallel. In conjunction to their analysis by confocal microscopy, the QD – cell interplay was explored as the QD concentrations were varied over extended (up to 72 hours) co-incubation times. Coupled to this investigation, cell viability, DNA quantification and cell proliferation assays were also performed to compare and contrast the various factors leading to cell stress and ultimately death.

The second aim of our study was to clearly analyse the viability, cytotoxicity and apoptosis at different time periods and discussed the effect of exposure of QDs on PC12 cells before and after the neurites were grown (chapter 4). The apoptotic process involved in the cell death machinery and also the intrinsic behaviour of QDs upon uptake by the cells have been analysed. CdTe QDs (gelatinised and non-gelatinised Thioglycolic acid (TGA) capped) have been investigated in this study with differentiated pheochromocytoma 12 (PC12) cells. The QD – cell interactions were investigated by MTT and APOTOX-Glo Triplex assays and also from confocal microscopic images to probe how individual cell functions (Cytotoxicity, Viability and Apoptosis) were affected by exposing the QDs to extended (up to 17 days) co-incubation times. In the same experiment, differentiated PC12 cells were also exposed to QDs after the neurites were grown for 10 days.

The third aim was to investigate the cytotoxicity and their differential gene expression of cells in the presence of QDs of gelatinated (gel) and non-gelatinated (non-gel) QDs in Human Pulmonary Microvascular Endothelial (HPMEC-ST1.6R) cells (chapter 5). The viability and DNA quantification of HPMEC-ST1.6R cells was done with alamarBlue and Pico-Green assays respectively. The effect of exposure of QDs on HPMEC-ST1.6R cells was done with Genome-wide microarray analysis and their differential expression of genes was identified.

The final experimental chapter was to examine the relationship between nanosurface topography and wound healing. The nanosurface roughnesses of silicone elastomer samples with rms surface roughnesses varying from ~88 nm to ~650 nm with characterisation of silicone samples by Fourier Transform Infrared Spectrophotometry (FTIR), Scanning Electron Microscopy (SEM) and Atomic Force Microscopy (AFM) and also measured the growth of NIH-3T3 fibroblasts on these surfaces for 24 hours by quantification of total amount of DNA by PicoGreen assay.

7.2 Conclusions

1. Red gel QDs are less toxic than orange gel QDs in the long term exposure of QDs to cells as observed from our studies on different cell lines i.e, undifferentiated PC12 cells, differentiated PC12 cells and HPMEC-ST1.6R cells for 72 hours, 17 days and 72 hours respectively.
2. Gelatination of QDs alleviated the toxicity of QDs upon exposure to cells.
3. Orange QDs, relatively smaller in size are more cytotoxic than the red QDs.
4. Gelatine coating on QDs is more stable and protected the cell from toxicity as there is no degradation of gelatine coating until 17 days as observed from our study.
5. The effect of size of QDs on the cytotoxicity is more pronounced than the effect of gelatination of QDs.
6. The cytotoxicity of QDs was found to increase in the following order from red gel, red non-gel, orange gel and orange non-gel.
7. There is uptake of QDs inside the cells and are distributed heterogeneously inside the cytoplasm around the perinuclear region. Heterogeneous cellular distribution is due to the nanoscale effect of QDs.
8. There are more genes differentially expressed in red QDs than the orange QDs. The more the cytotoxicity of QDs, the lesser the number of differentially expressed genes. The cells treated with red gel and red non-gel QDs expressed more differentially expressed genes than orange gel and orange non-gel QDs shows that the red gel and red non-gel QDs also triggered the stress and apoptotic machinery of the cell but the defensive mechanisms of the cell protected from apoptosis or cell death but is not the case in orange gel and orange non-gel QDs. The

overrepresentation of p53 and ATM (ataxia telangiectasia-mutated gene) signalling pathways in cells treated with orange gel and orange non-gel QDs shows that the orange gel and orange non-gel QDs were showing detrimental effect for the cells leading to apoptosis and finally cell death.

9. The genes of metallothionein superfamily are expressed along with involvement of MT-Heavy pathway in cells exposed to red non-gel and orange non-gel QDs shows that the cadmium ions are leaking from the QDs not coated with gelatine and leads to cytotoxicity. This shows that the gelatination of QDs acts as a barrier by preventing the leakage of cadmium ions from the core of QDs.
10. The smooth surface (~88nm) of PDMS (silicone) showed more fibroblast growth than the rough surfaces at the nano-scale level.
11. Roughness of PDMS (silicone) elastomers at the nano-scale level has the ability to control the fibroblast growth and fibrous capsule formation as observed in our *in vitro* studies.

7.3 Future directions

1. Validation of differentially expressed genes of microarray analysis using Real time-Polymerised chain reaction (RT-PCR).
2. Gene expression analysis using Microarray for HPMEC-ST1.6R cells exposed to QDs for 24 hours along with validation using real time-Polymerised chain reaction (RT-PCR).
3. Preclinical studies on animal models (*in vivo* studies)

CHAPTER 8: BIBLIOGRAPHY

Abbasi F, Mirzadeh H, Simjoo M. 2006. Hydrophilic interpenetrating polymer networks of poly(dimethyl siloxane) (PDMS) as biomaterial for cochlear implants. J Biomater Sci Polym Ed 17: 341-355.

Ai H, Mills DK, Jonathan AS, Jones SA. 2002. Gelatin-glutaraldehyde cross-linking on silicone rubber to increase endothelial cell adhesion and growth. In Vitro Cellular & Developmental Biology-Animal 38: 487-492.

Alivisatos AP. 1999. Semiconductor nanocrystals as fluorescent biological labels. Abstracts of Papers of the American Chemical Society 218: U296-U296.

—. 2004. The use of nanocrystals in biological detection. Nat. Biotech. 22: 47-52.

Alivisatos AP, Gu WW, Larabell C. 2005. Quantum dots as cellular probes. Annual review of biomedical engineering 7: 55-76.

Amane Shiohara, Akiyoshi Hoshino, Ken-ichi Hanaki, Kazuo Suzuki, Yamamoto K. 2004. Microbiology and Immunology 48: 669-675.

Azzazy HM, Mansour MM, Kazmierczak SC. 2007. From diagnostics to therapy: prospects of quantum dots. Clinical biochemistry 40: 917-927.

Backovic A, Wolfram D. 2007. Silicone mammary implants--can we turn back the time? Exp Gerontol 42: 713-718.

Bailey RE, Smith AM, Nie SM. 2004. Quantum dots in biology and medicine. Physica E-Low-Dimensional Systems & Nanostructures 25: 1-12.

Balbus JM, et al. 2007. Meeting report: hazard assessment for nanoparticles--report from an interdisciplinary workshop. Environmental health perspectives 115: 1654-1659.

Balthasar S, Michaelis K, Dinauer N, von Briesen H, Kreuter J, Langer K. 2005. Preparation and characterisation of antibody modified gelatin nanoparticles as drug carrier system for uptake in lymphocytes. Biomaterials 26: 2723-2732.

Barnsley GP, Sigurdson LJ, Barnsley SE. 2006. Textured surface breast implants in the prevention of capsular contracture among breast augmentation patients: A meta-analysis of randomized controlled trials. Plastic and reconstructive surgery 117: 2182-2190.

Barr S, Hill E, Bayat A. 2009. Current implant surface technology: an examination of their nanostructure and their influence on fibroblast alignment and biocompatibility. Eplasty 9: e22.

Barton G, et al. 2008. EMAAS: An extensible grid-based Rich Internet Application for microarray data analysis and management. Bmc Bioinformatics 9: -.

Bell AT. 2003. The impact of nanoscience on heterogeneous catalysis. Science 299: 1688-1691.

Bentolila LA, Ebenstein Y, Weiss S. 2009. Quantum dots for in vivo small-animal imaging. Journal of nuclear medicine : official publication, Society of Nuclear Medicine 50: 493-496.

Bhirde A, Xie J, Swierczewska M, Chen X. 2011. Nanoparticles for cell labeling. Nanoscale 3: 142-153.

Bisht S, Feldmann G, Soni S, Ravi R, Karikar C, Maitra A. 2007. Polymeric nanoparticle-encapsulated curcumin ("nanocurcumin"): a novel strategy for human cancer therapy. Journal of nanobiotechnology 5: 3.

Bruchez M, Jr., Moronne M, Gin P, Weiss S, Alivisatos AP. 1998a. Semiconductor Nanocrystals as Fluorescent Biological Labels. Science 281: 2013-2016.

Bruchez M, Jr., Moronne M, Gin P, Weiss S, Alivisatos AP. 1998b. Semiconductor nanocrystals as fluorescent biological labels. Science 281: 2013-2016.

Byrne SJ, Corr SA, Rakovich TY, Gun'ko YK, Rakovich YP, Donegan JF, Mitchell S, Volkov Y. 2006. Optimisation of the synthesis and modification of CdTe quantum dots for enhanced live cell imaging. Journal of Materials Chemistry 16: 2896-2902.

Byrne SJ, Williams Y, Davies A, Corr SA, Rakovich A, Gun'ko YK, Rakovich YP, Donegan JF, Volkov Y. 2007a. "Jelly Dots": Synthesis and Cytotoxicity Studies of CdTe Quantum Dot–Gelatin Nanocomposites. Small 3: 1152-1156.

Byrne SJ, Williams Y, Davies A, Corr SA, Rakovich A, Gun'ko YK, Rakovich YR, Donegan JF, Volkov Y. 2007b. "Jelly dots": Synthesis and cytotoxicity studies of CdTe quantum dot-gelatin nanocomposites. Small 3: 1152-1156.

Byrne SJ, Williams Y, Davies A, Corr SA, Rakovich A, Gun'ko YK, Rakovich YP, Donegan JF, Volkov Y. 2007c. "Jelly dots": synthesis and cytotoxicity studies of CdTe quantum dot-gelatin nanocomposites. Small 3: 1152-1156.

—. 2007d. "Jelly Dots": Synthesis and Cytotoxicity Studies of CdTe Quantum Dot-Gelatin Nanocomposites. Small 3: 1152-1156.

Byrne SJ, et al. 2007e. Synthesis, characterisation, and biological studies of CdTe quantum dot-naproxen conjugates. ChemMedChem 2: 183-186.

Calabrese EJ, Baldwin LA. 2002. Applications of hormesis in toxicology, risk assessment and chemotherapeutics. Trends Pharmacol. Sci. 23: 331-337.

Chan W-H, Shiao N-H, Lu P-Z. 2006a. CdSe quantum dots induce apoptosis in human neuroblastoma cells via mitochondrial-dependent pathways and inhibition of survival signals. Toxicology Letters 167 191-200.

Chan WC, Nie S. 1998a. Quantum Dot Bioconjugates for Ultrasensitive Nonisotopic Detection. Science 281: 2016-2018.

Chan WC, Nie S. 1998b. Quantum dot bioconjugates for ultrasensitive nonisotopic detection. Science 281: 2016-2018.

Chan WC, Maxwell DJ, Gao X, Bailey RE, Han M, Nie S. 2002a. Luminescent quantum dots for multiplexed biological detection and imaging. Curr Opin Biotechnol 13: 40-46.

Chan WCW, Maxwell DJ, Gao X, Bailey RE, Han M, Nie S. 2002b. Luminescent quantum dots for multiplexed biological detection and imaging. Curr. Op. Biotech. 13: 40-46.

Chan WH, Shiao NH, Lu PZ. 2006b. CdSe quantum dots induce apoptosis in human neuroblastoma cells via mitochondrial-dependent pathways and inhibition of survival signals. Toxicol Lett 167: 191-200.

Chang TY, Yadav VG, De Leo S, Mohedas A, Rajalingam B, Chen CL, Selvarasah S, Dokmeci MR, Khademhosseini A. 2007. Cell and protein compatibility of parylene-C surfaces. Langmuir 23: 11718-11725.

Chen F, Gerion D. 2004. Fluorescent CdSe/ZnS Nanocrystal-Peptide Conjugates for Long-term, Nontoxic Imaging and Nuclear Targeting in Living Cells. Nano Lett. 4: 1827-1832.

Cho SJ, Maysinger D, Jain M, Roder B, Hackbarth S, Winnik FM. 2007a. Long-Term Exposure to CdTe Quantum Dots Causes Functional Impairments in Live Cells. Langmuir 23: 1974-1980.

Cho SJ, Maysinger D, Jain M, Roder B, Hackbarth S, Winnik FM. 2007b. Long-term exposure to CdTe quantum dots causes functional impairments in live cells. Langmuir 23: 1974-1980.

Cho YH, Gokarna A, Jin LH, Hwang JS, Lim YT, Chung BH, Youn SH, Choi DS, Lim JH. 2008. Quantum dot-based protein micro- and nanoarrays for detection of prostate cancer biomarkers. Proteomics 8: 1809-1818.

Chouhan R, Bajpai A. 2009. Real time in vitro studies of doxorubicin release from PHEMA nanoparticles. Journal of nanobiotechnology 7: 5.

Coester C, Nayyar P, Samuel J. 2006. In vitro uptake of gelatin nanoparticles by murine dendritic cells and their intracellular localisation. European Journal of Pharmaceutics and Biopharmaceutics 62: 306-314.

Conroy J, Byrne SJ, Gun'ko YK, Rakovich YP, Donegan JF, Davies A, Kelleher D, Volkov Y. 2008. CdTe nanoparticles display tropism to core histones and histone-rich cell organelles. Small 4: 2006-2015.

Cooper GM. 2007. The Cell, A Molecular Approach: ASM Press Washington, D.C.

Cui BX, Wu CB, Chen L, Ramirez A, Bearer EL, Li WP, Mobley WC, Chu S. 2007. One at a time, live tracking of NGF axonal transport using quantum dots. Proceedings of the National Academy of Sciences of the United States of America 104: 13666-13671.

Dahan M, Levi S, Luccardini C, Rostaing P, Riveau B, Triller A. 2003. Diffusion dynamics of glycine receptors revealed by single-quantum dot tracking. Science 302: 442-445.

Dawson KA, Salvati A, Lynch I. 2009. Nanotoxicology: nanoparticles reconstruct lipids. Nat Nanotechnol 4: 84-85.

Delehanty JB, Medintz IL, Pons T, Brunel FM, Dawson PE, Mattoussi H. 2006. Self-assembled quantum dot-peptide bioconjugates for selective intracellular delivery. Bioconjugate Chemistry 17: 920-927.

denBraber ET, deRuijter JE, Ginsel LA, vonRecum AF, Jansen JA. 1996. Quantitative analysis of fibroblast morphology on microgrooved surfaces with various groove and ridge dimensions. Biomaterials 17: 2037-2044.

Derfus AM, Chan WCW, Bhatia SN. 2004a. Intracellular delivery of quantum dots for live cell labeling and organelle tracking. Advanced Materials 16: 961-+.

—. 2004b. Probing the cytotoxicity of semiconductor quantum dots. Nano Lett. 4: 11-18.

—. 2004c. Probing the cytotoxicity of semiconductor quantum dots. Nano Letters 4: 11-18.

Derfus AM, Chen AA, Min DH, Ruoslahti E, Bhatia SN. 2007. Targeted quantum dot conjugates for siRNA delivery. Bioconjug Chem 18: 1391-1396.

Dhawan A, Sharma V. 2010. Toxicity assessment of nanomaterials: methods and challenges. Analytical and bioanalytical chemistry 398: 589-605.

Drummen GP. 2010. Quantum dots-from synthesis to applications in biomedicine and life sciences. Int J Mol Sci 11: 154-163.

Duan HW, Nie SM. 2007. Cell-penetrating quantum dots based on multivalent and endosome-disrupting surface coatings. Journal of the American Chemical Society 129: 3333-3338.

Dubertret B, Skourides P, Norris DJ, Noireaux V, Brivanlou AH, Libchaber A. 2002a. In vivo imaging of quantum dots encapsulated in phospholipid micelles. Science 298: 1759-1762.

Dubertret B, Skourides P, Norris DJ, Noireaux V, Brivanlou AH, Libchaber A. 2002b. In Vivo Imaging of Quantum Dots Encapsulated in Phospholipid Micelles. Science 298: 1759-1762.

E. Chang, N. Thekkek , Yu WW, Colvin VL, Drezek R. 2006. Evaluation of Quantum Dot Cytotoxicity Based on Intracellular Uptake. Small 2: 1412-1417.

Fan YW, Cui FZ, Hou SP, Xu QY, Chen LN, Lee IS. 2002. Culture of neural cells on silicon wafers with nano-scale surface topograph. Journal of Neuroscience Methods 120: 17-23.

Foster KA, Galeffi F, Gerich FJ, Turner DA, Muller M. 2006. Optical and pharmacological tools to investigate the role of mitochondria during oxidative stress and neurodegeneration. Prog Neurobiol 79: 136-171.

Gao X, Cui Y, Levenson RM, Chung LW, Nie S. 2004a. In vivo cancer targeting and imaging with semiconductor quantum dots. Nat Biotechnol 22: 969-976.

Gao X, Cui Y, Levenson RM, Chung LWK, Nie S. 2004b. In vivo cancer targeting and imaging with semiconductor quantum dots. Nat. Biotech. 22: 969-976.

Gao X, Yang L, Petros JA, Marshall FF, Simons JW, Nie S. 2005. In vivo molecular and cellular imaging with quantum dots. Current opinion in biotechnology 16: 63-72.

Gaponik N, Talapin DV, Rogach AL, Hoppe K, Shevchenko EV, Kornowski A, Eychmüller A, Weller H. 2002. Thiol-capping of CdTe nanocrystals: An alternative to organometallic synthetic routes. J. Phys. Chem. B 106: 7177-7185.

George JM, Hasadsri L, Kreuter J, Hattori H, Iwasaki T. 2009. Functional Protein Delivery into Neurons Using Polymeric Nanoparticles. Journal of Biological Chemistry 284: 6972-6981.

Gerion D, Pinaud F, Williams SC, Parak WJ, Zanchet D, Weiss S, Alivisatos AP. 2001. Synthesis and properties of biocompatible water-soluble silica-coated CdSe/ZnS semiconductor quantum dots. Journal of Physical Chemistry B 105: 8861-8871.

Ghasemi Y, Peymani P, Afifi S. 2009. Quantum dot: magic nanoparticle for imaging, detection and targeting. Acta bio-medica : Atenei Parmensis 80: 156-165.

Goldman ER, Balighian ED, Mattoussi H, Kuno MK, Mauro JM, Tran PT, Anderson GP. 2002. Avidin: A Natural Bridge for Quantum Dot-Antibody Conjugates. J. Am. Chem. Soc. 124: 6378-6382.

Gomez N, Winter JO, Shieh F, Saunders AE, Korgel BA, Schmidt CE. 2005a. Challenges in quantum dot-neuron active interfacing. Talanta 67: 462-471.

Gomez N, Winter JO, Shieh F, Saunders AE, Korgel BA, Schmidt CE. 2005b. Challenges in quantum dot-neuron active interfacing. Talanta 67: 462-471.

Greene LA, Tischler AS. 1976. Establishment of a noradrenergic clonal line of rat adrenal pheochromocytoma cells which respond to nerve growth factor. Proc Natl Acad Sci U S A 73: 2424-2428.

Greene LA, Aletta JM, Rukenstein A, Green SH. 1987. PC12 pheochromocytoma cells: culture, nerve growth factor treatment, and experimental exploitation. Methods Enzymol 147: 207-216.

Greenham NC, Finlayson CE, Ginger DS. 2001. Enhanced Forster energy transfer in organic/inorganic bilayer optical microcavities. Chemical Physics Letters 338: 83-87.

Guan KL. 1994. The mitogen activated protein kinase signal transduction pathway: from the cell surface to the nucleus. Cellular signalling 6: 581-589.

Guo G, Liu W, Liang J, He Z, Xu H, Yang X. 2007a. Probing the cytotoxicity of CdSe quantum dots with surface modification. Mater. Lett. 61: 1641-1644.

Guo GN, Liu W, Liang JG, He ZK, Xu HB, Yang XL. 2007b. Probing the cytotoxicity of CdSe quantum dots with surface modification. Materials Letters 61: 1641-1644.

Halliwell B. 1999. Antioxidant defence mechanisms: from the beginning to the end (of the beginning). Free Radic Res 31: 261-272.

Han MY, Gao XH, Su JZ, Nie S. 2001. Quantum-dot-tagged microbeads for multiplexed optical coding of biomolecules. Nat Biotech 19: 631-635.

Hanaki K, Momo A, Oku T, Komoto A, Maenosono S, Yamaguchi Y, Yamamoto K. 2003. Semiconductor quantum dot/albumin complex is a long-life and highly photostable endosome marker. Biochemical and Biophysical Research Communications 302: 496-501.

Hoshino A, Hanaki K, Suzuki K, Yamamoto K. 2004a. Applications of T-lymphoma labeled with fluorescent quantum dots to cell tracing markers in mouse body. Biochemical and Biophysical Research Communications 314: 46-53.

Hoshino A, Fujioka K, Oku T, Suga M, Sasaki YF, Ohta T, Yasuhara M, Suzuki K, Yamamoto K. 2004b. Physicochemical properties and cellular toxicity of nanocrystal quantum dots depend on their surface modification. Nano Letters 4: 2163-2169.

—. 2004c. Physicochemical properties and cellular toxicity of nanocrystal quantum dots depend on their surface modification. Nano Lett. 4: 2163-2169.

Huang DW, Sherman BT, Lempicki RA. 2009a. Systematic and integrative analysis of large gene lists using DAVID bioinformatics resources. Nature Protocols 4: 44-57.

—. 2009b. Bioinformatics enrichment tools: paths toward the comprehensive functional analysis of large gene lists. Nucleic Acids Research 37: 1-13.

J. Lovrić, H. S. Bazzi, Y. Cuie, G. R. A. Fortin, F. M. Winnik, Maysinger. D. 2005. Differences in subcellular distribution and toxicity of green and red emitting CdTe quantum dots J. Mol. Med. 83: 377-385.

Jaiswal JK, Mattoussi H, Mauro JM, Simon SM. 2003. Long-term multiple color imaging of live cells using quantum dot bioconjugates. Nat Biotechnol 21: 47-51.

Jaiswal JK, Goldman ER, Mattoussi H, Simon SM. 2004. Use of quantum dots for live cell imaging. Nat. Methods 1: 73-78.

Jamieson T, Bakhshi R, Petrova D, Pocock R, Imani M, Seifalian AM. 2007. Biological applications of quantum dots. Biomaterials 28: 4717-4732.

Jan E, Byrne SJ, Cuddihy M, Davies AM, Volkov Y, Gun'ko YK, Kotov NA. 2008. High-Content Screening as a Universal Tool for Fingerprinting of Cytotoxicity of Nanoparticles. ACS Nano 2: 928-938.

Ji M, Jin L, Guo J, Yang W, Wang C, Fu S. 2008. Formation of luminescent nanocomposite assemblies via electrostatic interaction. Journal of colloid and interface science 318: 487-495.

Kagan CR, Murray CB, Bawendi MG. 1996a. Long-range resonance transfer of electronic excitations in close-packed CdSe quantum-dot solids. Physical Review B 54: 8633-8643.

Kagan CR, Murray CB, Nirmal M, Bawendi MG. 1996b. Electronic energy transfer in CdSe quantum dot solids (vol 76, pg 1517, 1996). Physical Review Letters 76: 3043-3043.

Kao WJ, Zhao QH, Hiltner A, Anderson JM. 1994. Theoretical analysis of in vivo macrophage adhesion and foreign body giant cell formation on polydimethylsiloxane, low density polyethylene, and polyetherurethanes. J Biomed Mater Res 28: 73-79.

Kaul Z, Yaguchi T, Kaul SC, Hirano T, Wadhwa R, Taira K. 2003. Mortalin imaging in normal and cancer cells with quantum dot immuno-conjugates. Cell research 13: 503-507.

Kheir JN, Leslie LF, Fulmer NL, Edlich RF, Gampper TJ. 1998. Polydimethylsiloxane for augmentation of the chin, malar, and nasal bones. J Long Term Eff Med Implants 8: 55-67.

Khorasani MT, Mirzadeh H. 2004. BHK cells behaviour on laser treated polydimethylsiloxane surface. Colloids Surf B Biointerfaces 35: 67-71.

Kidambi S, Udpa N, Schroeder SA, Findlan R, Lee I, Chan C. 2007. Cell adhesion on polyelectrolyte multilayer coated polydimethylsiloxane surfaces with varying topographies. Tissue Eng 13: 2105-2117.

Kirchner C, Liedl T, Kudera S, Pellegrino T, MunozJavier A, Gaub HE, Stolzle S, Fertig N, Parak WJ. 2005a. Cytotoxicity of Colloidal CdSe and CdSe/ZnS Nanoparticles. Nano Lett. 5: 331-338.

Kirchner C, Liedl T, Kudera S, Pellegrino T, Munoz Javier A, Gaub HE, Stolzle S, Fertig N, Parak WJ. 2005b. Cytotoxicity of colloidal CdSe and CdSe/ZnS nanoparticles. Nano Lett 5: 331-338.

Klaassen CD, Liu J, Diwan BA. 2009. Metallothionein protection of cadmium toxicity. Toxicology and applied pharmacology 238: 215-220.

Klenkler BJ, Griffith M, Becerril C, West-Mays JA, Sheardown H. 2005. EGF-grafted PDMS surfaces in artificial cornea applications. Biomaterials 26: 7286-7296.

Kloepfer JA, Mielke RE, Wong MS, Nealson KH, Stucky G, Nadeau JL. 2003. Quantum dots as strain- and metabolism-specific microbiological labels. Applied and environmental microbiology 69: 4205-4213.

Komarala VK, Rakovich YP, Bradley AL, Byrne SJ, Corr SA, Gun'ko YK. 2006. Emission properties of colloidal quantum dots on polyelectrolyte multilayers. Nanotechnology 17: 4117-4122.

Kondoh M, Araragi S, Sato K, Higashimoto M, Takiguchi M, Sato M. 2002a. Cadmium induces apoptosis partly via caspase-9 activation in HL-60 cells. Toxicology 170: 111-117.

Kondoh M, Araragi S, Sato K, Higashimoto M, Takiguchi M, Sato M. 2002b. Cadmium induces apoptosis partly via caspase-9 activation in HL-60 cells. Toxicol. 170: 111-117.

Kotov NA, Mamedova NN, Rogach AL, Studer J. 2001. Albumin-CdTe nanoparticle bioconjugates: Preparation, structure, and interunit energy transfer with antenna effect. Nano Letters 1: 281-286.

Krump-Konvalinkova V, Bittinger F, Unger RE, Peters K, Lehr HA, Kirkpatrick CJ. 2001. Generation of human pulmonary microvascular endothelial cell lines. Laboratory investigation; a journal of technical methods and pathology 81: 1717-1727.

Kyriakides TR, Leach KJ, Hoffman AS, Ratner BD, Bornstein P. 1999. Mice that lack the angiogenesis inhibitor, thrombospondin 2, mount an altered foreign body reaction characterized by increased vascularity. Proc Natl Acad Sci U S A 96: 4449-4454.

Lai CY, Trewyn BG, Jeftinija DM, Jeftinija K, Xu S, Jeftinija S, Lin VS. 2003. A mesoporous silica nanosphere-based carrier system with chemically removable CdS nanoparticle caps for stimuli-responsive controlled release of neurotransmitters and drug molecules. Journal of the American Chemical Society 125: 4451-4459.

Larson DR, Zipfel WR, Williams RM, Clark SW, Bruchez MP, Wise FW, Webb WW. 2003. Water-Soluble Quantum Dots for Multiphoton Fluorescence Imaging in Vivo. Science 300: 1434-1436.

Lee H-M SD-M, Song H-M, Yuka J-M, Lee Z-W, Lee S-H, Hwang S M, Kim J-M, Lee C-S, Jo E-K. 2009. Nanoparticles up-regulate tumor necrosis factor-α and CXCL8 via reactive oxygen species and mitogen-activated protein kinase activation Toxicol. Appl. Pharm. 238: 160-169.

Lee HM, Shin DM, Song HM, Yuk JM, Lee ZW, Lee SH, Hwang SM, Kim JM, Lee CS, Jo EK. 2009. Nanoparticles up-regulate tumor necrosis factor-alpha and CXCL8 via reactive oxygen species and mitogen-activated protein kinase activation. Toxicol Appl Pharmacol 238: 160-169.

Lee JN, Jiang X, Ryan D, Whitesides GM. 2004. Compatibility of mammalian cells on surfaces of poly(dimethylsiloxane). Langmuir 20: 11684-11691.

Li B, Chen J, Wang JH. 2006. RGD peptide-conjugated poly(dimethylsiloxane) promotes adhesion, proliferation, and collagen secretion of human fibroblasts. J Biomed Mater Res A 79: 989-998.

Li KG, Chen JT, Bai SS, Wen X, Song SY, Yu Q, Li J, Wang YQ. 2009a. Intracellular oxidative stress and cadmium ions release induce cytotoxicity of unmodified cadmium sulfide quantum dots. Toxicology in Vitro 23: 1007-1013.

—. 2009b. Intracellular oxidative stress and cadmium ions release induce cytotoxicity of unmodified cadmium sulfide quantum dots. Toxicol In Vitro 23: 1007-1013.

Li Y, Duan X, Jing L, Yang C, Qiao R, Gao M. 2011. Quantum dot-antisense oligonucleotide conjugates for multifunctional gene transfection, mRNA regulation, and tracking of biological processes. Biomaterials 32: 1923-1931.

Liao H, Andersson AS, Sutherland D, Petronis S, Kasemo B, Thomsen P. 2003. Response of rat osteoblast-like cells to microstructured model surfaces in vitro. Biomaterials 24: 649-654.

Lidke DS, Nagy P, Heintzmann R, Arndt-Jovin DJ, Post JN, Grecco HE, Jares-Erijman EA, Jovin TM. 2004. Quantum dot ligands provide new insights into erbB/HER receptor-mediated signal transduction. Nature Biotechnology 22: 198-203.

Limaye DA, Shaikh ZA. 1999. Cytotoxicity of Cadmium and Characteristics of Its Transport in Cardiomyocytes. Toxicol. Appl. Pharmacol. 154: 59-66.

Liu WT, Zhang Q, Zhu L, Feng HH, Ang S, Chau FS. 2006. Microbial detection in microfluidic devices through dual staining of quantum dots-labeled immunoassay and RNA hybridization. Analytica Chimica Acta 556: 171-177.

Lopez E, Figueroa S, Oset-Gasque MJ, Gonzalez MP. 2003. Apoptosis and necrosis: two distinct events induced by cadmium in cortical neurons in culture. Br. J. Pharmacol. 138: 901-911.

Lovric J, Cho SJ, Winnik FM, Maysinger D. 2005a. Unmodified cadmium telluride quantum dots induce reactive oxygen species formation leading to multiple organelle damage and cell death. Chem Biol 12: 1227-1234.

Lovric J, Bazzi HS, Cuie Y, Fortin GR, Winnik FM, Maysinger D. 2005b. Differences in subcellular distribution and toxicity of green and red emitting CdTe quantum dots. J Mol Med 83: 377-385.

Lovrić J, Cho SJ, Winnik FM, Maysinger D. 2005. Unmodified Cadmium Telluride Quantum Dots Induce Reactive Oxygen Species Formation Leading to Multiple Organelle Damage and Cell Death. Chem. Biol. 12: 1227-1234.

Madesh M, Hajnoczky G. 2001. VDAC-dependent permeabilization of the outer mitochondrial membrane by superoxide induces rapid and massive cytochrome c release. J Cell Biol 155: 1003-1015.

Mahto SK, Yoon TH, Rhee SW. 2010. Cytotoxic effects of surface-modified quantum dots on neuron-like PC12 cells cultured inside microfluidic devices. Biochip Journal 4: 82-88.

Mansur HS. 2010. Quantum dots and nanocomposites. Wiley interdisciplinary reviews. Nanomedicine and nanobiotechnology 2: 113-129.

McDevitt JT, et al. 2009. Nano-bio-chips for high performance multiplexed protein detection: Determinations of cancer biomarkers in serum and saliva using quantum dot bioconjugate labels. Biosensors & Bioelectronics 24: 3622-3629.

McLucas E, Moran MT, Rochev Y, Carroll WM, Smith TJ. 2006. An investigation into the effect of surface roughness of stainless steel on human umbilical vein endothelial cell gene expression. Endothelium 13: 35-41.

McStay GP, Clarke SJ, Halestrap AP. 2002. Role of critical thiol groups on the matrix surface of the adenine nucleotide translocase in the mechanism of the mitochondrial permeability transition pore. Biochem J 367: 541-548.

Medintz IL, Uyeda HT, Goldman ER, Mattoussi H. 2005. Quantum dot bioconjugates for imaging, labelling and sensing. Nature materials 4: 435-446.

Michalet X, Pinaud F, Lacoste TD, Dahan M, Bruchez MP, Alivisatos AP, Weiss S. 2001. Properties of fluorescent semiconductor nanocrystals and their application to biological labeling. Single Molecules 2: 261-276.

Michalet X, Pinaud FF, Bentolila LA, Tsay JM, Doose S, Li JJ, Sundaresan G, Wu AM, Gambhir SS, Weiss S. 2005. Quantum dots for live cells, in vivo imaging, and diagnostics. Science 307: 538-544.

Minet O, Dressler C, Beuthan J. 2004. Heat stress induced redistribution of fluorescent quantum dots in breast tumor cells. Journal of Fluorescence 14: 241-247.

Mirzadeh H, Abbasi F. 2004. Segmented detachable structure of cochlear-implant electrodes for close-hugging engagement with the modiolus. J Biomed Mater Res B Appl Biomater 68: 191-198.

Mirzadeh H, Shokrolahi F, Daliri M. 2003. Effect of silicon rubber crosslink density on fibroblast cell behavior in vitro. J Biomed Mater Res A 67: 727-732.

Monteiro-Riviere NA, Inman AO, Zhang LW. 2009. Limitations and relative utility of screening assays to assess engineered nanoparticle toxicity in a human cell line. Toxicology and Applied Pharmacology 234: 222-235.

Muller-Borer BJ, Collins MC, Gunst PR, Cascio WE, Kypson AP. 2007. Quantum dot labeling of mesenchymal stem cells. Journal of nanobiotechnology 5: 9.

Nabiev I, et al. 2007. Nonfunctionalized Nanocrystals Can Exploit a Cell's Active Transport Machinery Delivering Them to Specific Nuclear and Cytoplasmic Compartments. Nano Letters 7: 3452-3461.

Nel A. 2005. Atmosphere. Air pollution-related illness: effects of particles. Science 308: 804-806.

Nel A, Xia T, Madler L, Li N. 2006a. Toxic potential of materials at the nanolevel. Science 311: 622-627.

Nel A, Xia T, Madler L, Li N. 2006b. Toxic Potential of Materials at the Nanolevel. Science 311: 622-627.

Newmeyer DD, Ferguson-Miller S. 2003. Mitochondria: releasing power for life and unleashing the machineries of death. Cell 112: 481-490.

Nicolson PC, Vogt J. 2001. Soft contact lens polymers: an evolution. Biomaterials 22: 3273-3283.

Nie SM, Chan WCW. 1998. Quantum dot bioconjugates for ultrasensitive nonisotopic detection. Science 281: 2016-2018.

Oberdorster G, Oberdorster E, Oberdorster J. 2005. Nanotoxicology: an emerging discipline evolving from studies of ultrafine particles. Environ Health Perspect 113: 823-839.

Oh SH, Lim SC. 2006. A rapid and transient ROS generation by cadmium triggers apoptosis via caspase-dependent pathway in HepG2 cells and this is inhibited through N-acetylcysteine-mediated catalase upregulation. Toxicol Appl Pharmacol 212: 212-223.

Osaki F, Kanamori T, Sando S, Sera T, Aoyama Y. 2004. A Quantum Dot Conjugated Sugar Ball and Its Cellular Uptake. On the Size Effects of Endocytosis in the Subviral Region. Journal of the American Chemical Society 126: 6520-6521.

Park EJ, Yi J, Chung KH, Ryu DY, Choi J, Park K. 2008. Oxidative stress and apoptosis induced by titanium dioxide nanoparticles in cultured BEAS-2B cells. Toxicology letters 180: 222-229.

Park KH, Park JS, Na K, Woo DG, Yang HN, Kim JM, Kim JH, Chung HM. 2010. Non-viral gene delivery of DNA polyplexed with nanoparticles transfected into human mesenchymal stem cells. Biomaterials 31: 124-132.

Parker J, Walboomers XF, Von Den Hoff JW, Maltha JC, Jansen JA. 2002. Soft-tissue response to silicone and poly-L-lactic acid implants with a periodic or random surface micropattern. Journal of Biomedical Materials Research 61: 91-98.

Patel KR, Tang HY, Grever WE, Ng KYS, Xiang JM, Keep RF, Cao T, McAllister JP. 2006. Evaluation of polymer and self-assembled monolayer-coated silicone surfaces to reduce neural cell growth. Biomaterials 27: 1519-1526.

Pathak S, Cao E, Davidson MC, Jin S, Silva GA. 2006a. Quantum dot applications to neuroscience: new tools for probing neurons and glia. J Neurosci 26: 1893-1895.

Pathak S, Cao E, Davidson MC, Jin SH, Silva GA. 2006b. Quantum dot applications to neuroscience: New tools for probing neurons and glia. Journal of Neuroscience 26: 1893-1895.

Pelzl C, Arcizet D, Piontek G, Schlegel J, Heinrich D. 2009. Axonal guidance by surface microstructuring for intracellular transport investigations. Chemphyschem 10: 2884-2890.

Peng CW, Li Y. 2010. Application of Quantum Dots-Based Biotechnology in Cancer Diagnosis: Current Status and Future Perspectives. Journal of Nanomaterials: -.

Peng XG, Peng ZA. 2001. Formation of high-quality CdTe, CdSe, and CdS nanocrystals using CdO as precursor. Journal of the American Chemical Society 123: 183-184.

Pietrasanta LI, Echarte MM, Bruno L, Arndt-Jovin DJ, Jovin TM. 2007. Quantitative single particle tracking of NGF-receptor complexes: Transport is bidirectional but biased by longer retrograde run lengths. Febs Letters 581: 2905-2913.

Pinaud F, King D, Moore HP, Weiss S. 2004. Bioactivation and cell targeting of semiconductor CdSe/ZnS nanocrystals with phytochelatin-related peptides. J. Am. Chem. Soc. 126: 6115-6123.

Poeppl N, Schreml S, Lichtenegger F, Lenich A, Eisenmann-Klein M, Prantl L. 2007. Does the surface structure of implants have an impact on the formation of a capsular contracture? Aesthetic Plastic Surgery 31: 133-139.

Prasad BR, Brook MA, Smith T, Zhao S, Chen Y, Sheardown H, D'Souza R, Rochev Y. 2010a. Controlling cellular activity by manipulating silicone surface roughness. Colloids and surfaces. B, Biointerfaces 78: 237-242.

Prasad BR, Nikolskaya N, Connolly D, Smith TJ, Byrne SJ, Gerard VA, Gun'ko YK, Rochev Y. 2010b. Long-term exposure of CdTe quantum dots on PC12 cellular activity and the determination of optimum non-toxic concentrations for biological use. J Nanobiotechnology 8: 7.

Radio NM, Freudenrich TM, Robinette BL, Crofton KM, Mundy WR. 2010. Comparison of PC12 and cerebellar granule cell cultures for evaluating neurite outgrowth using high content analysis. Neurotoxicology and Teratology 32: 25-35.

Rajan SS, Liu HY, Vu TQ. 2008. Ligand-Bound Quantum Dot Probes for Studying the Molecular Scale Dynamics of Receptor Endocytic Trafficking in Live Cells. ACS Nano 2: 1153-1166.

Ratner BD, Hoffman AS, Schoen FJ, Lemons JE. 2004. Biomaterials science ; an introduction to materials in medicine. San Diego, CA: Academic Press.

Rice JM, Fisher AC, Hunt JA. 1998. Macrophage--polymer interactions. J Biomater Sci Polym Ed 9: 833-847.

Rikans LE, Yamano T. 2000a. Mechanisms of cadmium-mediated acute hepatotoxicity. J. Biochem. Molec. Tox. 14: 110-117.

—. 2000b. Mechanisms of cadmium-mediated acute hepatotoxicity. Journal of Biochemical and Molecular Toxicology 14: 110-117.

Romoser A, Ritter D, Majitha R, Meissner KE, McShane M, Sayes CM. 2011. Mitigation of Quantum Dot Cytotoxicity by Microencapsulation. PLoS One 6.

Rosenthal SJ, Tomlinson I, Adkins EM, Schroeter S, Adams S, Swafford L, McBride J, Wang Y, DeFelice LJ, Blakely RD. 2002a. Targeting cell surface receptors with ligand-conjugated nanocrystals. Journal of the American Chemical Society 124: 4586-4594.

—. 2002b. Targeting Cell Surface Receptors with Ligand-Conjugated Nanocrystals. J. Am. Chem. Soc. 124: 4586-4594.

Rosenzweig Z, Wang DS, He JB, Rosenzweig N. 2004. Superparamagnetic Fe2O3 Beads-CdSe/ZnS quantum dots core-shell nanocomposite particles for cell separation. Nano Letters 4: 409-413.

Ruan G, Winter JO. 2011. Alternating-color quantum dot nanocomposites for particle tracking. Nano letters 11: 941-945.

Ruan G, Agrawal A, Marcus AI, Nie S. 2007. Imaging and tracking of tat peptide-conjugated quantum dots in living cells: new insights into nanoparticle uptake, intracellular transport, and vesicle shedding. Journal of the American Chemical Society 129: 14759-14766.

Ryman-Rasmussen JP, Riviere JE, Monteiro-Riviere NA. 2007. Surface coatings determine cytotoxicity and irritation potential of quantum dot nanoparticles in epidermal keratinocytes. The Journal of investigative dermatology 127: 143-153.

Schumacher JF, Carman ML, Estes TG, Feinberg AW, Wilson LH, Callow ME, Callow JA, Finlay JA, Brennan AB. 2007. Engineered antifouling microtopographies - effect of feature size, geometry, and roughness on settlement of zoospores of the green alga Ulva. Biofouling 23: 55-62.

Sealfon SC, Chan PM, Yuen T, Ruf F, Gonzalez-Maeso J. 2005. Method for multiplex cellular detection of mRNAs using quantum dot fluorescent in situ hybridization. Nucleic Acids Research 33.

Seger R, Krebs EG. 1995. The MAPK signaling cascade. The FASEB journal : official publication of the Federation of American Societies for Experimental Biology 9: 726-735.

Shah B, Clark P, Stroscio M, Mao J. 2006. Labeling and imaging of human mesenchymal stem cells with quantum dot bioconjugates during proliferation and osteogenic differentiation in long term. Conference proceedings : ... Annual International Conference of the IEEE Engineering in Medicine and Biology Society. IEEE Engineering in Medicine and Biology Society. Conference 1: 1470-1473.

Shidoji Y, Hayashi K, Komura S, Ohishi N, Yagi K. 1999. Loss of molecular interaction between cytochrome c and cardiolipin due to lipid peroxidation. Biochem Biophys Res Commun 264: 343-347.

Shiohara A, Hoshino A, Hanaki K, Suzuki K, Yamamoto K. 2004. On the cyto-toxicity caused by quantum dots. Microbiol Immunol 48: 669-675.

Singh N, Manshian B, Jenkins GJ, Griffiths SM, Williams PM, Maffeis TG, Wright CJ, Doak SH. 2009. NanoGenotoxicology: the DNA damaging potential of engineered nanomaterials. Biomaterials 30: 3891-3914.

Stern ST, Zolnik BS, McLeland CB, Clogston J, Zheng J, McNeil SE. 2008. Induction of autophagy in porcine kidney cells by quantum dots: a common cellular response to nanomaterials? Toxicological sciences : an official journal of the Society of Toxicology 106: 140-152.

Su Y, Hu M, Fan C, He Y, Li Q, Li W, Wang LH, Shen P, Huang Q. 2010. The cytotoxicity of CdTe quantum dots and the relative contributions from released cadmium ions and nanoparticle properties. Biomaterials 31: 4829-4834.

Su YY, He Y, Lu HT, Sai LM, Li QN, Li WX, Wang LH, Shen PP, Huang Q, Fan CH. 2009. The cytotoxicity of cadmium based, aqueous phase - Synthesized, quantum dots and its modulation by surface coating. Biomaterials 30: 19-25.

Sukhanova A, Devy J, Venteo L, Kaplan H, Artemyev M, Oleinikov V, Klinov D, Pluot M, Cohen JH, Nabiev I. 2004. Biocompatible fluorescent nanocrystals for

immunolabeling of membrane proteins and cells. Analytical biochemistry 324: 60-67.

Tan WB, Huang N, Zhang Y. 2007. Ultrafine biocompatible chitosan nanoparticles encapsulating multi-coloured quantum dots for bioapplications. Journal of Colloid and Interface Science 310: 464-470.

Tang M, et al. 2008a. Unmodified CdSe quantum dots induce elevation of cytoplasmic calcium levels and impairment of functional properties of sodium channels in rat primary cultured hippocampal neurons. Environ Health Perspect 116: 915-922.

Tang ML, Wang M, Xing TR, Zeng J, Wang HL, Ruan DY. 2008b. Mechanisms of unmodified CdSe quantum dot-induced elevation of cytoplasmic calcium levels in primary cultures of rat hippocampal neurons. Biomaterials 29: 4383-4391.

Tang ML, et al. 2008c. Unmodified CdSe quantum dots induce elevation of cytoplasmic calcium levels and impairment of functional properties of sodium channels in rat primary cultured hippocampal neurons. Environmental Health Perspectives 116: 915-922.

Tang Z, Ozturk B, Wang Y, Kotov NA. 2004. Simple Preparation Strategy and One-Dimensional Energy Transfer in CdTe Nanoparticle Chains. J. Phys. Chem. B 108: 6927-6931.

Teeguarden JG, Hinderliter PM, Orr G, Thrall BD, Pounds JG. 2007. Particokinetics in vitro: dosimetry considerations for in vitro nanoparticle toxicity assessments. Toxicological sciences : an official journal of the Society of Toxicology 95: 300-312.

Texier I, Josser V. 2009. In vivo imaging of quantum dots. Methods in molecular biology 544: 393-406.

Toworfe GK, Composto RJ, Adams CS, Shapiro IM, Ducheyne P. 2004. Fibronectin adsorption on surface-activated poly(dimethylsiloxane) and its effect on cellular function. J Biomed Mater Res A 71: 449-461.

Travas-Sejdic J, Peng H, Zhang LJ, Kjallman THM, Soeller C. 2007. DNA hybridization detection with blue luminescent quantum dots and dye-labeled single-stranded DNA. Journal of the American Chemical Society 129: 3048-+.

Tsay JM, Michalet X. 2005. New light on quantum dot cytotoxicity. Chemistry & biology 12: 1159-1161.

Vanmaekelbergh D, Liljeroth P. 2005. Electron-conducting quantum dot solids: novel materials based on colloidal semiconductor nanocrystals. Chem Soc Rev 34: 299-312.

Vazquez M, Sabharwal N, Holland EC. 2009. Live Cell Labeling of Glial Progenitor Cells Using Targeted Quantum Dots. Annals of Biomedical Engineering 37: 1967-1973.

Vu TQ, Maddipati R, Blute TA, Nehilla BJ, Nusblat L, Desai TA. 2005. Peptide-conjugated quantum dots activate neuronal receptors and initiate downstream signaling of neurite growth. Nano Lett 5: 603-607.

Wan R MY, Zhang X, Chien S, Tollerud D J, Zhang Q. 2008. Matrix metalloproteinase-2 and -9 are induced differently by metal nanoparticles in human monocytes: The role of oxidative stress and protein tyrosine kinase activation Toxicol. Appl. Pharm. 233: 276-285.

Wang L, Nagesha DK, Selvarasah S, Dokmeci MR, Carrier RL. 2008a. Toxicity of CdSe Nanoparticles in Caco-2 Cell Cultures. J Nanobiotechnology 6: 11.

Wang L, Nagesha D, Selvarasah S, Dokmeci M, Carrier R. 2008b. Toxicity of CdSe Nanoparticles in Caco-2 Cell Cultures. Journal of Nanobiotechnology 6: 11.

Wang TH, Zhang CY, Yeh HC, Kuroki MT. 2005. Single-quantum-dot-based DNA nanosensor. Nature Materials 4: 826-831.

Watson P, Jones AT, Stephens DJ. 2005. Intracellular trafficking pathways and drug delivery: fluorescence imaging of living and fixed cells. Adv Drug Deliv Rev 57: 43-61.

Wick P, Manser P, Limbach LK, Dettlaff-Weglikowska U, Krumeich F, Roth S, Stark WJ, Bruinink A. 2007. The degree and kind of agglomeration affect carbon nanotube cytotoxicity. Toxicology letters 168: 121-131.

Wong CH, Samuel M, Tan BK, Song C. 2006. Capsular contracture in subglandular breast augmentation with textured versus smooth breast implants: A systematic review. Plastic and reconstructive surgery 118: 1224-1236.

Wong JY, Leach JB, Brown XQ. 2004. Balance of chemistry, topography, and mechanics at the cell-biomaterial interface: Issues and challenges for assessing the role of substrate mechanics on cell response. Surface Science 570: 119-133.

Wu X, Liu H, Liu J, Haley KN, Treadway JA, Larson JP, Ge N, Peale F, Bruchez MP. 2003a. Immunofluorescent labeling of cancer marker Her2 and other cellular targets with semiconductor quantum dots. Nat Biotechnol 21: 41-46.

Wu X, Liu H, Liu J, Haley KN, Treadway JA, Larson JP, Ge N, Peale F, Bruchez MP. 2003b. Immunofluorescent labeling of cancer marker Her2 and other cellular targets with semiconductor quantum dots. Nat. Biotech. 21: 41-46.

Xiao GG, Wang M, Li N, Loo JA, Nel AE. 2003. Use of proteomics to demonstrate a hierarchical oxidative stress response to diesel exhaust particle chemicals in a macrophage cell line. J Biol Chem 278: 50781-50790.

Xie HY, Xie M, Zhang ZL, Long YM, Liu X, Tang ML, Pang DW, Tan Z, Dickinson C, Zhou W. 2007. Wheat germ agglutinin-modified trifunctional nanospheres for cell recognition. Bioconjugate Chemistry 18: 1749-1755.

Yang Y, Xu K, Koike T, Zheng X. 2008. Transport of autophagosomes in neurites of PC12 cells during serum deprivation. Autophagy 4: 243-245.

Yim EK, Reano RM, Pang SW, Yee AF, Chen CS, Leong KW. 2005. Nanopattern-induced changes in morphology and motility of smooth muscle cells. Biomaterials 26: 5405-5413.

Yu WW, Qu LH, Guo WZ, Peng XG. 2003. Experimental determination of the extinction coefficient of CdTe, CdSe, and CdS nanocrystals. Chem. Mater. 15: 2854-2860.

Zhang CY, Hu J. 2010. Single Quantum Dot-Based Nanosensor for Multiple DNA Detection. Analytical Chemistry 82: 1921-1927.

Zhang H, Sachdev D, Wang C, Hubel A, Gaillard-Kelly M, Yee D. 2009a. Detection and downregulation of type I IGF receptor expression by antibody-conjugated quantum dots in breast cancer cells. Breast cancer research and treatment 114: 277-285.

Zhang T, Stilwell JL, Gerion D, Ding L, Elboudwarej O, Cooke PA, Gray JW, Alivisatos AP, Chen FF. 2006. Cellular effect of high doses of silica-coated quantum dot profiled with high throughput gene expression analysis and high content cellomics measurements. Nano letters 6: 800-808.

Zhang W, Chen G, Wang J, Ye BC, Zhong X. 2009b. Design and synthesis of highly luminescent near-infrared-emitting water-soluble CdTe/CdSe/ZnS core/shell/shell quantum dots. Inorganic chemistry 48: 9723-9731.

Zhang Y, Chen W, Zhang J, Liu J, Chen G, Pope C. 2007. In vitro and in vivo toxicity of CdTe nanoparticles. Journal of Nanoscience and Nanotechnology 7: 497-503.

Zhukov T, Zajac A, Song DS, Qian W. 2007. Protein microarrays and quantum dot probes for early cancer detection. Colloids and Surfaces B-Biointerfaces 58: 309-314.

PUBLISHED PAPERS

JOURNAL OF NANOBIOTECHNOLOGY

RESEARCH Open Access

Long-term exposure of CdTe quantum dots on PC12 cellular activity and the determination of optimum non-toxic concentrations for biological use

Babu R Prasad[1†], Natalia Nikolskaya[1], David Connolly[1], Terry J Smith[1], Stephen J Byrne[2*†], Valérie A Gérard[2], Yurii K Gun'ko[2], Yury Rochev[1*]

Abstract

Background: The unique and tuneable photonic properties of Quantum Dots (QDs) have made them potentially useful tools for imaging biological entities. However, QDs though attractive diagnostic and therapeutic tools, have a major disadvantage due to their inherent cytotoxic nature. The cellular interaction, uptake and resultant toxic influence of CdTe QDs (gelatinised and non-gelatinised Thioglycolic acid (TGA) capped) have been investigated with pheochromocytoma 12 (PC12) cells. In conjunction to their analysis by confocal microscopy, the QD - cell interplay was explored as the QD concentrations were varied over extended (up to 72 hours) co-incubation times. Coupled to this investigation, cell viability, DNA quantification and cell proliferation assays were also performed to compare and contrast the various factors leading to cell stress and ultimately death.

Results: Thioglycolic acid (TGA) stabilised CdTe QDs (gel and non - gel) were co-incubated with PC12 cells and investigated as to how their presence influenced cell behaviour and function. Cell morphology was analysed as the QD concentrations were varied over co-incubations up to 72 hours. The QDs were found to be excellent fluorophores, illuminating the cytoplasm of the cells and no deleterious effects were witnessed at concentrations of ~10^{-9} M. Three assays were utilised to probe how individual cell functions (viability, DNA quantification and proliferation) were affected by the presence of the QDs at various concentrations and incubation times. Cell response was found to not only be concentration dependant but also influenced by the surface environment of the QDs. Gelatine capping on the surface acts as a barrier towards the leaking of toxic atoms, thus reducing the negative impact of the QDs.

Conclusion: This study has shown that under the correct conditions, QDs can be routinely used for the imaging of PC12 cells with minimal adverse effects. We have found that PC12 cells are highly susceptible to an increased concentration range of the QDs, while the gelatine coating acts as a barrier towards enhanced toxicity at higher QD concentrations.

Background

Semiconductor nanoparticles or Quantum Dots (QDs) have been widely touted as new replacements for traditional dyes for the imaging of living cells and tissues. Due to their extremely small size QDs can, *via* specific and non-specific pathways penetrate and label both the exterior and interior of numerous cell types [1-7]. They are highly resistant to photobleaching [2,8-10] and their broad absorption ranges allow for their excitation and multiplexed detection across a wide spectrum of wavelengths [11-14].

Minute changes in the radius of QDs manifests as visible colour changes of the QDs in solution. This property may lead to their potential use as simultaneous multiple

* Correspondence: sbyrne3@tcd.ie; yury.rochev@nuigalway.ie
† Contributed equally
[1]National Centre for Biomedical Engineering Science, National University of Ireland, Galway, Ireland
[2]CRANN and The School of Chemistry, Trinity College Dublin, Dublin 2, Ireland

colour labels [15-17] The difference in size can also affect their uptake may lead to alterations in cellular activity and cytotoxicity [18,19].

Our studies are focussed on the analysis of PC12 cells which have the ability to be differentiated into neurons upon treatment with nerve growth factors (NGF). The application of QDs to neuroscience specific fields is currently emerging [20-25] and various groups have investigated the specific labelling of neurons with QDs. Nerve growth factors were QD tagged by Vu *et al* [26], QD micelles were up taken by rat hippocampal neurons as shown by Fan *et al* [27], while various antibody and peptide labelled QDs have also been explored [6,20,28-32]. However, advances in molecular medicine require the safe detection of individual biomolecules, cell components and other biological entities. One significant problem with QDs is their heavy metal composition [33-35], which has given genuine cause for concern due to their potential cytotoxicity [33,35,36]. In an effort to combat this problem, much research has been conducted into the mechanisms that result in QDs acting as toxic agents once exposed to a cellular environment [37-43] and ways of reducing their toxicological impact *via* non-toxic coatings [44].

While QDs have been investigated with a large variety of cell lines and types; more recently, in search of new neurotherapeutic and neuroprosthetic strategies, QDs have been explored to manipulate and create active cellular interfaces with nerve cells [19,20]. However, the application of such entities to neuron cell imaging is limited and while QDs have been used for cell labelling experiments, little work has been undertaken into measuring the ranges of neuron cell response over long time scales upon their perturbation by the QDs.

The purpose of the study was to explore the potential for labelling of undifferentiated Pheochromocytoma 12 (PC12) cells with gelatinised and non-gelatinised TGA capped CdTe QDs. We have studied serial co-incubations of 24, 48 and 72 hours and analysed the effect of three factors namely concentration, co-incubation time and surface modification in parallel to three assays measuring cell viability, proliferation and DNA quantification. Although shorter incubation periods have been used by some groups to investigate the toxicity [42,45], long term exposure is more reliable. There are a number of studies which have investigated the toxicity of QDs for 24 hour co-incubations and demonstrated that increasing concentrations increase cell toxicity significantly [23,45-48].

Results and Discussion

Optical characteristics

The two types of QDs utilised (gel and non-gel) were synthesised using a modification of a previously published procedure [49]. This synthetic route allows for the production of highly luminescent and crystalline CdTe QDs. Briefly, H_2Te gas was bubbled through an basic aqueous solution containing $Cd(ClO_4)_26H_2O$, thioglycolic acid (TGA) stabiliser and dissolved gelatine where appropriate. The resultant non-luminescent mixture was heated under reflux. The crude solutions were purified *via* size selective precipitation and individual fractions were characterised by UV-vis absorption and photoluminescence (PL) emission spectroscopy (λ_{ex} 425 nm). Prior to initiating cell culturing experiments, the QDs were further purified using sephadex (G25). This enabled us to remove any residual un-reacted moieties that may have been present from the original crude solution. Two differently sized batches of QDs (for both gel and non-gel QDs) were synthesised to allow us to investigate if the additional parameter of QD size had any impact on cell response. Figure 1 shows the typical absorption and emission profiles indicative of aqueous CdTe QDs. As there are no differences in the spectral characteristics of gel and non-gel QDs, one spectrum indicative of each size is shown for clarity.

The spectra shown in Figure 1 highlight the well resolved emission and absorption characteristics of the QDs. Narrow emission spectra (<40 nm full with half maximum [FWHM]) indicate <5% particle size distributions throughout. Gelatine was introduced during the synthesis of the QDs and its presence while altering QD growth rates and QYs [44], does not significantly alter the size distribution of the QDs and acts primarily as a co-capping agent.

Quantum yields (QYs) for the solutions (measured against Rhodamine 6G) were ~25% for the non-gel and ~35% for the gel QDs. As the presence of uncapped surface atoms provides alternate pathways for the non-radiative recombination of photons, the difference in QYs indicate the highly effective capping qualities of the gelatine.

To examine the quantity of gelatine on the QD surface we analysed the QDs using thermogravimetric analysis (TGA). This process involves burning the sample to be examined and measuring the weight loss against temperature (Figure 2).

For TGA experiments, each sample was first dried and subsequently weighed. The sample was then heated (from 30 to 900°C at a rate of 10°C/min) and as each component was burned off, the weight changes were recorded. For both types of QDs several steps can be seen. The initial drop in weight is due to the removal of water molecules. Following on, we can now see the weight loss due to the removal of the organic molecules from the QD surface. We can see a clear difference in the profiles of the two QD types. The gel QDs show an additional weight loss (~10%) at ~500°C compared to the non-gel QDs thus indicating the presence of excess

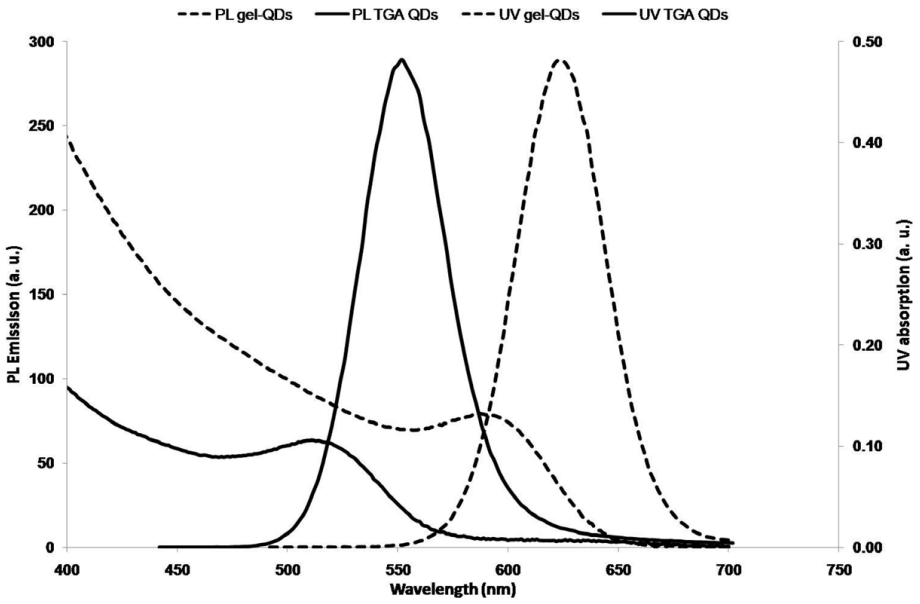

Figure 1 Absorption and emission spectra. UV-vis absorption and fluorescence emission spectra (λ_{em} 450 nm) of the differently sized (~2.5 nm - solid line & ~4.5 nm - dashed line) QDs synthesised and co-incubated with the PC12 cells.

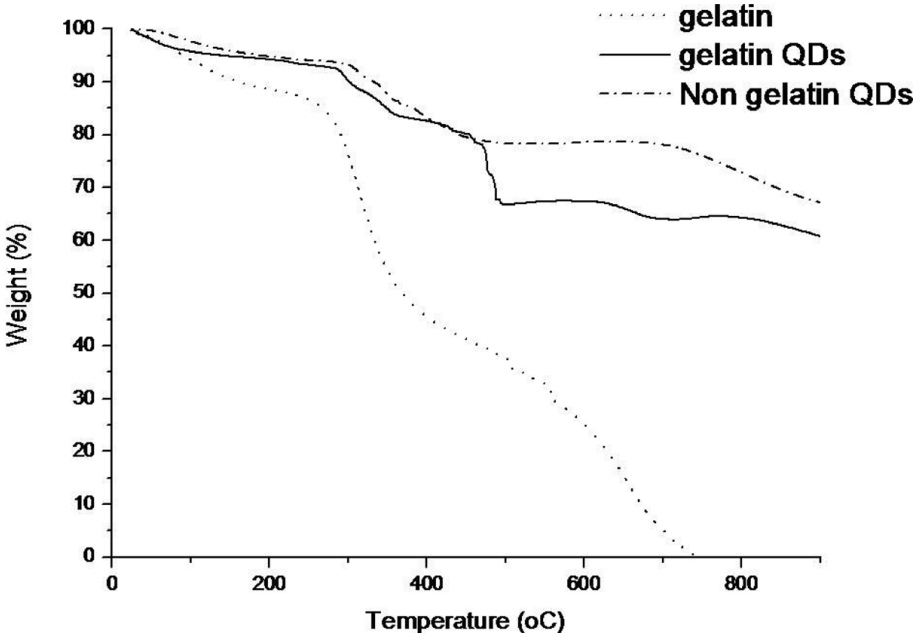

Figure 2 Thermogravimetric analysis. Graph showing the percentage weight loss for the QD and gelatine samples upon heating to 900°C.

organic groups that we are attributing the gelatine coating. We have also analysed the behaviour of gelatine under the same conditions as an additional guide.

High resolution transmission electron microscope (HRTEM) images were taken to examine the structure and morphology of the two differently sized types of QDs (Figure 3).

HRTEM images of the different sized QDs show the highly crystalline nature of both the gel and non-gel QDs (Figure 3). Lattice spacings are in agreement with those expected for the (111) plane of cubic zinc blend CdTe [50]. We have previously shown that although the presence of gelatine during the synthesis of the QDs can influence the rate of QD growth and QY [44], it does not

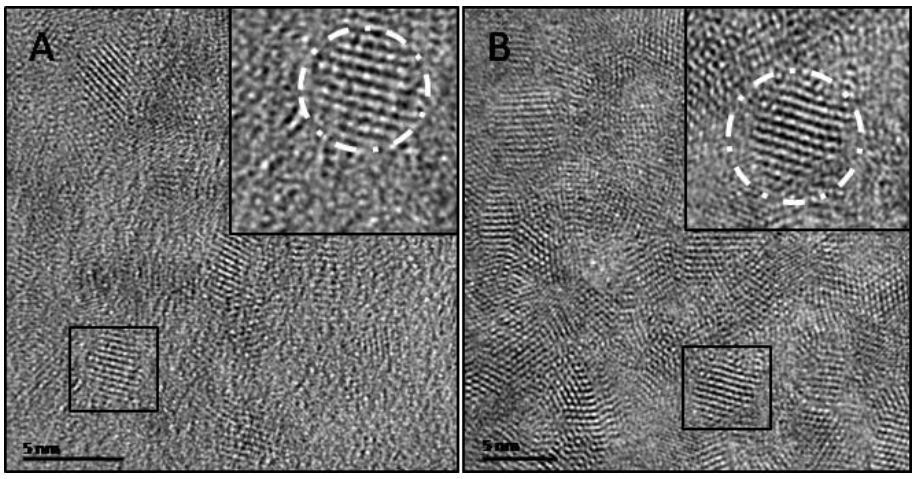

Figure 3 HRTEM QD characterisation. HRTEM images of (A) non-gel (~2.5 nm) and (B) gel (~4.5 nm) capped CdTe QDs. (Inserts are blown up images of highlight QDs).

seem to alter the physical structure of the QDs. Consequently, as can be seen from the resulting QY's, the gelatine must act solely as a co-capping agent for the protection of the QD surface and the reduction of non-radiative transitions. The incorporation of gelatine during the QD synthesis results in smaller QDs being produced under the same conditions compared to non-gel QDs but does not seem to alter or influence the size distribution with the particle ensemble. Following size selective purification, size distributions for spectroscopically similar gel and non gel samples were comparable with the only noticeable difference being their respective QYs.

The influence of this additional exterior coating upon uptake and any induced toxicity were some of the properties we wished to explore with the PC12 cells.

We have also conducted a number of experiments in an effort to empirically relate the actual mass (mg of QDs per ml) of the QDs used in solution to their determined concentration [17]. (note: QDs treated as individual molecules for the purpose of concentration determination). Several different batches of gel and non-gel QDs were dried under rotary evaporation. A measured amount of the resulting QD powder was then weighed and dissolved in exactly 1 ml of purified water. The molar concentration was then determined for each individual batch [17]. Figure 4 illustrates the relationship between QD weight and molar concentration (M) for our QDs used.

As expected there is a linear relationship between measured QD concentration and powdered weight. This

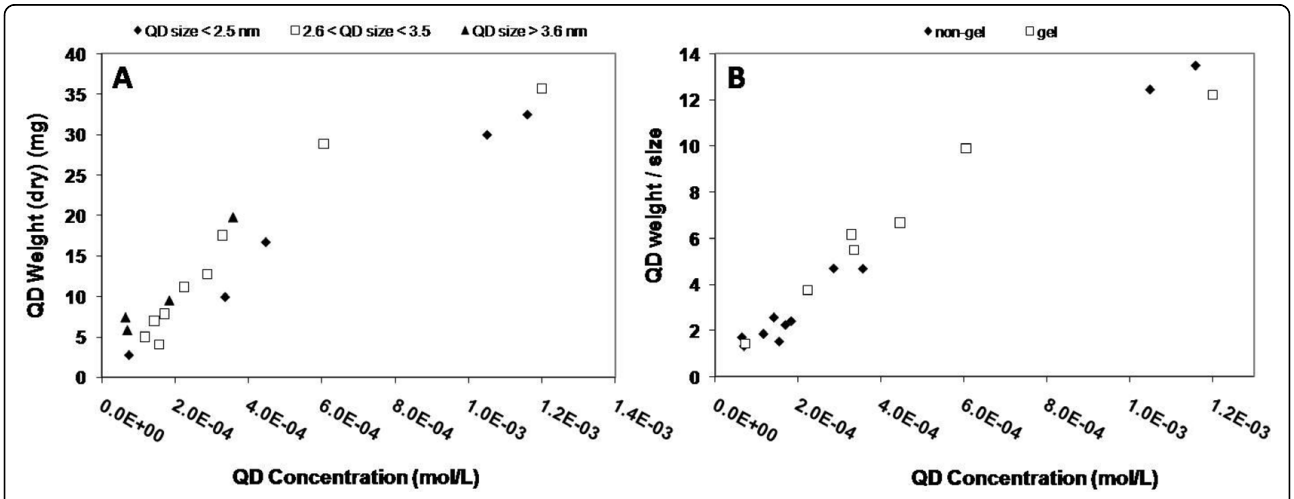

Figure 4 QD weight versus concentration profile. Graphs illustrating the relationship between measured QD concentration and QD powdered weight (A) and QD powdered weight/size (B).

allows us to postulate as to the concentration (mg/ml) of QDs that we have used throughout our experimental analysis. We have also included a plot of concentration against weight/size, to give a fuller empirical relationship for the system under investigation. It must be noted that as the QDs are dried from solution (although fully purified), there is the possibility that QD degradation may occur which increases the experimental error with regards to concentration, but overall it does give us a good general indication.

To investigate any possible degradation of the QDs without the presence of the PC12 cells, we carried out a number of experiments to analyse the effect of co-incubating the QDs with only the cell culture medium (Figure 5 and 6).

Figures 5 and 6 show the evolution of the UV-vis absorption and PL emission (λ_{ex} 480 nm) spectra of non-gel and gel QDs respectively in cell culture medium over time. The unusual shape of the UV spectra is due to the interference caused by the culture medium. This was used as a background throughout but its effect could not be completely removed. For the gel QDs at 0 hours, the UV spectrum is as expected but as the incubation times increased, the effect of the medium became apparent. Most importantly however, the UV spectra of both QD types remain consistent and do not drop even after 72 hours. This indicates that the core structures of the QDs remain intact and that no significant degradation to the QDs themselves is occurring. If degradation were occurring, the baseline would rise as the QD begin to precipitate from solution and the absorbance and structure of the spectrum would decrease significantly. This core stability is further corroborated by the PL spectra which show an initial drop after 48 hours, but stability thereafter. This quenching of the emission properties of the QDs is common when recorded in the presence of biological media.

Previously, we have investigated the effect of QD and protein charge on QD spectra and cellular interactive characteristics [51]. As the medium contains serum, these spectral changes can be attributed to the interaction of the various proteins present with the QD surface. These interactions do not lead to the degradation of the QDs, but do provide alternate pathways for radiative recombination, thus resulting in lower fluorescence intensities. If the QDs begin to degrade following cellular uptake, resulting in leeching of the core atoms; it must be attributable to the harsh intracellular conditions that the QDs face within the cytoplasm.

Our next aim was to analyse the effect of the QDs on cell behaviour and morphology also to then investigate any alterations to cell proliferation, viability and DNA quantification using pre-determined assays over extended co-incubation times.

1. Uptake of QDs and their effect on cell morphology

Stock gel and non-gel QD solutions (10^{-4} M) [17] were diluted to a range of concentrations ($10^{(-7)-(-9)}$ M) and

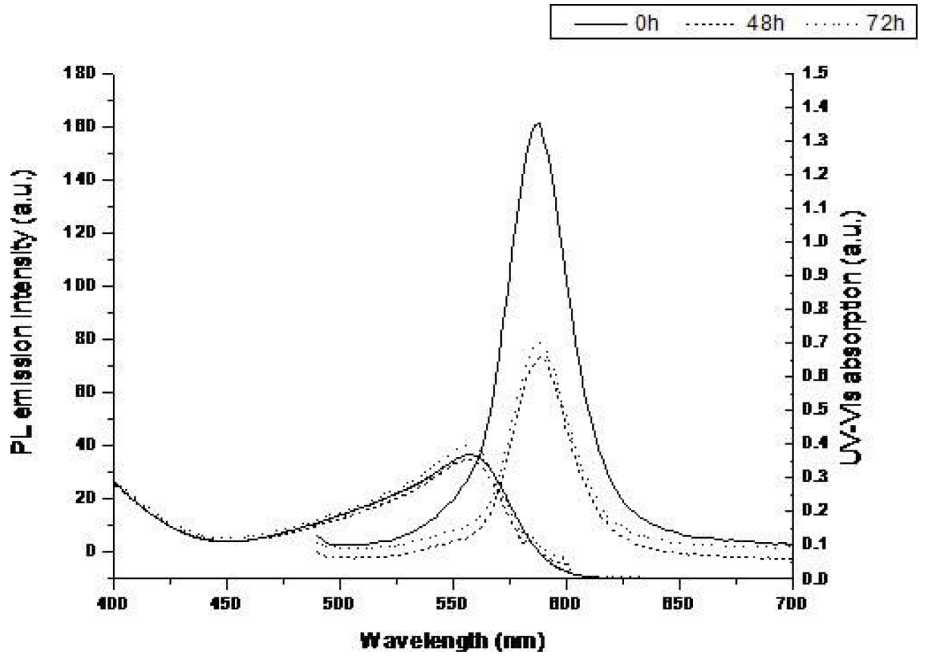

Figure 5 QD interactions with cell culture medium. Evolution of UV-vis absorption and PL emission spectra (λ_{exc} 480 nm) of non-gel QDs in cell culture medium over time.

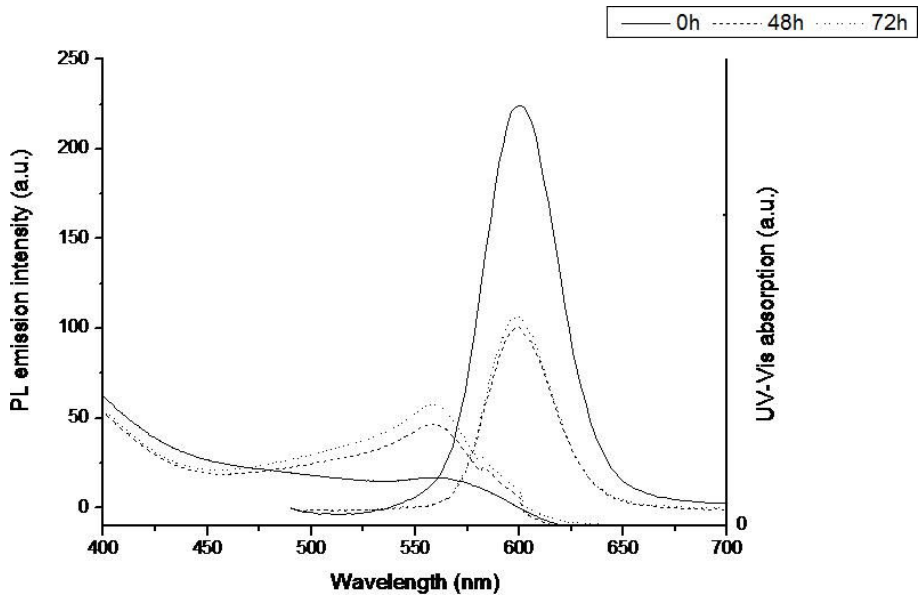

Figure 6 QD interactions with cell culture medium. Evolution of UV-vis absorption and PL emission spectra (λ_{exc} 480 nm) of gel QDs in cell culture medium over time.

incubated with the cells as described in the experimental section. Confocal images were taken to visually inspect QD uptake, localisation and cell morphology following incubation (Figures 7, 8, 9).

Figure 7, panels A and B show PC12 cells following 72 hours of co-incubation with 10^{-7} M and 10^{-9} M concentrations of QDs respectively. In panel A, the cells were seen to be rounded and floating in the nutrient rich medium. This contrasts the morphology of the cells in panel B and the control cells (panel C), which were attached to the culture plate and polygonal in shape. It can be noted that as QD concentrations were reduced, the effect on the cell morphology was eliminated and the cells were morphologically identical to the control cells (Figure 7, panels B and C). Although some earlier studies [23,48] have shown similar concentration dependence, there is no study investigating the effect on cell morphology at the extended time periods of 48 and 72 hours [45]. Green fluorescence in the PC12 cells is due to QDs localisation in the cytoplasm.

Figure 8 shows the fluorescent image (panel A) and overlaid corresponding differential interference contrast (DIC) image (panel B) of the PC12 cells treated with a 10^{-9} M concentration of QDs following 72 hours of co-incubation. The QDs are found to be located within the cytoplasm of PC12 cells.

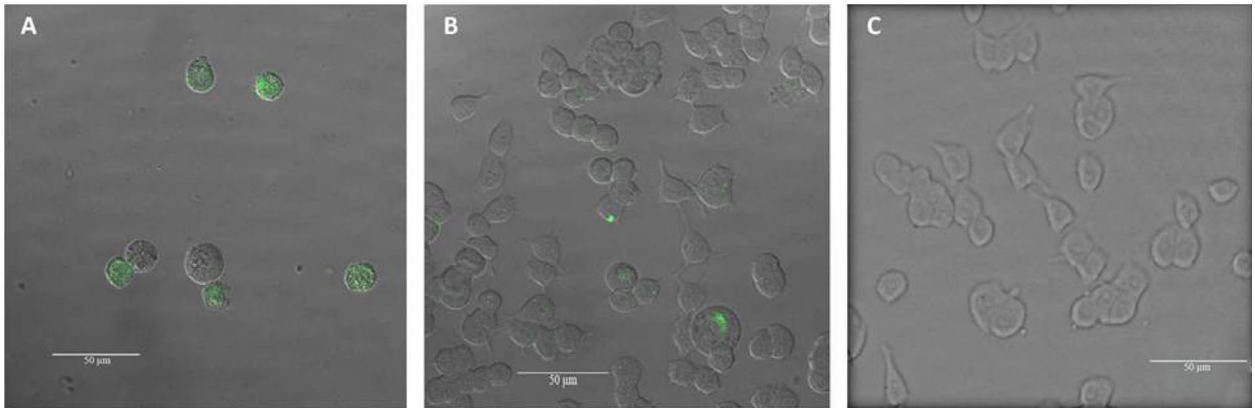

Figure 7 Confocal image. Fluorescent confocal image and corresponding differential interference contrast (DIC) images of PC12 cells exposed to a 10^{-7}M concentration of QDs (A), 10^{-9} M concentration of QDs (B) and a control sample with no QDs (C) following 72 hours of co-incubation. Scale bar = 50 µm.

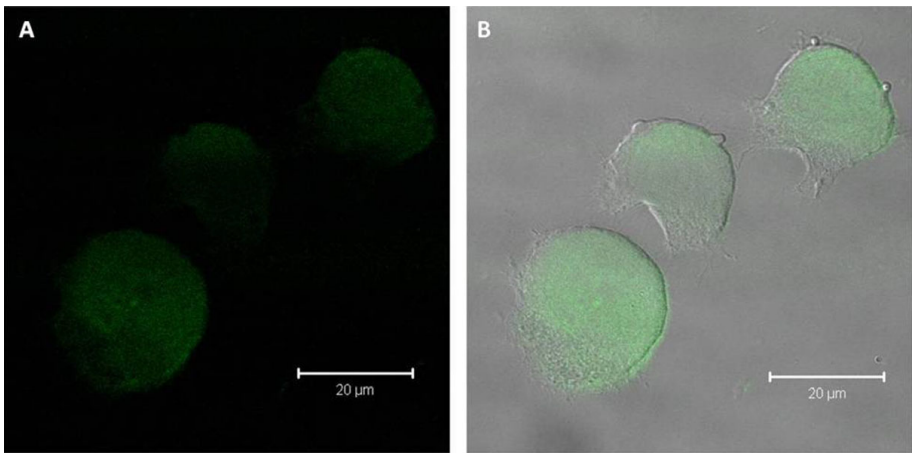

Figure 8 Confocal Image. Fluorescent confocal image of PC12 cells exposed to a 10^{-9} M concentration of QDs (A) and corresponding differential interference contrast (DIC) image (B) with A overlaid following 72 hours of co-incubation [scale bar = 20 μm].

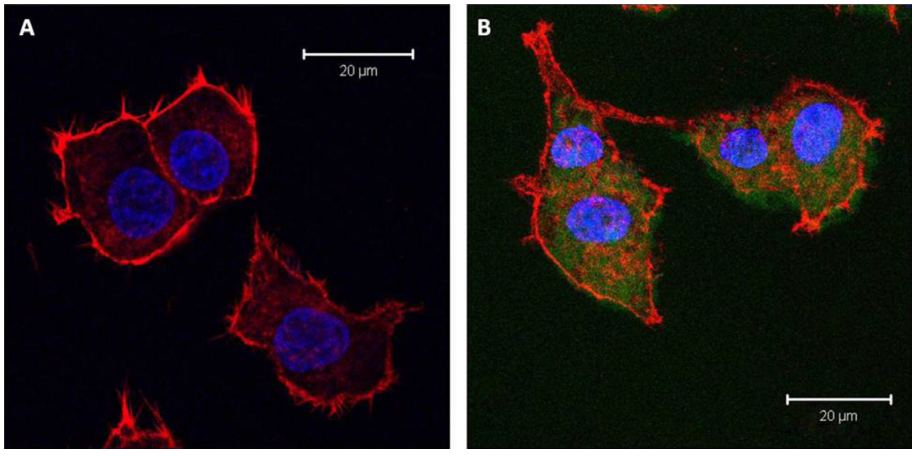

Figure 9 Confocal images. Fluorescent confocal images to illustrate the morphology of the actin stained PC12 cells with no QDs (A) as a control and PC12 cells exposed to the QDs (B) [conc. 10^{-9} M] following 72 hours of co-incubation. [Scale bar = 20 μm].

To enhance visualization, the nucleus and cellular membrane have been actin stained with blue and red colour respectively (Figure 9). The QDs (green luminescence) are visualized predominantly in the cytoplasm and their presence even after a 72 hour co-incubation in this region, does not seem to significantly perturb the cells. The cell morphology does not change when evaluated against the controls.

These initial observations illustrate the effect of changing QD concentration on cell survival and morphology and to further investigate cell behaviour, several assays were used to study the effect on cell proliferation, growth and metabolic activity.

2. Effect of QDs on cellular activity

The consequence of co-incubating classical molecules on the cell viability can be reliably predicted using single assays [52], however, the dynamics of nanomaterials are not as comprehensively understood and hence drawing conclusions from single cell viability assays can be misleading. As such additional assays are required to give a more comprehensive analysis when determining nanoparticle toxicity for risk assessment [52].

Consequently, alamarBlue (metabolic activity), PicoGreen (total DNA quantification) and ELISA BrdU (colorimetric assay for quantification of proliferating DNA) assays were run to analyse the effect of different QD concentrations, type and size following 24, 48 and 72 hour co-incubations with the PC12 cells.

The red/orange labels serve to differentiate the various QDs by size [~2.5 nm (orange) and ~4.5 nm (red)] and were used to investigate if the measured cell responses were in any way size dependant. The gel/non-gel label refers to the presence of gelatine during the synthesis of the QD and these different QDs were analysed to

investigate the influence that gelatine imparts on the QD induced cell toxicity.

The changes in luminescence intensity measured in response to the introduction of QDs to the cell cultures throughout all of our experiments can be solely attributed to direct interactions of the staining dyes upon entering the cells. Energy transfer to the dyes can be ruled out *via* a number of routes. Firstly, the dyes and QDs enter different regions of the cells and as such cannot interact directly on the scale required for FRET or other energy transfer phenomena. Secondly, the intensity (arbitrary units) of the dye emission is of the order of $\sim 10^3$ while the QDs display $\sim 10^2$. Thus, any energy transferred to the dye would be of an order of magnitude lower and would have a minimal effect on the emission intensity. Negative and background controls in our experiments also substantiate this fact.

2.1 AlamarBlue Assay

Viability of the PC12 cells, for different concentrations, sizes and types of QDs was investigated with an alamarBlue assay and the results graphed in Figure 10. This is a non-destructive assay and allows for the cells to be further utilised following analysis.

The graph shown in Figure 10 illustrates the alamarBlue response (percentage of reduced alamarBlue) for the PC12 cells following 24, 48 and 72 hour co-incubations with the QDs.

As seen in Figure 10, at 10^{-7} M QD concentrations the toxicity is extremely high at all incubation times, and approached the levels of negative controls after only 48 hours. We can see the influence of the gelatine coating up to 24 hours as cell viability responses are significantly higher for the gel QDs compared to their non-gel counterparts. Notably, all responses are lower than the controls indicating that at this concentration the presence of any foreign entities generate a detrimental environment for the cells and result in high levels of cell death.

At 10^{-8} M QD concentrations, we can now see a shift with respect to viability response. Initially after 24 hours, responses are comparable (note: orange non-gel QDs do show a slightly decreased response) between QD types and also to controls. This indicates that over this short incubation period, the cells are not significantly perturbed by the QDs at this concentration.

At 48 and 72 hours, the cell responses now mimic those seen for 10^{-7}M concentrations and have dropped in comparison to controls; however, significant differences are noted between the two QD types. Responses for the gel QDs are considerably higher than those of

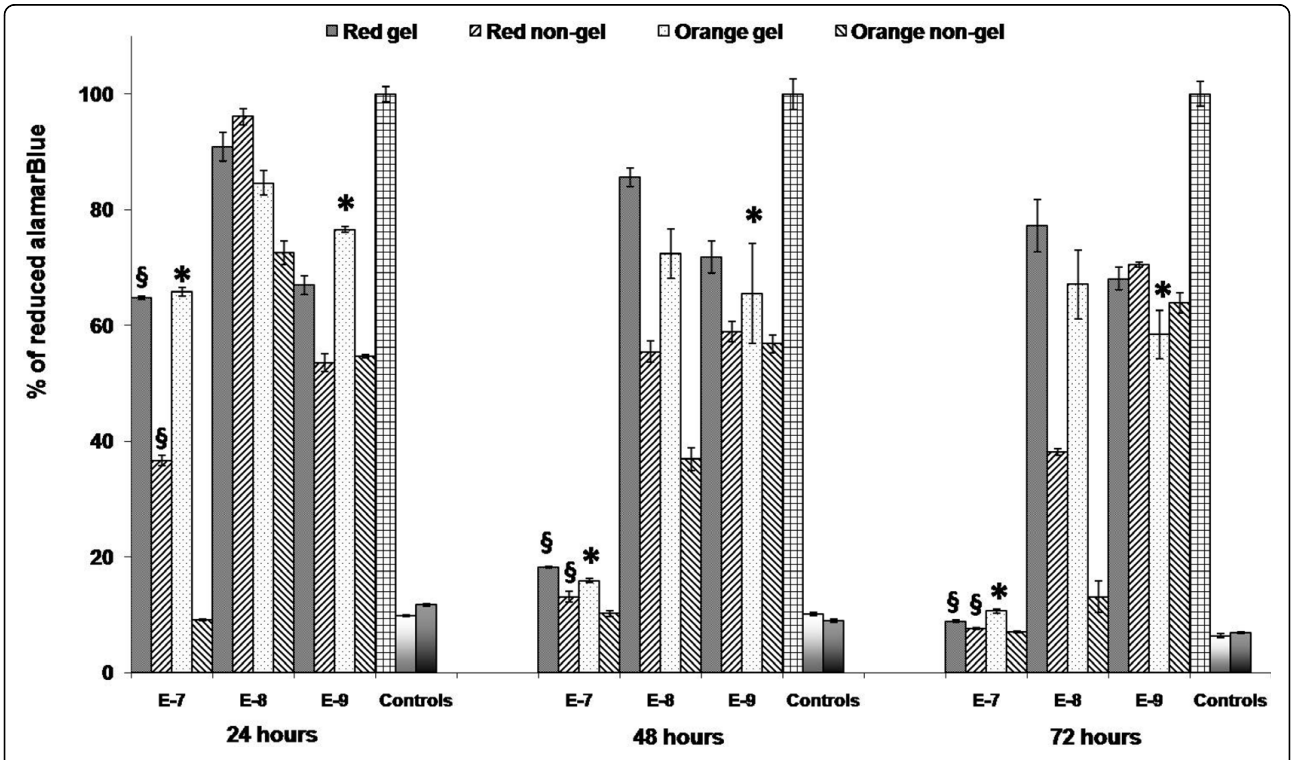

Figure 10 AlamarBlue histograms. AlamarBlue assay at 24, 48 and 72 hours showing the viability of PC12 cells after treatment with varying concentrations [10[[(-7)-(-9)] M] of the gel and non-gel QDs. From left to right, controls [positive, negative, background] are also shown. §denotes examples of statistical significance due to effect of gelatine, * denotes examples of statistical significance due to effect of concentration using a one- way ANOVA ($p < 0.05$) by Tukey's mean comparison.

the non-gel QDs and of note; the red QDs (whether gel or non-gel) are seemingly less toxic than the smaller orange QDs. This may be attributed to the fact that smaller QDs have been shown to penetrate further into cells than their larger counterparts. As nuclear pores are very small [45], nuclear staining of small "green" QDs and cytoplasmic localisation of larger "red" has demonstrated the size dependant nature of QD uptake [53]. Consequently, the smaller QDs may initiate deleterious cell reactions at far quicker rates than the larger ones.

Analysis of these responses at 48 and 72 hours reinforce the importance of the QD surface environment and the protective nature of the gelatine at this concentration. While the surface gelatine coating helps to reduce the toxicological impact of the QDs at 10^{-8} M concentrations, at 10^{-9} M we see the least amount of differences between QD types. Unlike previous concentrations, where alamarBlue responses decrease when comparing gel and non-gel QDs up to 72 hours, there is a certain amount of consistency when analysing the co-incubated QDs at 10^{-9} M concentrations. There are no significant changes in cell response, across the total incubation period. We can also see that final 72 hour cell responses are actually comparable to those recorded for gel QDs at 10^{-8} M. Throughout; all QDs types elicit responses below the levels of negative controls, however responses for gel QDs are far higher than non-gel QDs, indicating that even though their presence results in a certain level of toxicity, they are far less detrimental than their non-gel counterparts. As QDs are essentially a combination of toxic materials, their negative impact on cell health is to be expected, however as cell response seems to level off we can postulate as to the reasons for the induced QD toxicity.

The PC12s themselves can react to the presence of a foreign object, which may be the reason that overall QD cell responses are lower than the controls even after only 24 hours at low (10^{-9} M) concentrations. From our data it is also notable that at 10^{-9} M QD concentrations, the protective effect of gelatine coating was not obvious, with the sole exception of orange QDs at 24 hours. Thus, it can be argued that increases in cell viability at lower QD concentrations make it difficult for the protective effect of gelatine to be seen. CdTe QDs exert cytotoxicity characterised by decreases in the metabolic activity. The most common pathways involved in the toxicity of QDs are related to Reactive Oxygen Species (ROS). These free radicals act by activating different apoptotic pathways such as caspase-9-, caspase-3 and JNK [54]. Some studies have shown involvement of MAPK pathways *via* over-expression of TNF-α CxCl8 [55] or AP-1 and PTK pathways mediated by MMP2 and 9 over-expression [56]. Although there are different pathways involved, there is no obvious predilection for particular pathways in a particular cell line. A recent study with PC-12 cells has also shown involvement of reactive oxygen species (ROS) [45], where the authors have shown interactions of QDs with sub-cellular components and the detrimental effect of uncapped versus capped QDs [40]. This may indicate that the concentration of the leached atoms or reactive oxygen species even from non-gel QDs is so low at 10^{-9} M as to minimally impact the cells beyond the toxicity induced by their very presence.

Throughout the assay, we can see a progressive increase in cell viability for gel compared to non-gel QDs, indicating that the gelatine must act as an effective barrier towards these processes occurring. While it does not prevent the resulting negative impact on the cells, the gelatine seems to effectively slow down the adverse effects of the QDs on cell viability, allowing for longer cell survival, thus enhancing imaging and analysis over elongated co-incubation times.

These results have been focussed on cell respiratory responses. Our next objective was to find out if the impact of the QDs remains the same for other cellular activities.

2.2 PicoGreen Assay

PicoGreen kit Quant-iT™ dsDNA High-Sensitivity Assay Kit (Invitrogen) was used to quantify the amount of double stranded (ds) DNA in ng/μl.

The graph shown in Figure 11 illustrates the total amount of DNA present (ng/μl) in live PC12 cells after 24, 48 and 72 hours of co-incubation with both the gel and non-gel QDs. This assay allows us to directly relate the impact of the QDs on the overall cell population.

At 10^{-7} M QD concentrations, the histograms for the two QD types trend somewhat similarly to those seen for alamarBlue. Once again, responses never reach that of the control samples indicating the negative effect that the QDs have on this system. However, higher responses are once again recorded for the gel QDs after 24 hours and unlike the alamarBlue assay, the gel QDs show significantly higher results after 48 hours compared to the non-gel QDs. As before after 72 hours, both QD types elicit response similar to negative controls.

These data indicate that this assay seems to be more robust than the alamarBlue. This is an extremely sensitive assay to DNA concentrations and unlike the responses seen previously; there is an apparent shift in cell survival to longer co-incubation times. For example, responses for gel and non-gel QDs were comparable after only 48 hours with alamarBlue, while for PicoGreen this now occurs at 72 hours and this apparent shift continues as the concentrations are reduced.

As the QD concentrations are reduced to 10^{-8} M, we can see that after 24 hours DNA responses are approaching comparability with positive controls. Small differences once again favouring the gel QDs can be

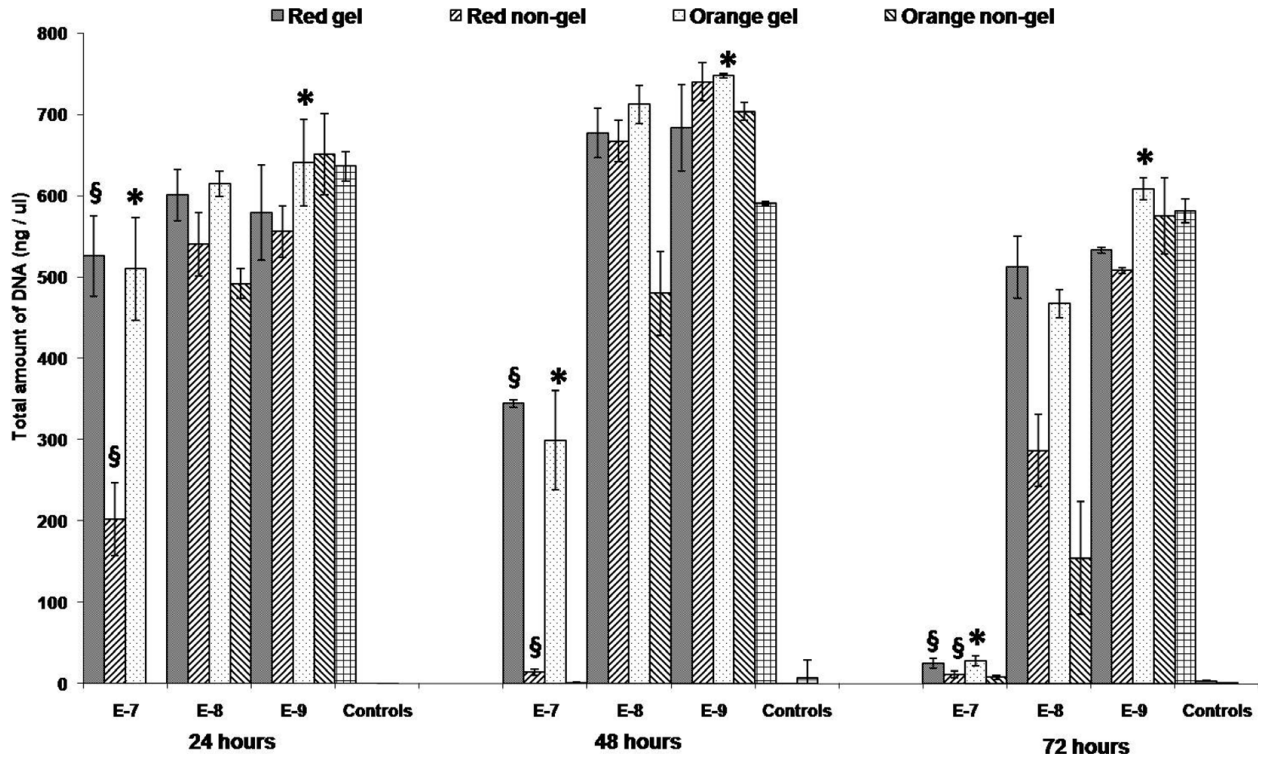

Figure 11 PicoGreen histograms. PicoGreen assay at 24, 48 and 72 hours illustrating the amount of DNA (ng/μl) measured from PC12 neurons following co-incubation with varying concentrations $10^{-7-(-9)}$ M of the gel and non-gel QDs. From left to right, controls [positive, negative, background] are also shown. §denotes examples of statistical significance due to effect of gelatine, * denotes examples of statistical significance due to effect of concentration using a one- way ANOVA ($p < 0.05$) by Tukey's mean comparison.

seen and these continue up to 48 hours. Notably, as recorded before, the orange non-gel QDs begin to show the lowest response indicating their increased impact on cell survival.

Only at 72 hours do we see responses drop below positive controls and significant differences can be seen between the two QD types with once again the gel QDs producing higher responses. Thus, comparing the two assays at this 10^{-8} M QD concentration, the shift to longer co-incubation times is clear indicating of increased cell survival rates and their ability to replicate for longer even in the presence of these toxic entities.

Similarly to the alamarBlue, there is a sense of consistency throughout the PicoGreen assay over all time points at 10^{-9} M QD concentrations. DNA responses are comparable to positive controls and do not drop significantly even after 72 hours of co-incubation. This highlights the robustness of this cellular process to toxic influences at this concentration and also emphasizes the hormetic effect [2,57].

These results further corroborate those from the alamarBlue assay verifying that the nature of the QD surface (gel or non-gel) greatly influences their behaviour and the resulting viability of the cells.

The QD surface must be protected from the harsh intracellular environment if the cells are going to survive long enough to enable useful information about their behaviour and response to be gathered. The presence of gelatine on the QD surface clearly helps to reduce the impact of low intra-cellular pH ranges and the interactions of the various proteins present from breaking down the surface structure and releasing the "naked" toxic core atoms. Overall however the gelatine helps to nullify the toxic effects induced by the QDs; however the localisation of the QDs and their final destination must also play a role as there are variations in the impact that the different QD sizes and types have on each distinct cell response. This is quite significant and will require further investigation to fully determine and understand how changes in QD type, structure, surface functionality and concentration may impinge on the various cellular processes that occur during co-incubation.

2.3 Proliferation ELISA BrdU

A Colorimetric Immunoassay was measured for the quantification of cell proliferation. This was based on the measurement of BrdU incorporation during DNA synthesis for the PC12 cells treated with different concentrations of gel and non-gel QDs. This cell

proliferation allows us to extrapolate the healthy nature of the cells following co-incubation times of up to 72 hours. This assay is somewhat different from those previously examined as those cellular processes may still occur in cells that are not proliferating.

Figure 12 illustrates the measured response for cell proliferation upon co-incubation with the QDs after 24, 48 and 72 hours. Notably, negative and background control responses are significantly higher than those seen for alamarBlue and PicoGreen.

Initially after 24 hours at 10^{-7} M QD concentrations, we can see a distinction between the less toxic gel and non-gel QDs however this levels off approaching negative controls at 48 and 72 hours. As the concentration drops to 10^{-8} M, we can once again see the significant influence of the gelatine capping. At 24 and 48 hours the non-gel QDs are substantially more toxic approaching negative controls, while gel QDs maintain parity with positive controls. Little distinction is recorded at 72 hours illustrating the negative impact that prolonged co-incubation with the QDs has on cell proliferation at this concentration.

Similarly to previous assays, little distinction can be made between QD types as the concentration is reduced to 10^{-9} M. After 24 hours, all QDs elicit responses in line with positive controls while after 48 and 72 hours, the red gel QDs once again showed the least detrimental effect on cell responses. Overall we can see a general trend towards a drop in cell proliferation with incubation time and the drop in responses for positive controls highlights the delicate nature of maintaining cell proliferation over extended co-incubation times. This also illustrates the extremely sensitive nature of this assay to external perturbation. Even though cell activity decreased during this assay application the results do show a similarity to those previously determined, albeit on a reduced scale.

Conclusion

In conclusion, we have co-incubated and analysed PC12 cells over extended incubation times (up to 72 hours) with both gelatinised (gel) and non-gelatinised (non-gel) thioglycolic acid capped CdTe QDs. We have visually inspected QD localisation, cell morphology and behaviour at a range of QD concentrations (10^{-7} - 10^{-9} M). The presence of the QDs at 10^{-7} M resulted in the death of all cells while at concentrations of 10^{-9} M, the QDs were up taken primarily in the cytoplasm of the PC12s and did not initiate any detrimental effects.

The presence of gelatine on the QD surface was investigated by thermogravimetric analysis (TGA) which shows an additional 10% weight loss for the gel compared to non-gel QDs. Experiments conducted on the possible degradation of the QDs in the cell culture

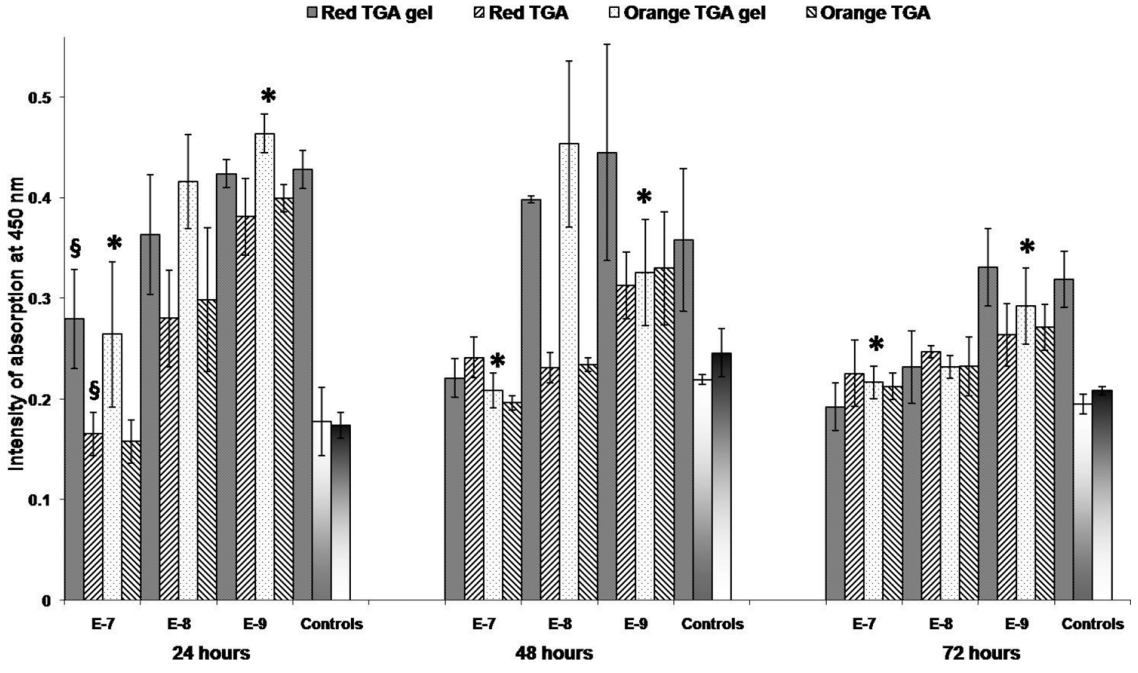

Figure 12 ELISA BrdU histograms. ELISA BrdU assay at 24, 48 and 72 hours illustrating (by intensity of absorption at 450 nm) the amount of cell proliferation following co-incubation with varying concentrations $10^{-7\text{-}(-9)}$ M of the gel and non-gel QDs. From left to right, controls [positive, negative, background] are also shown. §denotes examples of statistical significance due to effect of gelatine, * denotes examples of statistical significance due to effect of concentration using a one- way ANOVA ($p < 0.05$) by Tukey's mean comparison.

medium with serum have shown that quenching of the QD emission properties does occur due to protein-QD surface interactions. This does not induce a breakdown of the QD cores however, and indicates that any possible leeching of toxic core atoms must be induced by the internalisation of the QDs into the PC12 cells. We have also conducted experiments to enable us to empirically relate measured QD concentration to the actual weighed quantity of QDs present in mg/ml.

Utilising alamarBlue (cell viability) and Picogreen (DNA quantification) and ELISA BrdU (quantification of cell proliferation) assays we have measured and analysed cell response to co-incubations up to 72 hours with both gel and non-gel QDs. We have noted that throughout all our experiments, cell response varied in proportion to QD size, composition and concentration.

QD size significantly impacted measured responses. For the alamarBlue and PicoGreen assays at 10^{-7} &$^{-8}$ M QD concentrations, the orange non-gel QDs consistently produced lower cell responses. This indicates that the increased cellular penetration of these smaller QDs resulted in enhanced adverse effects compared to their larger red counterparts. Notably, these effects were significantly nullified by the gelatine coating with similarly sized gel QDs producing higher response throughout.

Increased QD concentrations also lead to a decrease in all measured cell responses. Notably however, it is evident at all time points that the gelatine coating has a protective effect as cell viability and survival rates are significantly higher for gel compared to non-gel QDs. Elongation of co-incubation times (up to 72 hours) also highlighted the importance and the significance of the gelatine for QD surface protection. The assays have shown that the gel QDs were consistently less toxic than their non-coated counterparts at concentrations up to 10^{-9} M. The presence of gelatine enables enhanced cell survival and proliferation at 10^{-8} M compared to non-gel QDs, while its influence is negated at 10^{-9} M concentrations over the longer co-incubation times. Thus, the 10^{-8} M QD concentration appears to act as a threshold for the initiation of deleterious effects. At 10^{-9} M concentrations, there appears to be a transition between the influences of QD surface structure (gel or non-gel) and QD concentration. The protective nature of the gelatine is countered by the drop in QD concentration and little variance was noted between the two QD types indicating that at this concentration the cells were unperturbed by the presence of either QD type.

Materials and methods

Chemicals and Reagents

PC12 cells (cancer cell line derived from a pheochromocytoma of the rat adrenal medulla) were used for this study. Dulbecco's Modification of Eagle Medium (DMEM) (Sigma-Aldrich) supplemented with 10% heat inactivated horse serum, 5% fetal bovine serum, 1% penicillin-streptomycin and, Trypsin-EDTA solution and all chemicals for QD synthesis were purchased from Sigma-Aldrich. Al_2Te_3 was purchased from Cerac Inc. AlamarBlue was purchased from Biosource International. A BrdU cell proliferation kit was purchased from Roche Diagnostics. Quant-iT PicoGreen DNA assay kit was obtained from Invitrogen. Permonax four-well chamber slide (Lab-Tek, Nalge Nunc International), Rhodamine-Phalloidin [Molecular Probes (Invitrogen)], DAPI (Vector Laboratories), Nunc tissue culture- treated 48-well plates were purchased from Biosciences and 96-well tissue culture plates were purchased from Sarstedt.

Quantum Dot Synthesis

Note: all values denoted are initial concentrations and follows previously published procedures [49,58]. Millipore water (150 ml) was degassed by bubbling argon for approximately 1 hour. $Cd(ClO_4)_2 6H_2O$ (3.22 g, [7.68 mmol]), TGA (thioglycolic acid) stabiliser (1.24 g, [13.46 mmol], 1.75 molar equivalents) was added and the pH was adjusted to 11.2-11.3 by the addition of a 2 M NaOH solution. For samples containing gelatine, 0.3 g was dissolved in 10 ml water by heating gently and added to the reaction mixture. H_2Te gas, generated from Al_2Te_3 (0.56 g, [0.128 mmol]) *via* drop-wise addition of a 0.5 M H_2SO_4 solution was bubbled through the cadmium/thiol solution under a slow argon flow for approximately 10 minutes. Note: 100% reaction and carryover is assumed, and cadmium is always in excess for this experiment. The resultant, non-luminescent solution was then heated to reflux. Following the reflux process, fractions were precipitated *via* the addition of isopropanol and were stored at 4°C. The concentration of stock solutions used was approximately 2×10^{-4} M [17] and were diluted by dissolving in de-ionised sterile water.

A Shimadzu UV-1601 UV - Visible Spectrophotometer was used to measure QD absorption while a Varian - Cary Eclipse Fluorescence Spectrophotometer was used to determine the fluorescence emission/photoluminescence (PL) spectra of QDs. A JEOL 3011 High Resolution Transmission Electron Microscope (HTREM) was used to image the QDs.

Relating QD mass to concentration

Different batches of both gel and non-gel QDs were individually dried under rotary evaporation. The resulting powder was scraped from the flask and weighed before being re-dissolved in exactly 1 ml of purified water. The concentration was then determined [17], thus giving a relationship between QD molar concentration and the mass of QDs (mg/ml).

Investigation of QDs in medium

Gel and non-gel QDs were diluted in cell culture medium to a final concentration of 10^{-6} M. UV-Vis absorption and PL emission spectra were recorded at various time points up to 72 hours after addition.

Thermogravimetric Analysis (TGA)

Samples of QDs (gel and non-gel) were dried on a rotary evaporator. The resulting powder was analysed by thermal gravimetric analysis on a Perkin Elmer Pyrus 1 instrument: it was heated from 30 to 900°C at a rate of 10°C/min and its weight was recorded continuously. The gelatine powder was also analysed.

Cell Culture

PC12 cells, were cultured in medium (DMEM supplemented with 10% heat inactivated horse serum, 5% fetal bovine serum, 1% penicillin-streptomycin) @ 37°C and a 5% CO_2 atmosphere. All the tissue culture plates and chamber slides were treated with 0.001% Poly-L-Lysine (PLL) for 24 hours.

Cell Staining

Cells were seeded into four-well chambers at density of 10^5 cells/cm^2. After 24 hours QDs were added (10% of amount of Medium) to make final concentrations in the range of $10^{(-7)-(-9)}$ M and the cells were incubated for different time periods from 24 - 72 hours. Cells were grown on 4 well Permonax Chamber slides in the presence of QDs. After the desired length of exposure, medium was removed and the coverslips were washed with 1% phosphate-buffered saline (BSA/PBS). Cells were fixed with 4% paraformaldehyde for 15 minutes and then washed 3 times with PBS. Then cells were permeabilized with permeabilizing solution (5 min, 0°C). Actin filaments of cytoplasm were labelled with Rhodamine Phalloidin (Molecular Probes (Invitrogen), at a 1:200 dilution with PBS for 15 minutes and again washed 3 times with PBS. Nuclei were labelled with Vectashield mounting medium with DAPI to preserve fluorescence and counter stained DNA with DAPI 1 μg/ml.

Confocal Microscopy

An LSM 510 (Carl Zeiss, Jena, Germany) Confocal Laser Scanning microscope was used to examine QDs inside PC12 cells and its morphology.

Cell Imaging was carried out using a LSM 510 Inverted Confocal Microscope which is equipped with the following excitation lasers: (a) Argon Laser Excitation -wavelengths (λ_{Ex}) = 458 nm, 488 nm, 514 nm, (b) HeNe1 - λ_{Ex} = 543 nm, (c) HeNe1 - λ_{Ex} = 633 nm and (d) Titanium Sapphire Tuneable Two-photon Laser tuneable from 710 nm to 1000 nm with a resulting excitation range of 355 nm to 500 nm.

Confocal laser scanning was carried out at laser scan speed of 7 with the Photomultiplier Tube settings adjusted to eliminate noise and saturation with the aid of the range indicator setting in the LSM 510 software. For image optimisation scan averaging was carried out on 8 scans per image.

Sequential acquisition was used to acquire the two colour images of the QDs in cells. For visualisation of the QDs, the samples were excited with the Argon 514 nm Laser and the microscope configuration was set up to capture the emitted fluorescence at 550 nm or 600 nm as desired. Differential Interference Contrast (DIC) or Nomarski Microscopy was used to visualise the cell morphology, and was carried out by using the HeNe1 488 nm laser with the Transmission Channel Detector selected and the DIC polariser and Nomarski prisms engaged. The two images were then over laid using the LSM 510 software.

Sequential acquisition was also used to acquire three colour images. Rhodamine phalloidin was excited using the HeNe1 543 nm laser and the emitted fluorescence was acquired at 575 nm. DAPI stain was excited with laser light at 390 nm (from the two photon laser tuned to 780 nm) and emitted fluorescence was acquired at 458 nm. The three separate images were over laid using the LSM510 software to make up the three colour images.

AlamarBlue Assay

During cellular respiration, mitochondria take in oxygen and release CO_2. During this process alamarBlue is substituted for molecular oxygen in the electron transfer chain and consequently becomes reduced. This reduction results in a change in both the colour and also the absorbance of the dye. These changes can be measured and are directly quantifiable against the number of healthy respiring cells present.

PC12 cells were seeded in 48-well micro-plates (Nunc) as triplicates. After 24 h, QDs were added (10% of amount of Medium) to make final concentrations in the range of $10^{(-7)-(-9)}$ M. Three different types of controls, namely: positive, negative and background were used throughout the study. Positive controls had cells with culture medium but without treatment with QDs. Negative controls were treated with QDs with culture medium and no cells. Background controls were cells treated with QDs but without culture medium. After 24 hours of treatment with QDs, the medium was removed and the wells were washed with HBSS. AlamarBlue solution was prepared by adding alamarBlue (Biosciences UK) and HBSS in the ratio of 1:10. 200 μl of alamarBlue solution was added to each well and the plates were incubated for 1 hour. 100 μl of reduced alamarBlue solution from each well was dispensed in a clear tissue

culture 96 well plate. The Plate was analysed using a Wallac Victor Fluorescent Plate Reader. Absorbance was measured at lower wavelength of 550 nm and higher wavelength of 595 nm with a measurement time of 5.0 s. This was repeated with incubation periods of 48 hours and 72 hours.

PicoGreen Assay

PicoGreen is a fluorescent stain that is highly selective for solubilised double-stranded DNA and is an extremely sensitive technique capable of nanogram DNA quantification. Unlike the non-destructive alamarBlue assay, a PicoGreen assay involves the freeze-thaw lysing of cells to analyse the quantity of dsDNA present. As the cells are washed to remove any dead cells before analysis, the assay only measures the DNA response from live healthy cells, thus allowing us to directly relate how the QDs impact cell survival rates.

The Quant-iT PicoGreen double-stranded DNA assay kit (Invitrogen) was used to assess DNA concentration. PC12 cells were grown in 48-well microplates (Nunc) as triplicates. After 24 h, QDs were added (10% of amount of Medium) to make final concentrations in the range of $10^{(-7)-(-9)}$ M. Three different types of controls, namely: positive, negative and background were used throughout the study. Positive controls had cells with culture medium but without treatment with QDs. Negative controls were treated with QDs with culture medium and no cells. Background controls were cells treated with QDs but without culture medium. After 24 hours of co-incubation with the QDs, the medium was removed and the wells were washed with HBSS. 200 μl of deionised double-distilled water was then added and the cells were lysed by freezing for 15 minutes at -80°C and thawing for 15 minutes at room temperature repeated 3 times. According to the assay kit a standard curve was then constructed. Final concentrations of the standards were 1000, 500, 100, 50, 25, 10, 5, and 0 ng/μl. 100 μl of lysed DNA solution of cells from each well were dispensed in a clear tissue culture 96-well plate. 100 μl of diluted PicoGreen solution were added to each of the test wells of 96-well plate. The Plate was analysed using a Wallac Victor Fluorescent Plate Reader by Fluorescence 485 nm/535 nm, 1.0 s protocol. Levels of DNA in each sample were calculated using the standard curve. This was repeated with incubation periods of 48 hours and 72 hours.

Cell Proliferation ELISA BrdU

An ELISA BrdU (BrdU) assay involves the detection of 5-bromo-2-deoxyuridine, an analogue of thymidine, which is incorporated into the DNA of proliferating cells. Incorporated BrdU is labelled with a peroxidase-conjugated anti-BrdU antibody (anti-BrdU-POD). The amount of bound anti-BrdU-POD is quantified calorimetrically through exposure to a peroxidase substrate (3,3,5,5-tetramethylbenzidine [TMB]). TMB is acted upon by peroxidase to form a blue product. Upon addition of a stop solution (H_2SO_4), a yellow product is formed, which absorbs at 450 nm. The level of absorbance is directly related to the amount of cell division that has occurred during the course of the incubation period.

Cellular proliferation was measured using an enzyme-linked immunosorbent assay (ELISA) (supplied as a kit [Roche]). Cell Proliferation ELISA BrdU (Colorimetric) was performed according to the protocol in the manual of the kit. PC12 cells were grown in 96-well microplates (Nunc) as triplicates. After 24 h, QDs were added (10% of amount of Medium) to make final concentrations in the range of $10^{(-7)-(-9)}$ M.

Three different types of controls, namely: positive, negative and background were used throughout the study. Positive controls had cells with culture medium but without treatment with QDs. Negative controls were treated with QDs with culture medium and no cells. Background controls were cells treated with QDs but without culture medium. BrdU labelling solution was added to each well after 24 hours of adding QDs and incubated at @ 37°C and 5% CO_2 atmosphere. The culture medium was removed and the cells denatured, and the anti-BrdU-POD added. This binds to the BrdU incorporated into cellular DNA. The level of incorporation is detected by means of a colorimetric substrate reaction. Quantification of the bound anti-BrdU-POD was accomplished by adding 100 μl TMB to each well and a further 20 minute incubation time at room temperature. 25 μl 0.1 M H_2SO_4 was then added, incubated for 1 minute and shaken at 300 rpm to stop the reaction. The Plate was analysed using the Wallac Victor Fluorescent Plate Reader (450-550 nm) protocol and measured absorbance for 2 minutes at room temperature. This was repeated with incubation periods of 48 hours and 72 hours.

Statistical Analysis

Results of alamarBlue and PicoGreen assays were analysed using one-way analysis of variance (ANOVA). A ρ value of less than 0.05 for the ANOVA was considered significant. Error was expressed as a standard deviation.

Abbreviations

QDs: Quantum Dots; CdTe: Cadmium Telluride; PC12: pheochromocytoma 12; NGF: nerve growth factors; TGA: Thioglycolic Acid; gel-QDs: gelatinised QDs; DNA: Deoxyribonucleic Acid; DMWM: Dulbecco's Modification of Eagle Medium EDTA; DAPI: 4: 6-diamidino-2-phenylindole; UV: ultraviolet; PL: photoluminescence; PLL: Poly-L-Lysine; BSA/PBS: Bovine serum albumin/phosphate-buffered saline; DIC: Differential Interference Contrast; HBSS: Hank's Balanced Salt Solution; TMB: 3,3,5,5-tetramethylbenzidine; HRTEM:

High Resolution Transmission Electron Microscopy; FRET: Förster Resonance Energy Transfer; TGA: Thermogravimetric Analysis.

Acknowledgements
This work has been funded by Science Foundation Ireland (SFI).

Author details
[1]National Centre for Biomedical Engineering Science, National University of Ireland, Galway, Ireland. [2]CRANN and The School of Chemistry, Trinity College Dublin, Dublin 2, Ireland.

Authors' contributions
BRP performed all cellular experiments and wrote the manuscript with SJB. SJB and VAG conducted the QD experiments. DC contributed with confocal imaging. YR, YG, NN, TJS designed the overall project and helped with data and manuscript revision. All authors read and approved the final manuscript.

Competing interests
The authors declare that they have no competing interests.

Received: 21 July 2009 Accepted: 25 March 2010
Published: 25 March 2010

References

1. Dubertret B, Skourides P, Norris DJ, Noireaux V, Brivanlou AH, Libchaber A: **In Vivo Imaging of Quantum Dots Encapsulated in Phospholipid Micelles.** *Science* 2002, **298**:1759-1762.
2. Gao X, Cui Y, Levenson RM, Chung LWK, Nie S: **In vivo cancer targeting and imaging with semiconductor quantum dots.** *Nat Biotech* 2004, **22**:969-976.
3. Goldman ER, Balighian ED, Mattoussi H, Kuno MK, Mauro JM, Tran PT, Anderson GP: **Avidin: A Natural Bridge for Quantum Dot-Antibody Conjugates.** *J Am Chem Soc* 2002, **124**:6378-6382.
4. Jaiswal JK, Goldman ER, Mattoussi H, Simon SM: **Use of quantum dots for live cell imaging.** *Nat Methods* 2004, **1**:73-78.
5. Pinaud F, King D, Moore HP, Weiss S: **Bioactivation and cell targeting of semiconductor CdSe/ZnS nanocrystals with phytochelatin-related peptides.** *J Am Chem Soc* 2004, **126**:6115-6123.
6. Rosenthal SJ, Tomlinson I, Adkins EM, Schroeter S, Adams S, Swafford L, McBride J, Wang Y, DeFelice LJ, Blakely RD: **Targeting Cell Surface Receptors with Ligand-Conjugated Nanocrystals.** *J Am Chem Soc* 2002, **124**:4586-4594.
7. Wu X, Liu H, Liu J, Haley KN, Treadway JA, Larson JP, Ge N, Peale F, Bruchez MP: **Immunofluorescent labeling of cancer marker Her2 and other cellular targets with semiconductor quantum dots.** *Nat Biotech* 2003, **21**:41-46.
8. Chen F, Gerion D: **Fluorescent CdSe/ZnS Nanocrystal-Peptide Conjugates for Long-term, Nontoxic Imaging and Nuclear Targeting in Living Cells.** *Nano Lett* 2004, **4**:1827-1832.
9. Bruchez M Jr, Moronne M, Gin P, Weiss S, Alivisatos AP: **Semiconductor Nanocrystals as Fluorescent Biological Labels.** *Science* 1998, **281**:2013-2016.
10. Chan WC, Nie S: **Quantum Dot Bioconjugates for Ultrasensitive Nonisotopic Detection.** *Science* 1998, **281**:2016-2018.
11. Alivisatos AP: **The use of nanocrystals in biological detection.** *Nat Biotech* 2004, **22**:47-52.
12. Han MY, Gao XH, Su JZ, Nie S: **Quantum-dot-tagged microbeads for multiplexed optical coding of biomolecules.** *Nat Biotech* 2001, **19**:631-635.
13. Larson DR, Zipfel WR, Williams RM, Clark SW, Bruchez MP, Wise FW, Webb WW: **Water-Soluble Quantum Dots for Multiphoton Fluorescence Imaging in Vivo.** *Science* 2003, **300**:1434-1436.
14. Chan WCW, Maxwell DJ, Gao X, Bailey RE, Han M, Nie S: **Luminescent quantum dots for multiplexed biological detection and imaging.** *Curr Op Biotech* 2002, **13**:40-46.
15. Vanmaekelbergh D, Liljeroth P: **Electron-conducting quantum dot solids: novel materials based on colloidal semiconductor nanocrystals.** *Chem Soc Rev* 2005, **34**:299-312.
16. Pathak S, Cao E, Davidson MC, Jin SH, Silva GA: **Quantum dot applications to neuroscience: New tools for probing neurons and glia.** *Journal of Neuroscience* 2006, **26**:1893-1895.
17. Yu WW, Qu LH, Guo WZ, Peng XG: **Experimental determination of the extinction coefficient of CdTe, CdSe, and CdS nanocrystals.** *Chem Mater* 2003, **15**:2854-2860.
18. Osaki F, Kanamori T, Sando S, Sera T, Aoyama Y: **A Quantum Dot Conjugated Sugar Ball and Its Cellular Uptake. On the Size Effects of Endocytosis in the Subviral Region.** *JACS* 2004, **126**:6520-6521.
19. Gomez N, Winter JO, Shieh F, Saunders AE, Korgel BA, Schmidt CE: **Challenges in quantum dot-neuron active interfacing.** *Talanta* 2005, **67**:462-471.
20. Jan E, Byrne SJ, Cuddihy M, Davies AM, Volkov Y, Gun'ko YK, Kotov NA: **High-Content Screening as a Universal Tool for Fingerprinting of Cytotoxicity of Nanoparticles.** *ACS Nano* 2008, **2**:928-938.
21. Rajan SS, Liu HY, Vu TQ: **Ligand-Bound Quantum Dot Probes for Studying the Molecular Scale Dynamics of Receptor Endocytic Trafficking in Live Cells.** *ACS Nano* 2008, **2**:1153-1166.
22. Cui BX, Wu CB, Chen L, Ramirez A, Bearer EL, Li WP, Mobley WC, Chu S: **One at a time, live tracking of NGF axonal transport using quantum dots.** *PNAS* 2007, **104**:13666-13671.
23. Tang ML, Xing TR, Zeng J, Wang HL, Li CC, Yin ST, Yan D, Deng HM, Liu J, Wang M, *et al*: **Unmodified CdSe quantum dots induce elevation of cytoplasmic calcium levels and impairment of functional properties of sodium channels in rat primary cultured hippocampal neurons.** *Environmental Health Perspectives* 2008, **116**:915-922.
24. Tang ML, Wang M, Xing TR, Zeng J, Wang HL, Ruan DY: **Mechanisms of unmodified CdSe quantum dot-induced elevation of cytoplasmic calcium levels in primary cultures of rat hippocampal neurons.** *Biomater* 2008, **29**:4383-4391.
25. Lopez E, Figueroa S, Oset-Gasque MJ, Gonzalez MP: **Apoptosis and necrosis: two distinct events induced by cadmium in cortical neurons in culture.** *Br J Pharmacol* 2003, **138**:901-911.
26. Vu TQ, Maddipati R, Blute TA, Nehilla BJ, Nusblat L, Desai TA: **Peptide-Conjugated Quantum Dots Activate Neuronal Receptors and Initiate Downstream Signaling of Neurite Growth.** *Nano Lett* 2005, **5**:603-607.
27. Fan H, Leve EW, Scullin C, Gabaldon J, Tallant D, Bunge S, Boyle T, Wilson MC, Brinker CJ: **Surfactant-Assisted Synthesis of Water-Soluble and Biocompatible Semiconductor Quantum Dot Micelles.** *Nano Letters* 2005, **5**:645-648.
28. Mamedova NN, Kotov NA, Rogach AL, Studer J: **Albumin-CdTe nanoparticle bioconjugates: Preparation, structure, and interunit energy transfer with antenna effect.** *Nano Lett* 2001, **1**:281-286.
29. Howarth M, Takao K, Hayashi Y, Ting AY: **Targeting quantum dots to surface proteins in living cells with biotin ligase.** *PNAS* 2005, **102**:7583-7588.
30. Sundara Rajan S, Vu TQ: **Quantum Dots Monitor TrkA Receptor Dynamics in the Interior of Neural PC12 Cells.** *Nano Letters* 2006, **6**:2049-2059.
31. Courty S, Luccardini C, Bellaiche Y, Cappello G, Dahan M: **Tracking Individual Kinesin Motors in Living Cells Using Single Quantum-Dot Imaging.** *Nano Letters* 2006, **6**:1491-1495.
32. Nan X, Sims PA, Chen P, Xie XS: **Observation of Individual Microtubule Motor Steps in Living Cells with Endocytosed Quantum Dots.** *P Phys Chem B* 2006, **109**:24220-24224.
33. Kondoh M, Araragi S, Sato K, Higashimoto M, Takiguchi M, Sato M: **Cadmium induces apoptosis partly via caspase-9 activation in HL-60 cells.** *Toxicol* 2002, **170**:111-117.
34. Limaye DA, Shaikh ZA: **Cytotoxicity of Cadmium and Characteristics of Its Transport in Cardiomyocytes.** *Toxicol Appl Pharmacol* 1999, **154**:59-66.
35. Rikans LE, Yamano T: **Mechanisms of cadmium-mediated acute hepatotoxicity.** *J Biochem Molec Tox* 2000, **14**:110-117.
36. Nel A, Xia T, Madler L, Li N: **Toxic Potential of Materials at the Nanolevel.** *Science* 2006, **311**:622-627.
37. Hoshino A, Fujioka K, Oku T, Suga M, Sasaki YF, Ohta T, Yasuhara M, Suzuki K, Yamamoto K: **Physicochemical properties and cellular toxicity of nanocrystal quantum dots depend on their surface modification.** *Nano Lett* 2004, **4**:2163-2169.
38. Derfus AM, Chan WCW, Bhatia SN: **Probing the cytotoxicity of semiconductor quantum dots.** *Nano Lett* 2004, **4**:11-18.
39. Guo G, Liu W, Liang J, He Z, Xu H, Yang X: **Probing the cytotoxicity of CdSe quantum dots with surface modification.** *Mater Lett* 2007, **61**:1641-1644.
40. Lovrić J, Cho SJ, Winnik FM, Maysinger D: **Unmodified Cadmium Telluride Quantum Dots Induce Reactive Oxygen Species Formation Leading to**

Multiple Organelle Damage and Cell Death. *Chem Biol* 2005, **12**:1227-1234.

41. Kirchner C, Liedl T, Kudera S, Pellegrino T, MunozJavier A, Gaub HE, Stolzle S, Fertig N, Parak WJ: **Cytotoxicity of Colloidal CdSe and CdSe/ZnS Nanoparticles.** *Nano Lett* 2005, **5**:331-338.
42. Chang E, Thekkek N, Yu WW, Colvin VL, Drezek R: **Evaluation of Quantum Dot Cytotoxicity Based on Intracellular Uptake.** *Small* 2006, **2**:1412-1417.
43. Wang L, Nagesha D, Selvarasah S, Dokmeci M, Carrier R: **Toxicity of CdSe Nanoparticles in Caco-2 Cell Cultures.** *J Nanobiotech* 2008, **6**:11.
44. Byrne SJ, Williams Y, Davies A, Corr SA, Rakovich A, Gun'ko YK, Rakovich YP, Donegan JF, Volkov Y: **"Jelly Dots": Synthesis and Cytotoxicity Studies of CdTe Quantum Dot-Gelatin Nanocomposites.** *Small* 2007, **3**:1152-1156.
45. Lovrić J, Bazzi HS, Cuie Y, Fortin GRA, Winnik FM, Maysinger D: **Differences in subcellular distribution and toxicity of green and red emitting CdTe quantum dots.** *J Mol Med* 2005, **83**:377-385.
46. Shiohara Amane, Hoshino Akiyoshi, Hanaki Ken-ichi, Suzuki Kazuo, Yamamoto K: *Microbiology and Immunology* 2004, **48**:669-675.
47. Cho SJ, Maysinger D, Jain M, Roder B, Hackbarth S, Winnik FM: **Long-Term Exposure to CdTe Quantum Dots Causes Functional Impairments in Live Cells.** *Langmuir* 2007, **23**:1974-1980.
48. Tan WB, Huang N, Zhang Y: **Ultrafine biocompatible chitosan nanoparticles encapsulating multi-coloured quantum dots for bioapplications.** *J Colloid and Interface Sci* 2007, **310**:464-470.
49. Byrne SJ, Corr SA, Rakovich TY, Gun'ko YK, Rakovich YP, Donegan JF, Mitchell S, Volkov Y: **Optimisation of the synthesis and modification of CdTe quantum dots for enhanced live cell imaging.** *J Mat Chem* 2006, **16**:2896-2902.
50. Tang Z, Ozturk B, Wang Y, Kotov NA: **Simple Preparation Strategy and One-Dimensional Energy Transfer in CdTe Nanoparticle Chains.** *J Phys Chem B* 2004, **108**:6927-6931.
51. Conroy JBSJ, Gun'ko YK, Rakovich YP, Donegan JF, Davies A, Kelleher D, Volkov Y: **CdTe Nanoparticles Display Tropism to Core Histones and Histone-Rich Cell Organelles.** *Small* 2008, **4**:2006-2015.
52. Monteiro-Riviere NA, Inman AO, Zhang LW: **Limitations and relative utility of screening assays to assess engineered nanoparticle toxicity in a human cell line.** *Toxicol Appl Pharmacol* 2009, **234**:222-235.
53. Nabiev I, Mitchell S, Davies A, Williams Y, Kelleher D, Moore R, Gun'ko YK, Byrne S, Rakovich YP, Donegan JF, *et al*: **Nonfunctionalized Nanocrystals Can Exploit a Cell's Active Transport Machinery Delivering Them to Specific Nuclear and Cytoplasmic Compartments.** *Nano Letters* 2007, **7**:3452-3461.
54. Chan W-H, Shiao N-H, Lu P-Z: **CdSe quantum dots induce apoptosis in human neuroblastoma cells via mitochondrial-dependent pathways and inhibition of survival signals.** *Toxicol Lett* 2006, **167**:191-200.
55. Lee H-M, Shin D-M, Song H-M, Yuka J-M, Lee Z-W, Lee S-H, Hwang SM, Kim J-M, Lee C-S, Jo E-K: **Nanoparticles up-regulate tumor necrosis factor-α and CXCL8 via reactive oxygen species and mitogen-activated protein kinase activation.** *Toxicol Appl Pharm* 2009, **238**:160-169.
56. Wan RMY, Zhang X, Chien S, Tollerud DJ, Zhang Q: **Matrix metalloproteinase-2 and -9 are induced differently by metal nanoparticles in human monocytes: The role of oxidative stress and protein tyrosine kinase activation.** *Toxicol Appl Pharm* 2008, **233**:276-285.
57. Calabrese EJ, Baldwin LA: **Applications of hormesis in toxicology, risk assessment and chemotherapeutics.** *Trends Pharmacol Sci* 2002, **23**:331-337.
58. Gaponik N, Talapin DV, Rogach AL, Hoppe K, Shevchenko EV, Kornowski A, Eychmüller A, Weller H: **Thiol-capping of CdTe nanocrystals: An alternative to organometallic synthetic routes.** *J Phys Chem B* 2002, **106**:7177-7185.

doi:10.1186/1477-3155-8-7
Cite this article as: Prasad *et al.*: Long-term exposure of CdTe quantum dots on PC12 cellular activity and the determination of optimum non-toxic concentrations for biological use. *Journal of Nanobiotechnology* 2010 **8**:7.

JOURNAL OF NANOBIOTECHNOLOGY

RESEARCH Open Access

Effects of long-term exposure of gelatinated and non-gelatinated cadmium telluride quantum dots on differentiated PC12 cells

Babu R Prasad[1], Gillian Mullins[1], Natalia Nikolskaya[1], David Connolly[1], Terry J Smith[1], Valérie A Gérard[2], Stephen J Byrne[2], Gemma-Louise Davies[2], Yurii K Gun'ko[2] and Yury Rochev[1*]

Abstract

Background: The inherent toxicity of unmodified Quantum Dots (QDs) is a major hindrance to their use in biological applications. To make them more potent as neuroprosthetic and neurotherapeutic agents, thioglycolic acid (TGA) capped CdTe QDs, were coated with a gelatine layer and investigated in this study with differentiated pheochromocytoma 12 (PC12) cells. The QD - cell interactions were investigated after incubation periods of up to 17 days by MTT and APOTOX-Glo Triplex assays along with using confocal microscopy.

Results: Long term exposure (up to 17 days) to gelatinated TGA-capped CdTe QDs of PC12 cells in the course of differentiation and after neurites were grown resulted in dramatically reduced cytotoxicity compared to non-gelatinated TGA-capped CdTe QDs.

Conclusion: The toxicity mechanism of QDs was identified as caspase-mediated apoptosis as a result of cadmium leaking from the core of QDs. It was therefore concluded that the gelatine capping on the surface of QDs acts as a barrier towards the leaking of toxic ions from the core QDs in the long term (up to 17 days).

Keywords: CdTe Quantum Dots, Differentiated PC12 cells, Cytotoxicity, Neuronal Growth Factor, Apoptosis

Background

Quantum Dots (QDs) represent an attractive diagnostic and therapeutic tool, however they possess the major disadvantage of being inherently cytotoxic, due to their cadmium components [1,2]. Cellular interaction with QDs is dependent on a variety of physicochemical parameters, including size, chemical composition, surface structure, solubility, shape and aggregation; all of which can influence or modify cellular uptake [3]. There is an inverse relationship between the size of QDs and their number of surface atoms or molecules that determines the material reactivity, which is the key to defining the chemical and biological properties of QDs [3,4]. The small size of QDs also gives them the ability to traverse cell membranes and possibly the blood-brain barrier, which cannot be achieved using conventional dyes, making their use as therapeutic tools an intriguing possibility. The size of QDs is fundamental to their cellular interaction and has to be considered while studying their toxicity and distribution in various cell compartments [5]. When coated with certain biocompatible polymers, QDs have been shown to be far less toxic to cells and living organisms in the short term [6]. A fundamental problem of QDs is that of aggregation and accumulation, which are particularly prevalent upon entrapment in organelles such as vesicles, endosomes and lysosomes inside living cells [7-9]. However, little information is known about the interactions of QDs with intracellular proteins and transportation methods of QDs inside living cells [10]. Even cell-penetrating peptides such as poly-arginine and TAT, when conjugated with QDs, still become trapped within vesicles and endosomes, therefore inhibiting their use as molecular diagnostic and therapeutic targeting tools [11,12]. Notably, accumulation of QDs over longer exposure periods of 8-24 hours results in a degradation of their

* Correspondence: yury.rochev@nuigalway.ie
[1]National Centre for Biomedical Engineering Science, National University of Ireland Galway, Galway, Ireland
Full list of author information is available at the end of the article

coatings, leading to a leakage of their toxic core particles or ions [8,13]. This core leakage has been shown to initiate the formation of reactive oxygen species (ROS), which are the key mediators in cell organelle damage and destruction. The high surface area to volume ratio of the QDs also lends itself to enhanced numbers of ROS sites [3]. Overload of Cd^{2+} and ROS in the mitochondria leads to permeability of the inner mitochondrial membrane. Cytochrome c is then released from mitochondrial intermembrane space which then activates the downstream caspases 9 and 3, finally causing cell death by apoptosis [2,14-17].

There has been significant advancement and progress in biological imaging, especially using fluorescent semiconductor nano-crystals due to their resistance to photo-bleaching [18-20]. This has paved the way for the development of medical diagnostics and drug delivery tools utilising QDs. One of the most important criteria for the future development of QDs as efficient cellular delivery, labelling and targeting agents is that their intracellular uptake depends on the selective detection of one molecule, or a small number of molecules. The QD probes must be able to selectively access various subcellular compartments which need to be targeted in order to understand the dynamics of cellular organisation without causing a cytotoxic effect during the time period required [21].

Currently, methods to access single molecule properties in living cells are limited due to the size of the probe or photo-bleaching of fluorescent biomarkers. QDs have great potential as fluorescent probes thanks to their sizes, which can range from approximately 2 to 5 nm and their enhanced photo-stability, whereby signal detection is not diminished even after exposure to the acidic cell environment [22].

Previously, we have investigated the cytotoxicity of QDs by analyzing the outcome of co-incubating a range of concentrations of various types of QDs with non-differentiated PC12 cells [23]. In this paper, we have studied the long-term cytotoxicity and localisation of gelatinated (gel) and non-gelatinated (non-gel) QDs of various sizes in differentiated PC12 cells. When treated with nerve growth factor (NGF), PC12 cells become differentiated and have functional properties enabling them to behave in a manner similar to neuronal cells [24]. Their phenotype may not be similar to primary nerve cells as their origin is from tumour cells, however, in the presence of NGF, they have the ability to produce neurites, synthesize neurotransmitters and receptors and exhibit the electrical activity, which are characteristic of neurons [25]. Although some cytotoxicity studies of QDs have been carried out with PC12 cells [26,27], in this study we clearly analyze the viability, cytotoxicity and apoptosis at different time periods and discuss the effect of exposure of QDs on PC12 cells before and after the neurites were grown. The apoptotic process involved in the cell death, as well as the intrinsic behaviour of QDs upon uptake by the cells is also analyzed.

Results

Our aim was to analyze the effect of CdTe QDs on cell behaviour and morphology and to investigate any alterations of cell proliferation, cytotoxicity, viability and apoptosis using pre-determined assays. PC12 cells were exposed to QDs over extended co-incubation periods before and after the formation of neurites. Stock solutions of gel and non-gel QDs (10^{-4} M) [28] were diluted to 10^{-9} M and incubated with the cells as described in the experimental section.

1. Characterisation of CdTe QDs

All types of QDs used in this study were fully characterised prior to their biological testing. UV-Visible absorption spectroscopy and photoluminescence emission spectroscopy provided information on their exciton band, core diameter, emission wavelength and quantum efficiency. These properties are summarized in Table 1 for all four types of QDs. Due to the presence of carboxylic groups on the surface of the particles, they were negatively charged and stable in basic pH solutions.

2. Uptake of QDs and their effect on cell morphology of differentiated PC12 cells

Confocal images were taken to visually inspect QD uptake, localisation and cell morphology following exposure to QDs before and after the differentiation of PC12 cells (Figures 1, 2 and 3).

As seen in Figure 1, the QDs were found to be located within the cytoplasm of differentiated PC12 cells in all the images. The cells exposed to gel QDs (red and orange) (panels A and C respectively) exhibited a similar morphology and neurite growth to the control (no treatment of QDs) in panel E. The cells exposed to non-gel QDs (panels B and D respectively) appeared rounded with partial inhibition of neurite growth (red non-gel) or no neurite growth (orange non-gel). Cell morphology changes are attributed to the absence of the protective gelatinated shell. These cellular morphologies indicated that the presence of gelatine provides a protective surface coating for the QDs and prevents the initiation of deleterious effects on the morphology and cellular activity of differentiated PC12 cells.

In Figure 2, the nucleus was stained with DAPI (blue) and the cytoplasm was actin stained (green). The gel QDs (red luminescence) in panel A are visible predominantly in the cytoplasm and their presence, even after 17 days of co-incubation, did not seem to significantly perturb the cells. The QDs were also parsimoniously

Table 1 Characteristics of QDs

QD type	Surface	Absorbance peak (nm)	PL emission peak (nm)	Quantum Yield	Size(nm) (+/- 0.1)	Hydrodynamic diameter (nm)	Zeta potential (mV)
Red non-gel	TGA	586	608	30%	4.7	11.7	-30
Orange non-gel	TGA	515	546	23%	2.4	3.6	-27
Red gel	TGA-gelatine	579	610	34%	4.5	14.3	-29
Orange gel	TGA-gelatine	522	550	29%	2.6	5.3	-42

distributed in the neurites. The cell morphology did not change compared to the controls in panel B.

Figure 3 shows the overlaid differential interference contrast (DIC) images with corresponding fluorescent images of the differentiated PC12 cells treated with NGF for 6 days prior to exposure to 10^{-9} M concentrations of the QDs. Red gel QDs are shown in panel A, red non-gel QDs in panel B, orange gel QDs in panel C and orange non-gel QDs in panel D following 7 days of co-incubation. The QDs were found to be located within the cytoplasm of differentiated PC12 cells in all the images. The cells exposed to red and orange gel QDs (panels A and C respectively) showed similar morphology and neurite growth compared to the control (no treatment of QDs) in panel E. There was evidence of slight neurite degeneration in the cells exposed to orange gel QDs more so than in the cells exposed to red gel QDs, illustrating that the red gel QDs are more cyto-protective than the orange gel QDs. The cells exposed to red non-gel and orange non-gel QDs (panels B and D respectively) appeared rounded with partial degeneration and full degeneration (fragmentation) of neurites respectively, which suggests that orange non-gel QDs are more cytotoxic than red non-gel QDs which is expected due to the enhanced cytotoxicity of the smaller orange QDs relative to their larger red counterparts.

These initial observations using confocal microscopy illustrate the effect of exposure of QDs before and after the differentiation of PC12 cells on cell survival and morphology. In order to further investigate the cell behaviour, several assays were used to study the effect on cell proliferation, cytotoxicity, viability and apoptosis.

3. Effect of QDs on cellular activity of differentiated PC12 cells

Results were analysed using a one-way ANOVA analysis by Tukey's mean comparison, where results with a p-value of less than 0.05 were reported as statistically significant and their occurrence can be deemed to be due to interactions in the system under investigation and chance variation can be eliminated. MTT (cell proliferation) and APOTOX Triplex (cytotoxicity, viability and apoptosis) assays were run to analyze the effect of different QD types and size following exposure of QDs before and after the differentiation of PC12 cells.

MTT Assay

The graph in Figure 4 depicts the results of an MTT assay for PC12 cells treated with NGF and exposed to QDs after periods of 10 and 16 days. After 10 and 16 days, the proliferation of cells exposed to red gel QDs was the same as the positive controls whereas the proliferation of cells exposed to smaller (orange) gel QDs was significantly reduced. This clearly showed that smaller orange gel QDs are significantly more toxic than larger red gel QDs towards differentiated PC12 cells. Similarly, smaller orange non-gel QDs appeared to be significantly more cytotoxic than larger red non-gel QDs as co-incubation periods were prolonged. Overall, gel QDs were found to be less cytotoxic than their non-gel counterparts. The absorption of MTT, and therefore cell proliferation, further decreased when the co-incubation time was extended up to 16 days. Even after prolonged exposure time, smaller QDs had a higher adverse effect on cell proliferation compared to their larger counterparts. As observed from the results displayed above, the gelatine layer on the surface of the gel QDs regardless of size proved to effectively reduce their cytotoxicity. This suggests that cell toxicity of QDs is due to the leakage of cadmium ions or from reactive oxygen species as we discussed in our previous paper with non-differentiated PC12 cells [23].

ApoTox-Glo™Triplex Assay

The graph in Figure 5 depicts the results of an APOTOX- Glo Triplex assay showing the cytotoxicity of PC12 cells treated with NGF and exposed to red and orange QDs of gel and non-gel types along with controls. The cells were also similarly treated after the neurites were grown for 10 days. After periods of 7, 12 and 17 days, the cytotoxicity of red gel QDs was comparable to the untreated cell controls but in the case of smaller gel QDs the cytotoxicity increased significantly. This clearly showed that smaller orange gel QDs are significantly more toxic than the larger red gel QDs. The smaller orange non-gel QDs also exhibited significantly higher cytotoxicity than the larger red non-gel QDs as co-incubation periods were prolonged, and non-gel QDs

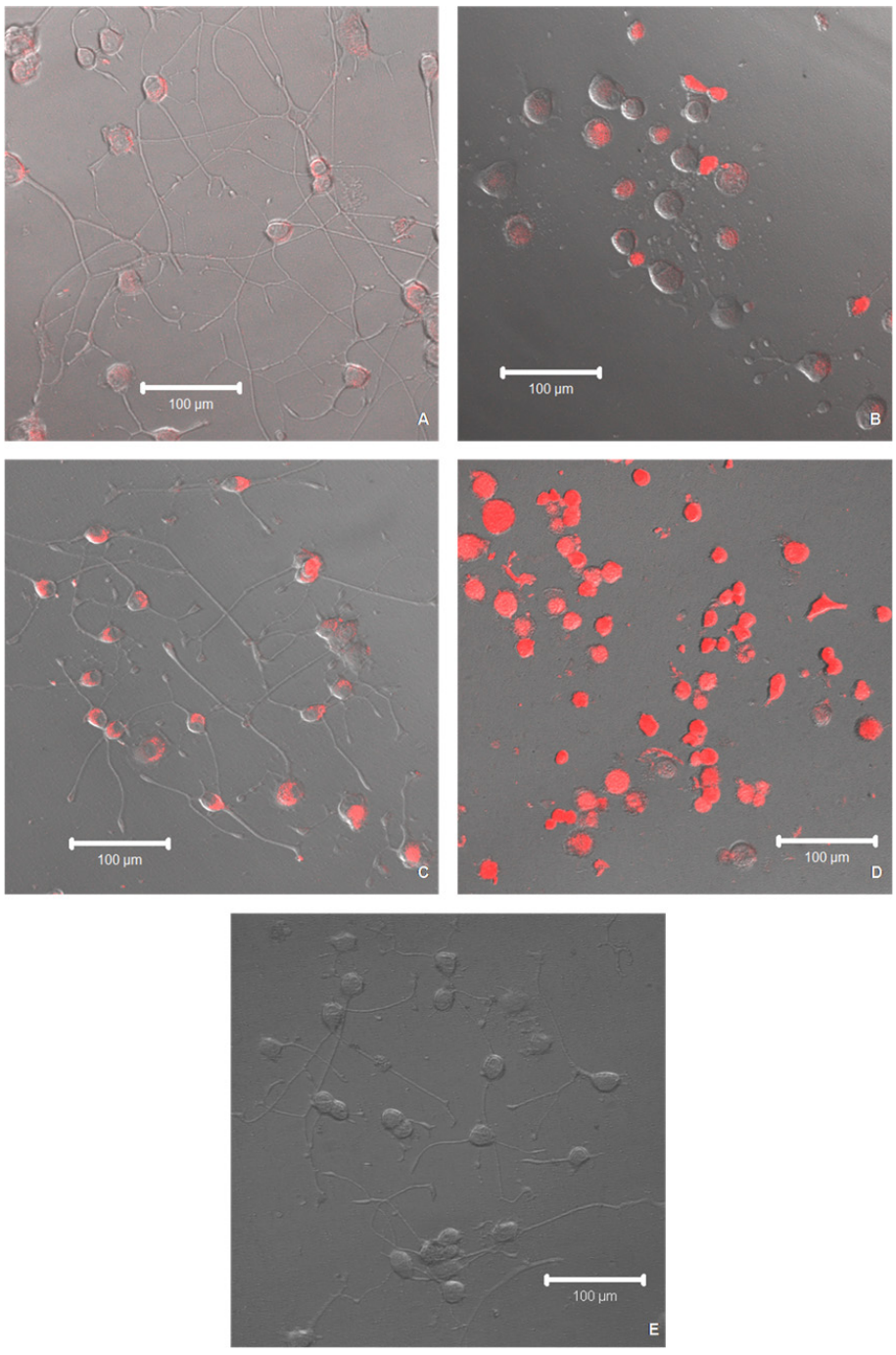

Figure 1 Live confocal images. Differential interference contrast (DIC) images of differentiated PC12 cells with overlaid corresponding fluorescent confocal images exposed to 10^{-9} M concentrations of QDs showing red gel QDs in (A), red non-gel QDs in (B), orange gel QDs in (C), orange non-gel QDs in (D) and the control in (E) without exposure to QDs following 14 days of co-incubation [scale bar = 100 µm].

were more cytotoxic than gel ones. Cytotoxicity levels increased as the co-incubation periods were prolonged up to 17 days. Gel and non-gel QDs exhibited the same trend with regards to the impact of particle size on cytotoxicity, with the smaller ones being the more toxic. Furthermore, the cells exposed to non-gel QDs were found to be more affected than those exposed to gel QDs. We found the same trend of cytotoxicity after neurites were grown for 10 days prior to QD exposure. This shows that there is absolutely no inhibition of

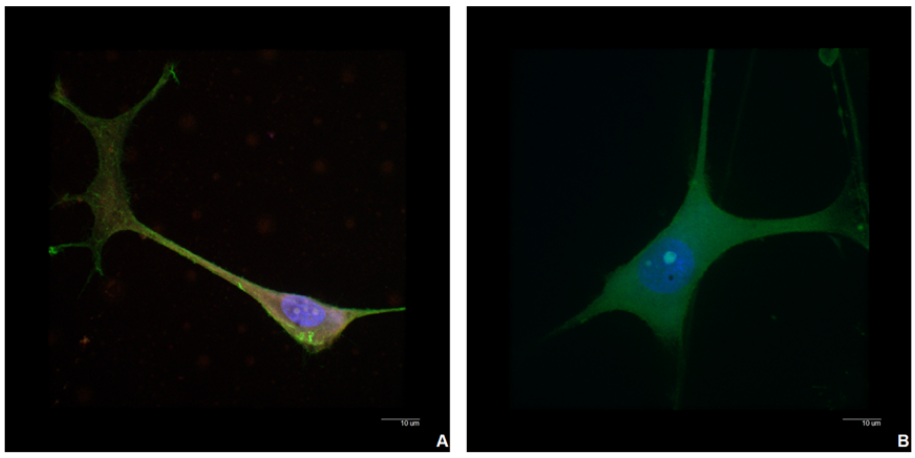

Figure 2 Stained confocal images. Overlaid fluorescent confocal images illustrating the morphology of the actin stained differentiated PC12 cells exposed to the red gel QDs (A) and differentiated PC12 cells without exposure to QDs as a control (B) following 17 days of co-incubation [Scale bar = 10 μm].

cellular interactions with QDs after the cells were grown with neurites.

The graph in Figure 6 depicts the results of an APOTOX Triplex assay showing the viability of PC12 cells treated with NGF and exposed to red and orange QDs of gel and non-gel types along with controls and the viability of cells treated with red and orange QDs of gel and non-gel types after neurites had been grown for 10 days. After periods of 7, 12 and 17 days, the viability of cells exposed to red gel QDs was the same as that of untreated control cells, however the viability of cells exposed to the smaller orange gel QDs decreased significantly. Similar to previous assays, cells exposed to the smaller orange QDs were significantly less viable than cells exposed to the larger red QDs (both gel and non-gel) as co-incubation periods were prolonged. Viability levels decreased as the co-incubation periods were prolonged up to 17 days, and retained the same trend with regards to gel/non-gel and size influence. The cells exposed to gel QDs were found to be more viable than the ones exposed to non-gel QDs and were equally viable as untreated controls (negative controls). We found the same trend of cellular viability after neurites were grown for 10 days and cells were subsequently treated with QDs. This also shows that there is absolutely no inhibition of cellular interactions with gel QDs after the cells were grown with neurites.

The graph in Figure 7 depicts the results of an APOTOX Triplex assay showing the apoptosis of PC12 cells treated with NGF and exposed to red and orange QDs of gel and non-gel types along with controls and also the apoptosis of cells which were treated with red and orange gel and non-gel QD types after neurites had been grown for 10 days. After periods of 7, 12 and 17 days, the apoptotic activity of cells exposed to red gel QDs was the same as that of untreated control cells, whereas the apoptotic activity of cells exposed to smaller orange gel QDs had significantly increased. This illustrated that smaller orange QDs were significantly more cytotoxic than the larger red QDs for both gel and non-gel QDs as co-incubation periods were prolonged. Overall, non-gel QDs induced more apoptosis than gel QDs. Apoptotic activity levels increased with both gel and non-gel QDs as the co-incubation periods were prolonged up to 17 days and retained the same trend with regards to gel/non-gel and size influence. The cells exposed to non-gel QDs were found to undergo more cell death than the cells exposed to gel QDs. We found the same trend of cell death after neurites were grown for 10 days and subsequent treatment of the cells with QDs. This shows that there is absolutely no inhibition of cellular interactions with gel QDs after the cells were grown with neurites.

Discussion

The present study is aimed at defining the effect of gelatinated CdTe QDs on differentiated PC12 cells. The cellular uptake of QDs is mediated by proteins such as clathrins, which are coated to membrane vesicles on the cell surface at the entry [29-31]. Non-specific binding occurred less frequently for PC12 cells [32] when compared to other cells like neuroblastoma cells as studied by Gomez *et al*. [33].

Confocal microscopy has been used to identify the localisation of the particles after cellular uptake, as shown in Figure 1 and 2. Similarly to previously reported non-differentiated PC12 cells [23], gel QDs were mostly found in the cytoplasm, which became

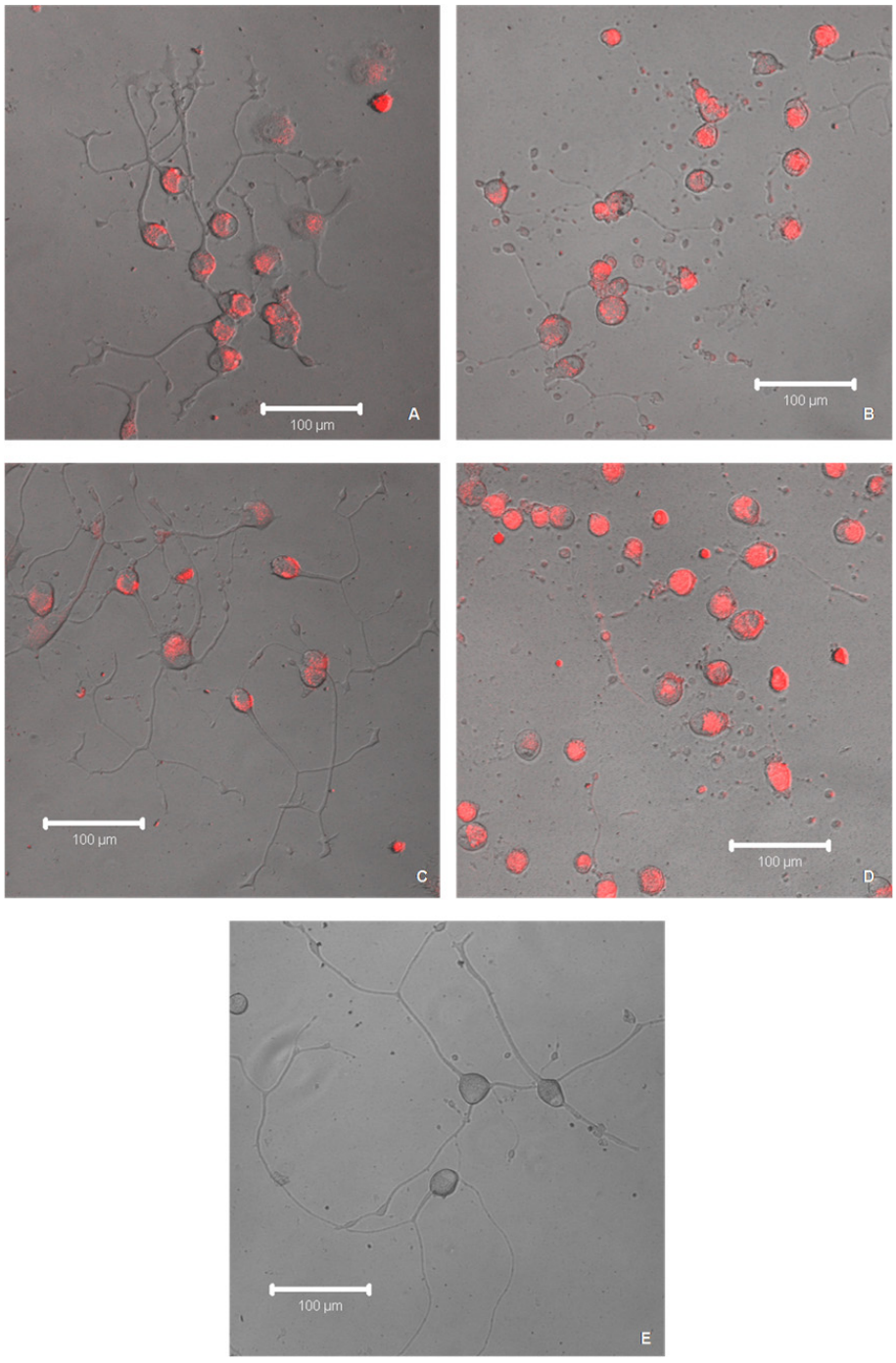

Figure 3 Live confocal images. Differential interference contrast (DIC) images of differentiated PC12 cells with overlaid corresponding fluorescent confocal images treated with NGF for 6 days prior to exposure to 10^{-9} M concentrations of QDs showing red gel QDs in (A), red non-gel QDs in (B), orange gel QDs in (C), orange non-gel QDs in (D) and control in (E) without exposure to QDs following 7 days of co-incubation [scale bar = 100 µm].

largely illuminated. This may be easily explained by the nature of the nanoparticles. The TGA-capped CdTe QDs used in this study were negatively charged thanks to the de-protonated carboxylic groups of the TGA molecules and they exhibit an average zeta potential of -40 mV. It has been shown in previous studies that negatively charged QDs have a strong tropism to core histones and histone-rich cell organelles [10]. This

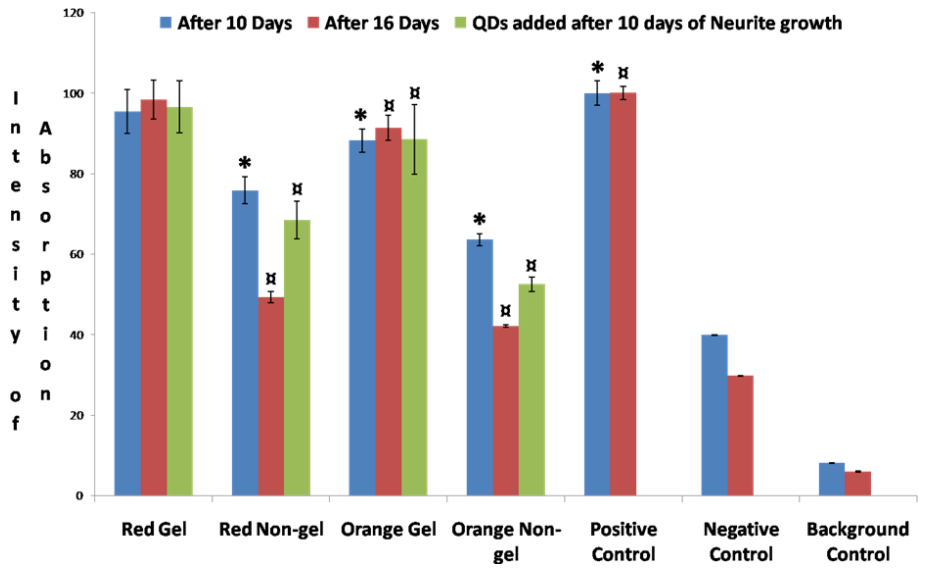

Figure 4 Proliferation assay. Graph of MTT assay after 10 and 16 days showing the rate of proliferation of differentiated PC12 cells after exposure to concentrations [10^{-9} M] of the gel and non-gel QDs. Positive control shows differentiated PC12 cells without exposure to QDs; the graph also shows differentiated PC12 cells which were exposed with red and orange QDs of gel and non-gel types after neurites were grown for 10 days. Symbols * and ¤ denote examples of statistical significance in comparison with positive controls using a one-way ANOVA ($P < 0.05$) by Tukey's mean comparison.

research suggested that the surface charge of these nanoparticles may ultimately determine their cellular uptake and therefore their location within the cell. It has been suggested that the negatively charged QDs are drawn towards the nucleus due to molecular interactions with positively charged histones. This may explain why the majority of TGA-capped CdTe QDs reside in the cytoplasm [5], surrounding the nucleus as opposed to the neurites.

Macromolecules, such as proteins and RNA, responsible for genome structure and function must be transported by selective, energy-dependent mechanisms from

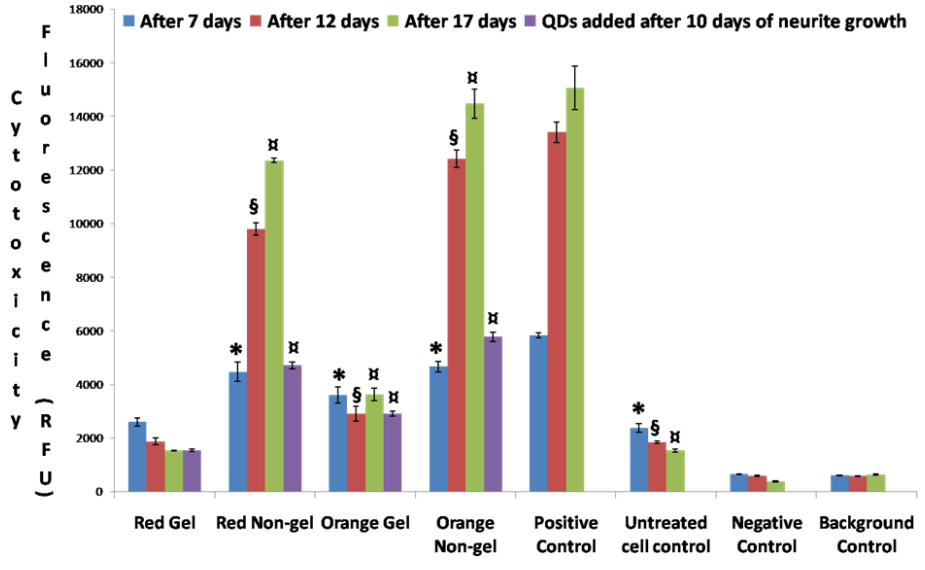

Figure 5 Cytotoxicity assay. Graph of APOTOX GLO Triplex assay showing the cytotoxicity of differentiated PC12 cells after 7, 12 and 17 days treated with red and orange QDs of gel and non-gel types along with controls. The cells were also treated with red and orange QDs of gel and non-gel types and neurites were subsequently grown for 10 days. Symbols *, § and ¤ denote examples of statistical significance in comparison with untreated cell controls using a one-way ANOVA ($P < 0.05$) by Tukey's mean comparison.

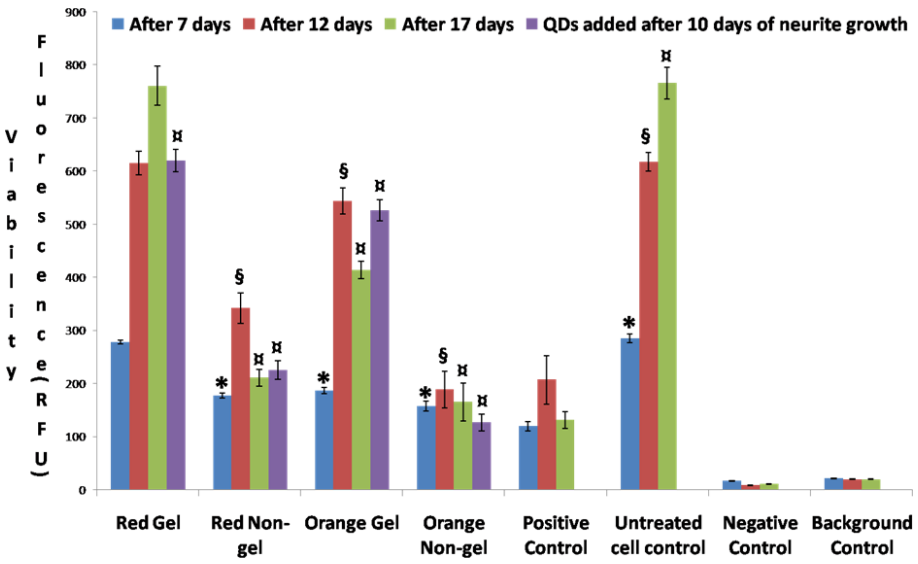

Figure 6 Viability assay. Graph of APOTOX GLO Triplex assay showing the viability of differentiated PC12 cells after 7, 12 and 17 days treated with red and orange QDs of gel and non-gel types along with controls. The cells were also treated with red and orange QDs of gel and non-gel types and neurites were subsequently grown for 10 days. Symbols *, § and ¤ denote examples of statistical significance in comparison with untreated cell controls using a one-way ANOVA ($P < 0.05$) by Tukey's mean comparison.

the cytoplasm to the nucleus. The karyopherin family of proteins maintain this process of selective import and export into the nucleus and cytoplasm. The nuclear localisation signals, nuclear transport receptors and the proteins in the nuclear pore complex ensure that no unwanted molecules are transported into the nucleus [34]. This selective transport system could be the reason why QDs are not localised within the nucleus. A second reason why QDs seem to localise only in the cytoplasm could be due to entrapment within cell organelles such as endosomes, lysosomes and vesicles. However, examination of images of differentiated PC12 cells (Figures 1 and 2), shows some localisation of QDs within the neurites. This would mean that not all the QDs are

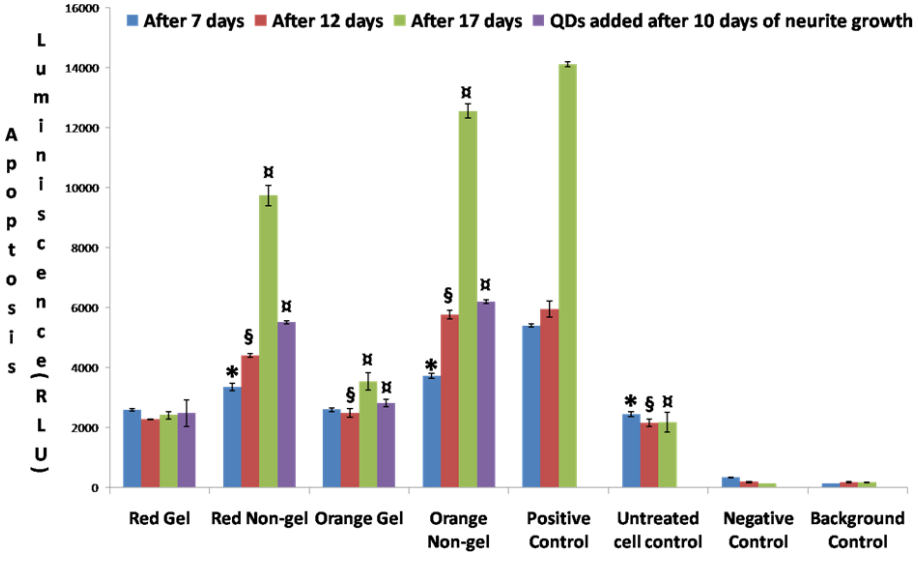

Figure 7 Apoptosis assay. Graph of APOTOX GLO Triplex assay showing the apoptosis of differentiated PC12 cells after 7, 12 and 17 days treated with red and orange QDs of gel and non-gel types along with controls. The cells were also treated with red and orange QDs of gel and non-gel types and neurites were subsequently grown for 10 days. Symbols *, § and ¤ denote examples of statistical significance in comparison with untreated cell controls using a one-way ANOVA ($P < 0.05$) by Tukey's mean comparison.

accumulated within these cell organelles, but still are not observed within the nucleus [12,31].

Figure 3 displays a comparison of the morphological changes induced by exposure of cells to QDs of different sizes and structure. The degeneration of neurites observable mostly in the case of non-gel QDs was attributed to neuronal cell death and direct axonal toxicity, as evidenced by the study of Sanjeev Kumar Mahto *et al*., with differentiated PC12 cells inside microfluidic devices [26]. Another study also showed that the degeneration of neurites was due to autophagosomes or lysosomes produced in the cell cytoplasm and in the neurites, which traverse in both anterograde and retrograde directions to destroy the already impaired mitochondria due to the toxicity of QDs [35].

Although observation of the cell morphology gave a rather clear idea of the trend in cytotoxicity among the different types of QDs, quantitative assays of the metabolic activity could provide a better understanding of the mechanisms involved. The MTT proliferation assay was designed to probe the activity of reductase enzymes as a measure of cell viability and proliferation. The results shown in Figure 4 indicated that gel QDs (both red and orange) did not significantly affect cell proliferation as compared to untreated control cell cultures. Non-gel QDs, however, caused a reduction of about 50% in cell proliferation. Interestingly, whether the cell differentiation occurred simultaneously or prior to QD treatment did not change the outcome of the assay. The MTT assay correlated well with the viability part of the APOTOX GLO Triplex assay (Figure 6), although the latter gave more subtle results, showing a discrepancy between red and orange QDs. This assay essentially assessed the cell membrane integrity and is therefore more sensitive than MTT which measures the enzyme level. Orange QDs are smaller in size and appeared to be slightly more cytotoxic then their larger red counterparts. It was previously reported by Lovric *et al.* [5] that QD cytotoxicity was inversely related to their size due to the fact that smaller particles may enter cells more readily thus interfering to a higher degree with the cell machinery. As expected, the cytotoxicity part of the APOTOX GLO Triplex assay produced similar results (Figure 5); gel QDs appeared to be much less cytotoxic than non-gel QDs, and orange (smaller) ones were more cytotoxic than red (larger) ones.

A recent study on the toxicity of QDs with PC12 cells has shown involvement of reactive oxygen species (ROS) [5] and the most common pathways involved in relation to toxicity of QDs with ROS has been discussed previously [23]. In the cell, mitochondria are cellular factories for the production of Adenosine Triphosphate (ATP) and are also a prime source of ROS production. In addition, they help to regulate the cytoplasmic calcium levels, pH and apoptosis. Abnormally increased levels of ROS (oxidative stress) during ischemia make it difficult for the neuronal cells to survive due to overwhelming multiple buffering mechanisms of ROS [15]. Oxidative stress is a state in which glutathione (GSH) is depleted with accumulation of oxidized glutathione (GSSG) [3,36]. Lower levels of ROS are easily neutralized by generation of GSH and antioxidant enzymes. Protective or injury responses in the cells are characterized by the drop in GSH/GSSG ratio [3,36-39]. At lower oxidative stress, cellular redox hemostasis occurs, intermediate oxidative stress leads to inflammation and higher oxidative stress leads to cytotoxicity which finally leads to apoptosis [3,36].

Apoptosis is one form of cell death which involves the cell death machinery, Caspase-9, Apaf-1 and Cytochrome c. Chromatin margination along the nuclear membrane, nuclear condensation, budding and fragmentation are some of the features of apoptosis which can be seen in the cell morphology. DNA fragmentation, which is one of the hallmarks of apoptosis is thought to be induced by cadmium. Cadmium toxicity is thought to affect the cells by the production of ROS and can induce apoptosis through a mitochondrial caspase dependent pathway [40]. Caspases, a family of cysteine proteases, carry out these complex biochemical events which cause cell morphology changes. Caspases are made up of initiator caspases such as caspases-8, -9 and -12, whose function is to activate downstream caspases, and executor caspases, such as caspases-3, -6 and -7, their function being to degrade cellular protein [1,41].

In previous research on human neuroblastoma cells, Chan *et al.* described the apoptotic chain of events induced by CdSe QDs through the mitochondrial release of cytochrome c and activation of caspase-9 and caspase-3 [14]. The trigger is the intracellular degradation of QDs, which leads to the release of free cadmium ions (Cd^{+2}) inside the cytoplasm. These free cadmium ions inside the cells are responsible for the formation of ROS, leading to oxidation of the phospholipid Cardiolipin, which helps in associating the cytochrome c with inner mitochondrial membrane [42]. Due to oxidation of cardiolipin, cytochrome c is released, an important event in apoptotic signaling [43]. Release of cytochrome c is also due to ROS-induced changes in the conformation of the adenine nucleotide translocase, a protein which is involved in the formation of the mitochondrial permeability transition pore [44], and the voltage-dependent anion channel-selective permeabilization of the mitochondrial outer membrane [45]. It is thought that this release of Cytochrome *c* into the cytosol leads to Caspase-9 activation by Cytochrome c/Apaf-1 complex. Caspase-9 is the upstream caspase in the mitochondria-dependent apoptosis pathway and activates Caspase-3.

In our study, the apoptosis assay, while confirming the general trend among the various types of QDs, provided valuable information about the mechanisms involved in cell death upon QD treatment (Figure 7). The assay itself is based on the measurement of the activity of caspase 3/7 as an indicator of apoptosis. Therefore it can be concluded that QDs, in particular non-gel types, cause cell death *via* cadmium-induced mitochondrial release of cytochrome c and activation of caspase-3 leading to apoptosis [41].

Long term exposure (up to 17 days) of PC12 cells to QDs both before and after undergoing differentiation displayed dramatic differences between non-gel and gel QDs. While the former exhibited a dramatic increase in cytototoxicity as measured by MTT and APOTOX GLO Triplex assays (Figures 4 to 7), the latter remained at a comparable level of toxicity as after 7 and 12 days of incubation. It was therefore concluded that the gelatine coating durably stabilized the QDs and created virtually no interference with cell functions over significant periods of time.

The results presented here are consistent with our previously published findings on non-differentiated PC12 cells [23]. Differentiated PC12 cells mimic neuronal cells behaviour, thus providing a model for QD interaction with neurons. The accumulation of nanoparticles in neurites was minor compared to the rest of the cytoplasm and did not appear to disturb the cell functions any further, even over extended periods of time (up to 17 days). In addition, we found that QDs did not affect differentiation itself, as proved by the growth of neurites in their presence.

Conclusion

There is clear evidence from MTT and APOTOX-Glo Triplex assay (Cytotoxicity, Viability and Apoptosis) and also from microscopic images that the gelatine-coating helps to reduce the toxicity of CdTe QDs and assists in protecting the cells themselves. This was observed indiscriminately when neurites were grown prior to or after exposure to QDs. The difference in toxicity and resulting cell death between the orange and red gel QDs is due to the smaller size of the orange QDs. By preventing leakage of cadmium ions from the QD core and providing a biocompatible interface, the gelatine coating helps to delay caspase activation events that eventually lead to apoptosis. Gel QDs were shown neither to inhibit cell differentiation nor to be any more cytotoxic towards neuron-like differentiated cells than non-differentiated ones. This provided a good indication that these particles can remain in healthy and sensitive tissue for several days (up to 17 days) without damaging it, which opens applications in diagnostics and targeted drug delivery. This is an important starting point that can be used for development of other non-toxic nanoparticle-gelatine composites, which might have a range of potential biomedical applications such as controlled drug delivery, *in vivo* and *in vitro* diagnostics and anticancer therapy.

Materials and methods

Chemicals and Reagents

PC12 cells (cell line derived from a pheochromocytoma of the rat adrenal medulla) were used for this study. Dulbecco's Modification of Eagle Medium (DMEM) (Sigma-Aldrich) supplemented with 10% heat inactivated horse serum, 5% fetal bovine serum, 1% penicillin-streptomycin and Trypsin-EDTA solution and all chemicals for QD synthesis were purchased from Sigma-Aldrich. Al_2Te_3 was purchased from Cerac Inc. Mouse Nerve Growth Factor (mNGF 2.5S Grade 2) was purchased from Alomone labs. MTT assay to measure cell proliferation, MTT Reagent and stop solution was kindly received from Dr. Afshin Samali Group of NCBES, NUI Galway. APOTOX-Glo™ Triplex assay kit to measure cytotoxicity, viability and apoptosis was purchased from Promega Corporation. Permonax four-well chamber slide (Lab-Tek, Nalgene Nunc International), Phalloidin-FITC (Sigma-Aldrich), DAPI (Vector Laboratories), 96-well flat tissue culture plates were purchased from Sarstedt.

Quantum Dot Synthesis

Note: all values denoted are initial concentrations and synthesis follows previously published procedures [46,47]. Millipore water (150 ml) was degassed by bubbling argon through it for approximately 1 hour. Cd $(ClO_4)_2 \cdot 6H_2O$ and 1.3 molar equivalents of thio-glycolic acid (TGA) stabilizer were added to the water and the pH was adjusted to 11.2-11.3 by the addition of a 2 M NaOH solution. For samples containing gelatine, 0.3 g was added to the reaction mixture. H_2Te gas was generated from Al_2Te_3 (0.25 molar equivalents as compared to cadmium per-chlorate) *via* drop-wise addition of a 0.5 M H_2SO_4 solution and was bubbled through the cadmium/thiol solution under a slow argon flow for approximately 10 minutes. Note: 100% reaction and carryover is assumed and cadmium is always in excess for this experiment. The resultant, non-luminescent solution was then heated to reflux (at 130°C). Following the reflux process, fractions were precipitated *via* the addition of isopropanol and were stored at 4°C. The stock solutions were further purified on a Sephadex G25 column. A Shimadzu UV-1601 UV - Visible Spectrophotometer was used to measure QD absorption while a Varian - Cary Eclipse Fluorescence Spectrophotometer was used to determine the fluorescence emission/photoluminescence (PL) spectra of QDs. Throughout the text,

gel and non-gel refer to the presence of gelatine during the synthesis of the QDs. Smaller QDs (~2.5 nm) are referred to as orange QDs and larger ones (~ 4.5 nm) as red QDs. Hydrodynamic diameters and zeta potentials were measured on a Malvern Zetasizer Nano Series V5.10. The concentration of samples used for these measurements was typically corresponding to an absorbance around 0.2 in the plasmon band. Three measurements were usually taken for each sample, each made of 10 to 20 accumulations as optimised by the machine.

Cell Culture

PC12 cells, were cultured in medium (DMEM supplemented with 10% heat inactivated horse serum, 5% fetal bovine serum, 1% penicillin-streptomycin) @ 37°C and a 5% CO_2 atmosphere. All the tissue culture plates and chamber slides were treated with 0.001% Poly-L-Lysine (PLL) for 24 hours.

Cell Staining

Cells were seeded into four-well chambers at a density of 5000 cells/cm^2. After 24 hours, QDs were added (10% of amount of Medium) to make final concentrations of 10^{-9} M and the cells were incubated for 17 days. Cells were grown on 4 well Permonax Chamber slides in the presence of QDs and were washed with 1% phosphate-buffered saline (BSA/PBS). Cells were fixed with 4% paraformaldehyde for 15 minutes and then washed 3 times with PBS. Then cells were permeabilized with permeabilizing solution (5 min, 0°C). Actin filaments of cytoplasm were labelled with Phalloidin FITC (Sigma-Aldrich), at 1:50 dilution with PBS for 20 minutes and again washed 3 times with PBS. Nuclei were labelled with Vectashield mounting medium with DAPI to preserve fluorescence and counterstain DNA with DAPI 1 μg/ml.

Confocal Microscopy

An LSM 510 (Carl Zeiss, Jena, Germany) Confocal Laser Scanning microscope was used to examine QDs inside PC12 cells and their morphology.

Cell imaging was carried out using a LSM 510 Inverted Confocal Microscope which is equipped with the following excitation lasers: (a) Argon Laser excitation wavelengths (λ_{Ex}) = 458 nm, 488 nm, 514 nm, (b) HeNe1 - λ_{Ex} = 543 nm and (c) Titanium Sapphire Tuneable Two-photon Laser tuneable from 710 nm to 1000 nm with a resulting excitation range of 355 nm to 500 nm.

All Confocal laser scanning was carried out at laser scan speed of 7 with the Photomultiplier Tube settings adjusted to eliminate noise and saturation with the aid of the range indicator setting in the LSM 510 software. For image optimisation, scan averaging was carried out on 8 scans per image.

Sequential acquisition was used to acquire the two-colour images of the QDs in cells. For visualisation of the QDs, the samples were excited with the Argon 514 nm Laser and the microscope configuration was set up to capture the emitted fluorescence at 550 nm or 600 nm as desired. Differential Interference Contrast (DIC) or Nomarski Microscopy was used to visualise the cell morphology, and was carried out by using the HeNe1 488 nm laser with the Transmission Channel Detector selected and the DIC polariser and Nomarski prisms engaged. The two images were then overlaid using the LSM 510 software.

Sequential acquisition was also used to acquire three-colour images. Rhodamine phalloidin was excited using the HeNe1 543 nm laser and the emitted fluorescence was acquired at 575 nm. DAPI stain was excited with laser light at 390 nm (from the Two Photon laser tuned to 780 nm) and emitted fluorescence was acquired at 458 nm. The three separate images were overlaid using the LSM510 software to make up the three-colour images.

MTT Assay

The yellow tetrazolium MTT (3-(4, 5-dimethylthiazolyl-2)-2, 5 diphenyltetrazolium bromide) is reduced by metabolically active cells, in part by the action of dehydrogenase enzymes, to generate reducing equivalents such as Nicotinamide adenine dinucleotide (NADH) and nicotinamide adenine dinucleotide phosphate (NADPH). The resulting intracellular purple formazan can be solubilized and quantified by spectrophotometry. The MTT Cell Proliferation Assay measures the cell proliferation rate and conversely, when metabolic events lead to apoptosis or necrosis, the reduction in cell viability. PC12 cells of approximately 1000/well were seeded in a flat 96-well micro-plate (Sarstedt) as triplicates. Three different types of controls, namely: positive, negative and background were used throughout the study. Positive control had cells with culture medium treated with NGF but not exposed to QDs. Negative control had QDs without cells. Background control had culture medium without cells. After 24 h, QDs (10% of amount of medium) of size ~ 4.5 nm (red gel, red non-gel) and ~2.5 nm (orange gel and orange non-gel) were added to make final concentrations of QDs to 10^{-9} M. After 48 hours of seeding, the cells were treated with final concentration of 200 ng/ml of Nerve Growth Factor (NGF) on every second day with 200 μl of fresh medium in each well.

After 10 days of exposure to QDs, old medium was removed from all the wells and 100 μl of fresh medium was added. 10 μl of MTT reagent was then added to each well and incubated for 3 hours. To stop the reaction of the assay, 100 μl of stop solution was added to

each well. The 96-well plate was left on a shaker overnight at a speed of 300 rpm and was then analyzed using a Perkin Elmer Victor$^3{}_{TM}$V Wallac plate reader at absorbance of 570 nm. This was repeated again for another 96 well plate with incubation period of 16 days after adding QDs [27].

ApoTox-Glo™Triplex Assay

This combines three assay chemistries to assess viability, cytotoxicity and caspase activation events within a single assay well. In the first part of the assay, it measures two protease activities simultaneously; one being a marker of cell viability and the other being a marker of cytotoxicity. Peptide substrate (glycylphenylalanyl-aminofluorocoumarin; GF-AFC) enters intact cells where it is cleaved by the live-cell protease activity to generate a fluorescent signal proportional to the number of living cells. This live-cell protease becomes inactive upon loss of cell membrane integrity and leakage into the surrounding culture medium. Peptide substrate (bis-alanylalanyl-phenylalanyl-rhodamine 110; bis-AAF-R110) is used to measure dead-cell protease activity, which is released from cells that have lost membrane integrity. Bis-AAF-R110 is not cell-permeable, so no signal from this substrate is generated by intact, viable cells. The live- and dead-cell proteases produce different products, AFC and R110, which have different excitation and emission spectra, allowing them to be detected simultaneously. In the second part of the assay, the Caspase-Glo® 3/7 Reagent, added in an "add-mix-measure" format, results in cell lysis, followed by caspase cleavage of the substrate and generation of a "glow-type" luminescent signal produced by luciferase.

PC12 cells of approximately 500/well were seeded in a flat 96-well micro-plate (Sarstedt) as triplicates. Four different types of controls, namely: positive, untreated, negative and background controls were used throughout the study. Positive control had cells with culture medium treated with NGF and exposed to Staurosporine of 500 nM final concentration for 16 hours to induce apoptosis. Control cell cultures contained cells treated with NGF, without QDs. Optional test compound control (negative control) consisted of QDs without cells. No-cell control (background) contained only culture medium without cells. After 24 h, QDs (10% of amount of medium) of size ~ 4.5 nm (red gel, red non-gel) and ~2.5 nm (orange gel and orange non-gel) were added to make final concentrations of QDs to 10^{-9} M. After 48 hours of seeding, the cells were treated with final concentration of 200 ng/ml of Nerve Growth Factor (NGF) on every second day with 200 μl of fresh medium in each well [27].

After 7 days of exposure to QDs, old medium was removed from all the wells and 100 μl of fresh medium was added. 20 μl of Viability/Cytotoxicity reagent containing both GF-AFC and bis-AAF-R110 substrates was added to each well, and briefly mixed by orbital shaking at 300-500 rpm for 30 seconds and then incubated at 37°C for 30-180 minutes. Fluorescence was measured at $400_{Ex}/505_{Em}$ (Viability) and $485_{Ex}/520_{Em}$ (Cytotoxicity) by using PerSeptive Biosystems CYTOFLUOR® multi-well plate reader series 4000. After that 100 μl of Caspase-Glo 3/7 reagent was added to each well, and briefly mixed by orbital shaking at 300-500 rpm for 30 seconds and then incubated at room temperature for 30-180 minutes. Luminescence was measured using a Perkin Elmer Victor$^3{}_{TM}$V Wallac plate reader by Luminiscence (1.0 s) protocol which is proportional to the amount of caspase activity present. This was repeated again for another 96 well plates with incubation period of 12 and 17 days after adding QDs.

Statistical Analysis

Results of MTT assay were analysed using one-way analysis of variance (ANOVA). A ρ value of less than 0.05 for the ANOVA was considered significant. Error was expressed as standard deviation.

Abbreviations

QDs: Quantum Dots; CdTe: Cadmium Telluride; PC12: Pheochromocytoma 12; NGF: nerve growth factor; TGA: Thioglycolic Acid; gel-QDs: gelatinised QDs; DNA: Deoxyribonucleic Acid; DMEM: Dulbecco's Modification of Eagle Medium; EDTA: Ethylenediaminetetraacetic acid; DAPI: 4, 6-diamidino-2-phenylindole; UV: ultraviolet; PL: photoluminescence; PLL: Poly-L-Lysine; BSA/PBS: Bovine serum albumin/phosphate-buffered saline; DIC: Differential Interference Contrast; HBSS: Hank's Balanced Salt Solution.

Acknowledgements and Funding

The authors would like to thank Dr. Ayswaria Deepti, Apoptosis Group, NCBES, National University of Ireland, Galway and Dr. Kerry Thomson, Department of Anatomy, School of Medicine, National University of Ireland, Galway, Ireland. This work was funded by Science Foundation Ireland (SFI).

Author details

[1]National Centre for Biomedical Engineering Science, National University of Ireland Galway, Galway, Ireland. [2]CRANN and the School of Chemistry, Trinity College Dublin, Dublin 2, Ireland.

Authors' contributions

BRP performed all the experiments and wrote the manuscript. GM contributed with cellular experiments. VAG, SJB and GLD synthesised QDs and contributed with manuscript preparation. DC contributed with confocal imaging. YR, YG, NN, TJS designed the overall project and helped with data and manuscript revision. All authors read and approved the final manuscript.

Competing interests

The authors declare that they have no competing interests.

Received: 22 June 2011 Accepted: 20 January 2012
Published: 20 January 2012

References

1. Li KG, Chen JT, Bai SS, Wen X, Song SY, Yu Q, Li J, Wang YQ: **Intracellular oxidative stress and cadmium ions release induce cytotoxicity of unmodified cadmium sulfide quantum dots.** *Toxicol In Vitro* 2009, **23(6)**:1007-1013.

2. Lovric J, Cho SJ, Winnik FM, Maysinger D: **Unmodified cadmium telluride quantum dots induce reactive oxygen species formation leading to multiple organelle damage and cell death.** *Chem Biol* 2005, **12(11)**:1227-1234.
3. Nel A, Xia T, Madler L, Li N: **Toxic potential of materials at the nanolevel.** *Science* 2006, **311(5761)**:622-627.
4. Oberdorster G, Oberdorster E, Oberdorster J: **Nanotoxicology: an emerging discipline evolving from studies of ultrafine particles.** *Environ Health Perspect* 2005, **113(7)**:823-839.
5. Lovrić J, Bazzi HS, Cuie Y, Fortin GRA, Winnik FM, Maysinger D: **Differences in subcellular distribution and toxicity of green and red emitting CdTe quantum dots.** *J Mol Med* 2005, **83**:377-385.
6. Byrne SJ, Williams Y, Davies A, Corr SA, Rakovich A, Gun'ko YK, Rakovich YP, Donegan JF, Volkov Y: **"Jelly dots": synthesis and cytotoxicity studies of CdTe quantum dot-gelatin nanocomposites.** *Small* 2007, **3(7)**:1152-1156.
7. Derfus AM, Chan WCW, Bhatia SN: **Intracellular delivery of quantum dots for live cell labeling and organelle tracking.** *Advanced Materials* 2004, **16(12)**:961-+.
8. Derfus AM, Chan WCW, Bhatia SN: **Probing the cytotoxicity of semiconductor quantum dots.** *Nano Letters* 2004, **4(1)**:11-18.
9. Lee HM, Shin DM, Song HM, Yuk JM, Lee ZW, Lee SH, Hwang SM, Kim JM, Lee CS, Jo EK: **Nanoparticles up-regulate tumor necrosis factor-alpha and CXCL8 via reactive oxygen species and mitogen-activated protein kinase activation.** *Toxicol Appl Pharmacol* 2009, **238(2)**:160-169.
10. Conroy J, Byrne SJ, Gun'ko YK, Rakovich YP, Donegan JF, Davies A, Kelleher D, Volkov Y: **CdTe nanoparticles display tropism to core histones and histone-rich cell organelles.** *Small* 2008, **4(11)**:2006-2015.
11. Duan H, Nie S: **Cell-penetrating quantum dots based on multivalent and endosome-disrupting surface coatings.** *J Am Chem Soc* 2007, **129(11)**:3333-3338.
12. Ruan G, Agrawal A, Marcus AI, Nie S: **Imaging and tracking of tat peptide-conjugated quantum dots in living cells: new insights into nanoparticle uptake, intracellular transport, and vesicle shedding.** *J Am Chem Soc* 2007, **129(47)**:14759-14766.
13. Cho SJ, Maysinger D, Jain M, Roder B, Hackbarth S, Winnik FM: **Long-term exposure to CdTe quantum dots causes functional impairments in live cells.** *Langmuir* 2007, **23(4)**:1974-1980.
14. Chan WH, Shiao NH, Lu PZ: **CdSe quantum dots induce apoptosis in human neuroblastoma cells via mitochondrial-dependent pathways and inhibition of survival signals.** *Toxicol Lett* 2006, **167(3)**:191-200.
15. Foster KA, Galeffi F, Gerich FJ, Turner DA, Muller M: **Optical and pharmacological tools to investigate the role of mitochondria during oxidative stress and neurodegeneration.** *Prog Neurobiol* 2006, **79(3)**:136-171.
16. Tang M, Xing T, Zeng J, Wang H, Li C, Yin S, Yan D, Deng H, Liu J, Wang M, *et al*: **Unmodified CdSe quantum dots induce elevation of cytoplasmic calcium levels and impairment of functional properties of sodium channels in rat primary cultured hippocampal neurons.** *Environ Health Perspect* 2008, **116(7)**:915-922.
17. Tang M, Wang M, Xing T, Zeng J, Wang H, Ruan DY: **Mechanisms of unmodified CdSe quantum dot-induced elevation of cytoplasmic calcium levels in primary cultures of rat hippocampal neurons.** *Biomaterials* 2008, **29(33)**:4383-4391.
18. Gao X, Cui Y, Levenson RM, Chung LW, Nie S: **In vivo cancer targeting and imaging with semiconductor quantum dots.** *Nat Biotechnol* 2004, **22(8)**:969-976.
19. Chan WC, Nie S: **Quantum dot bioconjugates for ultrasensitive nonisotopic detection.** *Science* 1998, **281(5385)**:2016-2018.
20. Bruchez M, Moronne M, Gin P, Weiss S, Alivisatos AP: **Semiconductor nanocrystals as fluorescent biological labels.** *Science* 1998, **281(5385)**:2013-2016.
21. Delehanty JB, Medintz IL, Pons T, Brunel FM, Dawson PE, Mattoussi H: **Self-assembled quantum dot-peptide bioconjugates for selective intracellular delivery.** *Bioconjugate Chem* 2006, **17(4)**:920-927.
22. Dahan M, Levi S, Luccardini C, Rostaing P, Riveau B, Triller A: **Diffusion dynamics of glycine receptors revealed by single-quantum dot tracking.** *Science* 2003, **302(5644)**:442-445.
23. Prasad BR, Nikolskaya N, Connolly D, Smith TJ, Byrne SJ, Gerard VA, Gun'ko YK, Rochev Y: **Long-term exposure of CdTe quantum dots on PC12 cellular activity and the determination of optimum non-toxic concentrations for biological use.** *J Nanobiotechnology* 2010, **8**:7.
24. Greene LA, Aletta JM, Rukenstein A, Green SH: **PC12 pheochromocytoma cells: culture, nerve growth factor treatment, and experimental exploitation.** *Methods Enzymol* 1987, **147**:207-216.
25. Radio NM, Freudenrich TM, Robinette BL, Crofton KM, Mundy WR: **Comparison of PC12 and cerebellar granule cell cultures for evaluating neurite outgrowth using high content analysis.** *Neurotoxicol Teratol* 2010, **32(1)**:25-35.
26. Mahto SK, Yoon TH, Rhee SW: **Cytotoxic effects of surface-modified quantum dots on neuron-like PC12 cells cultured inside microfluidic devices.** *Biochip J* 2010, **4(1)**:82-88.
27. Pelzl C, Arcizet D, Piontek G, Schlegel J, Heinrich D: **Axonal guidance by surface microstructuring for intracellular transport investigations.** *Chemphyschem* 2009, **10(16)**:2884-2890.
28. Yu WW, Qu LH, Guo WZ, Peng XG: **Experimental determination of the extinction coefficient of CdTe, CdSe, and CdS nanocrystals.** *Chem Mater* 2003, **15(14)**:2854-2860.
29. Dawson KA, Salvati A, Lynch I: **Nanotoxicology: nanoparticles reconstruct lipids.** *Nat Nanotechnol* 2009, **4(2)**:84-85.
30. Watson P, Jones AT, Stephens DJ: **Intracellular trafficking pathways and drug delivery: fluorescence imaging of living and fixed cells.** *Adv Drug Deliv Rev* 2005, **57(1)**:43-61.
31. Byrne SJ, le Bon B, Corr SA, Stefanko M, O'Connor C, Gun'ko YK, Rakovich YP, Donegan JF, Williams Y, Volkov Y, *et al*: **Synthesis, characterisation, and biological studies of CdTe quantum dot-naproxen conjugates.** *ChemMedChem* 2007, **2(2)**:183-186.
32. Vu TQ, Maddipati R, Blute TA, Nehilla BJ, Nusblat L, Desai TA: **Peptide-conjugated quantum dots activate neuronal receptors and initiate downstream signaling of neurite growth.** *Nano Lett* 2005, **5(4)**:603-607.
33. Gomez N, Winter JO, Shieh F, Saunders AE, Korgel BA, Schmidt CE: **Challenges in quantum dot-neuron active interfacing.** *Talanta* 2005, **67(3)**:462-471.
34. Cooper GM: *The Cell, A Molecular Approach*. Fourth edition. ASM Press Washington, D.C; 2007.
35. Yang Y, Xu K, Koike T, Zheng X: **Transport of autophagosomes in neurites of PC12 cells during serum deprivation.** *Autophagy* 2008, **4(2)**:243-245.
36. Halliwell B: **Antioxidant defence mechanisms: from the beginning to the end (of the beginning).** *Free Radic Res* 1999, **31(4)**:261-272.
37. Nel A: **Atmosphere. Air pollution-related illness: effects of particles.** *Science* 2005, **308(5723)**:804-806.
38. Bell AT: **The impact of nanoscience on heterogeneous catalysis.** *Science* 2003, **299(5613)**:1688-1691.
39. Xiao GG, Wang M, Li N, Loo JA, Nel AE: **Use of proteomics to demonstrate a hierarchical oxidative stress response to diesel exhaust particle chemicals in a macrophage cell line.** *J Biol Chem* 2003, **278(50)**:50781-50790.
40. Oh SH, Lim SC: **A rapid and transient ROS generation by cadmium triggers apoptosis via caspase-dependent pathway in HepG2 cells and this is inhibited through N-acetylcysteine-mediated catalase upregulation.** *Toxicol Appl Pharmacol* 2006, **212(3)**:212-223.
41. Kondoh M, Araragi S, Sato K, Higashimoto M, Takiguchi M, Sato M: **Cadmium induces apoptosis partly via caspase-9 activation in HL-60 cells.** *Toxicology* 2002, **170**:(1-2):111-117.
42. Shidoji Y, Hayashi K, Komura S, Ohishi N, Yagi K: **Loss of molecular interaction between cytochrome c and cardiolipin due to lipid peroxidation.** *Biochem Biophys Res Commun* 1999, **264(2)**:343-347.
43. Newmeyer DD, Ferguson-Miller S: **Mitochondria: releasing power for life and unleashing the machineries of death.** *Cell* 2003, **112(4)**:481-490.
44. McStay GP, Clarke SJ, Halestrap AP: **Role of critical thiol groups on the matrix surface of the adenine nucleotide translocase in the mechanism of the mitochondrial permeability transition pore.** *Biochem J* 2002, **367(Pt 2)**:541-548.
45. Madesh M, Hajnoczky G: **VDAC-dependent permeabilization of the outer mitochondrial membrane by superoxide induces rapid and massive cytochrome c release.** *J Cell Biol* 2001, **155(6)**:1003-1015.
46. Byrne SJ, Corr SA, Rakovich TY, Gun'ko YK, Rakovich YP, Donegan JF, Mitchell S, Volkov Y: **Optimisation of the synthesis and modification of CdTe quantum dots for enhanced live cell imaging.** *J Mat Chem* 2006, **16(28)**:2896-2902.
47. Gaponik N, Talapin DV, Rogach AL, Hoppe K, Shevchenko EV, Kornowski A, Eychmüller A, Weller H: **Thiol-capping of CdTe nanocrystals: An**

alternative to organometallic synthetic routes. *J Phys Chem B* 2002, 106(29):7177-7185.

doi:10.1186/1477-3155-10-4
Cite this article as: Prasad *et al.*: Effects of long-term exposure of gelatinated and non-gelatinated cadmium telluride quantum dots on differentiated PC12 cells. *Journal of Nanobiotechnology* 2012 **10**:4.

Colloids and Surfaces B: Biointerfaces xxx (2010) xxx–xxx

Contents lists available at ScienceDirect

Colloids and Surfaces B: Biointerfaces

journal homepage: www.elsevier.com/locate/colsurfb

Controlling cellular activity by manipulating silicone surface roughness

Babu R. Prasad[a], Michael A. Brook[b,d,*], Terry Smith[a], Shigui Zhao[b], Yang Chen[b], Heather Sheardown[c,d], Renita D'souza[d], Yuri Rochev[a,**]

[a] National Centre for Biomedical Engineering Science, National University of Ireland, Galway, Ireland
[b] Department of Chemistry and Chemical Biology, McMaster University, Hamilton, Ontario, Canada L8S 4M1
[c] Department of Chemical Engineering, McMaster University, Hamilton, Ontario, Canada L8S 4M1
[d] School of Biomedical Engineering, McMaster University, Hamilton, Ontario, Canada L8S 4M1

ARTICLE INFO

Article history:
Received 26 December 2009
Received in revised form 11 March 2010
Accepted 11 March 2010
Available online xxx

Keywords:
Silicones
Surface topology
Cellular activity
3T3 fibroblasts
Biocompatibility

ABSTRACT

Silicone elastomers exhibit a broad range of beneficial properties that are exploited in biomaterials. In some cases, however, problems can arise at silicone elastomer interfaces. With breast implants, for example, the fibrous capsule that forms at the silicone interface can undergo contracture, which can lead to the need for revision surgery. The relationship between surface topography and wound healing – which could impact on the degree of contracture – has not been examined in detail. To address this, we prepared silicone elastomer samples with rms surface roughnesses varying from 88 to 650 nm and examined the growth of 3T3 fibroblasts on these surfaces. The PicoGreen® assay demonstrated that fibroblast growth decreased with increases in surface roughness. Relatively smooth (~88 nm) PDMS samples had *ca.* twice as much fibroblast DNA per unit area than the 'bumpy' (~378 nm) and very rough (~604 and ~650 nm) PDMS samples. While the PDMS sample with roughness of ~650 nm had significantly fewer fibroblasts at 24 h than the TCP control, fibroblasts on the smooth silicone surprisingly reached confluence much more rapidly than on TCP, the gold standard for cell culture. Thus, increasing the surface roughness at the sub-micron scale could be a strategy worthy of consideration to help mitigate fibroblast growth and control fibrous capsule formation on silicone elastomer implants.

1. Introduction

Biomaterials, from breast implants to coronary stents, have evolved over time without a clear understanding of the properties that lead to optimal biocompatibility [1]. It is well known that surface characteristics such as roughness, texture, surface free energy, surface charge and chemical composition all play key roles in cell adhesion and growth, and that the nature of a biomaterial surface governs the phenotypic response of interacting cells [1].

Surface topography plays a significant role in biological processes such as cell attachment [2–5], motility, proliferation [3,6,7], differentiation [8], as well as regulation of gene expression [9]: these biological processes are important criteria for implant acceptance. The roughness of the implant surface can have significant influence on the cellular behaviour [10] and thus the foreign body reaction [9,11,12] can be minimized by critical adjustment of the roughness [13].

Poly(dimethylsiloxane) (PDMS or silicone) is a versatile polymer because of its biological stability [14,15] and low toxicity [14], the ease with which the hardness of silicone elastomers can be controlled, and its ability to be easily molded and shaped [15]. These properties make it suitable for a variety of applications such as breast implants [16], cochlear implants [17,18], maxillofacial reconstruction [15], artificial corneas [19], artificial skin, soft contact lenses [20], and coatings for pacemaker leads. The wound healing response at the external surface of a silicone implants leads to the formation of a fibrous capsule. Capsule formation can be either interrupted or unduly enhanced by infection, immune reaction, implant migration, or extrusion [15]. In the case of breast implants, the capsule can undergo significant contracture (shrinkage), a condition that can be painful and require revision operations [21].

Silicone breast implants are sold with smooth surfaces, or surfaces that are rough at the hundreds of microns scale. The rough surfaces are designed to facilitate tissue infiltration. However, the impact of silicone roughness at the sub-micron level on healing has not been examined in detail. Changing the roughness of PDMS at this length scale may modulate fibroblast growth and proliferation, which in turn may affect post-implantation fibrous capsule

* Corresponding author at: Department of Chemistry and Chemical Biology, McMaster University, Hamilton, Ontario, Canada L8S 4M1. Tel.: +1 905 525 9140x23483; fax: +1 905 522 2509.
** Corresponding author. Tel.: +353 91 492806; fax: +353 91 494596.
E-mail addresses: mabrook@mcmaster.ca (M.A. Brook), yury.rochev@nuigalway.ie (Y. Rochev).

0927-7765/$ – see front matter © 2010 Elsevier B.V. All rights reserved.
doi:10.1016/j.colsurfb.2010.03.006

Table 1
Showing varying roughness obtained by the optical profiler and atomic force microscopy in nanometer scale.

Technique	Different surface roughness of PDMS by controlled etching			
	Smooth (nm)	Bumpy (nm)	Very rough (nm)	
Optical profiler (Rq roughness)	20	150	300	400
Atomic force microscopy (Ra roughness)	88	378	604	650

formation and could also facilitate tissue reconstruction procedures [3].

We have recently developed synthetic methodologies that introduce roughness on silicone elastomer surfaces of up to hundreds of nanometers without changing the chemical composition of the surface. In the report below, we correlate the ability of 3T3 fibroblasts to adhere and proliferate on silicone surfaces with different surface topographies at the sub-micron scale.

2. Materials and methods

KOH was obtained from Aldrich and organic solvents were purchased from Caledon Laboratories. Water used was purified by treating in a reverse osmosis unit followed by a Millipore unit (18 mΩ resistivity). SYLGARD 184 (silicone elastomer kit) was purchased from Dow Corning.

2.1. Fabrication of PDMS

The elastomer was formed by combining the curing agent (1 part) with the silicone prepolymer (10 parts), and pouring the mixture into a Petri dish, where it was allowed to cure for 48 h at room temperature. Silicone slabs were cut into small circular disks of *ca.* 0.65 mm thickness and area 0.36 cm^2 and were used directly.

2.1.1. Etching

PDMS samples with varied surface roughness were prepared by controlled etching with KOH in mixed organic/aqueous solvents. The starting silicone elastomers had rms roughness (WYKO NT1100 optical profiler, Veeco) of 15–20 nm (see below for AFM roughness, which gave different values), which could be increased in a controlled manner to *ca.* 800 nm over 0.5–24 h. KOH was dissolved in water and then mixed with MeOH, ratio KOH:H_2O:MeOH = 1:10:90. One silicone elastomer disk was placed in a vial that contained the basic etchant solution and shaken for 6 h at room temperature (orbital shaker, 2 rps). At the conclusion of the etching process, the elastomer disks were removed from the vials, and washed extensively to remove any physically adhering materials. In a typical washing cycle, the rubber slabs were washed with acetone, THF, acetone, hexanes, acetone, water, acetone, and finally flushed with nitrogen then placed in vacuum chamber at room temperature overnight to dry. Finally, surface characteristics were determined.

2.2. Surface property characterization

FTIR: PDMS samples were characterized for chemical composition by Fourier transform infrared spectrophotometer FTIR-8300 system (Shimadzu).
SEM: Surface topography of gold coated PDMS samples were analysed by scanning electron microscopy (SEM) using a Hitachi S-4700 instrument.
AFM: The PDMS samples were also analysed by atomic force microscopy (AFM) using a Digital Instruments Dimension 3100 in tapping mode in air with scanning size of 100 μm × 100 μm area. Note that the measured roughnesses from the AFM were higher than the values obtained from the optical profiler, see text.

2.2.1. Optical profilometer

Surface roughnesses were obtained using a Veeco WYKO NT1100 optical profiling system (Mode: VSI, objective 50×, FOV 2.0×).

2.3. Cell culture

The PDMS samples were sterilized by treating with 70% ethanol for 20 min followed by successive washes four times with sterile PBS. NIH-3T3 (mouse) fibroblasts were cultured in Dulbecco's Modification of Eagle Medium (DMEM) (Sigma–Aldrich) supplemented with 10% fetal bovine serum (Sigma–Aldrich), 1% penicillin–streptomycin (Sigma–Aldrich) and 200 mM L-glutamine (Sigma–Aldrich) and kept in an incubator at 37 °C and 5% CO_2 atmosphere. Sterilized PDMS samples were kept in sterile 24-well plates, seeded with approximately 50 μl of a suspension of NIH-3T3 fibroblasts at a density of 40,000 cells/cm^2. This was just enough to cover the PDMS samples so that the cells could not flow off of the PDMS sample surface. The cells were kept in an incubator for 1 h so that they became fixed on the PDMS surface and then Dulbecco's Modification of Eagle Medium (DMEM) was added to give a final volume of 800 μl in each well, and again the plates were placed in an incubator at 37 °C under 5% CO_2 for 24 h. DNA was quantified according to the calibration curve by PicoGreen® assay. Twelve samples (4 PDMS samples × 3 repeats) were prepared three times with different passages, each time in triplicate. We used 14, 15 and 16 passages for our experiments.

2.4. PicoGreen® assay

The PicoGreen® assay was performed 24 h after seeding the cells on the surface of PDMS to measure the amount of DNA in micrograms per millilitre. After 24 h, media was removed from the wells and the wells were rinsed with Hanks Balanced salt solution (Sigma–Aldrich) once and 250 μl of double distilled water was added to each well. The cells were repeatedly subjected to lysis by freeze–thaw cycles three times (cooled for 15 min at −80 °C and then thawed for 15 min). Buffer and different DNA stock solutions were prepared for the calibration curve and 100 μl of diluted PicoGreen solution was added to an equal amount of lysed cell solution in a 96-well plate, according to the manufacturer's instructions (Invitrogen/Molecular probes™, Quant-iT™, PicoGreen®dsDNAAssay kit). The readings were obtained using the fluorescein (485/535 nm, 1.0 s) setting from the plate reader, a Perkin-Elmer Wallac Victor^3 ™1420 Multilabel counter.

2.5. Statistical analysis

Results of PicoGreen® assay were analysed using one-way analysis of variance (ANOVA) by Tukey's mean comparison. A ρ value of less than 0.05 for the ANOVA was considered significant. Error was expressed as standard deviation.

3. Results

Silicones readily undergo both polymerization and depolymerization with acidic and basic catalysts [22]. The by-products,

Please cite this article in press as: B.R. Prasad, et al., Controlling cellular activity by manipulating silicone surface roughness, Colloids Surf. B: Biointerfaces (2010), doi:10.1016/j.colsurfb.2010.03.006

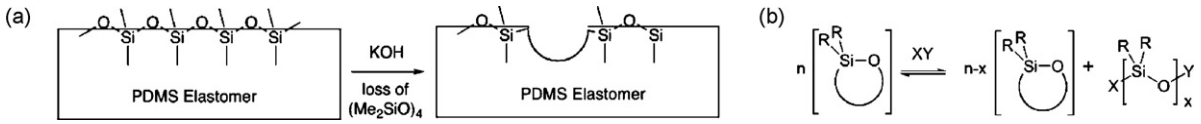

Fig. 1. (A) Elastomer etching process. (B) Silicone polymerization/depolymerization by equilibration.

typically cyclic siloxanes, can be removed by evaporation. When appropriate solvents are used, the depolymerization process occurs asymmetrically, leading to roughened surfaces (Fig. 1). Silicone elastomers were first cured by hydrosilylation using a commercial kit, Sylgard 184. Different degrees of roughness on the elastomer surface were created by the controlled chemical etching of the surface catalyzed with KOH (Table 1) [23]. FTIR spectra of the PDMS samples of different roughness demonstrated that chemical etching did not affect the surface chemical composition, which remained that of pure poly(dimethylsiloxane) (Fig. 2).

Surfaces of different roughness could be obtained by controlling reaction time, etchant (KOH) concentration, and particularly the solvent: a key requirement was the use of solvents that were poorly soluble in silicones in order to limit reactions to the interface. Thus, KOH was dissolved in a 10:90 mixture of water:methanol. Surface roughnesses of the samples prepared were investigated by SEM, AFM and optical profilometry. SEM demonstrated qualitatively that the PDMS surfaces exhibited different degrees of roughness (Fig. 3), which were quantified using AFM: the four surfaces exhibited root mean square roughness of ~88, ~378, ~604 and ~650 nm, respectively, as shown in Fig. 4. Optical profilometry, a technique based on interferometry, reported the same trends in roughness: the differences in roughness values between the two techniques are a consequence of the reporting of roughness on the profilometer as Rq, rather than the Ra values recorded by the AFM. In addition, because the two techniques derive roughness from an optical and electrical response, respectively, a perfect correlation is unexpected. Abbadie et al. have examined the correlation between the two techniques in detail [24].

The response of 3T3 fibroblasts to the PDMS elastomer of different surface roughnesses was examined over 24 h. Cells were seeded at a density of 40,000 cells/cm^2, allowed to adhere for 1 h, and then supplemented with DMEM for 24 h. The morphology of cells on different surfaces was examined microscopically, and the efficiency of cell proliferation was determined using a PicoGreen® assay that determines the amount of fibroblast cellular DNA on different surfaces.

Morphologically, the cells readily distinguished between the PDMS surfaces of different roughnesses. The growth on tissue culture plastic (TCP) was used as a control. As shown in Fig. 5, after 24 h very significant differences were observed in the degree of proliferation and the appearance of the cells. 3T3 cells on TCP were adherent after 24 h, proliferating although not to confluence, and exhibited their normal elongated (high aspect ratio) shape (Fig. 5a). Flat, smooth silicone surfaces were far more productive for cell growth than TCP: dense, near confluent cell layers were produced (Fig. 5c). By contrast, very rough PDMS surfaces with the same chemical structure exhibited only a few adhering and rounded up cells (Fig. 5b).

The selectivity of the 3T3 cells for smoother surfaces was further demonstrated by the use of the PicoGreen® assay, which is a more objective method to quantify cellular proliferation by measuring the DNA produced. As shown in Fig. 6, the fibroblast growth decreased with an increase in surface roughness. Smooth (~88 nm rms roughness) PDMS elastomers had significantly higher and statistically different ($p < 0.05$) amounts of fibroblast DNA per unit area than the 'bumpy' (~378 nm) and very rough (~604 nm and ~650 nm) PDMS samples. The smooth silicone surface exhibited far more cells at 24 h than the TCP, which is normally considered the gold standard for tissue culture.

4. Discussion

A key step in wound healing is the proliferation of fibroblasts, and the generation of ECM, including collagen. In the case of some implants, notably breast implants, excessive production of collagen, particularly when the fibres are well oriented, leads to

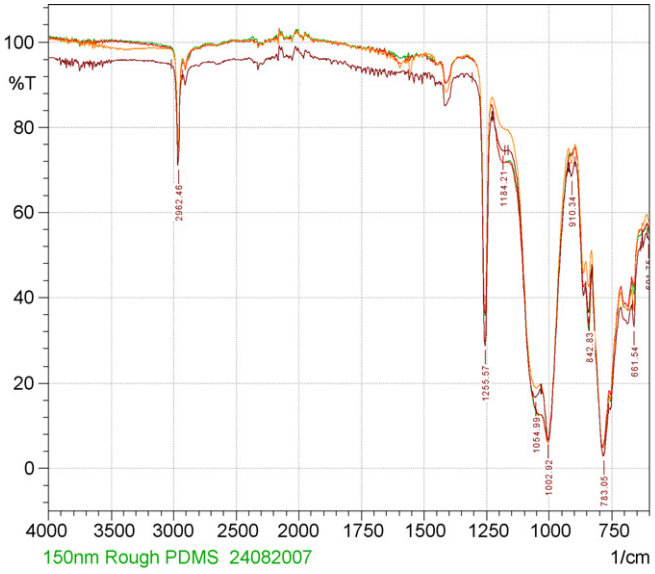

Fig. 2. Overlay of FTIR spectra from ~88 nm smooth PDMS (dark brown spectrum), ~378 nm bumpy PDMS (green spectrum), and ~604 nm (red spectrum) and ~650 nm (orange spectrum) very rough PDMS.

Please cite this article in press as: B.R. Prasad, et al., Controlling cellular activity by manipulating silicone surface roughness, Colloids Surf. B: Biointerfaces (2010), doi:10.1016/j.colsurfb.2010.03.006

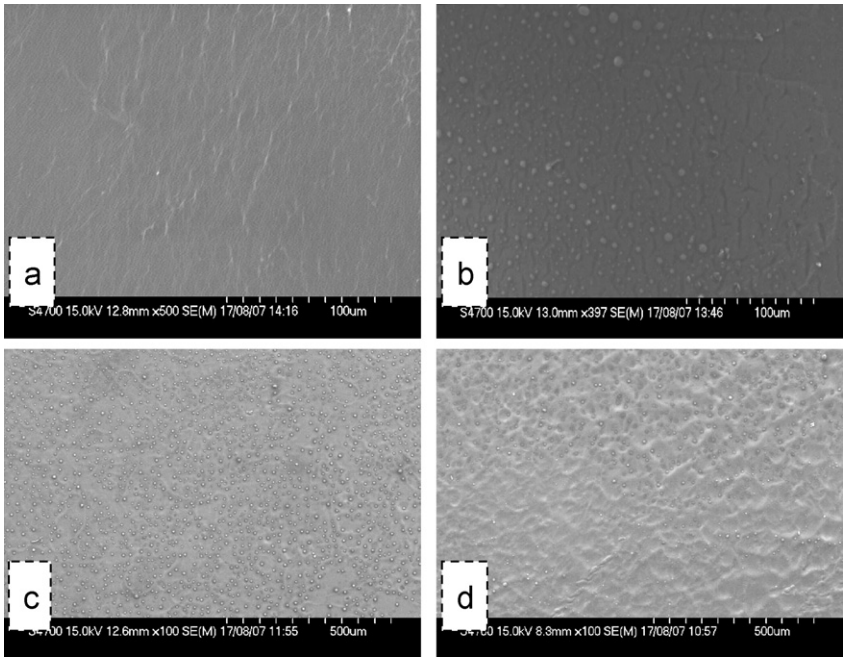

Fig. 3. SEM pictures showing (a) smooth (b) bumpy and (c and d) very rough PDMS surfaces.

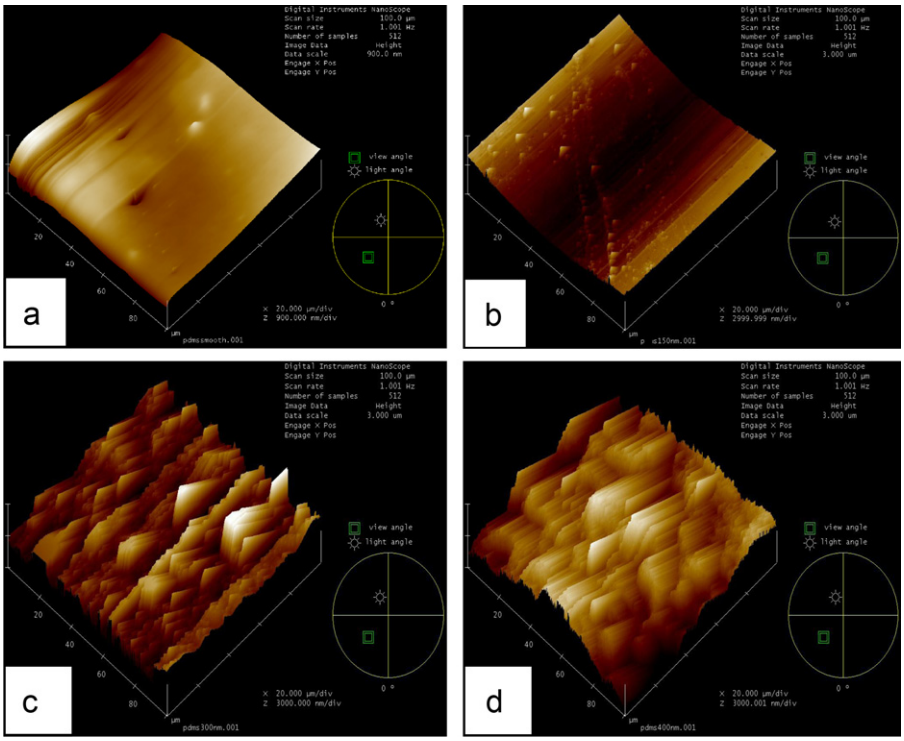

Fig. 4. 3D AFM pictures showing (a) smooth, (b) bumpy and (c and d) very rough PDMS surfaces.

'contracture', which can be painful and, in many cases, requires a surgical revision [25].

A variety of factors associated with a given surface can affect cellular compatibility. For example, low cell growth has been associated with hydrophobic surfaces such as silicones [26,27]. However, the rough, bumpy and smooth surfaces described above are comprised of the same silicone of the same low surface energy. Thus, the distinction observed in the ability of cells to proliferate can be associated with roughness alone.

While some investigations have suggested that the topography of the silicone surface does not have a significant effect on contracture [28], more studies suggest that a correlation exists [29,30]. These studies have compared 'smooth surfaces', prepared by dip coating with uncured silicone elastomers, to multi-micron scale rough surfaces, prepared either by molding operations or by exposing the uncured silicone surface to salt, which is washed away after cure [21]. The additional effect of softness of the material has been reviewed [31]. On smooth surfaces, fibroblasts more

Please cite this article in press as: B.R. Prasad, et al., Controlling cellular activity by manipulating silicone surface roughness, Colloids Surf. B: Biointerfaces (2010), doi:10.1016/j.colsurfb.2010.03.006

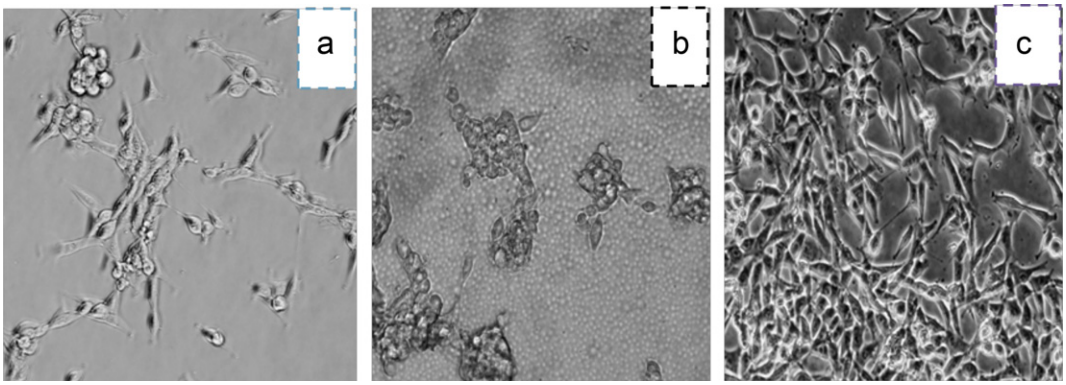

Fig. 5. (a) 3T3 fibroblasts on TCP; (b) 3T3 cells clumped on a very rough PDMS surface; (c) dense 3T3 cells on smooth PDMS. In all cases, photos were taken 24 h after seeding.

easily orient, leading to collagen fibres that can effectively contract. Deep, oriented multi-micron wide grooves lead to contact guidance of cellular growth along the groove [32]. The response of fibroblasts to oriented grooves was found to be better than to randomly oriented rough surfaces: thicker capsules formed in the former case, although when implanted the thinner capsules that were associated with random rough surfaces led to greater inflammatory responses [25]. Therefore, in addition to the benefits that could arise from tissue ingrowth on rough surfaces, which can be important for holding the implant in place, particularly with reconstruction patients post-mastectomy, rough surfaces at the micron scale length may be associated with reduced contracture [29,30].

While the effect on cellular growth of both smooth and very rough silicone implant surfaces have been examined [33], very little is known about the effect on cellular adhesion and proliferation of silicone surface roughness at the sub-micron scale. On silicon (the rigid element), slightly rougher surfaces (>70 nm) and very smooth (<10 nm) surfaces were detrimental to cell adhesion when compared with intermediate surfaces (20–50 nm) [34]. One report suggests that nanotexturing may affect contracture [21]. In the work above, we compared smooth surfaces with intermediate (bumpy) and very rough surfaces on the hundreds of nm scale. Smooth surfaces were associated with extremely efficient fibroblast proliferation, much better even than TCP.

The decrease in cellular compatibility of rougher silicone elastomer surfaces at the nm scale may be beneficial in a practical sense. The initial steps of the wound healing process involve protein adsorption on the silicone surface followed by cellular adsorption, particularly by fibroblasts. Since the ultimate outcome of over-proliferation of fibroblasts can be a thick and contracted capsule, surfaces that are less attractive to such surfaces may be beneficial in silicone-based implantable devices as they may lead to lower rates of contraction. Further research on in vivo responses to such surfaces will address this question.

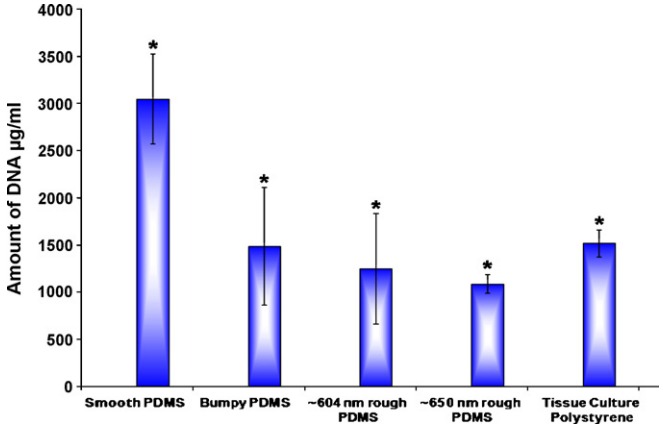

Fig. 6. PicoGreen® assay results showing the amount of DNA on silicone surfaces in microgram per millilitre (* denotes statistical significance using a one-way ANOVA ($p < 0.05$) by Tukey's mean comparison when compared with smooth PDMS).

5. Conclusions

Controlled levels of surface roughness could be introduced on PDMS elastomer samples using KOH-catalyzed etching as demonstrated by SEM, optical profilometry and AFM. Smooth PDMS surfaces supported 3T3 fibroblast cell growth better than both TCP and rougher silicone surfaces. The decreased ability of fibroblasts to proliferate on the rougher surfaces may be beneficial for in vivo applications, as it could lead to lower levels of capsular contracture than on smoother surfaces.

Acknowledgements

We want to acknowledge Dr. Natalia Nikolskaya of NCBES for helping with the PicoGreen® assay procedure and Dr. Eadaoin Timmins of NCBES for assisting with FTIR and AFM procedures. We thank Science Foundation Ireland and the Natural Sciences and Engineering Research Council of Canada for financial support. MAB wishes to acknowledge with gratitude Science Foundation Ireland for granting him an E.T.S. Walton Visiting Research Professorship in 2007.

References

[1] B.D. Ratner, et al., Biomaterials Science; An Introduction to Materials in Medicine, 2nd ed., Academic Press, San Diego, CA, 2004.
[2] M.T. Khorasani, H. Mirzadeh, BHK cells behaviour on laser treated polydimethylsiloxane surface, Colloids Surf. B Biointerf. 35 (1) (2004) 67–71.
[3] S. Kidambi, et al., Cell adhesion on polyelectrolyte multilayer coated polydimethylsiloxane surfaces with varying topographies, Tissue Eng. 13 (8) (2007) 2105–2117.
[4] J.N. Lee, et al., Compatibility of mammalian cells on surfaces of poly(dimethylsiloxane), Langmuir 20 (26) (2004) 11684–11691.
[5] G.K. Toworfe, et al., Fibronectin adsorption on surface-activated poly(dimethylsiloxane) and its effect on cellular function, J. Biomed. Mater. Res. A 71 (3) (2004) 449–461.
[6] B. Li, J. Chen, J.H. Wang, RGD peptide-conjugated poly(dimethylsiloxane) promotes adhesion, proliferation, and collagen secretion of human fibroblasts, J. Biomed. Mater. Res. A 79 (4) (2006) 989–998.
[7] E.K. Yim, et al., Nanopattern-induced changes in morphology and motility of smooth muscle cells, Biomaterials 26 (26) (2005) 5405–5413.
[8] H. Liao, et al., Response of rat osteoblast-like cells to microstructured model surfaces in vitro, Biomaterials 24 (4) (2003) 649–654.
[9] T.R. Kyriakides, et al., Mice that lack the angiogenesis inhibitor, thrombospondin 2, mount an altered foreign body reaction characterized by increased vascularity, Proc. Natl. Acad. Sci. U.S.A. 96 (8) (1999) 4449–4454.

Please cite this article in press as: B.R. Prasad, et al., Controlling cellular activity by manipulating silicone surface roughness, Colloids Surf. B: Biointerfaces (2010), doi:10.1016/j.colsurfb.2010.03.006

[10] E. McLucas, et al., An investigation into the effect of surface roughness of stainless steel on human umbilical vein endothelial cell gene expression, Endothelium 13 (1) (2006) 35–41.
[11] W.J. Kao, et al., Theoretical analysis of in vivo macrophage adhesion and foreign body giant cell formation on polydimethylsiloxane, low density polyethylene, and polyetherurethanes, J. Biomed. Mater. Res. 28 (1) (1994) 73–79.
[12] J.M. Rice, A.C. Fisher, J.A. Hunt, Macrophage–polymer interactions, J. Biomater. Sci. Polym. Ed. 9 (8) (1998) 833–847.
[13] H. Mirzadeh, F. Shokrolahi, M. Daliri, Effect of silicon rubber crosslink density on fibroblast cell behavior in vitro, J. Biomed. Mater. Res. A 67 (3) (2003) 727–732.
[14] T.Y. Chang, et al., Cell and protein compatibility of parylene-C surfaces, Langmuir 23 (23) (2007) 11718–11725.
[15] J.N. Kheir, et al., Polydimethylsiloxane for augmentation of the chin, malar, and nasal bones, J. Long Term Eff. Med. Implants 8 (1) (1998) 55–67.
[16] A. Backovic, D. Wolfram, Silicone mammary implants—can we turn back the time? Exp. Gerontol. 42 (8) (2007) 713–718.
[17] F. Abbasi, H. Mirzadeh, M. Simjoo, Hydrophilic interpenetrating polymer networks of poly(dimethyl siloxane) (PDMS) as biomaterial for cochlear implants, J. Biomater. Sci. Polym. Ed. 17 (3) (2006) 341–355.
[18] H. Mirzadeh, F. Abbasi, Segmented detachable structure of cochlear-implant electrodes for close-hugging engagement with the modiolus, J. Biomed. Mater. Res. B Appl. Biomater. 68 (2) (2004) 191–198.
[19] B.J. Klenkler, et al., EGF-grafted PDMS surfaces in artificial cornea applications, Biomaterials 26 (35) (2005) 7286–7296.
[20] P.C. Nicolson, J. Vogt, Soft contact lens polymers: an evolution, Biomaterials 22 (24) (2001) 3273–3283.
[21] S. Barr, E. Hill, A. Bayat, Current implant surface technology: an examination of their nanostructure and their influence on fibroblast alignment and biocompatibility, Eplasty 9 (2009) e22.
[22] M.A. Brook, Silicones, in Silicon, in Organic, Organometallic and Polymer Chemistry, Wiley, New York, 2000, pp. 256–308.
[23] M.A. Brook, et al., in: S.J. Clarson, et al. (Eds.), Etching of Silicone Elastomers: Controlled Manipulation of Surface Roughness, in Synthesis and Properties of Silicones and Silicone-modified Materials, American Chemical Society, Washington, DC, 2010.
[24] A. Abbadie, et al., Low thermal budget surface preparation of Si and SiGe, Appl. Surf. Sci. 225 (1–4) (2004) 256–266.
[25] J. Parker, et al., Soft-tissue response to silicone and poly-L-lactic acid implants with a periodic or random surface micropattern, J. Biomed. Mater. Res. 61 (1) (2002) 91–98.
[26] K.R. Patel, et al., Evaluation of polymer and self-assembled monolayer-coated silicone surfaces to reduce neural cell growth, Biomaterials 27 (8) (2006) 1519–1526.
[27] H. Ai, et al., Gelatin-glutaraldehyde cross-linking on silicone rubber to increase endothelial cell adhesion and growth, In Vitro Cell. Dev. Biol. Anim. 38 (9) (2002) 487–492.
[28] N. Poeppl, et al., Does the surface structure of implants have an impact on the formation of a capsular contracture? Aesthet. Plast. Surg. 31 (2) (2007) 133–139.
[29] G.P. Barnsley, L.J. Sigurdson, S.E. Barnsley, Textured surface breast implants in the prevention of capsular contracture among breast augmentation patients: a meta-analysis of randomized controlled trials, Plast. Reconstr. Surg. 117 (7) (2006) 2182–2190.
[30] C.H. Wong, et al., Capsular contracture in subglandular breast augmentation with textured versus smooth breast implants: a systematic review, Plast. Reconstr. Surg. 118 (5) (2006) 1224–1236.
[31] J.Y. Wong, J.B. Leach, X.Q. Brown, Balance of chemistry, topography, and mechanics at the cell-biomaterial interface: issues and challenges for assessing the role of substrate mechanics on cell response, Surf. Sci. 570 (1–2) (2004) 119–133.
[32] E.T. denBraber, et al., Quantitative analysis of fibroblast morphology on microgrooved surfaces with various groove and ridge dimensions, Biomaterials 17 (21) (1996) 2037–2044.
[33] J.F. Schumacher, et al., Engineered antifouling microtopographies—effect of feature size, geometry, and roughness on settlement of zoospores of the green alga Ulva, Biofouling 23 (1) (2007) 55–62.
[34] Y.W. Fan, et al., Culture of neural cells on silicon wafers with nano-scale surface topograph, J. Neurosci. Methods 120 (1) (2002) 17–23.

Please cite this article in press as: B.R. Prasad, et al., Controlling cellular activity by manipulating silicone surface roughness, Colloids Surf. B: Biointerfaces (2010), doi:10.1016/j.colsurfb.2010.03.006